An Investigation of the Synthesis and Properties of Nano Crystalline $Y_2O_3:Eu^{3+}$ (Prepared using Micelle- based Precursors)

A thesis submitted for the degree of Doctor of Philosophy

By

Yecheskel Kelly Saltoun

Wolfson Centre for Materials Processing

Brunel University

September 2013

Dedication

To my wife Shoshi Saltoun thank you for all your help and support.

Abstract

The work described in this thesis was aimed at understanding the reactions taking place on heating $Y_2O_3:Eu^{3+}$ phosphor precursors in the nano particle size regime.

Herein combustion syntheses to prepare nanometer sized crystallites of cubic $Y_2O_3:Eu^{3+}$ using precursors containing sacrificial long chain alkylammonium cations (the fuel) are reported. Using this method it proved possible to produce cubic $Y_2O_3:Eu^{3+}$ crystallites in the 20-70nm size range. The presence of CO_2 bands in the infra red spectra of the surface of the cubic $Y_2O_3:Eu^{3+}$ crystallites are also reported. These bands are identical in position to those found in [(Y, Eu)$OHCO_3.H_2O$], and are explained as arising from the spontaneous reaction of the surface of the nanometer sized particles of cubic $Y_2O_3:Eu^{3+}$ with atmospheric CO_2 and water vapour. This indicates that nanometer sized particles of cubic $Y_2O_3:Eu^{3+}$ are thermodynamically unstable in the atmosphere and must be protected against such back reactions. This could be done with surface coatings.

Precursors of the products were prepared from methanolic and ethanolic solutions and then these were fired at temperatures of 650 and 900°C.
Products (samples) prepared at a temperature of 900°C were observed to be all white powders in colour. Under 254nm uv excitation the samples prepared at 650°C displayed a weak red luminescence which was in contrast to the strong red luminescence from the samples prepared at 900°C that is characteristic of the Eu^{3+} ion in cubic Y_2O_3. The strongest red luminescence comes from 1:3 material sample ratios prepared at 900°C. The understanding of the chemistry behind the reactions and the characterisation and properties of the products formed are the major aims of the work reported here.

Table of Contents

Table of Contents

Table of Contents

Table of Contents

Table of Contents

Table of Contents

List of Figures

List of Figures

List of Figures

List of Figures

List of Figures

List of Figures

List of Figures

List of Figures

List of Figures

List of Figures

List of tables

Acknowledgements

I would like to thank from the bottom of my heart all the people that helped me to start and finish this work. Firstly, I would like to thank my supervisor Professor Jack Silver, for both constant encouragement and strong support through the years of this work.

The late Professor Rob Withnall, from the Wolfson centre, assisted me with great insight and guidance on the experimental part of Raman spectroscopy and also for help with the papers published during this work.

I wish to thank Dr. Terry Ireland, for help in every area of my work including all experimental work and results.

Thanks are also due to Dr. George Fern, for help with XRD analysis and results.

My thanks are also due to Prof. J. Silver and the late Prof. R. Withnall for use of all the lab and office facilities and I acknowledge the help of the technical staff whose help included their vast experience.

I would also like to thank the staff at the Experimental Techniques Centre (ETC) at Brunel University, including Dr. Alan Reynolds, Mrs Nita Verma, Dr.Lorna Anguilano and Dr Jesus Ojeda.

I owe a great deal to the many friends and colleagues, named and unnamed, that contributed to the completion of this work.

Finally, my wife, my son and my daughter for their continuous support and encouragement,

List of Abbreviations

Abbreviation	Meaning
ATR	Attenuated Total Reflectance
CRT	Cathode Ray Tube
CIE-	Commission internationale de l’éclairage
CCT	Colour Correlated Temperature (K)
Cd	Candela
CRI	Colour Rendering Index
FESEM	Field Emission Scanning Electron Microscope
FTIR	Fourier Transform Infrared Spectroscopy
FPD	Flat panel displays
lm	Lumens
LED	Light Emitting Diode
LCD	Liquid crystal displays
OLED	Organic Light Emitting Diode
PLED	Polymer Light Emitting Diode
QE	Quantum Efficiency (%)
SEM	Scanning Electron Microscope
TGA	Thermo gravimetric Analysis
XRD	X-Ray Diffraction

Chapter One

Introduction

1.0 Luminescence

It is of interest to review some historical facts about luminescence and luminescent materials to put the work in this thesis in context with its field of interest. Historically, the Chinese were the first to refer to the subject of luminescence observed in fireflies and glow-worms in the book "**Shih Ching**" (Book of Odes) written sometime in the period 1500-1000 BC [1]. Luminescence is also referred to in the "**Vedas**", the sacred books of India (of similar antiquity) by the word "khadoyta" (glow-worms in Sanskrit) which is used frequently. However, it was Aristotle (384-322 BC), who in his treatise "**De Coloribus**" (About Colours), introduced the idea of light of non incandescent origin and stated that "Some bodies, though they are not fire, nor participate in any way of nature of fire, yet seem to produce light" which is a very reasonable definition of the process of luminescence [1]. He went on to write:-"There are materials and substances in nature that are capable of producing light which is not obtained from candles or fire wood"**.** This statement can also be considered as a definition of luminescence [1].The Japanese were reported to have prepared phosphorescent paint from seashells in the 10^{th} century. It is of note that the credit for the preparation of the first phosphor should go to the Japanese.

At the start of the modern era a number of interesting observations [1, 2] in the field of phosphorescence, were reported:-

- 1610 Vincent Cascariolo: - The first phosphor preparations were barium sulfide (BaS and related compounds, for their good electro luminescence. These phosphors were reinvestigated in the 1970s, 1980s, 1990s).
- 1670 Henning Brandt: - Discovery of phosphorus. (He was an alchemist).
- 1700 F Hoffman: - Discovery of CaS.
- 1885 W Crookes: - Luminescence of phosphors investigated.
- 1886 Lecoq de Boisbaudran: - Activators Mn (Mn still best for EL).
- 1886 Sidot: - ZnS phosphors (ZnS: Ag still used in blue TV phosphors).

In the past 110 years the luminescence effect has been the subject of extensive systematic scientific research:-

- 1904 Klatt and Lenard: - CaS and ZnS phosphors (used fluxes still employed today).
- 1928 Lenard *et al.*:- Systematic study of phosphors.
- 1936 Destriau: - Electroluminescence (ZnS: Cu still best EL powder phosphor).
- 1938 Zinc silicate, various inventors Oxide lattice phosphors.

- 1949 McKeag, Ranby: - Calcium halo phosphate lamp phosphors (Still used in some present day lamps).
- 1964 Pallila and Levine: - YVO_4: Eu for colour TV (stimulated investigation of rare earth activators in phosphors).
- 1974 T Inoguchi *et al.:* Stable AC thin film EL.
- 1978 A Vecht *et al.*:- Alkaline earth phosphors for EL.
- 1980s Various, RGB backlit active matrix LCDs.
- 1992 Fujitsu: - High brightness full colour plasma display.
- 1993 Planar :- Saturated blue EL from thiogallates

Over the past 60 years, research on phosphors and solid state luminescence has blossomed, coinciding with advances in solid-state physics and optical spectroscopy, it has led to the development of phosphors as important industrial/ technological materials. They have found widespread use impacting on the lives of people all over the world. They are to be found in:-

- Cathode ray tubes (CRTs) for televisions and computer display monitors,
- CRT in radar,
- Plasma televisions (photoluminescent devices)
- As colour convertors for blue light emitting diodes (LEDs) to change the emitted light to white or another colour.

1.01 Luminescence and Fluorescence

The luminescent light that is emitted from materials can appear in three spectral regions of the electromagnetic spectrum [2]:
(1) the visible region, (2) the near Infrared region and (3) Ultraviolet region.
Luminescence is observed in the liquid, Solid or gas phases of certain organic and inorganic compounds.
Fluorescence was the term introduced to denote the imperceptible short after-glow of the mineral fluorite, CaF_2, following its excitation. This allowed it to be readily distinguished from phosphorescence, which denotes long-afterglow (which may stretch into a few hours). Light emission from a material during the time it is exposed to exciting radiation is referred to as fluorescence, if the after-glow is detectable visually after the end of the excitation, it is called phosphorescence.

1.1 Definition of Phosphor

- Phosphors (or luminophors) may be defined as solid materials showing luminescence. Phosphors essentially consist of very pure inorganic materials doped with suitable ions called activators [2, 3].

- The activator is usually present in concentration levels varying from one to five parts per million of the host lattice.

Often, additional ions act as charge compensators or donors in the lattice. These are termed co-activators. Luminescence [4] is produced when activators are inserted into the host lattice. They create local centres that can be excited to produce Luminescence. See figure 1.1a - when an activator with the desired emission does not have the required absorption for the available excitation energy, it may be possible to incorporate a co-activator, which absorbs the excitation energy and then transfers it to the neighbouring activator, this is explain in figure 1.1b

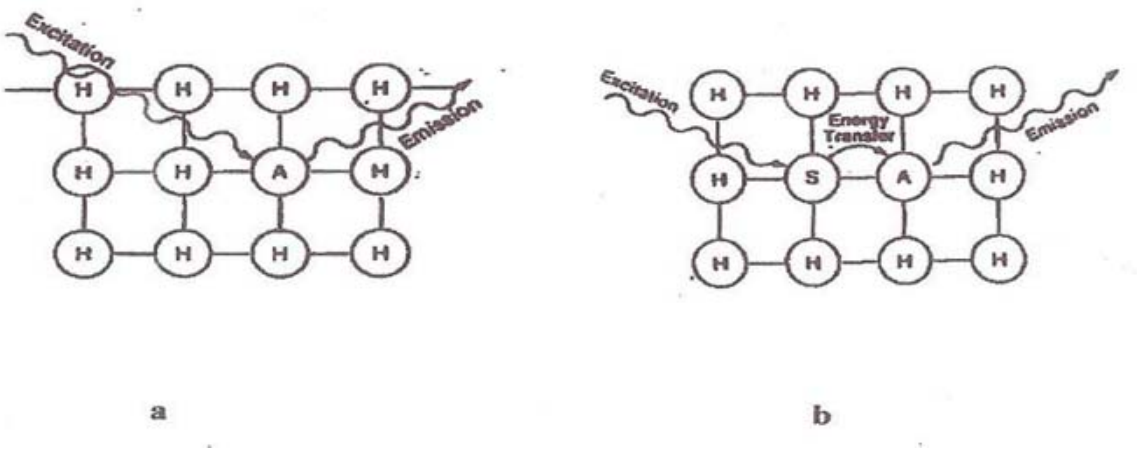

Figure 1.1 a) Shows the excitations and emission processes of the activator (A) in the host lattice (H). b) Shows the role of the co-activator (S) in excitation and emission processes [38].

Normally phosphors are made from crystalline materials that act as host crystals. They contain x amount of controlled impurities which are called activators, that generate the luminescence.

Different methods and type of excitation gives rise to various kinds of luminescence [5]. Emission obtained

a) from the absorption of photons (light) is called photoluminescence.
b) By applying electric currents or electric fields (a.c or d.c) is called electroluminescence.
c) by bombardment with an electron beam is called cathodoluminescence.
d) from the use of pressure is called triboluminescence.
e) by the use of heat is called thremoluminescence.
f) from a chemical reaction is called chemiluminescence.

Phosphors have seen wide spread use (see section 1.16) in for example televisions tubes, cathode ray tubes, fluorescent lighting (strips and compact light bulbs).The cathode ray tubes have now been almost totally replaced by flat screen technologies [5, 6]. Colour television technology was invented and started by

John.L.Baird in 1928 and was further developed in 1940 by Peter Goldmark. Initially the colour television was transmitted in red, blue and green [7].

1.2 Stokes' Law of Luminescence.

Sir George Stokes (1852) stated the first Law of Luminescence [8]. He said that "the wavelength of emitted light has to be longer than that of the absorbed light," The scientific world considered this statement as the first Law of Luminescence **(s**ee figure 1.2).

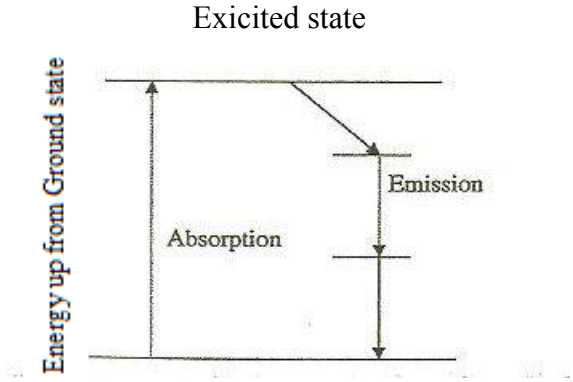

Figure 1.2 A conventional phosphor obeying Stokes' Law [8].

For photo Luminescence:- E excitation > E emission, λ excitation < λ emission.

Other phosphors known as up -convertors do not follow Stokes' law. These are called Anti–Stokes' phosphors and can convert infrared light into visible light by using two or more photons for excitation [9, 10] (see section 1.8).

1.3 The introduction of Activators into a Phosphor lattice

Lattice defects produce luminescence. The luminescence can occur either by addition or subtraction as follows:

a. Addition of atoms to the lattice to create luminescence.
b. Subtraction of atoms from lattice to create luminescence.

In both instances, a and b can be defined as activators that aim to increase luminescence. When an activator is introduced into any material, a new material forms which rearranges the crystal stoichiometry for better or worse in producing luminescence. This can also be achieved by rearranging the crystal or material lattice using chemical processes to introduce more activator to the crystal.
There are two different methods for adding activator to a phosphor host lattice:-

a) Adding activator to the reaction solution before precipitation of the phosphor precursor takes place; then precipitating the activator and host lattice simultaneously, this method is called co-precipitation.

b) Adding the activator solution to the dry phosphor lattice and then firing the dried solid.

Luminescent emission can be presented by three general models [11], which are shown in Figure 1.3. The location of the activator and coactivator levels in the forbidden energy gap and the energy transitions that make up luminescent emission are shown.

I. The Schon-Klasens model, (a) shows that luminescence is due to a radiative recombination of an electron from the conduction band with a localised acceptor level which lies above the valence band.
II. The Lambe- Klick model, (b) represents the luminescent transition as a free hole combining with a trapped electron at a level, which lies below the conduction band.
III. The Prener- Williams model, (c) considers that a localised association of the activator and co-activator is necessary to give luminescent emission.
See below, Figure 1.3 ZnS lumicient emission as per above [12].

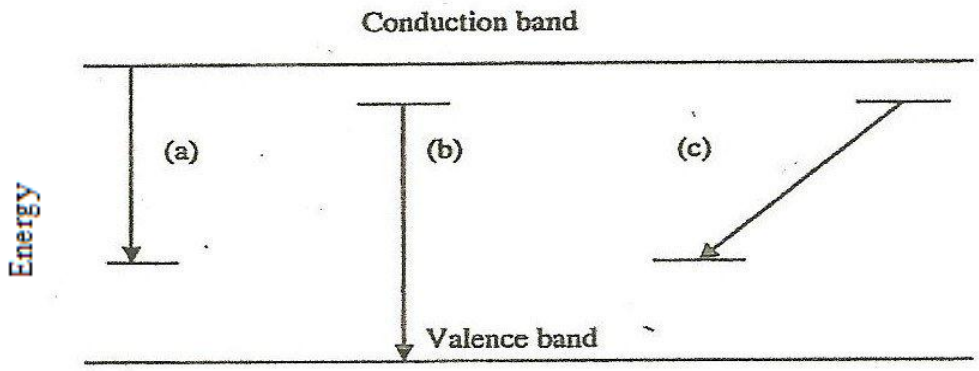

Figure 1.3 Energy models for luminescent emission ZnS :(a) Schon-Klasens; (b) Lambe-Klick, and (c) Prener-Williams [12].

A good inorganic phosphor consists of a lattice and an activator; the materials have to be of high purity. The activator may be introduced into the phosphor lattice in a variety of ways, such as: co-precipitation, e.g. by adding activator to the reaction solution, before precipitation takes place and precipitating the activator and host lattice simultaneously.

1.4 The introduction of Sensitisers into a Phosphor lattice

Definition of a sensitiser: - Sensitised photoluminescence is defined as a process whereby an impurity species (activator or acceptor) having no appreciable light

absorption ability in a given spectral domain, is made to emit radiation upon excitation as a result of absorption by and transfer from another impurity species (sensitiser, or donor) as shown below: - (Figure 1.4) [13]. The activator (A) is made to emit light after being excited via an energy transfer from the photo- excited donor (D)

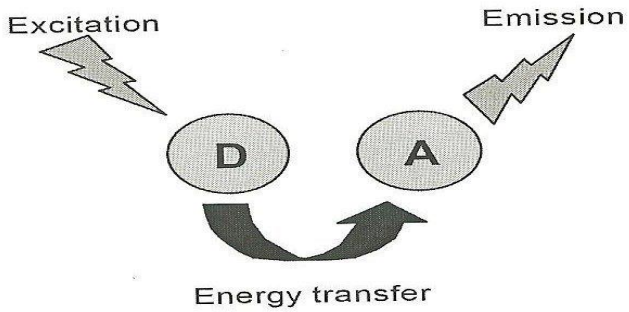

Figure 1.4 Principle of sensitised photoluminescence [13].

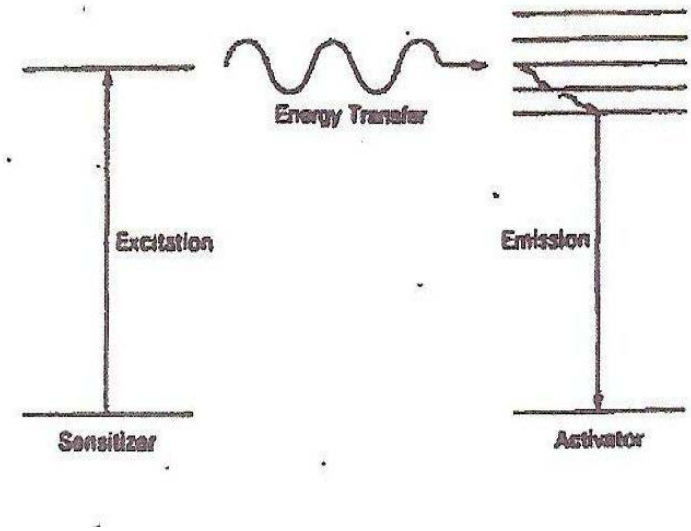

Figure 1.5 The energy transfer between a sensitiser and an activator [13].

The processes of excitation and emission depend on the activator being excited by absorbing a quantum of energy, and undergoing a transition to an excited state. Because the potential curves of the two states are non symmetrical, the activator ends up in a high vibrational state within the exited state. Initially the exited state phase relaxes to its lowest vibrational level. At which the system returns to its ground electronic state giving off the energy difference as luminescence. Note that the

excitation energy is higher than the emission energy. The energy transfer process is illustrated in Figure 1.4.and 1.5. The co activator is first excited to an upper energy state by the absorption of the incident radiation. This excitation energy is transferred by exciting a neighbouring activator, which then returns to its ground state via luminescent emission, the process of transfer is called non radiative energy transfer. For it to occur, the activator and the co-activator must have excited state levels of equal energy. Also they must be close enough in the host lattice. The distance may range from 4 to 30 Å [13]. Figure 1.4 illustrating the energy transfer between a sensitizer and an activator [13].

1.5 The introduction of Quenchers into a Phosphor lattice

Metals such as cobalt, nickel and iron are called Quenchers. They are normally used in small quantities of 10^{-6} to 10^{-8} g atom per mol of phosphor. Using quenchers in the phosphor can: - increase the speed of response, shorten the phosphor afterglow and help the activator to increase the phosphor luminescence [13].

1.6 Excitation and Emission spectra

The variations of response of a phosphor with wave length give rise to its excitation and emission spectra .The spectra show the interaction of the excitation energy with the activator and the host lattice. Figure 1.6 shows the excitation and emission spectra of the Y_2O_3: Eu phosphor [14].

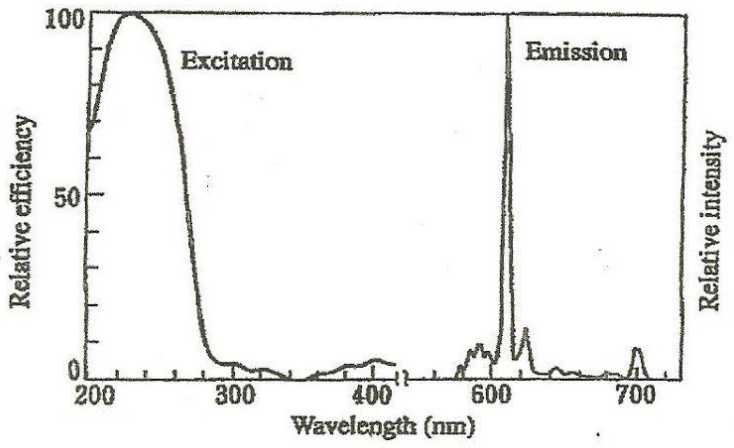

Figure 1.6 Excitation and emission spectra of the red Y_2O_3: Eu [14].

1.7 Phosphors emit light.

- Essentially, when an ion is in an excited state it reverts to its initial unexcited state by either :-
- (a) emitting photons, (or visible light), or (b) emitting phonons (or heat energy), e.g. lattice vibrations

Typical life times of activator ions in seconds are:

- Mn^{2+} (3d→3d) ~10^{-2}
- Cu^{+} (4s→3d) ~10^{-3}-10^{-4}
- Ag^{+} (5s→4d) ~10^{-6}-10^{-5}
- Eu^{3+} (4f→4f) ~10^{-4}-10^{-2}
- Tb^{3+} (4f→4f) ~10^{-4}-10^{-2}
- Ce^{3+} (5d→4f) ~ $3x10^{-7}$
- Eu^{2+} (5d→4f) ~ $8x10^{-7}$

The emission of light from inorganic solids is often split into two categories which are related to the lifetime of the activator: -

Phosphorescence, where the perceptible emission of light continues after excitation has ceased.

Fluorescence, where the perceptible emission of light ceases with the cessation of excitation

1.8 Upconversion or Anti Stokes phosphors

- Upconversion is an anti-Stokes phenomenon whereby two or more photons of low energy are added together to give a photon of higher energy (see Figure 1.7).

Up-conversion processes [15, 16] occur when the emitted radiation is of a higher energy than that absorbed. Many mechanisms have been proposed for this type of luminescence and are dependent upon a variety of factors. In general, several photons are absorbed for each one emitted.

The principle of the up-conversion process is illustrated in Figure 1.7. To understand the Anti-Stokes process we can consider an ion having a series of energy levels, which are fairly evenly spaced. As the ion absorbs a photon it enters an intermediate excited state, and will enter further excited states (upon each absorption) until it can absorb no more and the energy is released as a single photon of higher energy than those absorbed. Up-conversion processes occur in some trivalent rare earth activated phosphors which accept infrared light excitation (low energy and long wavelength) and emit visible light (high energy and short wavelength). Such processes occur due to higher lying excited states of rare earth ions being populated by two or three successive excitation steps with infrared quanta or by energy transfer from other

cations in the lattice. A downward transition to the ground level or to an intermediate excited level produces the visible luminescence [17].

Figure 1.7 shows Energy verses ground state. The 3 horizontal levels from bottom to top are first, second and third exited level.

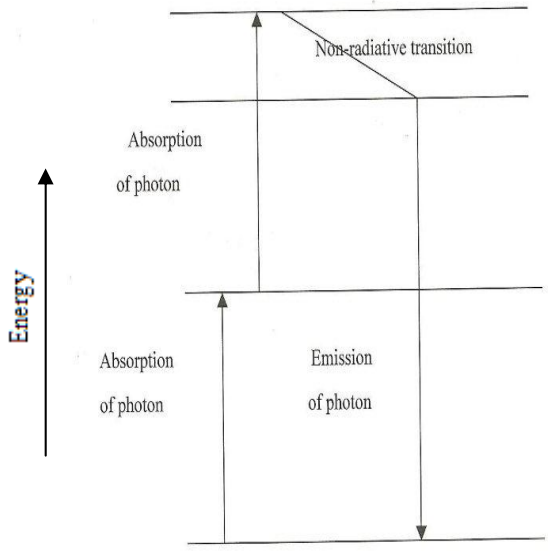

Figure 1.7 General mechanisms for Anti-Stokes' process [15].

Anti-Stokes phosphors were developed for up-conversion of long-wave IR-radiation (1.5-1. 6 μm) into short-wave (0.8-1.02 μm) and radiation of IR-range 0.9-1.07 μm into visible light of various colours. They are useful in night viewing devices for spectral sensitivity broadening of electron-optical image converters (up to 1.6 μm), in light-emitting diodes (LED) of various types, for visualization of IR-radiation and laser adjustment, as well as for marking of documents and valuable papers for security. The Anti-Stokes phosphors are usually powders, consisting of rare earth activated compounds based on yttrium (and some other elements) oxides, fluorides, oxysulphides, and oxychlorides. Such phosphors can provide stable emission for over > 100000 hours and within a temperature range of -60°C +70°C [18].

Anti-Stokes and Stokes emissions have been observed in cubic Y_2O_3:Eu^{3+} stimulated by 632.8 nm ruby laser light excitation [19]. All the emission features exhibited a marked thermal dependence, decreasing in intensity as the temperature was lowered. Arrhenius plots of this thermal behaviour indicated that the Eu^{3+} ions were thermally excited to a low-lying level ca. 1300 cm^{-1} above the ground state; this low-lying excited state was assigned to the $^7F_2$ level. Subsequent absorption of a 632.8 nm photon by the thermally excited Eu^{3+} ion promoted the electron to its $^5D_0$ level. Anti-Stokes emission bands at wavelengths longer than 580 nm exhibited a one photon dependence on the 632.8 nm exciting light and are assigned to the $^5D_0 \rightarrow 7F_0$, $^5D_0 \rightarrow$

$^7F_1$, and $^5D_0 \rightarrow {}^7F_2$ transitions of the Eu^{3+} ion. Stokes' emission bands also showing one photon dependence were assigned to the $^5D_0 \rightarrow 7F_3$ and $^5D_0 \rightarrow {}^7F_4$ transitions. Upconversion anti-Stokes emission bands were observed at wavelengths shorter than 580 nm and showed a two photon dependence on the 632.8 nm exciting light. These emission bands were assigned to Eu^{3+} ions on the C_2 sites of cubic Y_2O_3 with the only exception being a band at 582.2 nm. Although this emission band showed a thermal behaviour similar to that of the other emission bands, it was assigned to the Eu^{3+} ion on the S_6 site of cubic Y_2O_3, in keeping with previous assignments of others [19].

1.9 Efficiency

There are several definitions of the efficiency of a phosphor. The luminous efficiency - Ɛ- is the ratio between luminance and the input power. Luminance is a measure of the total energy output of a light source emitting in the visible region of the spectrum. This type of energy is known as brightness. Luminance is measured by candelas per sq meter = cd/m^2. The luminance efficiency of a phosphor under an electron beam excitation is measured in units of lumens per watt (lm/W).It can be measured using the efficiency equation $Ɛ= \pi$ L x.A/ P where π =3.14 is included since the emission of phosphor is measured is Lambertian, L is the luminance in (cd/m^2), **A** is the electron beams spot area in m^2, P is the power of the incident electron beam in watts, calculated by: **P =** accelerating potential in volts (V) x current in amperes (A). As a general rule, efficiency Ɛ is used to describe the efficiency of a phosphor excited by sources that produce electron – hole pairs in the host lattice for examples cathode-rays, X-rays, α (alpha) particles and γ (gamma)-rays.

The intrinsic luminous efficiency is the efficiency of a powder phosphor sample .The screen luminous efficiency is the efficiency of a thin layer phosphor powder deposited onto substrate. Screen efficiencies are lower than intrinsic efficiencies, due to the presence of binders that can absorb part of the excitation and emitted energies, and may also chemically react with the phosphor. There are two methods to measure screen efficiencies, (I) in back reflection mode light emitted directly from the front of the phosphor screen and (II) in transmission mode light emitted through the phosphor layer and substrate, measured from the back of the phosphor screen. A good phosphor screen should have efficiency comparable to its intrinsic efficiency [20].

1.10 Operating life and stability

Phosphors degrade with exposure to light, under an electric field, or when exposed to electron bombardment. The stability of a phosphor is often extremely sensitive to even traces of moisture and oxygen, the relative resistance to degradation under cathode ray. Excitation is rated as follows:-
Fluorides < Sulphides < Oxysulphides <silicates < $Y_3 Al_5 O_{12}$ (Yttrium Aluminium Garnet) and Aluminates.

In a CRT system there are four basic factors that can affect the stability of phosphor - (a) thermal quenching, (b) burning, (c) coloumbic ageing and (d) poisoning.
Thermal quenching in conventional CRT if high in a conditions where the phosphor is unable to dissipate the heat generated, leading to an increase in temperature and hence a reduction in phosphor efficiency. A return to low energy conditions leads again to normal phosphor efficiency.

Poisoning: - phosphors can be very sensitive to the presence of foreign ions other than the activators and co-activators. If the phosphor is contaminated with impurities such as iron, or nickel it may have a small fraction of its potential efficiency. If the contaminating ion is present in high concentration it can prevent the luminescence from occurring [9, 10, and 20].

1.11 Particle size and Morphology

Particle size and morphology of the phosphor powder are critical in determining the actual resolution and also the minimum pixel size and uniformity of the screen produced. When considering different display systems, the phosphors will have to be designed for each specific application. Phosphors do not obey simple rules, for example CRT phosphors used for TV screens may not respond in an electroluminescent cell and on the other hand phosphors that show good response under shorter wave UV excitation (254nm) may show poor response under longer wave UV (365 nm). Normally phosphors are optimised efficiently for their specific application [9, 10].

1.12 Cost

The cost of the phosphor is not critical as it represents a small fraction of the price of the display. The current material cost is around £750 (GBP) for a kilogram of phosphor. However one gram of phosphor can cover between 0.12 to 0.15 square meters so that one kilogram can cover approximately up to 150 m^2 of display surface [10].

1.13 Reproducibility

Production methods for a successful phosphor must produce a stable and good phosphor product from batch to a batch. The production must avoid the smallest traces of impurities, stiochometric variations or surface contamination. This requires strict

quality control and sophisticated instrumentation. For some phosphors the production process is operated at laboratory scale and cannot be scaled up for commercial use. Therefore it is essential to be aware of all the problems when synthesising/manufacturing a phosphor.

1.14 How phosphors convert electrical signals into light

Technology	Method of Excitation
Direct	
AC or DC electroluminescence	High field electrons

Here, the energy source is electrical; the conversion to light being direct or indirect.
In direct emission, electrical energy is converted directly into light. This is termed "electroluminescence". This term is most frequently applied to high field devices while low field devices are termed "light emitting diodes" (LEDs). The high field can be applied under direct or alternating current conditions, hence AC and DC EL displays.

Indirect	
Gas Plasma	Gas plasma generates ultraviolet light
LCD backlight	Gas plasma generates ultraviolet light
Cathodoluminescence	
Cathode ray tubes (CRTs) (~15-17 keV)	High voltage electrons
Field effect devices (FEDs) (~300-6000 eV)	High voltage electrons
Vacuum fluorescence (VF) (10-500 eV)	Low voltage electrons

The emission involves a cascade of events so indirectly the electricity causes other things to happen before the light is generated in, for example:- cathodoluminescent displays, such as cathode ray tubes (CRT), field effect displays (FEDs) and vacuum fluorescent devices (VFDs), the mechanism sequence can be described as involving:-

- Generation of free electrons.
- The passage (or acceleration) of electrons through a vacuum.
- The penetration of the electrons into the phosphor resulting in inducing excitation.

- The recombination process resulting in the generation of light.

In the case of photo luminescent displays such as DC or AC plasma displays (PDPs) where the UV light is generated by gas plasma.

The plasma can be generated under DC or AC conditions. This, in turn, excites the phosphor.

1.15 Luminescence types and display devices

Luminescence type	Excitation	Applications
Cathodoluminescence,	Electron beams (10kV-30kV) (10V-10kV)	CRT for TV, for display, for measurement, for other. Vacuum fluorescent display, Field emission display, large sized outdoor display.
Radioluminescence (X-rays and others)	High energy radiation (above 50 kV)	Fluoroscopic screen, intensifying screens, scintillator, image (input screen), dosimeter, radiographic imaging plate.
Photoluminescence	Ultraviolet rays (Vacuum UV) (254nm)	Plasma display, neon sign, neon tubing, Fluorescent display.
	(254-400nm)	High pressure mercury lamp, luminous paint, fluorescent pigment, fluorescent marking.
Upconversion or Anti-Stokes'	Visible infra red	IR-visible upconversion, solid state lasers, laser dye material.
Electroluminescence	Electric fields	DC inorganic electroluminescence, DC organic electroluminescence (OLED), AC inorganic electroluminescence, light emitting diodes (LED), semiconductor laser.

1.16 Phosphor Applications

Phosphors are important constituents of energy efficient fluorescent lamps, cathode ray tubes, high definition TVs, oscilloscopes, radar screens, low voltage field emission displays (FED), flat panel displays (FPD), liquid crystal displays (LCD) and plasma displays. The goal of all manufacturers is to produce efficient phosphors under low excitation energy. The importance of phosphors can be seen as industrial display materials for the display industry. These are employed in:-

1. Cathode ray tubes (cathodoluminescent devises) (CRT) [21] (see Figure 1.8 which presents a phosphor pattern of a striped picture tube) in which a mask control above whom the three different electron beams are only lit these owen phosphors. These used to be found commonly in televisions, computer monitors and radar systems. It is no longer the leading display technology-though it dominated the market for 60 years from 1940, $Y_2 O_3$ Eu was the first good red phosphor widely used for colour television [22].
2. Fluorescent lighting.
3. Flat screen plasma televisions.
4. Safety and military use (for further applications of phosphors) see [23].
   Phosphors can be classified according to their excitation in terms of duration (time) and brightness.
5. LED lighting sources as the colour changing elements [24]
   and LED screen televisions.
6. Electroluminescent displays [25, 26].
7. Emergency lighting systems based on electroluminescent devices.
8. Intensifying screens for medical and industrial radiography.
9. Infrared up-conversion phosphors.
10. Infrared phosphors for luminous paints.
11. For marking (security uses on currency etc.).
12. Stamps printed with phosphor-containing inks (see Figure 1.9)
    which shows phosphors stripes printed over the stamps.
13. Application of near-infrared phosphors for marking.

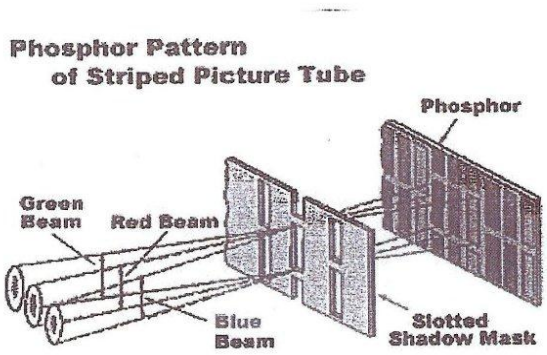

Figure1.8 Simplified diagram of a CRT [21].

Figure 1.9 Stamps printed with phosphor-containing inks [19].

1.17 Chromaticity.

Chromaticity is explained as the characterisation of colour known as CIE (Commission international Del 'Eclairage)-any colour can be given x, y, z chromaticity coordinates. The CIE chromaticity coordinates are equal to 100% so therefore the equation is x+y+z=1.Normally the value of x and y are given so z can be calculated as follows – z=1-(x +y). See figures 1.10&1.11 [27, 28] that show the CIE chromaticity diagram obtained from the "basic law of colour" [30].

CIE Chromaticity Diagram

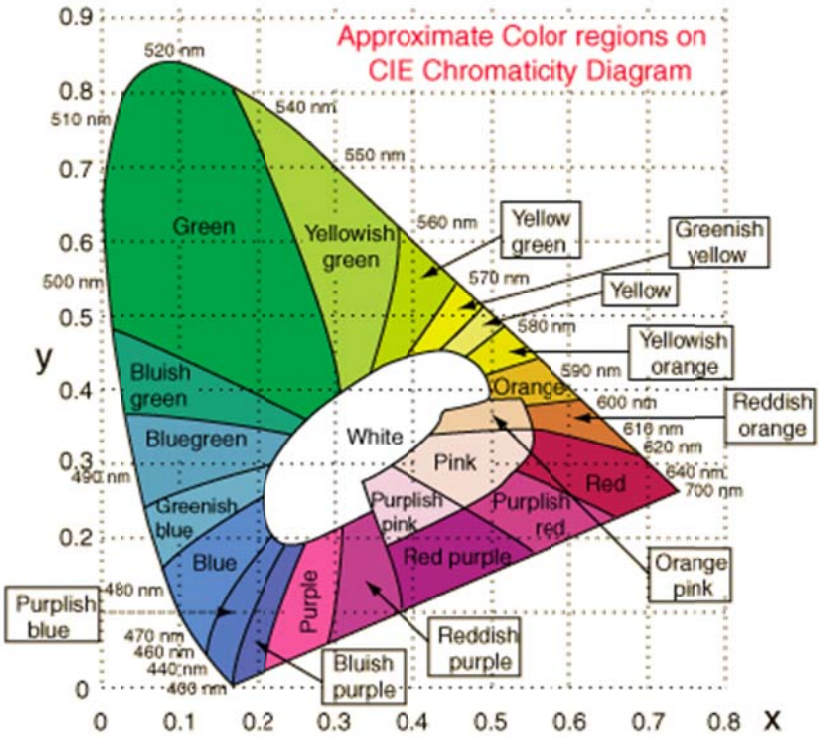

Figure 1.10 C.I.E.chromaticity diagram [29]. “The Colour regions”

Axis Y versus X

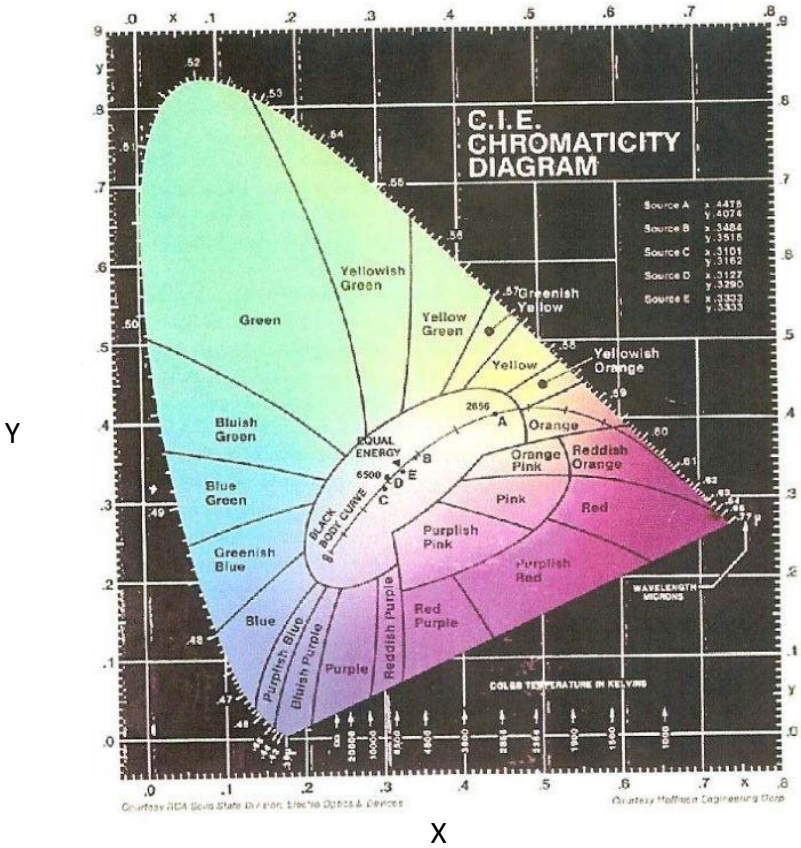

Figure 1.11 C.I.E.chromaticity diagram. [30]".

This tridimensionality of colour matching has a great advantage for both basic and applied colour work. If we define three standard primary sources for the matching light and define a standard observer's colour matching behaviour, then any test light can be described by just three numbers, the intensities of the primaries that produce a colour match for the standard observer. The 1931 CIE XYZ system implements this scheme. The CIE standard observer's colour matching was defined by averaging colour matching data from several human observers in several research laboratories, using three real light sources for the matching light. To simplify the logic and computation in applications, the committee decided to mathematically transform the data in such a way that the red, green, and blue real light sources used in the laboratory measurements were replaced by three theoretical light sources. In this system, then, any test light is characterized by three numbers ("tristimulus values"), X, Y, and Z, which are the amounts of each of the three primaries needed by the standard observer to match the test light. Y, for example, was defined to be mathematically identical to the luminance of the test light. For convenience in plotting colours graphically, the chromatic variables are characterized by a two-dimensional derivative statistic (the "chromaticity coordinates") which are derived from X, Y and Z by normalizing each to their sum:

$X = X / (X + Y + Z)$
$Y = Y / (X + Y + Z)$
$Z = Z / (X + Y + Z) = 1 - (X + Y)$

Any two of these (conventionally x and y are used) plus the luminance Y, fully capture the standard observer's colour match to the test light. Graphs of the x and y coordinates of lights are called chromaticity diagrams. Chromaticity diagrams show two of the three dimensions of colour, the third being luminance.

One of the most useful properties of chromaticity diagrams is their convenient representation of mixtures of two lights. Under the assumed laws of colour mixture that underlie this system, the chromaticities of all mixtures of any two lights lie on the straight line connecting the chromaticities of the two lights. Any individual colour emitted in a display can be characterised within the triangle connecting its three primaries: Any mixture of the red and blue primaries lies on the lower side of the triangle. If the green primary is then added to any of those lights, the mixture lies on a line connecting that light to the green primary. These mixtures together populate the triangle which is therefore the (x y) range of the display. By the same logic, all mixtures of any of the spectrum lights lie on straight lines interconnecting the points on the spectrum locus. These all lie within the area bounded by the spectrum locus, which therefore is the 2D range of physically realizable lights.

1.18 Retina

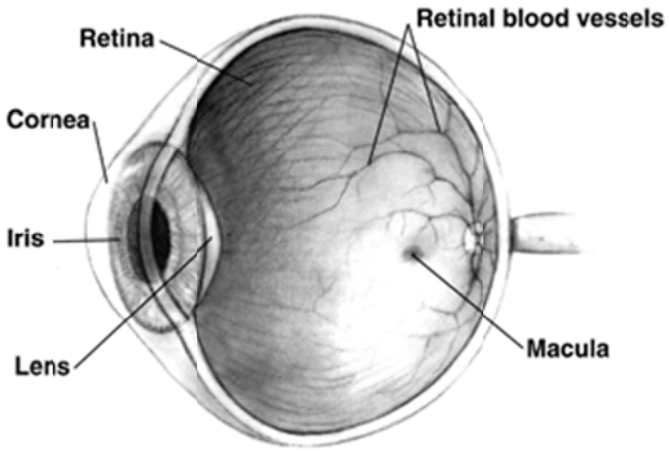

Figure 1.12. The basic structure of human retina and eyeball [18].

The vertebrate retina is a light-sensitive tissue lining the inner surface of the eye. The optics of the eye creates an image of the visual world on the retina, which initiates a cascade of chemical and electrical events that ultimately trigger nerve impulses. These

are sent to various visual centres of the brain [31]. The retina is a layered structure with several layers of neurons interconnected by synapses. The only neurons that are directly sensitive to light are the photoreceptor cells. These are mainly of two types: the rods and cones. Rods function mainly in dim light and provide black-and-white vision, while cones support daytime vision and the perception of colour. Recently evidence for a third photoreceptor system which does not involve rods and cone [32, 33] has been discovered. This much rarer type of photoreceptor, the photosensitive ganglion cell, is important for reflex responses to bright daylight. Neural signals from the rods and cones undergo processing by other neurons of the retina. The output takes the form of action potentials in retinal ganglion cells whose axons merge to form the optic nerve. Several important features of visual perception can be traced to the retinal encoding and processing of light. In adult humans the entire retina is approximately 72% of a sphere about 22 mm in diameter. The entire retina contains about 7 million cones and 75 to 150 million rods. The optic disc, a part of the retina sometimes called "the blind spot" because it lacks photoreceptors, is located at the optic papilla, where the optic-nerve fibers leave the eye. It appears as an oval white area of 3mm². Temporal to this disc is the macula. At its centre is the fovea, a pit that is responsible for sharp central vision is less sensitive to light because of its lack of rods.

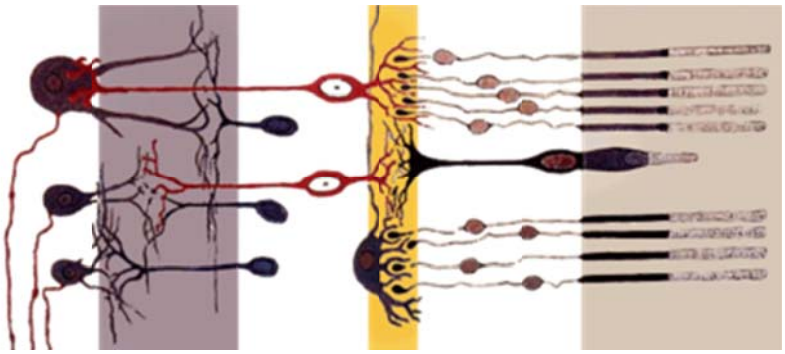

Figure 1.13 Rods, cones and nerve layers in the retina [18].

In the figure 1.13, the front (anterior) of the eye is on the left. Light passes through several transparent nerve layers to reach the rods and cones (far right). A chemical change in the rods and cones sends a signal back to the nerves. The signal goes first to the bipolar and horizontal cells (yellow layer), then to the anacrine cells and ganglion cells (purple layer), then to the optic nerve fibers. The signals are processed in these layers. First, the signals start as raw outputs of points in the rod and cone cells. Then the nerve layers identify simple shapes, such as bright points surrounded by dark points, edges, and movement [34]. In section the retina is no more than 0.5 mm thick. It has three layers of nerve cells and two of synapses, including the unique ribbon synapses. The optic nerve carries the ganglion cell axons to the brain and the blood vessels that open into the retina. The ganglion cells lie innermost in the retina while the photoreceptive cells lie outermost. Because of this counter-intuitive arrangement, light must first pass through and around the ganglion cells and through the thickness of the

retina, before reaching the rods and cones. The central retina is cone-dominated and the peripheral retina is rod-dominated. The area directly surrounding the fovea has the highest density of rods converging on a single bipolar cell. Since the cones have a much lesser power of merging signals, the fovea allows for the sharpest vision the eye can attain [31]. Though the rod and cones are a mosaic of sorts, straight forward transmission from receptors via bipolar to ganglion cells is not the case, since there are about 150 million receptors and only 1 million optic nerve fibres [35], there must be convergence and thus mixing of signals. Moreover, the horizontal action of the horizontal and amacrine cells can allow one area of the retina to control another (e.g., one stimulus inhibiting another). This inhibition is key to the sum of messages sent to the higher regions of the brain. In some lower vertebrates, (e.g., the pigeon) there is a "centrifugal" control of messages, that is, one layer can control another, or higher regions of the brain can drive the retinal nerve cells, but in primates this does not occur [31].

An image is produced by the patterned excitation of the cones and rods in the retina. The retina receives via the lenses. An image then forms on 6 to 8 million light sensitive receptors that transfer the colour image to the brain through a nerve bundle which contains one million fibres [35]. The excitation is processed to form a representation of the external environment. The cones respond to bright light and mediate high-resolution colour vision during daylight illumination (also called photopic vision). The rods are saturated at daylight levels and don't contribute to pattern vision. However, rods do respond to dim light and mediate lower-resolution, monochromatic vision under very low levels of illumination (called scotopic vision). The illumination in most office settings falls between these two levels and is called mesopic vision. At these light levels, both the rods and cones are actively contributing pattern information. The response of cones to various wavelengths of light is called their spectral sensitivity. In normal human vision, the spectral sensitivity of a cone falls into one of three subgroups. These are often called blue, green, and red cones but more accurately are short, medium, and long wavelength sensitive cone subgroups. When light falls on a receptor it sends a proportional response synaptically to bipolar cells which in turn signal the retinal ganglion cells. The receptors are also 'cross-linked' by horizontal cells and amacrine cells, which modify the synaptic signal before reaching the ganglion cells. Rod and cone signals are intermixed and combine, although rods are mostly active in very poorly lit conditions and saturate in broad daylight, while cones function in brighter lighting because they are not sensitive enough to work at very low light levels. Although there are more than 130 million retinal receptors, there are only approximately 1.2 million fibers (axons) in the optic nerve; a large amount of pre-processing is performed within the retina. The fovea produces the most accurate information. Despite occupying about 0.01% of the visual field (less than 2° of visual angle), about 10% of axons in the optic nerve are devoted to the fovea. The resolution limit of the fovea has been determined at around 10,000

points. The information capacity is estimated at 500,000 bits per second without colour or around 600,000 bits per second including colour [18].

1.19 Human Eye response

The eyes response to all colours is not linear and has a visual spectrum of 400 to 700 nm. In daylight the eye is more sensitive to green at 555nm and less to blue and red. The rods have a maximum response at 507 nm and this causes the light sensitivity curve for daytime vision, to be photonic and at night scotopic. Night vision is explained by the rods activity [33] and can be seen in Figure 1.14 and 1.15.The pigments in the human eye have peak sensitivities at about 650 nm (red), 530 nm (green), and 425 nm (blue) (see Figure 1.16).

The relative sensitivity of the three receptors for the "normal" human eye, designated by Greek letters beta, gamma and rho (β, γ, and ρ), is illustrated by the blue, green, and red curves on the right in Figure 1.16. Although the beta and gamma sensors correspond closely to blue and green, the rho sensor (the red curve) isn't even close to red. An ink with the same reflectivity spectrum would appear yellow-orange. The eye/brain discriminates colour by processing the relative stimuli in the three sensors. R, G, and B are used as additive primary colours because their distribution across the visible spectrum produces a wide-gamut colour image, not because they match the eye's response. Fewer than three colours are insufficient to reproduce full spectra. Additional colours offer some advantage- that's why recent inkjet photo printers have 6 to 8 colours. Combining three colours- even monochromatic (spectrally pure) colours produced by lasers- can produce most, though not all, of the colours the eye can see.

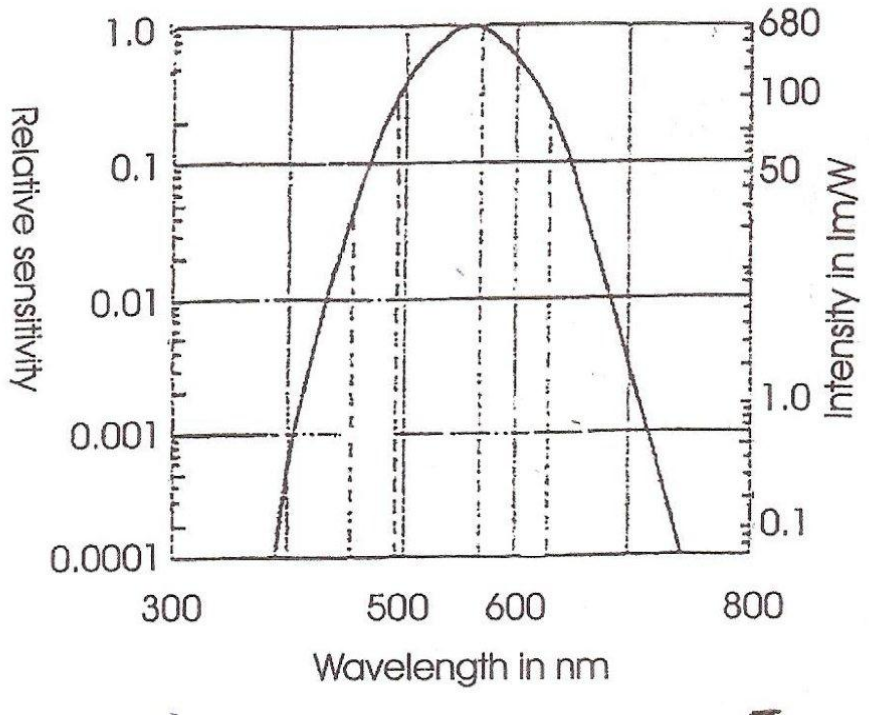

Figure 1.14 Spectral response of the human eye [36].

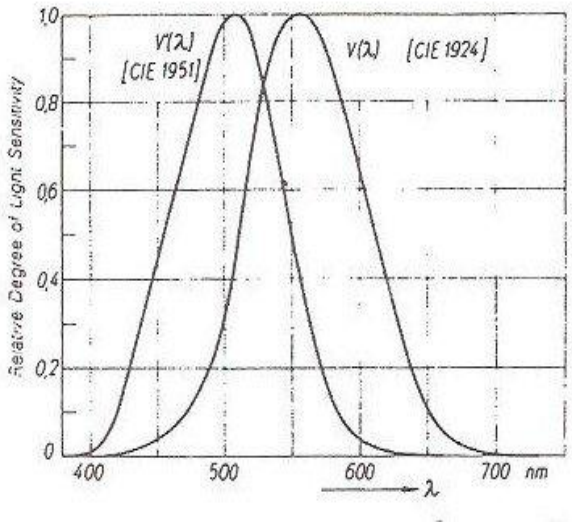

Figure 1.15 Difference in light sensitivity for daytime, V' and night-time vision [37].

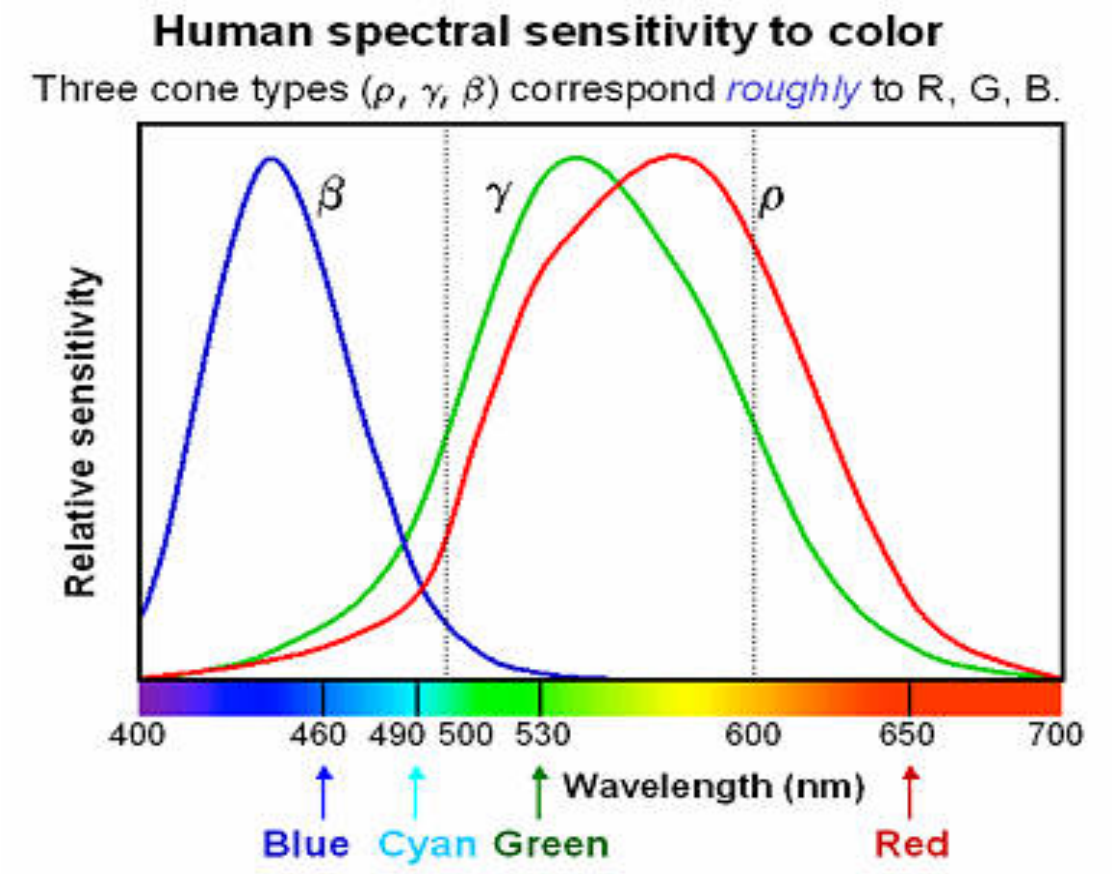

Figure 1.16 Human eye spectral sensitivity to colour [36].

References

[1] G, Blasse and B.C Grabmaier,"Luminesent Materials", pages 11-32 Springer- Verlag, Berlin 1994

[2] B.Valeur and M.Berberan-Santos." Brief history of Fluoscence and Phosphorescence." . Journal Chem. Education.88, 731-738.2011.

[3] P. Goldberg "Luminescence of Inorganic Solids ". Academic Press, New York and London.2.1966.

[4] M.A. Cayless and A.M. Marsden "Lamps and Lighting "Third Edition Edward Arnolds London.139.1966.

[5] J. Wilson and J.F.B. Hawkes "Optoelectronics: An introduction" Prentice Hall International, London.126.1983.

[6] J. Hallet. "Information Display". Vol.14, (I), 24. January 1998.

[7] Albert Abramson." The history of Television, 1942-2000."13-14, 2003.

[8] P. Goldberg "Luminescence of Inorganic Solids ". Academic Press, New York and London.4.1966.

[9] J.Hewett, "Opto & Laser Europe ".Issue106, 17. May2003.

[10] J Silver, D.A Davis, P. Marsh, A. Newport and J Ovenstone. "Phosphors and their specific application" International conference SID, London 21-23-November 2000.

[11] A.Vecht, Talk" notes from course on Luminescence emission and display". SID June 2001.

[12] B. Ray "II-IV Compounds "Pergamon Press Edinburgh.92-93.1969.

[13] J.A Deluca, "Insert of quenchers into a phosphor lattice". Journal Chem. Education .57, 8.541-545.1980.

[14] G, Blasse and B.C Grabmaier,"Luminesent Materials", pages 91-107 Springer- Verlag, Berlin 1994.

[15] N.Pelletier-Allard and R. Pelletier.”Luminescence”. 34, 323-324.1986.

[16] F.Auzel.” Visible luminescence”. Proc, IEEE, 61-62, 758, 1973.

[17] S. Shionoya and W. M. Yen “Phosphor Handbook “chapter 12, P643.CRC press LLC, 1999.

[18] F.Spedding and AH. Daane . "The Rare Earths". John Wiley & Sons, Inc.,105-106. 1961.

[19] J. Silver, M. I. Martinez-Rubio, T. G. Ireland, G. R. Fern and R.Withnall.” Eu^{3+} ion on the S_6 site of cubic Y_2O_3”. Phys. Chem. B, 2001, 105, 38, pp 9107– 9112,

[20] S.J.wiliamson and H.Z.Cummins ”light and coulor in nature and art”. Pages 173-180 .Wiley,1983.

[21] A.Vecht , C.Gibbons,T.Ireland, J.Silver and D. Barber.”Engineering Phosphors for field emission display”. Journal of Vacuum Science and technology B,17:750-757,1999.

[22] H. Kueppers “The Basic law of colour theory”. Baro. New York. Page 105-106, 1982.

[23] S.Shionoya, W.M Yen, “Phosphor Handbook “CRC press. London.7.1999.

[24] J. Hewett, Opto & Laser Europe.” LED lighting sources” .106, 17. May 2003.

[25] A.Bol, J.Ferwerda , J.A.Bergwerff and A.Meijerink.”Luminescent screen display”. Journal Electroluminescent displays. 99, 325-326, 2002.

[26] L.V.Zavyalova, A.K.Savin and G.S.Svechnikov.”Emissive display.” ” Journal Electroluminescent displays” 18, 73-74.1997.

[27] H. Kueppers “ The Basic law of colour theory “ .Barons. K New York. 142-143, 1982.

[28] J. Schanda.”CIE colorimetry” pages 25-28.John Wiley and Son, Inc. 2007.

[29] CIE(1932). Commission internationale de l'Eclairage proceedings, 1931. Cambridge: Cambridge University Press..

[30] H. Kueppers “The Basic law of colour theory” Barons K New York. 145-146.1982.

[31] "Sensory Reception: Human Vision: Structure and function Of the Human Eye"Vol. 27, Encyclopaedia Britannica, 1987.

[32] K.Thapan, J, Arendt, and D.J.Skene, J Physiology."Eye development and retinogenesis." 1, 261, 535-536, 2001.

[33] M.S.Rea, J.D.Bullough and M.G.Figueiro. "Induction of ectopic eyes". Journal of Pineat resech. 32,209-210, 2002.

[34] A drawing by Ramón Y Cajal for Human Vision: Structure and function of the Human Eye " Histologie du Système Nerveux de l'Homme et des Vertébrés, Maloine, Paris, 1911.

[35] T.Sherman."Connecting large vessels to small in the retina". Journal of General Physiology 78, 431–453, 1981.

[36] B.Cassin "Dictionary of eye technology" Barbara Cassin and triad Communications, 1984.

[37] H. Kueppers "The Basic law of colour theory", Barons K New York.104, 106, 1982.

[38] J. A. Rose. " Studies of luminescent materials including Novel preparation of phosphors". PhD thesis Greenwich University March 2004.

Chapter Two

Y, Eu, Y_2O_3, Y_2O_3: Eu and micellar material used for this thesis.

2.0 Introduction

The main aim of this thesis was to prepare nanometre sized particles of the red emitting phosphor yttrium oxide doped with europium. To appreciate the chemistry and properties of this phosphor it is useful to introduce the chemistry and properties of its constituent elements. In addition as the synthetic methods used involve the use of micelles it is useful to also discuss their properties here.

History:-Europium is a member of the group of metals known as the rare earth elements. Yttrium has many properties in common with these elements and is often found associated with them. Much of its chemistry is similar to that of the rare earth elements in their 3+ oxidation state.

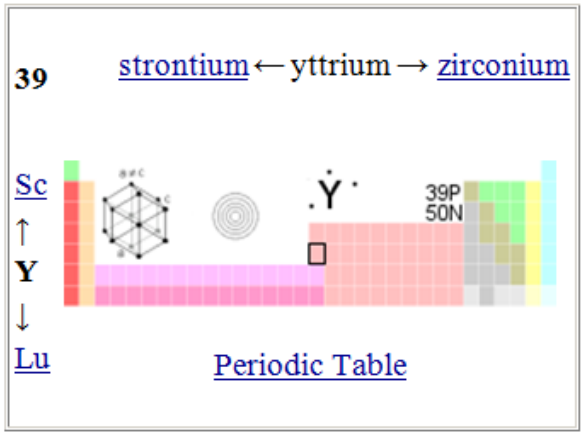

2.1 Yttrium [1] has the symbol **Y** and atomic number 39. A silvery metallic transition metal, yttrium occurs commonly with rare-earth minerals. Yttrium (named for Ytterby, a Swedish village near Vaxholm) was discovered by Finnish chemist, physicist and mineralogist Johan Gadolin in 1794 in a gadolinite mineral from Ytterby. It was isolated by Friedrich Wohler in 1828 as an impure extract of yttria through the reduction of yttrium anhydrous chloride (YCl_3) with potassium. In 1843, the great Swedish chemist Carl Mosander was able to show that yttria could be divided into the oxides (or earths) of three different elements. "Yttria" was the name used for the most basic one and the others were re-named erbia and terbia. The quarry located near the village of Ytterby yielded many unusual minerals that contained rare earths and other

elements. The elements erbium, terbium, ytterbium, and yttrium have all been named after this same small village.

Occurrence: This element is found in almost all rare earth minerals and in uranium ores but not as a free element. Yttrium is commercially recovered from monazite sand (3% content, [(Ce, La, etc.)PO_4]) and from bastnasite (0.2% content, [(Ce, La, etc.)$(CO_3)F$]). It is commercially produced by reducing yttrium fluoride with calcium metal but it can also be produced using other techniques. It is difficult to separate from other rare earths and when extracted, is a dark gray powder. Lunar samples from the Apollo program have relatively high yttrium content.

Isotopes: Natural yttrium is composed of only one isotope (Y-89).

Yttrium is a silver-metallic, lustrous rare earth metal that is relatively stable in air and chemically resembles the lanthanides. Shavings or turnings of the metal can ignite in air when they exceed 400°C. The metal has a low neutron cross-section for nuclear capture. The common oxidation state of yttrium is +3. Yttrium (III) oxide is the most important yttrium compound and is widely used to make the red emitting $YVO_4:Eu^{3+}$ and $Y_2O_3:Eu^{3+}$ phosphors that were used in the early colour television picture tubes. Yttrium oxide has many other uses in modern technology such as in yttrium iron garnets which are very effective microwave filters. Yttrium iron, aluminium, and gadolinium garnets (e.g. $Y_3Fe_5O_{12}$ and $Y_3Al_5O_{12}$) have interesting magnetic properties. Yttrium iron garnet is very efficient as an acoustic energy transmitter and transducer. Yttrium aluminium garnet, yttrium lithium fluoride, and yttrium vanadate are used in combination with dopants such as neodymium or erbium in infrared lasers.

2.2 Eu [2,3] Europium

Samarium ← europium → gadolinium

-
↑
Eu
↓
Am

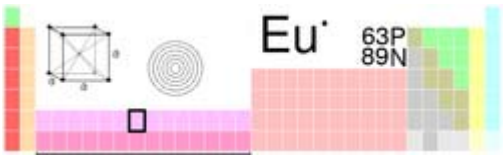

Periodic Table

Eu has atomic number 63. It was named after the continent Europe. Europium is the most reactive of the rare earth elements; it instantly oxidizes in air, and resembles calcium in its reaction with water. Europium metal ignites in air at about 150°C to 180°C. Its hardness approximate to that of lead and it is ductile. The existence of Europium was first found by Paul Émile Lecoq de Boisbaudran in 1890, who obtained a basic fraction from samarium-gadolinium concentrates which had spectral lines not

accounted for by samarium or gadolinium. However, the discovery of europium is generally credited to French chemist Eugène-Antole Demarçay, who suspected

samples of the recently discovered element samarium were contaminated with an unknown element in 1896,which isolated europium in 1901.

Applications: There are few commercial applications for europium metal, although it has been used to dope some types of glass to make lasers, as well as being used for screening for Down's syndrome and some other genetic diseases. Due to its ability to absorb neutrons, it is also being studied for use in nuclear reactors.

As discussed in chapter 1 and above Y_2O_3 doped with Eu^{3+} has been widely used as a red phosphor in television sets and in fluorescent lamps. Eu^{3+} is also used and as an activator for many other yttrium-based phosphors. Eu^{2+} is used as an activator for a group of phosphors that are used to convert the colour of blue LED s to yellow green or red for current lighting applications.,

Europium fluorescence is used to interrogate bimolecular interactions in drug-discovery screens. It is also used in the anti-counterfeiting phosphors in Euro banknotes.

Occurrence [2, 3, and 4]: Europium is never found in nature as the free element; however, there are many minerals containing europium, with the most important sources being bastnasite and monazite. Europium has also been identified in the spectra of the sun and certain stars, most lanthanides form compounds with an oxidation state of +3.

Isotopes: Naturally occurring europium is composed of 2 stable isotopes, 151-Eu and 153-Eu, with 153-Eu being the most abundant (52.2% natural abundance).

2. 3 Yttrium Oxide (Y_2O_3).

Y_2O_3 is a refractory material. It has less thermal expansion than alumina, magnesia and zirconium. It is soluble in acids and slightly soluble in water. It is available on the market in various purities between 99.9% and 99.99%.

Chapter 2 Y, Eu, Y_2O_3, Y_2O_3: Eu and Micelles Material used for this thesis.

Figure 2.1 Crystal shapes of Y_2O_3 [5].

Background: Yttrium oxide is mainly extracted from the mineral Xenotime (YPO_4). Its properties include high thermal stability and good transparency to infrared radiation. It has an affinity for oxygen and sulphur and is used as an additive to stabilise zirconia and as a sintering aid in silicon nitride. As an optical ceramic, it transmits well in the infrared range, from 1 to 8 μm wavelength. The high infrared transmission, together with good resistance to erosion and thermal shock, makes it ideal for protection domes for infrared sensors.

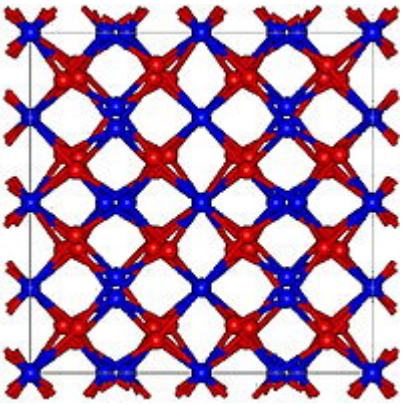

Figure 2.2 The crystal structure of Y_2O_3 [6].

The crystal structure of Y_2O_3 used in phosphors application is a body-centered cube where each Y^{3+} cation is surrounded by six oxygens located at the corners of a cube. There are two different Y^{3+} cation sites in the lattice. These are shown in figure 2.3 below. Two of the corners are vacant and can be along a body or face diagonal of the cube which results in two Y^{3+} site symmetries called S_6 and C_2 ,respectively it is believed that the activators substitute these Y^{3+} sites.(ref).The ratio of C_2 to S_6 sites is

3 to 1 [6].

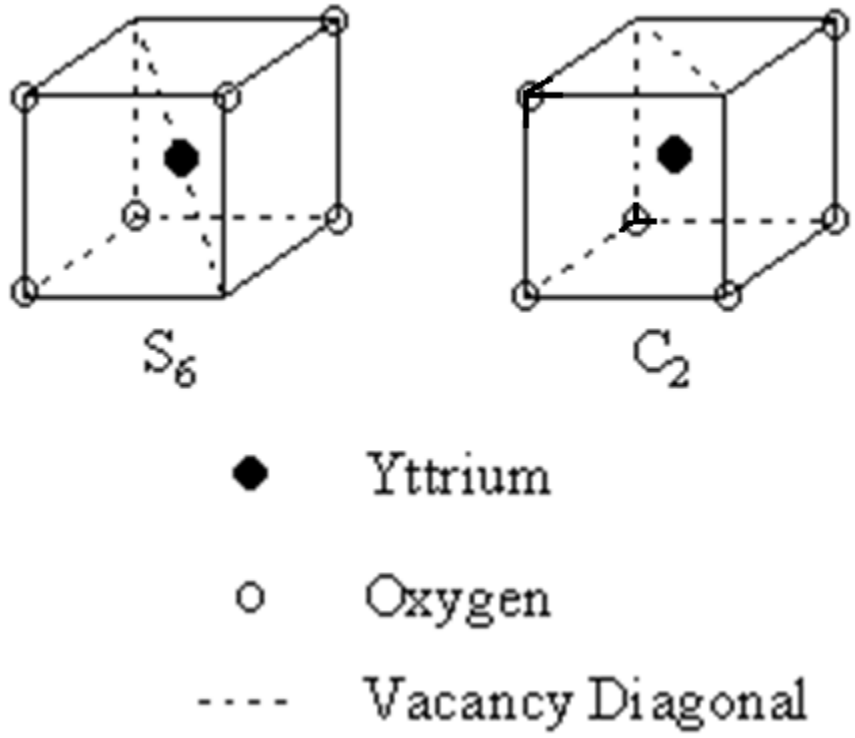

Figure 2.3 The two Y^{3+} crystallographic symmetry sites in cubic-Y_2O_3 [6].

2.4 $Y_2O_3:Eu^{3+}$

The red emitting phosphor, $Y_2O_3:Eu^{3+}$, is prepared by adding Eu^{3+} cations to the Y_2O_3 lattice as activators. The emission spectra from the Eu^{3+} cations in the S_6 sites show weak emission lines, whereas the spectra from the Eu^{3+} cations in the C_2 site have sharp emission lines, dominated by the red emission at 611nm from the $^5D_0 \rightarrow {}^7F_2$ transition. The different properties are due to different crystallographic site symmetries. Over the period from 1963 to 1968 studies by Mandel, Toma and Palumbo of $Y_2O_3:Yb^{3+}$ and $Y_2O_3:Bi^{3+}$ respectively showed that the Y_2O_3 activated phosphors substitute at both C_2 and S_6 sites [7]. The research carried out on $Y_2O_3:Eu^{3+}$ phosphors by previous researchers identified it as an extremely efficient phosphor for use in CRT's and fluorescent lamps and is still used at present in these devices. In 1977 three-band fluorescent lamps were fabricated [8].These contained [$Zn_2SiO_4:Mn^{2+}$], green, for red [$Y_2O_3:Eu^{3+}$] and blue [$Sr_5(PO_4)_3Cl:Eu^{2+}$] phosphors instead of the previously used calcium halo phosphate phosphors. There has been significant research into the development of $Y_2O_3:Eu^{3+}$ nanometre sized-particles in the last fifteen years [9-12]. ≤1μm spherical phosphor powders of $Y_2O_3:Eu^{3+}$ [9] were developed in the late 1990's especially for field emissive devices because thin layers of closely packed phosphor particles were required. In 1999 Ireland et al [10] produced $Y_2O_3:Eu^{3+}$ phosphors from solution by using a sacrificial Micellar phase. These phosphorescent

materials had significantly smaller sized particles (approximately 0.1-1.0nm) compared with commercial Y_2O_3:Eu^{3+} phosphor particles. In 2000 Martinez-Rubio et al [11] used EDTA to control particle size during the synthesis of ultrafine Y_2O_3: Eu phosphors. Martinez- Rubio et al developed another method for producing a range of particle sizes in 2002; however this was via a copolymer microgel of NIPAM and AMPS [12]. Anti-Stokes and Stokes emission bands were assigned to the Eu^{3+} ions on the C_2 and S_6 sites of the Y_2O_3:Eu^{3+} phosphor under 632.8nm light excitation during 2001 by Silver et al [13]. The early 21st century witnessed growing demands for innovative flat screen technology which led to the development of novel nano-structured phosphors such as unfilled and inverse photonic crystals. Silver et al [14] researched this new area of phosphor technology and produced Y_2O_3:Eu^{3+} photonic crystal lattices for various display applications. Silver et al [15] also showed in 2004 that whilst controlling the dopant level in cubic Y_2O_3: Eu^{3+} phosphors the activators in the Y_2O_3:Eu^{3+} phosphor, i.e. the Eu^{3+} ions were distributed evenly and homogeneously in the developed phosphor particles. Chen et al [16]. Investigated the luminescent properties of $Sr_{2-x}Ca_xMgSi_2O_7$: Eu^{2+}, Dy^{3+} where x = 0 or 1 in 2006. A VUV laser source (157.6 nm) was used to excite the sample and the results showed rich line structures in the laser-excited emission spectra which partly result from the 4f-4f transitions of Eu^{3+}, indicating an efficient photon-induced process which promotes Eu^{2+} to Eu^{3+} [16].

Eu^{3+} has five narrow emission bands as shown in the Dieke diagram (figure-2.4). Corresponding to the $^5D_0 \rightarrow {}^7F_i$ transitions where i = 0, 1, 2, 3 and 4 [17]. In cubic Y_2O_3:Eu^{3+} bands give rise to the characteristic red emission of the phosphor.

In research conducted by Camenzind [18] continuous, single-step synthesis of cubic, monocrystalline Y_2O_3:Eu^{3+} nanophosphors particles were achieved by flame spray pyrolysis. Synthesis of monoclinic or cubic Y_2O_3:Eu^{3+} nanoparticles were achieved by controlling the high temperature residence time of these particles.

Reasons for choosing this phosphor for use in FEDs and high definition flat screens include :-

1) Yoo et al [19, 20]. Predicted that as the particle size decreased so would the optimum CL work voltage.
2) The decrease in phosphor particle size will also result in a higher number of particles per unit volume and increase the possibility of electron penetration to the dopant site.
3) Additionally, a smaller phosphor size could result in a smaller screen pixel size and a higher degree of transparency for phosphors dispersed in other substances.

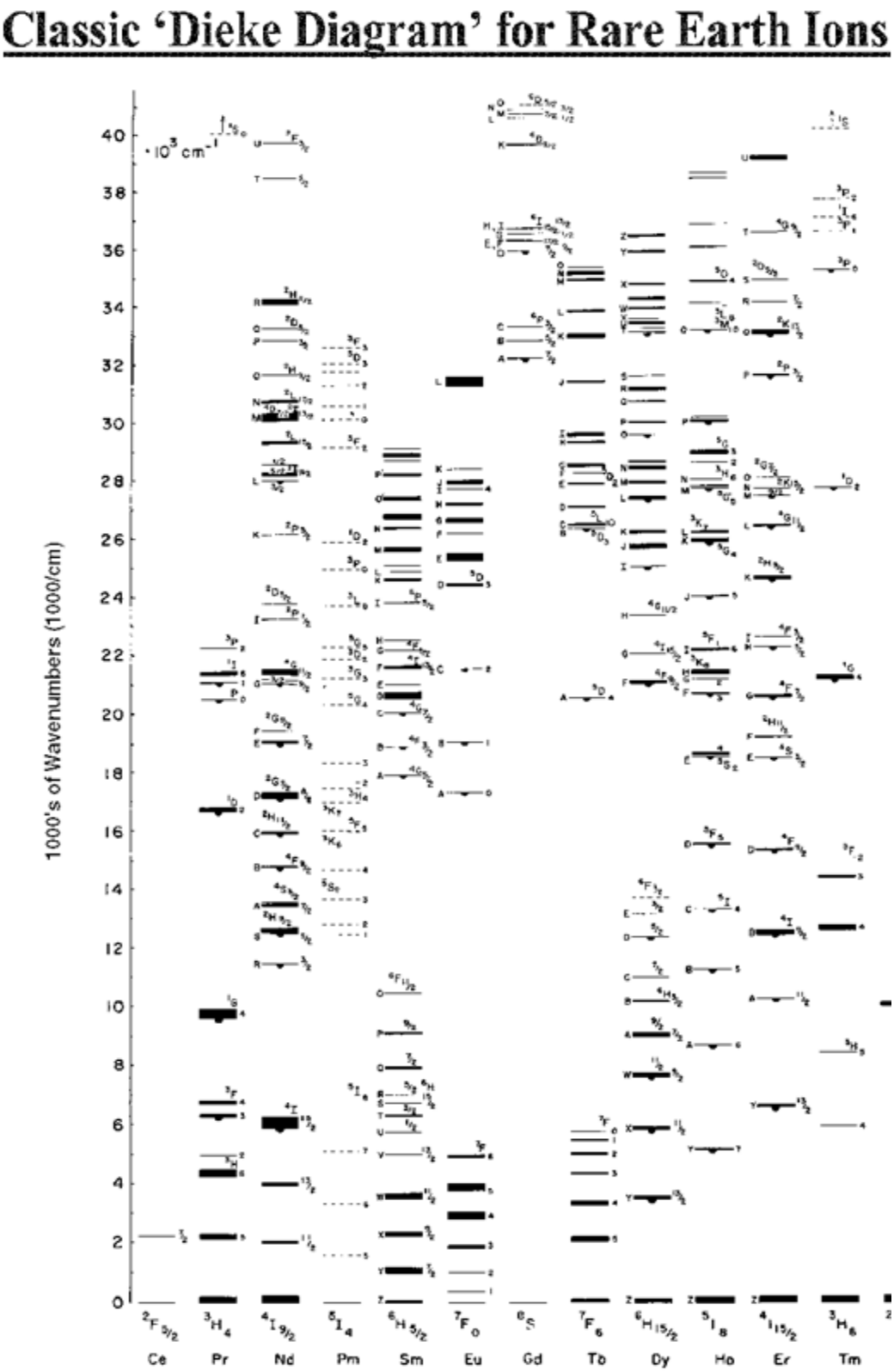

Figure 2.4 Dieke diagrams [20].

Chapter 2 Y, Eu, Y_2O_3, Y_2O_3: Eu and Micelles Material used for this thesis.

2.5 Nanometre sized particles of $Y_2O_3:Eu^{3+}$ [21].

Since the first reports on quantum confined effects in nano-particle zinc sulphide based phosphors by Bhargarva and co-workers [22-27], there has been interest in the properties and uses of many traditional phosphors in nano-particle (or nanocrystalline) form. Nanocrystalline phosphors are thought to have more perfect lattices [28] and therefore fewer bulk defects compared to conventional μm size phosphor particles. Emission studies of, for example, $ZnS:Mn^{2+}$ have shown that the intrinsic luminescence efficiency of the doped phosphors can be improved if the particle size is reduced to nanodimensions; in addition, lifetime shortening of the excited state has been reported [22,23,25]. In this section a brief review of published literature methods for making nanometre sized particles of $Y_2O_3:Eu^{3+}$ are covered. Methods of making nanocrystalline monoclinic $Y_2O_3:Eu^{3+}$ and novel nano-structures containing Y_2O_3: Eu^{3+} are also reviewed here.

2.5.1 Chemical synthesis of nanocrystalline cubic europium doped yttria particles. Nanocrystalline europium doped yttria particles have been synthesised using a wide variety of methods that have given rise to nanoparticles or nanocrystallites of different particle size. There are five main methods to produce nanocrystalline $Y_2O_3:Eu^{3+}$. These are:-

(a) Solution methods.
(b) Aerosol spray methods
(c) Chemical vapour techniques for europium doped yttria.
(d) Combustion methods.
(e) Synthesis of phosphors novel structures

Of these five processes, solution methods, aerosol spray and combustion methods can be scaled up for industrial production.

(a) Solution methods (suitable for industrial use).

Homogeneous precipitation of phosphors from solution makes it possible to introduce the dopant into the host lattice at the atomic level without needing high temperature diffusion. This often involves the initial preparation of a phosphor precursor lattice such as in the most versatile method for preparing $Y_2O_3:Eu^{3+}$ nanocrystalline phosphor, the urea precipitation method. This method has been pioneered for phosphor application by Matijevic et al [29] It is based on synthetic methods developed for the preparation of other metal oxides for a variety of uses (none phosphor uses) [29]. This method shows promise for industrial scaled up production. It provides more effective control over stoichiometry in the final product and also allows good control over phosphor morphology which, for example, has facilitated the generation of spherical particles that will pack well into small pixel areas for high definition display screens [30, 31]. In addition the size of the final phosphor particle can be controlled by

manipulating solution conditions in the precipitation process [32, 33, 34]. The technique which was been shown to be successful involves the addition of urea to metal salts in aqueous solution under conditions of pH and temperature which facilitate the decomposition of the urea and precipitation of metal hydroxycarbonates [31].

(b) Aerosol Spray methods (suitable for industrial use).

In the past ten years Aerosol Spray methods have become widely used in industry and at least one company has marketed Y_2O_3:Eu^{3+} nanoparticles and reported on their products. Spray pyrolysis is said to have a number of advantages in the preparation of metal oxide based phosphor particles for applications in displays and fluorescent lamps [35]. The phosphor particles prepared by this method have spherical morphologies uniform size and were non-aggregated [36-39]. However although these particles have sub-micron size and many attractions in new types of flat panel displays, they have the problem of poor luminescence characteristics due to many defects and scattering of emitted light. To overcome some of the problems several types of carbonate fluxes have been used to prepare Y_2O_3:Eu^{3+} nanoparticles. The fluxes tried were K_2CO_3 (Tm = 900 ºC), Na_2CO_3, Li_2CO_3, Li_2CO_3 + Na_2CO_3, and K_2CO_3 + Li_2CO_3 (Tm = 491 ºC), these are in the order of their melting temperatures. The amount of flux was fixed at 20 wt% based on the Y_2O_3:Eu^{3+} product [35]. The flux materials were dissolved in the spray solution. The added metal carbonate flux formed a precipitate on reaction with Y and Eu cations. To obtain non-aggregated particles they were directly prepared by ultrasonic spray pyrolysis at 1300 ºC without post treatment. The particles manifested good PL characteristics. The alkali metal carbonate fluxes are said to have eliminated the surface defects of particles by partial melting of particles at high temperature. The best performing flux was pure Li_2CO_3 [35].

A new synthetic method to prepare spherical phosphors for emissive screen applications was based on dissolving the phosphor precursor's europium chloride hexahydrate and yttrium nitrate in deionised water [40]. The resulting solutions were transformed into aerosols through a ceramic filter and passed through a furnace. Solid spherical particles of diameter between 500nm and 2 μm where formed at relatively low temperatures (900 ºC). The brightness of the particles is said to have been up to 130% compared to commercial powders. The phosphor particle size and surface shape could be easily controlled [40]. In a further paper by the same group it was found that the surface states of the cubic Y_2O_3:Eu^{3+}spherical particles influenced the photo-luminescent properties of the particles, whereas the cathode-luminescence (under 500V excitation) is less sensitive to the surface state [41]. That is the surface material act as quencher's sites for photo-luminescence but not for the higher energy cathodeluminescence.

(c) Chemical vapour synthesis, (CVS).

Nanocrystalline europium doped yttria particles have been synthesized using a chemical vapour technique.[42] $Y_2O_3:Eu^{3+}$ nanometre sized particles (NPs) were prepared in a tubular flow reactor by Chemical vapour synthesis using tris (tetramethyl-heptaanedionato) yttrium Y $(C_{11}H_{19}O_2)_3$ as the precursor for the host lattice and tris (tetramethyl-heptaanedionato) europium Eu $(C_{11}H_{19}O_2)_3$, for the europium doping. The powder was characterised using X-ray diffraction and transmission electron microscopy. The $Y_2O_3:Eu^{3+}$ nanoparticles (NPs) crystallised in the cubic structure with an average particle size of only 10 nm. Reflection, excitation, and emission spectra were reported. They showed that the nanoparticles manifested blue shifted absorption bands with respect to coarse grained material [42].$Y_2O_3:Eu^{3+}$. (NPs) were prepared in a tubular furnace by CVS [43]. This is the same method as Konrad et al [42].

(d) Combustion methods. General application

One of the problems with making such sub micrometer sized particles; is that during annealing of the precursor particles at high temperatures (often necessary for good crystallite quality and hence emission properties) the particles tend to sinter. One way partially to alleviate this problem is to synthesise the particles as rapidly as possible at a high temperature. A method that has been explored for this purpose is combustion synthesis using an organic fuel that is ignited when a crucible or other vessel containing the phosphor precursors and the fuel is placed in a furnace preheated to 900^0C. The fuel ignites and raises the temperature in the vessel very quickly. The residence time of the vessel in the furnace is controlled by the operator and removed at any desired time after ignition.

$Gd_2O_3:Eu^{3+}$ and $(Gd_2Y)_2O_3:Eu^{3+}$ nanocrystals were prepared by the glycine assisted combustion method using rare earth nitrate precursors [44]. The as-prepared products were found to be porous networks from the HTEM and isolated NPs could be observed after further annealing. From the luminescence spectra and XRD patterns, the prepared $Gd_2O_3:Eu^{3+}$ nanocrystals were found to be monoclinic. When the Y^{3+} was doped into the Gd_2O_3 to form the complex host, it was found that the structure changed from monoclinic to cubic at the point when Y^{3+}/Gd^{3+} was 0.3. The luminescent intensity of the $(Gd, Y)_2O_3:Eu^{3+}$ nanocrystals was higher than that of pure $Y_2O_3:Eu^{3+}$ or $Gd_2O_3:Eu^{3+}$ materials. It was found that along with the XRD pattern, the luminescence spectra was another powerful piece of evidence in deducing the crystal structure [44]. The effects of lithium doped yttria were investigated in an attempt to improve luminescent properties of nanosized $Y_2O_3:Eu^{3+}$ phosphors synthesized by the glycine combustion method using rare earth element and lithium nitrate salts as precursors [45]. $Lu_2O_3:Eu^{3+}$ luminescent NPs were prepared with Eu^{3+} concentrations of 1-13 (m/o) via a combustion route [46], although this is not a paper on $Y_2O_3:Eu^{3+}$ phosphors

it is covered here for comparison as the emission spectra is similar. The metal nitrates were mixed in a small amount of water with urea; the solution was dried at 130-150º C. The solid was then fired at 650 ºC where a vigorous reduction took place yielding the desired oxide. Their morphology was determined with TEM measurements. It was found that the sizes of nanocrystallites were around 10-13 nm. These powders were sintered at 1700 ºC into tablets whose grains were a few μm wide. Absorption and emission spectra of all materials were measured [47]. A series of Y^{3+} and Eu^{3+} complexes have been synthesised by taking benzoic acid, o-nitrobenzoic acid, m-nitrobenzoic acid, p-nitrobenzoic acid and 3, 5-dinitrobenzoic acid as ligands. Based upon the properties of the explosive decomposition of the complexes, a number of Y_2O_3:Eu^{3+} nano-crystals have been prepared by solid state thermo-decomposition [47]. TEM, X-ray diffraction analyses show that the Y_2O_3:Eu^{3+} nano-crystallites have spherical structure, and the average size of the crystals is within 40 to 60 nm. Introduction of Eu^{3+} has little effect upon the crystal structure of the oxides. Furthermore, change in the structure of the ligands of the complexes does not affect the morphology and sizes of the final products significantly. Compared with the products from the nitro substituted benzoic acid complexes. However, the Y_2O_3:Eu^{3+} nano-crystals obtained from benzoic acid complex aggregated severely. It is to be noted that annealing temperature has an obvious effect upon the sizes of the final products. The higher the temperature is, the larger the nano-crystals will be. Fluorescence measurements demonstrated clearly that all the Y_2O_3:Eu^{3+} nano-crystallites luminescence similarly. But, the luminescent property of the one prepared by the benzoic acid complex is the superior. Nanosized Y_2O_3:Eu^{3+} was synthesised [48] using a solution-combustion method very similar to that of Sun et al [24]. The samples were characterised by x-ray diffraction, extended x-ray absorption fine structure (EXAFS), and photoluminescence spectroscopy. The structure of nanocrystalline Y_2O_3:Eu^{3+} prepared by a combustion reaction was analyzed by XRD and high-resolution electron microscopy [49]. The combustion method involved dissolving the rare earth nitrates in glycine and distilled water. The water was evaporated off. The powder was then ignited. The reaction is given as: -

$$6M(NO_3)_3 + 10HCOOH + 18\ O_2 \rightarrow 3M_2O_3 + 20CO_2 + 5N_2 + 25H_2O \quad (M = Y^{3+}, Eu^{3+}),$$

Compared with large-scale particles, 5 nm Y_2O_3:Eu^{3+} particles presented as distorted crystallites with rough surfaces. Luminescent and absorption properties of these Y_2O_3:Eu^{3+} NPs showed remarkable effects related to their size. For those Y_2O_3:Eu^{3+} NPs that were smaller than 10 nm some new results were observed: (a) a red shift of the charge-transfer-state absorption; (b) new emission bands of Eu^{3+} in the $^5D_0 \rightarrow {}^7F_7$ region; (c) luminescent decay of the energy level $^5D_0$ of Eu^{3+} turning to a two-step exponential; and (d) a pronounced increase in the quenching concentration and much lower phonon density compared with those of the bulk material. All these phenomena were attributed to the effect of the softened lattice (caused by the loss of long range

order) and surface state of the nanomaterials. The latter was confirmed by stronger excitation by the host absorption after the surface modification [49]. Nanocrystalline Y_2O_3:Eu^{3+} (10% Eu doped) of cubic crystal structure with different particle size was prepared by a combustion reaction (metal nitrates and glycine) [50]. Sizes of particals studied range from several nanometres to 200 nm. High-resolution electron microscope images and extended X-ray absorption fine structure (EXAFS) analysis of the nanoscale samples indicated both the presence of crystalline particles showing evidence of many defects and the co-existence of an amorphous phase. The preparation, optical properties and application potential of some nanomaterials based on Y_2O_3:Eu^{3+},Tb^{3+},Er^{3+},Yb^{3+} have been reported [51]. Y_2O_3 nanophosphors were prepared by the combustion method using different dopant concentrations. The Y_2O_3 nanophosphors precursors were the basic carbonates. The size of Y_2O_3:Eu^{3+} was from 4.4 to 72.2nm depending on the conditions used. The luminescent spectra, up-conversion and lifetimes were measured and compared. The influence of the technological conditions on the luminescent properties was investigated in detail. The energy transfer process was studied using the luminescent spectra, the lifetimes of the emission bands and their temperature dependence for the samples with rare-earth concentrations of 5mol%, the relative concentration needed between Eu and Tb is 8:2 for energy transfer to take place from Tb to Eu [51].

(e) Synthesis of novel structures.

Y_2O_3: Eu^{3+} nanotubes where fabricated by a surfactant assembly mechanism. The surfactant (sodium dodecasulfonate) was dissolved together with yttrium and europium chlorides (latter salts in mole ratio of 98:2), the mixture was stirred till clear and urea was added to adjust the *p*H till precipitation occurred. The resulting solids were then fired in stages. The resulting tubular structures were characterized by transmission electron microscopy. Eu nanotubes where synthesized in the same way [52]. An unusual Eu^{3+}-doped-yttria-silica nanocomposite has been synthesized using a deposition-precipitation technique. Silica was impregnated with an aqueous solution containing the rare earth nitrates a few drops of HNO_3 and urea. The impregnated solid was removed by centrifugation, dried and fired at 1000 ºC for 1h.Y_2O_3:Eu^{3+} nanocrystalline particles with a mean size of 12 nm, dispersed in an amorphous silica matrix, were characterised using XRD in a sample treated at 900 ºC. The nanoparticles were coated with an amorphous layer visible in the high resolution TEM micrographs. The authors suggest that this amorphous layer is likely to interact with the silica matrix through Si-O-Y bonds, which is consistent with Si-29 NMR MAS results. In contrast the nanocomposite treated at 1000 ºC was found to partially evolve to give an alpha-$Y_2Si_2O_7$ crystalline phase. The luminescence spectra of the nanocomposites are taken as evidence that the sites in which the Eu^{3+} ions are accommodated are disordered. The authors also report that the decay times of the Eu^{3+} ions $^5D_0$ emissions are rather long in the nanocomposites indicating that multiphonon relaxation is not effective in

quenching the luminescence. They conclude that the reduced coupling to OH vibrations in the materials could be ascribed to the presence of the amorphous layer coating the nanoparticles and effectively shielding the Eu^{3+} ion from the silanol groups [53].Y_2O_3:Eu^{3+} (NPs) inside porous optical inert materials such as MCM-41 (a silica based mesopororous molecular sieve), porous silica, and porous alumina were synthesized and structurally and electronically characterized. Typically the precursors of the Y_2O_3:Eu^{3+} (NPs) $Y(C_{11}H_{19}O_2)_3$ and $Eu(C_{11}H_{19}O_2)_3$ are dissolved in a suitable solvent such as CH_3Cl or ethanol. The substrate is dipped into the solution for a period of time then dried and fired in a tube furnace under flowing oxygen for the europium doping [54]. Y_2O_3:Eu^{3+} filled porous MCM-41, porous silica, and porous alumina with pore size between 2.7 to 80nm were prepared and structurally and electronically characterized [54].

2.6 Combustion methods employed for this thesis

The work in this thesis builds on the combustion methods pioneered in 1999 in the paper by Ireland et al [55]. They reported a combustion synthesis to prepare nanometer sized crystallites of cubic Y_2O_3:Eu^{3+} using a precursor containing a sacrificial long chain alkylammonium cation (the fuel). Using this method it proved possible to produce cubic Y_2O_3:Eu^{3+} crystallites in the 50-70nm size range. The presence of CO_2 bands in the infra red spectra of the cubic Y_2O_3:Eu^{3+} crystallites were also reported. These bands are identical in position to those found in [(Y, Eu)$OHCO_3.H_2O$], and are explained as arising from the spontaneous reaction of the surface of the nanometer sized particles of cubic Y_2O_3:Eu^{3+} with atmospheric CO_2 and water vapour. This indicates that nanometer sized particles of cubic Y_2O_3:Eu^{3+} are thermodynamically unstable in the atmosphere and must be protected against such back reactions. This could be done with surface coatings. This was the first report of the facile self-assembly of the red emitting phosphor yttrium oxide europium (Y_2O_3:Eu^{3+}) from solution using a sacrificial micellar phase [55]. The micellar phase was assembled using the alkylammonium chloride salt ($C_{12}H_{25}NH_3Cl$) in an ethanolic solution. The resulting fine powder had smaller particles, ranging in size from 0.1 to 1.0 μm, than the commercial cubic Y_2O_3:Eu^{3+} phosphor [55]. One of the problems with making such sub micrometer sized particles is that during annealing of the precursor particles at high temperatures (often necessary for good crystallite quality and hence emission properties) the particles tend to sinter. A more sophisticated way to control the rate of crystallization of the phosphor particles would be to vary the ratio of phosphor precursor to fuel. In theory the presence of more fuel around the phosphor precursor should facilitate/influence the combustion process and possibly lead to more crystalline products. In the work on which this thesis is based longer and shorter chain hydrochlorides alkylammonium are used as fuel and the effect of varying the ratio of these to the Y_2O_3:Eu^{3+} precursor on the cathodoluminescence (CL) and

photoluminescence (PL) properties of the resulting phosphors is reported herein.

2.7 Micelles [19]

A **micelle** can be formed when one or more of a variety of molecules such as soaps and detergents are added to water [19]. The molecules making up the micelles may be a fatty acids, a salt of a fatty acid (soap), phospholipids, or other similar molecules. The molecule must have a strongly polar "head" and a non-polar hydrocarbon chain "tail". When this type of molecule is added to water, the non-polar tails of the molecules clump into the centre of a ball like structure called a micelle, because they are hydrophobic or "water hating". The polar head of the molecule presents itself for interaction with the water molecules on the outside of the micelle [19].

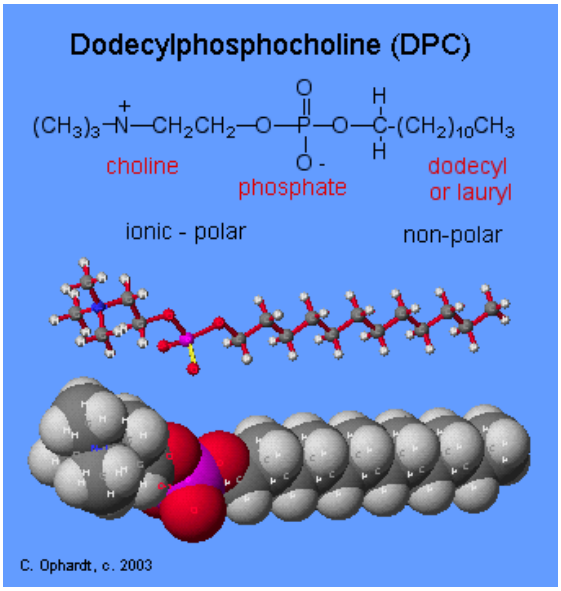

Figure 2.5 Dodecylphosphocholine [57].

To understand the structures of a micelle see Figure 2.5. It is useful to consider the structure of dodecylphosphocholine (DPC). The phosphoric acid group has ester bonds between (1) choline, $(CH_3)_3N\ (CH_2)_2OH$, and (2) dodecyl (or lauryl) alcohol, $CH_3(CH_2)_{11}OH$. The choline, which contains a quaternary amine with a positive charge, and the phosphate are ionic and polar. The dodecyl part is the non-polar hydrocarbon chain.

Structure of a Micelle [57]: The theoretical model shows 54 molecules of dodecylphosphocholine (DPC) and about 1200 H_2O molecules. Each lipid has a polar

head group (phosphocholine) and a hydrophobic tail (dodecyl = C_{12}).

Figure **2.6** presents a micelle cross section The gray spheres on the interior represent the long hydrocarbon chains of the dodecyl groups which are massed together because they are non-polar. The polar head groups of the phosphate are shown as red and orange spheres. The amine nitrogen is shown in blue surrounded by the gray methyl groups. The water molecules are represented as red and white spheres surrounding the outside of the micelle and they penetrate all of the spaces in the head group region. The hydrophobic tails are shown (as space fill). H_2O is excluded from this entire interior volume. The hydrocarbon chains vary in their individual conformations (e.g. Trans/gauche configuration at each carbon-carbon bond), but adapt so as to fill all of the interior space.

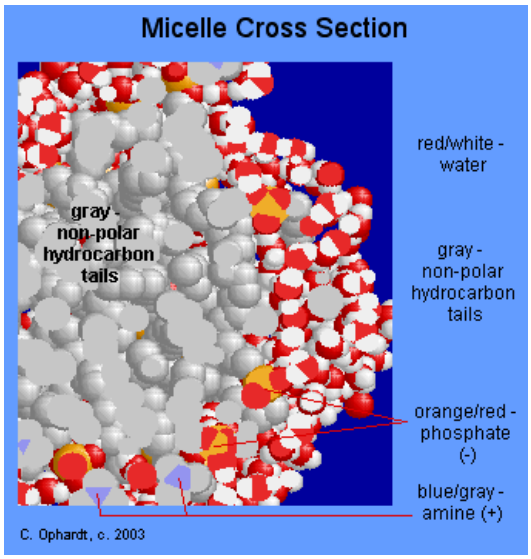

Figure 2.6 Micelle cross section [57].With cations and anions on the outside.

Single DPC and Surrounding Molecules: [56,57,58]

The close-up of a DPC molecule (space fill) in the micelle is shown in Figure 2.7. Other DPC neighbour molecules are shown in thick wire form. The rest of the micelle is white sticks. The DPC is in contact with 10-15 H_2Os (red/white spheres) that make favourable H-bond or ion-dipole interactions (<3.5 Å). Neighbouring DPC molecules that are within 4.0 Å of each DPC are thicker sticks; the atoms on each that can make favourable van der Waals interactions are colour yellow. This is in contrast to protein crystal structures where interior atoms are relatively fixed. The micelle interior is highly dynamic, i.e. each lipid may have 4-8 contacting neighbour lipids at any instant, but these partners change several times every nanosecond on average.

Chapter 2 Y, Eu, Y_2O_3, Y_2O_3: Eu and Micelles Material used for this thesis.

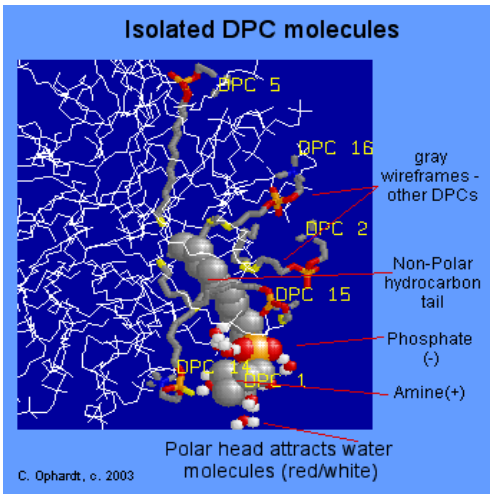

Figure 2.7 Isolated DPC molecules [57].

Cationic Detergents: [56] Another class of detergents have a positive ionic charge and are called "cationic" detergents. In addition to being good cleansing agents, they also possess a germicidal property which makes them useful in hospitals. Most of these detergents are derivatives of ammonia. A cationic detergent is most likely to be found in a shampoo or clothes "rinse". The purpose is to neutralize the static electrical charges from residual anionic (negative ions) detergent molecules. Since the negative charges repel each other, the positive cationic detergent neutralizes this charge [56].

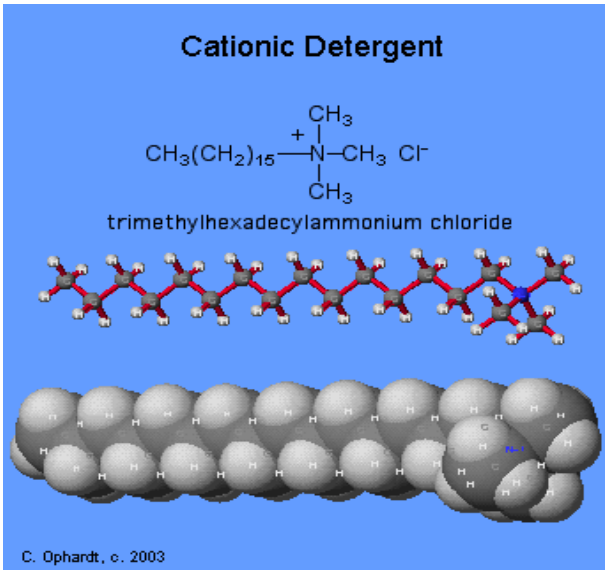

Figure 2.8 Cationic Detergents [57].

In this thesis all of the micelles prepared were of the positively charged variety. The positive charge resides on the alkyl ammonium nitrogen.

References

[1] S. Cotton. "Scandium, Yttrium & the Lanthanides: Inorganic & Coordination Chemistry". Encyclopedia of Inorganic Chemistry.03-15-2006.

[2] R. Cooley, Y. Don, M. Stone and W. Hosmer. "Europium Salts". Inorganic Syntheses 2, 69–73, 1946.

[3] P.Belli. "Search for α decay of natural europium". Nuclear Physics A 789, 15–29, 2007.

[4] B.Johansson and A. Rosengren. "Generalized phase diagram for the rare-earth elements". "(Calculations and correlations of bulk properties)". Physical Review B 11 (8), 2836–2857, 1975.

[5] P. H.Klein and W. J. Croft. "Thermal conductivity, Diffusivity, and Expansion of Y_2O_3, $Y_3Al_5O_{12}$, and LaF_3 in the Range 77-300 K". Journal. Appl. Phys. 38 (4), 1602-1603, 1967.

[6] Y.Nian Xu, Z.Quan Gu and W.Y.Ching. "Electronic, structural, and optical properties of crystalline yttria". Journal Phys. Rev. B56 (23), 1493–1500, 1997.

[7] A. Parker. "Colour in Burgess Shale animals and the effect of light on Evolution in the Cambrian". 99-100, 1998.

[8] M.Xu." Electric_field Monte Carlo simulation of polarized light Propagation in turbid media". OPEX-12-26-6530, 2004.

[9] J.Nam."Making 1μm spherical phosphor powders of Y_2O_3:Eu^{3+}". Journal Semiconductor Materials and Devices.25-29, 2003.

[10] T. Ireland and J.Silver."Facile self-assembly of yttrium oxide europium phosphor from Solution using a sacrificial Micellar phase". Journal of the Electrochemical Society. 2, 1.52-54, 1999.

[11] R. Martinez. "Effect of EDTA on controlling nucleation And morphology in the synthesis of ultrafine Y_2O_3 : Eu phosphors" Journal of the Electrochemical Society. 3, 9.446-449, 2000.

[12] R. Martinez."A synthetic method for the production of a range of

Particle sizes for Y_2O_3 : Eu phosphors using a copolymer microgel of NIPAM and AMPS". Journal of the Electrochemical Society. 149. 253-5, 2002.

[13] J.Silver. "Upconversion Luminescent emission from europium-doped Yttrium oxide under at 632.8 nm light Excitation". Journal of Physical Chemistry. B, 105. 9107-9112, 2001.

[14] R.Withall and J.Silver."Photonic phosphors based on cubic Y_2O_3:Tb^{3+} In filled into a synthetic opal lattice". E.J.abstract.1464-1468, 2003.

[15] J.Silver."Fine control of the dopant level in cubic Y_2O_3 : Eu^{3+} Phosphors". Journal of the Electrochemical Society.151, 66-68, 2004.

[16] Y.Chen."Luminescent properties of blue-emitting long afterglow phosphors Sr-Ca_2MgSiO_7 : Eu^{2+}". Journal of Luminescence.118,70-78, 2006.

[17] G.Novak." Chelated Rare Earth Ions". Optical Spectroscopy. II, 151-158, 2006.

[18] A.Camenzind, "Cubic or Monoclinic Y_2O_3:Eu^{3+} Nanoparticles by One Step Flame Spray Pyrolysis'. Journal of Luminescence. 119,66-76, 2006.

[19] J.S. Yoo, J.D. Lee and J. Appl. "Making up micelles from fatty acids". Journal Phys. 81, 6-8, 1997.

[20] G.H.Dieke. "Spectra and energy levels of rare earth ions in crystals". Interscience publishers. New York 1968.

[21] J.Silver. J. A. McCleverty." Metal Compounds as Phosphors in comprehensive coordination Chemistry II. The Synthesis, Reactions, Properties and Applications of Coordination Compounds". Pergamon Press, New York. 9.15, 689-717, 2003.

[22] R.N.Bhargava, D. Gallagher, X.Hong and A.Nurminkko. "Nanometre sized particles of Y_2O_3:Eu^{3+}". Journal Phys.72, 416-419, 1994.

[23] R.N.Bhargava, D. Gallagher and T.J. Welker. "Luminescence efficiency of the doped phosphors". Journal Lumines.60&61, 275-280, 1994.

[24] T.A. Kennedy, E.R. Glaser, P.B. Klien and R.N. Bhargava. "Luminescent emission of ZnS:Mn^{2+} ". Journal Phys. B 52,143-156, 1995.

[25] R.N.Bhargava, D. Gallagher, W.E. Heady and J.M. Racz. "Phosphor lifetime shortening". Journal Mater. Res 10, 870-878, 1995.

[26] R.N. Bhargava."Quantum confined effects in nano-particle Zinc sulphide Based phosphors". Journal Lumens. 70, 85-94, 1996.

[27] E.Goldburt and R.N. Bhargava. "Preparation and characterization of rare earth activators". Journal Electrochem Soc. Proc. 95-25, 368, 1996.

[28] M.A.Hines and P.Guyot-Sionnest. "Nanocrystalline phosphors Have more perfect lattices". Journal Phys. Chem.100, 468-471, 1996.

[29] Y.S.Her, E. Matijevic and W.R. Wilcox. "Urea precipitation method for preparing Y_2O_3:Eu^{3+} nanocrystalline phosphor". Journal Mater. Res 7, 2269-2272, 1992.

[30] Y.D.Jiang, Z.L. Wang, F. Zhang, H.G. Paics and C.J. Summers."Spherical particles for high definition display screens". Journal Mater. Res 13, 2950-2955, 1998.

[31] A.Vecht, X. Jing, C. Gibbons, T. Ireland, D. Davies and P. Marsh. "Field emission display". Newport.SID98.Digest 29, 1043-1047, 1998.

[32] M.I .Martinez-Rubio, T.G. Ireland, G. Fern, M.J. Snowden and J. Silver. " Novel Method for the Synthesis of spherical particles of the Y_2O_3: Eu Phosphor Using a Copolymer Microgel of Nipam and Acrylic Acid". Langmuir 17, 7145-7149, 2001.

[33] M.I .Martinez-Rubio, T.G. Ireland, G. Fern, M.J. Snowden and J. Silver. "A Synthetic Method for the Production of a range of particle sizes for Y_2O_3: Eu Phosphors". Journal Electrochem Soc. 149, H53-H58, 2002.

[34] J. Silver, M.I. Martinez-Rubio, S. Gebretensae, G.R. Fern, M.J. Snowden and R. Withnall." Novel Synthetic Method for the Controlled Production of Particle Desired Size for Y_2O_3: Eu Phosphor using Copolymer Micro gels of NIPAM". SID Digest. 393-396, 2002.

[35] Y.C.Kang, S.B. Park, H.S. Roh and D.J. Seo."The effect of metal carbonate fluxes on the crystallinity morphology and photoluminescence characteristics of Y_2O_3: Eu phosphor in spray pyrolysis". Journal Mat Sci. Lett 19, 1225-1227, 2000.

[36] Y.C.Kang, S.B. Park, I.W. Lenggoro and K. Okuyama. ." Metal carbonate Fluxes controls the crystallinity morphology of Y_2O_3: Eu phosphor in Spray pyrolysis". Journal Phys. Chem. Solids, 60(3), 379-380, 1999.

[37] Y.C.Kang, S.B. Park, I.W. Lenggoro and K. Okuyama." Y_2O_3: Eu phosphor Photoluminescence characteristics in spray pyrolysis". Journal Electrochem. Soc 146(3), 1226- 1227, 1999.

[38] Y.C.Kang, S.B. Park, I.W. Lenggoro and K. Okuyama."Luminescent properties of phosphor powder Y_2O_3: Eu." Journal Mat Sci. Lett 19,778- 779, 1999.

[39] Y.C.Kang, S.B. Park, I.W. Lenggoro and K. Okuyama." Spray pyrolysis Production method for Y_2O_3: Eu phosphor for display screens". Journal Mater. Res 14(6), 2611- 2615, 1999.

[40] S. H. Cho, J. S. Yoo and J.D. Lee." A new synthetic method to prepare spherical phosphors for emissive screen applications." Journal Electrochem. Soc.145 (3), 1017-1019, 1998.

[41] J.S.Yoo, C.J. Summers, G.Y.Hong, K.Won and S.H. Optical." Characteristics of spherical Yttrium Oxide Doped European prepared by Ultrasonic Aerosol Pyrolysis. 5th International Conference on the Science and Technology of Display Phosphors, San Diego, USA, 8-10th, November. 187-190, 1999.

[42] A.Konrad, T. Fries, A. Gahn, F.Kummer, U. Herr, R. Tidecks and K. Samwer."Chemical vapour synthesis and luminescence properties of nanocrystalline cubic Y_2O_3 : Eu. Journal Appl. Phys 86, (6). 3129-3133, 1999.

[43] T.Igarashi, M. Ihara, T. Kusunoki, K. Ohno, K. Isobe and T. Senna. " Relationship between optical properties and crystallinity of nanometer Y_2O_3 : Eu phosphor**."** Journal Appl. Phys. Lett. 76, (12), 1549-1551, 2000.

[44] LD. Sun, J.Yao, C.G. Liu, C.S. Liao and C.H.Yan. "Rare earth activated nanosized oxide phosphors, synthesis and optical properties." Journal. Lumines 87-9, 447-450, 2000.

[45] LD.Sun, C.Qian, CS. Liao, XL. Wang and CH. Yan." Luminescent proper-ties of Li+ doped nanosized Y_2O_3 : Eu ." Journal Solid State Commune. 119(6), 393-396, 2001.

[46] PK. Sharma, MH. Jilavi, VK. Varadan and H.Schmidt." Influence of initial pH on the particle size and fluorescence properties of the nano scale Eu (III) doped yttria." Journal Phys.Chem Solids 63(1), 171-177, 2002.

[47] GL.Gao,Y.Fang, MZ.Wang and TD.Hu."Properties of Y_2O_3 : Eu Nano-crystals prepared by thermo- decomposition of benzoic acid and nitro benzoic acid complexes".Phys Chem. Sin.18(5), 399-403, 2002.

[48] ZM.Qi, CS.Shi, WW.Zhang, WP.Zhang and TD.Hu."Local structure and luminescence of nanocrystalline Y_2O_3 : Eu." Journal Appl. Phys. Lett 81(15), 2857-2859, 2002.

[49] WW.Zhang, PB.Xie, M.Yin, HT.Chen, L. Jing and YS. Lou. "Optical properties of nanocrystalline Y_2O_3 : Eu depending on its odd structure." Journal Colloid Interface Sci. 262(2), 588-593, 2003.

[50] WW.Zhang, X.Mei, Z.Wei-Ping, Y.Min, ZM.Qi, SD.Xia and C.Garapon. "Site-selective spectra and time-resolved spectra of nanocrystalline Y_2O_3 :Eu." Chem. phys. Lett. 376 (3-4), 318-323, 2003.

[51] T.K. Minh, L.Q. Vu, N. Huong, C. Barthou and W. Strek, "Nanomaterials containing rare-earth ions Tb, Eu, Er and Yb: Preparation, optical properties and application potential". Journal Lumines. 102,391-394, 2003.

[52] CF. Qin, WP. Zhang, JS. Qin and GS. Zhao. "Site selective spectroscopy of surfactant-assembled Y_2O_3 : Eu nanotubes." Journal of Rare Earth.21 (6), 601-604, 2003.

[53] C.Casu, M. Mainas, M. Musinu, A.Piccaluga, G .Polizzi and S.Speghini "Synthesis, characterisation and optical properties of nanocrystalline Y_2O_3:Eu^{3+} Dispersed in a silica matrix by a deposition-precipitation method Cannas." Journal. Mater. Chem. 13 (12), 3079-3084, 2003.

[54] R, Kennedy, M.Von Seggem, H.Winkler, H. Kolbe, M. Fischer, R.A. Xaomao and Li. Benker."Luminescence properties of nanocrystalline Y_2O_3:Eu^{3+} in different host materials." Journal. Appl. Phys. 89, (3), 1679-1686, 2001.

[55] T. Ireland, J.Silver, C. Gibbons and A.Vecht. ."Facile self-assembly of Y_2O_3 : Eu phosphor from solution using a sacrificial micellar phase". Journal of Electrochem and Solid State. Lett 2, 50- 51, 1999.

[56] W. McClure."Micellar structure and lipid chain relaxation." Solid State. Phys. 13, 2695-701, 1980.

[57] D. Van der Spoel, H.J.C. Berenson and D. P. Tieleman. "Molecular dynamics simulations of dodecyl phosphocholine micelles at three Different aggregate sizes".J. Phys. Chem. B 104, 6380-6388, 2000.

[58] D.P. Tieleman. "Micelle structures details". J. Phys. Chem. B 104, 6378-6380, 2000.

Chapter Three

Experimental Techniques

3.0 Introduction

A number of different characterisation/analytical techniques were used in the work described in this thesis and are introduced in this chapter. These were:-

1. Scanning electron microscopy (SEM).
2. X-Ray powder diffraction (XRPD).
3. Direct current Cathodoluminescence.
4. Bentham spectrometer UV- visible spectroscopy.
5. ATR-FTIR infra-red spectroscopy.
6. Raman spectroscopy.
7. Flurorolog-3 UV-visible spectroscopy.
8. Thermal Methods of characterisation. A. SDT-Q500 (TGA).B. SDT-Q600.

Each of these techniques will now be briefly described along with how they were used in this work.

3.1 Scanning electron microscope (SEM)

Scanning electron microscopy was used to investigate the morphology and particle sizes of the Y_2O_3: Eu products. The basic function of an SEM [1, 2] is to produce an image of three dimensional appearances derived from the action of an electron beam scanning across the surface of a specimen [1]. The technique revealed a wide range of interesting structures and nano-sized structures in the samples annealed at 650 and 900°C. Over 200 images were obtained.

The instrument used shown in Figure 3.1 is a SEM Zeiss Supra 35 VP [3]. This was used to analyse the samples and the average particle size of each sample was obtained. The Zeiss Supra 35 VP SEM has a resolution down to 1.0 nm. Field emission scanning electron microscopy (FESEM) was used to study the microstructure of the samples using this instrument (see Figure 3.1).The powder samples were mounted on carbon tabs attached to aluminium pin stubs. The stub was then coated in gold using a sputter coater to cover the sample with a thin conducting layer of gold. The following technique was used: an aluminium stub covered with double sided carbon black conducting tape was pressed into the phosphor powder sample that was to be measured, any excess of material was removed by gently tapping the stub against the hard surface of the sample box. The stub was then coated in gold using a sputter coater before being placed into the SEM chamber. Only six samples at a time were placed in the SEM chamber. The sample material sizes were measured using the photographs of particles. The sizes of particles in the photographs were determined using an appropriate scale once the magnification factors had been established. The SEM chamber was evacuated to vacuum conditions to a pressure below 10^{-4} mbar the

images were observed on a screen and printed out onto individual micrographs. Various points on the sample were taken to get an accurate assessment of the sample. For each of the 42 samples 4 or 5 pictures were taken, at magnifications of 1k, 6k, 30k and 50k. The SEM - Zeiss Supra 35 VP features [3] are-(1) A unique ZEISS GEMINI FESEM column which delivers nano scale high resolution imaging over the entire voltage range; (2) SEM capable of delivering high quality imaging solutions for the many demanding applications in the field of nano technology; (3) that the GEMINI FESEM column has an extremely low magnetic field outside the objective lens enabling investigation of magnetic materials and devices (data storage, FE-RAM, steel, alloys and magnets); (4) GEMINI® column provides the best resolution values currently available: 1 nm/15 kV, 1.7 nm/1 kV and 4 nm/0.1 kV with high flexibility, a specimen current of 20 nA and a current stability of 0.2%/h. The Zeiss Supra 35VP is an ultra-high performance field emission scanning electron microscope, with both high-vacuum and variable operating pressure (VP) capability. The field emission source and gemini column in this instrument result in a very high resolution capability, and this is complemented by the variable pressure system, which enables imaging and analysis of samples in their natural state, without artefacts' induced by surface charging.

Figure 3.1 SEM the Zeiss Supra 35 VP [3].

3.2 X – RAY POWDER DIFFRACTION (XRPD)

XRPD can be used for qualitative and quantitative crystalline phase identification, for structure determination and refinement, for microstructure determination.

X-ray diffraction (XRD) [4, 5] is a versatile, non-destructive technique that reveals detailed information about the chemical composition and crystallographic structure of natural and manufactured materials. It utilises knowledge of a number of physical properties:-

1) A crystal lattice is a regular three-dimensional distribution (cubic, rhombic, etc) of atoms or ions in space. These are arranged so that they form a series of parallel planes separated from one another by a distance *d*, which varies according to the nature of the material. For any crystal, planes exist in a number of different orientations - each with its own specific *d*-spacing.
2) Bragg's Law: - By varying the angle theta, the Bragg's Law conditions are satisfied by different *d*-spacing in polycrystalline materials. Plotting the angular positions and intensities of the resultant diffracted peaks of radiation produces a pattern which is characteristic of the sample. Where a mixture of different phases is present, the resultant Diffractogram is formed by addition of the individual patterns.
3) Constructive interference, when a monochromatic X-ray beam with wavelength lambda is projected onto a crystalline material at an angle theta(θ), diffraction occurs only when the distance travelled by the rays reflected from successive planes differs by a complete number *n* of wavelengths.

X-ray powder diffraction studies were used to identify the phases present in the combusted products synthesized in this work, their degree of disorder/order and their crystallite sizes [6]. Diffractograms were collected using the Y_2O_3:Eu powders and other product in a conventional holder, on aluminium stubs and on a silicon substrate, a total of 108 Diffractograms were collected. XRPD was carried out on 42 samples. The crystalline phases of the products [6] were determined by X-ray powder diffraction (XRPD) using a Bruker D8 Advance X-ray powder diffractometer (AXRPD) fitted with a nickel-filtered copper source and a Lynx-Eye™ silicon strip detector (see Figures 3.2 and 3.3). Data were recorded from X-ray intensity as a function of Bragg angle θ to 2θ and 5 to 100° at 293 K. The diffractometer was previously calibrated using an aluminium oxide line position standard from Bruker and LaB_6 NIST SRM 660a line profile standard [7]. The emission of the nickel filtered Cu source and hence the instrumental line broadening was determined by fitting the NIST standard using Bruker Topas

version 3 [8]. Phases were indentified from the XRD patterns by peak search matching using the ICCD PDF-2 data files. The identifiable phases were refined using Bruker Topas version 3 [8].

The samples were put in a holder which was placed into the diffractometer, which in turn was linked to a computer which had an internal reference data base for comparing samples. Prints were taken for comparison and in some cases ASCI files, so that the spectra could be overlapped and compared. In each analysis six samples at a time were put into the AXRPD and each sample were bombard by X-ray at angles of 5 to 100 degrees for 35 minutes. The AXRPD was connected to the computer and results were obtained for each sample in form of scan. Every 4 h a further set of 6 samples was inserted into the AXRPD till the entire 42 sample had been analysed.

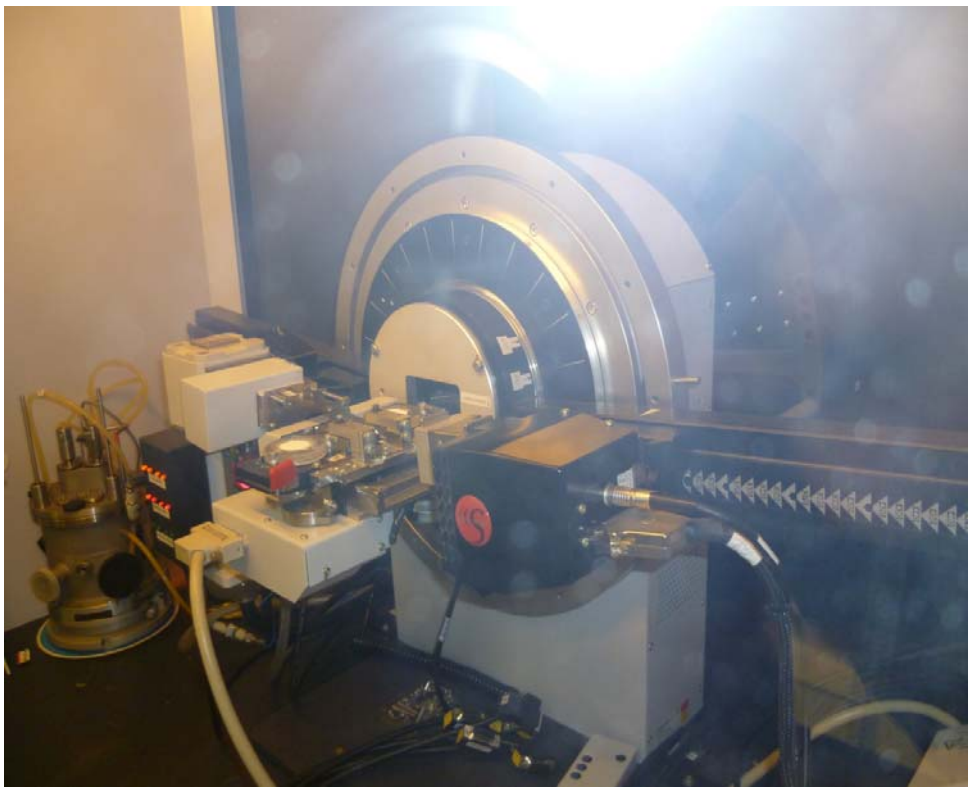

Figure 3.2 AXRPD

Figure 3.3 XRPD

3.3 Direct current Cathodoluminescence measurements [9-13].

Cathodoluminescent light intensity measurements were measured in a low-voltage electron gun vacuum chamber at voltages between 1000 to 5000V over a range of e-beam currents. The light intensity of these samples was in some cases comparable with much larger particles that have been produced as bulk materials. Luminance measurements were carried out using Jeti Spectroradiometer Specbos 1200 and Specbos 1200 Spectroradiometer for fast data gathering of emission spectrum, and luminance. The Spectroradiometer Specbos 1200 photometer is a self calibrating instrument [14], with automatic calibration based on every twenty minutes or when temperature changes by a half of a degree since the last calibration. The Luminance of the sample was calculated in metric-Candelas per square meter. For consistent results for the above samples the same measuring procedure was adopted for each set of measurements. The electron beam was focused so that the beam spot and the monitoring spot on the photometer covered

about 100% of the emission area. To keep the measuring angle consistent Luminescence was measured at the centre of each phosphor sample. One hour was allowed each day as a warm up period for the electron gun power supply to reduce the beam current drift .The emission current was regularly checked to ensure that it remained at desired position of 50μA. Each sample on its aluminium stub (-see preparation method below) was carefully aligned to ensure that the beam was in the centre of the phosphor sample and then a complete measurement set was taken before moving onto the next sample. The low voltage cathodoluminescent equipment used is presented in Figure 3.4. The low voltage equipment is composed of a cylindrical stainless steel Vacuum chamber, which has six ports at equal distances around its circumference, only four of these ports were used .The first port contained the electron gun, the second port adjacent was used for viewing the sample, the third port was the pressure gauge measuring system and the fourth port was used for electrical connections. The two remaining ports were sealed and blacked out to avoid any light entering the system (see Figures 3.4 & 3.5). The viewing port is positioned next to the electron gun port to allow reflectance measurements to be collected from each sample; the other ports are positioned to collect transmittance measurements at an angle of 180°. 42 samples were measured Six Y_2O_3: EU-C16 phosphor coated aluminium sample stubs were mounted around a central manipulator. Six samples each time were mounted on the central arm which had complete rotational freedom and limited vertical movement of the samples in the chamber. It can attain a vacuum of 1.33x 10^{-3} Pa and deliver an electron beam at energy of 5 kV. This allows the sample being stubbed to be moved in the direction of the electron beam. To maintain the vacuum in the chamber, two pumps were used constantly so that a suitable vacuum was obtained in the chamber the first pump used to maintain a pressure of 1.33x10^{-2} Pa in the chamber, and this way monitored by a Pirani gauge. The second pump used was a turbo-molecular pump capable of producing a pressure of 1.33μ Pa this was monitored by an ionisation gauge. All low voltage measurements were taken at a pressure below 1.33m Pa. The Cl measurement data and spectra were undertaken and using a high-vacuum chamber with a Kimball Physics Inc. (Walton, USA), model EFG-7 Flood electron gun with its matching EGPS-7 Power supply. A measurement was obtained over an excitation range from 1000 to 5000 Volts and an emission current of 8.5 μA .The Electron beam was Defocused for Spectra collection and tightly focused for light output measurements. The Cl luminance measurements were obtained by means of a Jeti spectroradiometer (Specbos 1200, Jeti Technische Instruments GmbH and Jena, Germany) [14]. The phosphor sample screens were excited with electron beam energies from 1000 to 5000V, and emission currents from 1.1 to 9.8μA/cm^2, with an electron beam spot size of 9.0mm for defocused measurements and 1.41 mm for the focussed measurements. For the above samples Cl emission and excitation spectra were collected using the Bentham system previously described except that the fibre optic bundle (Bentham TEL-600 fiberoptic connected to monochromator) was disconnected from the in-built sealed chamber and attached to a telescope (TEL 301D). The

Cathodoluminescence spectra were collected, with a TFL301 photometer telescope, with an aperture mirror viewing system to focus precisely on the area of the measurement. The photometer telescope collects the light output through the front viewing port of the low-voltage chamber which light passes to the M300 monochromator through the integral flexible fiberoptic for the CL luminance measurements and spectra of the prepared samples phosphor screens were prepared in the following manner. After cleaning the aluminium pin stubs in an ultrasonic bath containing ethanol and drying in an oven at a temperature of 100°C, they were weighed. A stub was then placed in an electrochemical cell containing an ultrasonically dispersed solution of the phosphor powder (0.5g), in a solution of magnesium nitrate (0.075g/L) in isopropanol (50mL). The stub was positioned so that its flat surface was forming a meniscus with the surface of the phosphor/electrolyte solution and also acting as an electrode, the counter electrode was a strip of magnesium ribbon. A field of 300V was applied to facilitate the coating of the stub by electrode position. This procedure was repeated till all the stubs were coated with approximately 3.0mg (±0.10mg) of phosphor. After drying the stubs at 100°C they were introduced into the vacuum chamber for Cl measurements.

For the 42 samples, Cl measurements were used to measure and obtain spectra. Cathodoluminescence from 1kV-5kV (low voltage) Cl apparatus which used for testing phosphor and used for other applications. The first experiment used a defocused beam, carried out through a 9mm hole using a spectroradiometer 1200. The experiment then continued by setting the equipment at values from 1000 to 5000V using currents from 10uA through to 50μA. Thus for 1000Vcurrents of 10, 20, 30, 40 and 50 μA were used and Cl measurements were recorded using the spectroradiometer 1200 which is connected to the computer. The results were recorded using the Jeti program. Using the results a graph was plotted, in total 42 graphs has been produced. To avoid burning the sample defocused measurements were always carried out first before focused measurements. The second experiment (focused beam) utilised a 1.41mm hole using the spectroradiometer 1200. The experiments than continued by setting the equipment from 1kV through to 5kV.

Using the results 42 graphs were produced. The third set of experiments used a defocused beam followed by a focused beam to produce spectra rather than measurements. Again the same conditions were used as laid out above. For example for a series of experiments the method was to start from 1000V Vs 10μA and then Vs 50μA, then progressively to 5000V. 4 sets of results was obtained 2 defocused and 2 focused for each sample and in total 168 spectra of intensity in arbitrary units wavelength nm were produced.

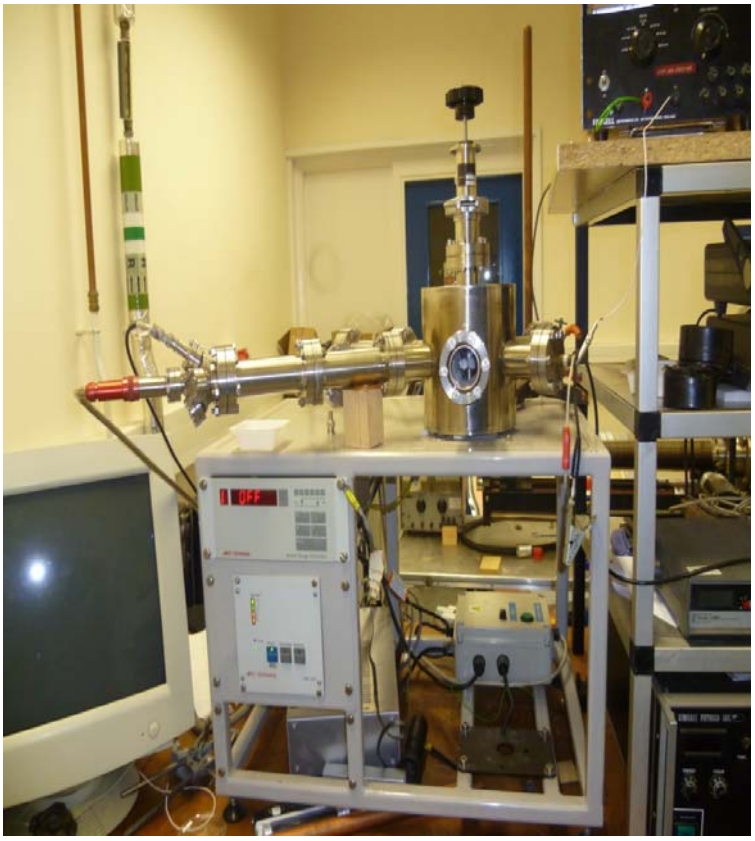

Figure 3.4- Direct current cathodoluminescent measurements.

Figure 3.5- Direct current cathodoluminescent measurements

3.4 Bentham spectrometer

The Bentham monochrome apparatus (see Figure-3.6 and 3.7) can be used for measuring the excitation and emission spectra of materials across the UV, Visible and near IR spectral regions. Also it is possible to calculate and measure the luminous efficiency for the produced samples.

The PL excitation and emission spectra were obtained using a Bentham power (Reading, UK) M300 programmable grating monochromator photometer system with computer controlled wavelength scanning and intensity data collection, using in the visible region a 1800 lines/mm grating. The stepping motor and sine drive allows wavelength scanning to be completely controlled from a remote stepping drive unit (SMD3B). Sample excitation and collection was collected inside an in-built sealed chamber connected to the M300 monochromator via a fibre-optic bundle. The Bentham spectrometer has a monochromator, which measures the radiation emitted by the phosphor at a single wavelength. It also has combination filters, which enable it to measure over a range of wavelengths. The Bentham spectrometer was linked to a computer, which displays the emission and excitation spectra and calculates the C.I.E coordinates. The set-up used for D.C Cathodoluminescent measurements utilised a telescope to focus on the sample in the low voltage chamber and as with the intensity measurements the samples were moved into the electron beam.

From each sample a small amount of material was put on an aluminium stud and put into the Bentham spectrometer measuring chamber. Each sample was scanned twice, first for its emission when excited at 254 nm and collected over a range from 300 to 800 nm (the emission scan was plotted as intensity in arbitrary units against wavelength (nm)); second to collect the excitation spectrum. The excitation scans were taken monitoring the 612 nm emission band and collecting the spectra over the range from 200 nm to 500 nm. The excitation scan was plotted as intensity in arbitrary units Vs wavelength in nm. A total of 42 scans were obtained. To achieve better results the above experiments were repeated in an alternative way with a small amount of powder placed in a 2cm x2cm x1cm black plastic holder and this was inserted into Bentham spectrometer measuring chamber to obtain emission and excitation spectra.

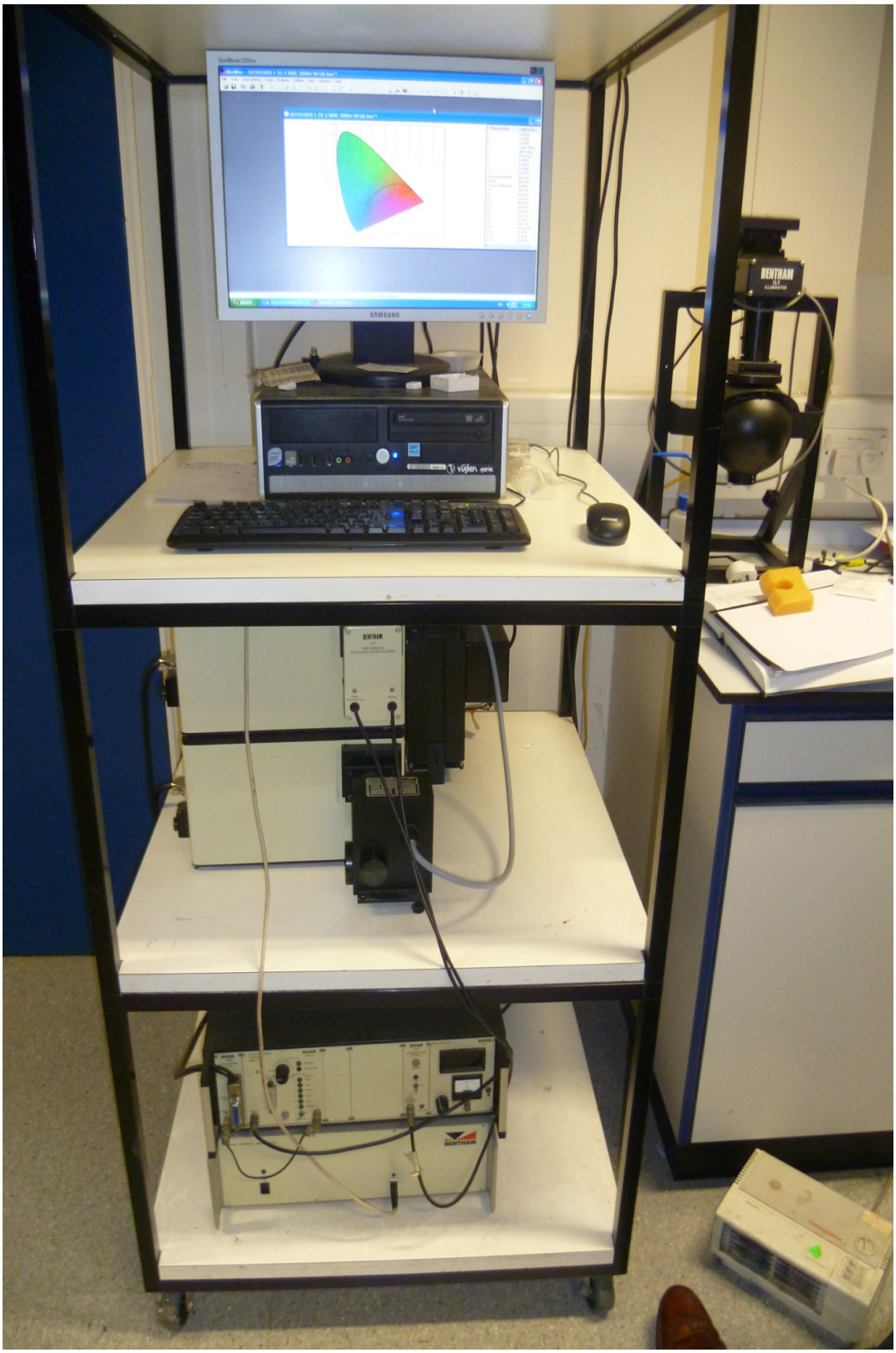

Figure 3.6 The Bentham spectrometer

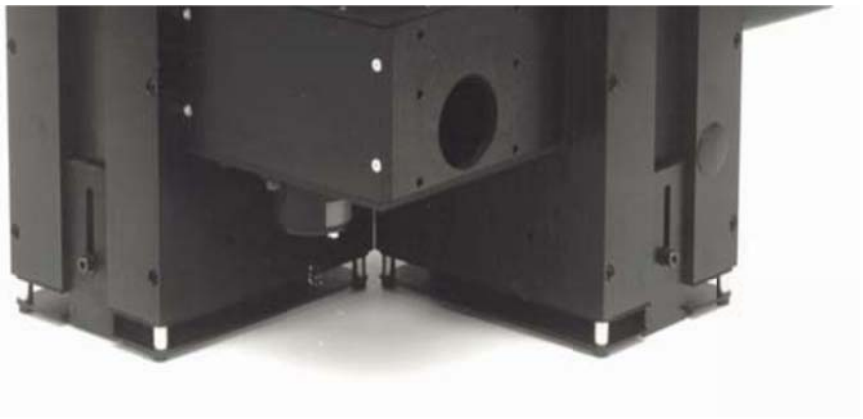

Figure -3.7 Bentham spectrometer measuring chamber

3.5 ATR-FTIR

ATR (Attenuated Total Reflectance) - FTIR (Fourier Transform Infrared Spectroscopy).

Infrared spectroscopy is a reliable technique widely used in both organic and inorganic chemistry, in research and industry. It is used in quality control, dynamic measurement, and monitoring applications such as the long-term unattended measurement of CO_2 concentrations in greenhouses and growth chambers by infrared gas analyzers. It is also used in forensic analysis in both criminal and civil cases.

Sample measurements were made using a Perkin Elmer one FTIR spectrometer, with a specac ATR accessory consisting of a diamond crystal and using a 45°. 36 samples were used for the experiment. Six new samples of $Y_2O_3:Eu^{3+}$ - C_{16} $H_{33}NH_3Cl$ ethanol base fired at 900°C and 650°C were prepared, and were measured twice, once then after 14 days to find out if there are any changes in the results. The ATR analysis was carried out with a small portion taken from each sample; this was placed onto the ATR diamond crystal. To insure a complete coverage of the crystal, a slight pressure was applied to the sample using an anvil to ensure complete contact between the sample and the ATR crystal. The sample was analysed using a spectral resolution of $4cm^{-1}$ with 20 scan accumulation collected for each sample (see Figure 3.8). The ATR method of infra red investigation of the structure and properties of the surface area of solid sample material is based on an effect induced by the penetration of the light wave into the investigated sample.

Figure 3.8 ATR chamber for Single Reflection Diamond Attenuated Total Reflectance (ATR) cell used for analysis of solids, liquids, pastes, films and micro samples.

FTIR

Fourier transform infrared (FTIR) spectroscopy is a measurement technique that allows one to record infrared spectra. Infrared light is guided through an interferometer and then through the sample (or vice versa). A moving mirror inside the apparatus alters the distribution of infrared light that passes through the interferometer. The signal directly recorded, called an "interferogram", represents light output as a function of the mirror position. A data-processing technique called Fourier transform turns this raw data into the desired result (the sample's spectrum). Light output is recorded as a function of infrared wavelength (or equivalently, wave number).

As described above, the sample's spectrum is always compared to a reference. Fourier Transform infrared spectroscopy (FTIR) was carried out in KBr Pellets (42 sample measurements were collected using the FTIR spectrometer). The 42 pellets in the KBr were each prepared by taking 150 mg of dry KBr and 1mg of sample mixed together and put into a 10,000kg pressure to form a pellet. The pellet was placed into an alumina desiccators to stop the pellets absorbing water. Each pellet in term was placed into the FTIR spectrometer to obtain an infrared spectrum. The Y axis presents absorbance (A) and the X axis is Wave number (cm^{-1}). Each sample was analysed using a spectral resolution of 4 cm^{-1} with 20 scan accumulation and data were collected individually for each sample [15].

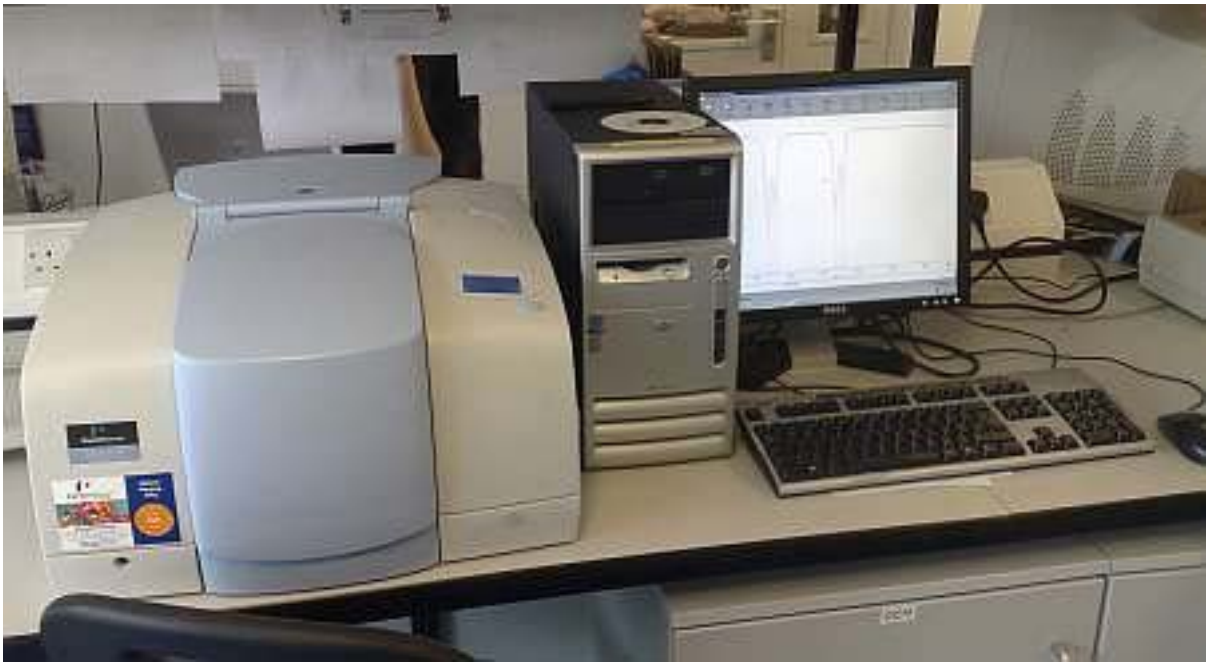

Figure 3.9 FTIR photospectometer

3.6 Raman spectroscopy

3.6.1 Introductions

1. **Raman spectroscopy:** (named after C. V. Raman) is a spectroscopic technique used to study vibrational, rotational, and other low-frequency modes in a system [16]. It relies on inelastic scattering, or Raman scattering, of monochromatic light, usually from a laser in the visible, near infrared, or near ultraviolet range. The laser light interacts with molecular vibrations, phonons or other excitations in the system, resulting in the energy of the laser photons being shifted up or down. The shift in energy gives information about the phonons modes in the system. The Raman effect occurs when light impinges upon a molecule and interacts with electron cloud and bonds of that molecule [17].
2. The equipment has dual capabilities that enable more routine low/medium resolution Raman analysis and even broader band laser induced luminescence to be conducted on the same bench-top instrument.
3. The Labram HR equipment is configured with UV, visible and NIR capability. Also it has an upright microscope for materials analysis for Raman analysis and Raman spectra scan.
4. The Labram HR equipment is also configured with fast Raman imaging technologies. The Labram HR allows the collection of large area Raman images in the matter of seconds/minutes. The unique combination of innovative optics, detectors and software combine to provide true confocal Raman imaging with an unmatched speed of data acquisition.

5. The Labram HR equipment is configured with the ultra low frequency (ULF) module allows Raman spectroscopic information in the sub-100cm^{-1} region, with measurements below <10cm^{-1}, and measurements are obtained in just a few minutes. The measurement of each sample took around five minutes each.

The Labram HR equipment is also configured with a motorized XY sample stage for automated Raman Imaging, autofocus attachment for automatic z-axis imaging (depth profiling), Polarizing filters in excitation and scattering beam-paths, Dual laser excitation at (785 nm or 488 nm), Liquid Nitrogen cooled 1024x256 pixel CCD detector, and Cuvette and macro sample holders. The Labram infinity system has a spatial resolution of about 1 micron which allows for the analysis of single cells, (see Figure –3.10 which presents the Labram HR video –Raman spectroscopy by Horiba). The figure shows the confocal microscope located in the centre, with the control PC on the left. At the rear are a video monitor and the lasers with the cooling fan for the Ar ion laser above He monitor.

3.6.2 The Labram HR Raman by Horiba equipment overview and features.

The Labram HR equipment provides high spectroscopic resolution and a unique wavelength range capability that offers both great flexibility and high performance. Labram HR equipment is widely used for standard Raman analysis, and photoluminescence (PL) the equipment has the following functions:-

6. High spectral resolution the unique high resolution mode is ideal for subtle band analysis such as that for phase (crystalline/amorphous); weak bonding forces (such as hydrogen bonding).
7. The equipment permits precise characterization of position or shape of the Raman spectral features. Band analysis with a resolution in the order of 0.3 cm^{-1} to 1 cm^{-1} is particularly suited to the high resolution mode.

Figure 3.10 Labram HR video –Raman spectroscopy by Horiba

Raman spectra and emission spectra were obtained using a Labram Raman spectrometer equipped with a 1800 g/mm holographic grating, a holographic super notch filter and a Peltier-cooled CCD detector. Samples were excited using a helium-neon laser with an output of 8 mW of power at the sample on the 632.8 nm line. 42 samples were analysed individually and for each sample the emission spectra were collected simultaneously with the Raman spectra, both excited by the same helium-neon laser. The greatest intensity in the photoluminescence spectra was from the largest particles which were the densest material encountered by the exciting laser beam. The samples used were laid flat ensuring good contacts, which is essential for photo-luminescence. In this work, small size (cubic shape) material made by the combustion method was established and found to have the ideal shape and size for the best photo-luminescence performance because of their self packing property.

From each sample a small quantity of the material was put on a small fine glass sheet and put on the microscope frame on the confocal pinhole with user controlled variable aperture the confocal pinhole fully matches the laser spot and provides the highest spatial resolution with maximum signal throughput. Typically [17], a sample was illuminated with a laser beam. Light from the illuminated spot was collected with a lens and sent through a monochromator. Wavelengths close to the laser line, due to elastic Rayleigh scattering, are filtered out while the rest of the collected light is dispersed onto a detector. Than a measurement for each sample was taken, a graph plotted and the results transmitted into Raman spectra scan of Raman shift Vs intensity (nm). 42 Raman scans were obtained.

3.7 Spectrophotometer Flurorolog-3

I H R 320 -Horiba Spectrofluorometer equipment.

System Description: - A diagram of the optical path of the spectrometer is presented in Figure 3.11 and is discussed below. The spectrometer consists of: A source of radiation that produces a beam of light that is filtered by an excitation spectrometer that allows a single wavelength of light to reach the sample. In the sample compartment, the sample responds to the incoming radiation. The resulting radiation is filtered by an emission spectrometer that feeds the signal to a photomultiplier detector. By stepping either or both spectrometers through a wavelength region, and recording the variation in intensity as a function of wavelength, a spectrum is produced.

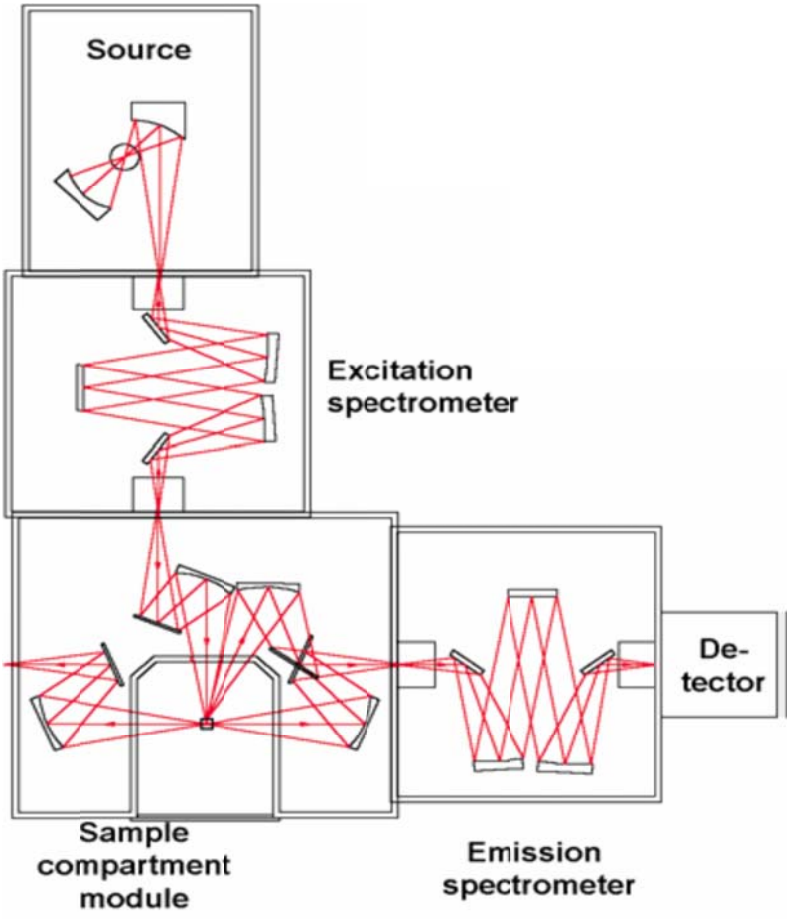

Figure 3.11 Optical path of Spectrometer

The spectrofluorometer components (spectrometers, sample-compartment module, accessories) are connected to a controller which, in turn, transfers information to and from the computer. The Fluorolog-3 Basic components Spectrometers-The Fluorolog-3 comes equipped with a double-grating spectrometer in the excitation and emission positions. Double-grating spectrometers offer a significant increase in sensitivity, resolution and stray-light rejection. Sample compartment-The standard sample-compartment module is a T-Box, which provides efficient throughput with a choice of standard right-angle emission collection or optional front-face emission collection. The sample-compartment module comes equipped with a silicon photodiode reference detector to monitor and compensate for variations in the xenon lamp output. The spectrometer is shown in Figure 3.12.

Figure 3.12 Flurorolog-3, I H R 320 -Horiba Spectrofluorometer.

The Model 1907 450-W xenon lamp delivers light from 240 nm to 850 nm for sample excitation. The lamp has an approximate life of 2000 h, and is ozone-free. The lamp is designed to fit into the FL-1039 Xenon Lamp Housing and the FL-1040 Dual Lamp Housing. And fan to cool the Lamp (see Figures 3.13 and 3.14)

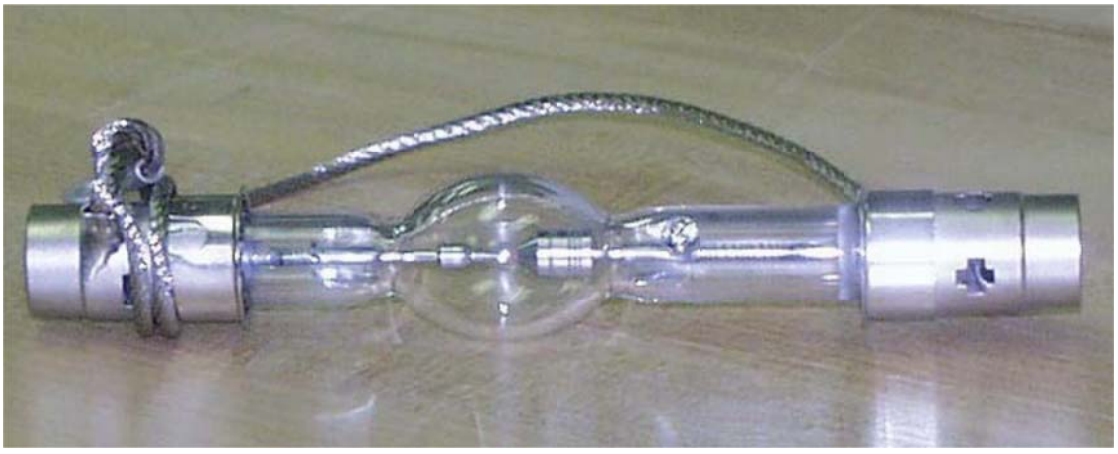

Figure 3.13 Model 1907 450-W Xenon Lamp

Figure 3.14- FL-1040 Dual Lamp Housing. And fan to cool the Lamp

The Model 1933 solid sample holder as shown in Figure 3.15 is designed for samples such as thin films, powders, pellets, microscope slides, and fibbers. The holder consists of a base with graduated dial, upon which a bracket, a spring clip, and a sample block rest with the ability to rotate the sample towards the light beam.

From each sample a small amount of material was taken to fill the whole well of the block. The material placed on the block on the side opposite that of the well (see Figure 3.15). Then immediately a quartz cover slip or a thin film of glass (microscope slides), is placed over the well; this holds the sample in place when vertically positioned. The block is carefully inserted between the bracket and spring clip, so that the sample is perpendicular to the excitation light and fluorescence collected using front-face detection.

Samples were placed in a special black cell, as explained above, (see Figure 3.15) at an angle of 30° to the UV beam of the Spectrofluorometer- Flurorolog-3 Equipment to obtain emission and excitation spectral graphs. For this experiment emitted EMR from

the samples were passed through two different types of filters. The first one was the yellow filter "SCHOTT AG-KV-450". For each sample excitation and emission spectra graphs were produced plotting Intensity CPS/Micro Amps Vs Wave length (nm). By monitoring the 612nm band an excitation spectrum was produced for each sample, and at 395 nm (excitation energy) an emission spectrum was recorded for each sample. The above experiment was repeated with the second filter Type-KV 370, Mat. Nr 1011820, Dicke (mm) =3.0, Abm. (mm) 50.0x 50.0 SCHOTT AG. For each sample excitation spectra graph was produced of Intensity CPS versus wave length (nm) this time monitoring at 609nm and for excitation spectra each sample, and emission spectra were produced using 254 nm exciting radiation.

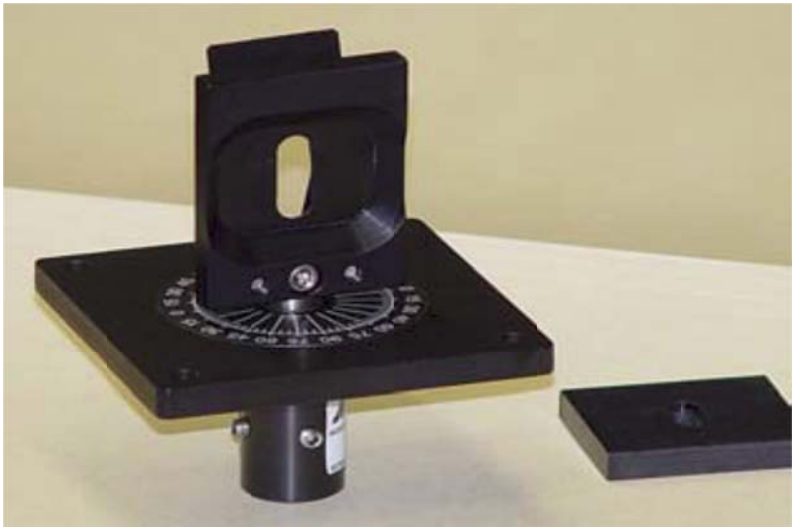

Figure 3.15 Sample holders.

3.8 Thermal Methods of characterisation

3.8.1 SDT-Q500 (TGA)

Thermo gravimetric analysis (TGA) measures the amount and rate of change in the weight of a material as a function of temperature & time in a controlled atmosphere. The SDT-Q500 thermo gravimetric analyzer (TGA) (see Figure 3.16) was used for each sample, to analyse, measure and record its weight change (TGA) from room temperature to 1000C. All samples were individually analysed to obtain their weight changes from ambient temperature and on heating to 1000C. A small amount of material from each sample was taken and put into the SDT Q500 sample chamber. The chamber was sealed and then the temperature was raised in the chamber from 20°C to 900°C. Each experiment took 2h to complete and as a result a TGA graph was obtained. Graphs plotted of weight loss in % against temperature increase from 20°C

to 900°C over 120 min. The experimental technique consisted of heating at a constant rate until weight change occurred as determined by selecting the temperature rate increase of 8°C per min at each weight loss the temperature was held isothermally until the weight change was complete. This sequence of heating, and isothermal holding is repeated for each weight change encountered. The result was optimum weight loss resolution for the duration of 120 min. Using SDT Q500 the experimental results obtained for the samples included:-

1) Weight loss as a function of temperature,
2) Thermal stability and heat resistance,
3) The moisture content of the samples.
4) Analyses between ambient and up to 1000°C.

The main features of the equipment are listed below.

SDT Q500 (TA) Technical information

- Temperature Range: Ambient to 1000 °C
- Isothermal Temperature Accuracy: 1 °C
- Isothermal Temperature Precision: 0.1 °C
- Continuous Weighing Capacity: 1.0 g
- Heating Rate: 0.1-100 °C /min
- 30-position auto sampler
- Dual range microbalance (0-200 mg and 0-1 g) with auto switching
- Vertical balance design with a horizontal gas purge
- Automated pan loading and furnace movement
- Software controlled, dual mass flow controllers with automated gas switching
- Full VGA colour touch screen display for convenient operator control and monitoring of instrument status
- Temperature Compensated Thermobalance Included
- Maximum Sample Weight 1 g
- Weighing Precision +/- 0.01%
- Sensitivity 0.1 μg
- Baseline Dynamic Drift* < 50 μg
- Furnace Heating Resistance Wound.
- Temperature Calibration Curie point.
- Sample Pans Platinum 50, 100 μL.
- Ceramic pan 100, 250, 500 μL.

The advantage of using SDT Q500 (TGA)

The advantages of this instrument stem from its inherent design and careful user use:- Reproducibility:- (Powders best), Sample weight,10-20mg for most applications,50-100mg for measuring volatiles, Most TGA instruments have baseline drift of +/- 0.025mg which is 0.25% of a 10mg sample, Use brass tweezers to eliminate static

effects, use a clean sample pan before every run and distribute sample evenly over bottom of pan.

Figure 3.16 TA Instruments SDT Q500 Thermo gravimetric Analyzer (TGA)

The method is especially important for measuring small weight, losses associated with volatilization or small amounts of residue. To calibrate the instrument it is first ran clean, empty, over temperature, range of interest, at desired heating rate. Then the sample is ran over the same range. A plot of weight in µg versus. Temperature is then made. Ideally the surface area of the sample should be maximised to improve weight loss resolution and temperature response

3.8.2 SDT Q600

Figure 3.17 SDT Q600

Chapter 3 Experimental Techniques

Introduction:

The SDT Q600 instrument is an analysis instrument capable of performing both differential scanning calorimetry (DSC) and thermo gravimetric analysis (TGA) at the same time. Simultaneous DSC-TGA provide a true measurement of heat flow DSC and weight change TGA on the same sample from ambient temperature to 1000°C (see Figure 3.17).

SDT Q600 noise is <4 microwatts and the TGA balance sensitivity is 0.1 μg. A heat flux DSC design with separate sample and reference pans is used, and is calibrated for heat flow measurements using sapphire. The SDT Q600 features automated furnace movement and a horizontal purge gas system with digital mass flow controllers and programmable gas switching capability. A separate inlet tube permits introduction of reactive gases into the sample chamber. The accessory kit contains platinum and ceramic sample pans, calibration and test materials, plus tools. The platinum cups are recommended for operation up to 1000 °C, and for their general inertness and ease of cleaning. The ceramic cups are advised for operation to 1,500 °C, Equipment description from TA manufacture [19]. The TA Instruments SD Q600 provides an accurate simultaneous measurement of weight change (Thermo gravimetric analysis - TGA) and differential heat flow (Differential scanning calorimetric - DSC) on the same sample in a temperature range from ambient to 1000 °C. TGA applications include studying absorbed moisture content, level of organic and inorganic components, degradation temperatures, solvent residues, and estimation of corrosion kinetics in high temperature oxidation of materials. DSC applications include studying phase transitions (melting, glass transitions, and exothermic decompositions), curing processes, and oxidative stability of materials. Materials studied by the Q600 include organic and inorganic chemicals, polymers, pharmaceuticals, food/biological samples, etc. The SDT- Q600 features a horizontal dual beam balance design (sample capacity: 200 mg) that supports precise TGA (balance sensitivity: 0.1 μg) and DSC (heat flow sensitivity: 4 μW) measurements. The dual beam design allows two TGA samples to be analyzed simultaneously and delivers superior weight signal measurements (sensitivity, accuracy, and precision). DSC heat flow data is dynamically normalized using the instantaneous sample weight at any given temperature. The SDT- Q600 features a horizontal furnace. A matched Platinum/Platinum-Rhodium thermocouple pair within the ceramic beams provides direct sample, reference, and differential temperature measurements. A horizontal purge gas system with digital mass flow control and integral gas switching capability provides for precise metering of purge gas to the sample and reference pans. A separate gas inlet tube delivers reactive or inert gas to the sample. The SDT- Q600 also includes Advantage software for complete automatic experimental control and Universal Analysis 2000 software for comprehensive data analysis.

Thus this SDT measures the heat flow and weight changes associated with transitions and reactions in materials over the temperature range ambient to 1000°C. The information provided differentiates endothermic and exothermic events, which have no associated weight change (e.g. melting and crystallization) from those which involve a weight change (e.g. degradation). In addition, performing both DSC and TGA measurements at the same time, on the same instrument and same sample.

For this experiment new samples were specially prepared as follows : 3 samples of (Y_2O_3: Eu^{3+})Cl_3- (C_{16} $H_{33}NH_3Cl$) methanol base with material ratio 1:1, 1:2, 1:3 and 3 samples (Y_2O_3: Eu^{3+})Cl_3-(C_{16} $H_{33}NH_3Cl$) ethanol base with material ratio 1:1, 1:2, 1:3 . A small amount of material from each sample was taken and put into the SDT Q600 Chamber. The chamber was sealed and the experiment started by raising the temperature in the chamber from 20^0 C to 900^0C each experiment took around 2 hr to complete, and each resulted in a DSC-TGA graph. The graph plotted weight loss and heat loss as a percentage against temperature increase from 20^0 C to 900° C.

References

[1] J.I Goldestein and D.E Newbury, P.Echlin and E.Lifshin "Scanning Electron Microscopy and X-ray Microanalysis". London. Chapter-4 page 124, 1981.

[2] D.A Skoog and J.Leary."Principle of instrumental analysis 4th. " Ed Saunders College Publishing, 1992.

[3] Manual Operating Instruction for quality electron microscopy analysis Zeiss Gemini supra 35 VP.

[4] R. Jenkins and R.L. Snyder." Introduction to X-ray Powder Diffractometer". J. Wiley & Sons, Inc. 1996.

[5] R. Jenkins "Modern Powder diffraction", Reviews in Mineralogy, 20, 47-72. 1989.

[6] L.S. Dent Glasser;" Crystallography and its applications" .London. Van Nostrand Reinhold (UK) Co. Ltd, 1982.

[7] Bruker D8 –XRD, advanced powder diffraction file search user Instruction Manual and Tutorials for inorganic compound.

[8] Bruker AXS GMBH, XRPD, advanced powder diffraction evaluation Package Manual with Bragg Brentano geometry.

[9] H.W.Leverenz "An introduction to the luminescence of Solids " Dover publication New York page 211, 1968.

[10] H.W.Leverenz "An introduction to the luminescence of Solids " Dover publication New York page 72, 1968.

[11] L, Ozawa." Cathodoluminescence theory and applications" Kodansha Japan, Page 251- 252, 1990.

[12] G.Balasse and B.C.Grabmaier,"Luminescent Materials". Springer-Verlag, Berlin, Page 137.1994.

[13] L.Ozawa." Cathodoluminescence theory and applications" Kodansha Japan page 237- 238.1990.

[14] EFG-7, EGPS-7H Electron gun and power supply.EFG-7H-2011, EGPS-7H-219, user Instruction Manual by Kimball Physics Inc USA.

[15] Perkin Elmer analytical instrument, general technique for obtains Infrared spectra for FT/IR, FTNIR, ATR user Manual with Instrument Verification report.

[16] D.J. Gardiner," Practical Raman spectroscopy. Springer-Verlag. ISBN 978-0387502540, 1989.

[17] G.Placzek. "Rayleigh Streeung und Raman Effekt", J.In: Hdb. der Radiologie, Vol VI. 2. 209 .1934.

Chapter Four

Synthetic Methods used to prepare the Phosphor Materials Studied in this Thesis

4.1 Introduction

The work presented in this chapter describes the methods by which the materials studied were synthesized. The synthetic methods used was based on (but modified from) one that was previously published [1].The preparations all made use of amine hydrochlorides $(C_nH_{2n+1})NH_3Cl$ (n=8,12,16) to form micellar phases (see chapter 2 section,2.6) in methanol or in ethanol and these were used to self assemble yttrium and europium cations from YCl_3:Eu^{+3} (Eu 2.0 Mol%). The solution chemistry produces the precursor for the Y_2O_3:Eu^{3+} lattice. There follows experimental, descriptions of how a number of samples were prepared in alcohol of micelles containing the amine hydrochlorides and rare earth cations. These in turn are followed by details of the combustion methodology (the heating of reagents) at 650°C and 900°C. The ethanol and hydrocarbon chains with the amine hydrochlorides forming the micellar backbone acted as the fuel for the combustion process and provided the energy to synthesis the formation of the europium-doped yttrium oxide products
[2, 3].

4.1.1 Chemicals

The chemicals used in this work are as follows:- Yttrium oxide (99.99%), europium oxide (99.99%), yttrium nitrate (99.99%) and europium nitrate (99.99%) (all obtained from Aldrich Chemical Company), magnesium nitrate (AnalaR, BDH Merck), hydrochloric acid (37%, Fisher), ethanol (99.7-100% v/v, BDH Merck), isopropanol (AnalaR, BDH Merck) and methanol (AnalaR, BDH Merck). The alkyl ammonium salt $C_{16}H_{33}NH_3Cl$ was prepared from the amine see 4.3.

4.1.2 Experiment 1. The preparation of Y_2O_3:Eu^{3+}

A solution of 98% of $Y(NO_3)_3$ and 2% $Eu(NO_3)_3$ was made up as follows to produce $Y_{0.98}Eu_{0.02}(NO_3)_3$. First Eu_2O_3 =152x2 +16x3 = 352 g /4 = 88 g, but as only 2% was required then a mother solution containing 1.76g of Eu_2O_3 was needed. Similarly 98% Y_2O_3 = 89x2 +16x3= 226 grams /4 =56.5 g, but as only 98% was required then the mother solution required 55.37 g.

A solution in water was prepared by taking 1.76 g of Eu_2O_3 and 55.375 g of Y_2O_3, adding nitric acid to convert the oxides to nitrates following which water was added to make 1000mL of solution "A". (This is now referred to as solution "A"). Then 15 g of urea ($CO(NH_2)_2$) were added to 25 ml of solution" A" together with 450 ml of distilled water. The mixture was put on hot plate to reach 85°C. The reaction started and a white colour was produced that ended in a solid deposit, the heating was continued for an hour. The solution was heated at 100°C on hot plate for a further hour to stabilize and to evaporate down in volume. After an hour a clear solution was obtained. This method is dependent on the addition of, and hydrothermal decomposition of, urea in acid solution in the presence of metal salts that are soluble at acid pHs. The chemistry involved includes:-aqueous decomposition of urea (<85 ºC, ~ pH 3) which produced (resulting) in the following ions, of which,

$$H_2NCONH_2 \rightarrow NH_4^+ + OCN^-$$

The cyanate ion rapidly reacted as follows:

$$OCN^- + 2H^+ + 2H_2O \rightarrow H_2CO_3 + NH_4^+$$

In the presence of Y^{3+} and Eu^{3+} cations which were added as acid salts the solution pH dropped to ~2.5. The urea was added and the resulting hydroxonium ions (H_3O^+) promoted the decomposition of urea. The subsequent release of carbonate ions causes precipitation of the metal hydroxycarbonate phosphor precursor, once the concentration of reactants reached supercritical saturation

$$[(Y, Eu)\,OH\,(H_2O)_n]^{2+} + H_2CO_3 \rightarrow [(Y,Eu)OHCO_3.H_2O] + (n-1)\,H_2O + 2H^+_{(aq)}$$

The precipitate was filtered and placed in a crucible in a furnace then fired to 980°C for 30 min. The resulting white powder was $Y_2O_3:Eu^{3+}$.

4.1.3 Experiment 2. The Preparations of [(Y, Eu)$OHCO_3.H_2O$].

50mL of solution A was mixed with a solution of 15 g of urea ($CO(NH_2)_2$) in 450 mL distilled water. The solution was put on a hot plate set at 85°C. The reaction started and the solution turned from a clear colour to white solution (at pH = 3). The white colour solution started to crystallize and became a solid deposit; the heating was continued for 1 hour. The solution was heated to 100°C on hot plate for a further hour to stabilize and to evaporate down in volume. After 1h the white solution changed to clear solution. The $CO(NH_2)_2$ had decomposed, a solid deposit and solid in suspension was left without a trace of ($CO(NH_2)_2$).A vacuum filter was used to remove (filter off) the water. (The precipitate was rinsed with 100 mL of distilled water to filter off any urea trace) .The resulting dry white powder was [(Y, Eu)$OHCO_3.H_2O$].

4.1.4 Experiment 3. The Preparations of more [(Y, Eu)$OHCO_3.H_2O$].

For 4 days on a daily basis experiment 2 was repeated to obtained a pure product in large quantity of [(Y,Eu)$OHCO_3.H_2O$]. The dry white powder product was used for further experiments/measurements.

4.1.5. Experiment 4. The Preparations of a solution of $Y_{0.98}Eu_{0.02}Cl_3$

A solution of 1.76g of 2% Eu_2O_3 and 55.375g of 98% Y_2O_3 was made up in distilled water. The solution colour became white. Then to this solution 180 mL of HCl was added very slowly at the rate of 10mL per 5 min, to get the reaction going slowly and not over heated, to achieve a controlled reaction. At the end of the reaction the solution changed colour from white to clear. The result was a one liter solution of $Y_{0.98}Eu_{0.02}Cl_3$.

4.2 Experimental work using Micellar methods.

4.2.1 Experiment 5. To prepare the amine hydrochloride $CH_3(CH_2)_nNH_3Cl$ (where n = 7, 11 or 15)

The amines were quaternised with excess dilute hydrochloric acid in a warm solution of ethanol. The resulting yellow masses were recrystallised from ethanol, whereby the alkylammonium chloride was observed to have crystallized into soft white thin salt laths.

A typical method was: - To 50mL warm solution of ethanol, a 20g of $C_{12}H_{26}NH_3$ was added and fully dissolved. Then 100mL of HCl at the rate of 10mL per 4 min was added to the solution (to get the reaction going slowly and not over heated). The solution was put on hot plate set at 85°C in the fume cubed; the solution was heated for a further hour to stabilize and to evaporate down in volume. The following equation describes the reaction and the chemistry:- $C_{12}H_{26}NH_3 + HCl \rightarrow (C_{12}H_{25}NH_3Cl)$.A white viscose solution was formed. A vacuum filter was used to remove (filter off) the water from the solid produced. Then the precipitate was rinsed with 50mL of ethanol and filtered. Then the product was dried in an oven at 100°C for 1h, to obtain $C_{12}H_{25}NH_3Cl$ as a white powder.

4.2.2 Experiment 6. To produce micelles containing phosphor precursors with $C_{12}H_{25}NH_3Cl$

The europium content in the phosphor prepared herein by the micellar method was 2.0 Mol%. A solution of 1.76g of 2% Eu_2O_3 and 55.375g of 98% Y_2O_3 was made up in distilled water. The solution colour became white. Then to this solution 180 mL of HCl was added very slowly at the rate of 10mL per 5 min, to get the reaction going slowly and not over heated, to achieve a controlled reaction. The solution was made up to 1litre volume. 25 mL of this solution was added to a warm alcoholic solution (25 mL) containing $C_{12}H_{25}NH_3Cl$ (2.21g, 0.01M) and 25 mL water. This gave a stiochometric ratio of 1:1 for the combined metal chloride to alkylammonium chloride present in the solution. In other preparations the metal chloride to alkylammonium chloride ratio was 1:2

or 1:3 using. The solution was heated on a hot plate to about 100°C until it was reduced in volume and became viscous (some alcohol was still present. This assisted in speeding up ignition of alkylammonim chloride fuel).
The following equation describes the reaction and the chemistry:-

$EuCl_3 + YCl_3 + C_{12}H_{25}NH_3Cl \rightarrow [(Y,Eu)Cl_3](C_{12}H_{25}\text{-}NH_3Cl)n$ (where n = 2).

4.2.3 Experiment 7 to convert the phosphor precursor to the phosphor.

A vacuum filter was used to filter off the water from the solid produced in section 4.2.2. Then the precipitate was rinsed with 100 mL of ethanol and filtered. Then the product was dried in an oven at 100°C for 1h. The resulting dry or almost dry white powder was $[(Y,Eu)Cl_3]$ - $C_{12}H_{25}NH_3Cl$.This powder was divided into 6 samples. Each sample was placed in a crucible and then fired in the furnace at different temperatures: 500°C, 600°C, 700°C, 800°C, 900°C and 1000°C. Each sample was fired in a crucible in a furnace for 30 min. The XRPD data of the sample fired at 500°C is presented in Figure 4.1.This shows the presence of mainly amorphous material with some very broad peaks from a crystalline phase that could not be identified. These are most likely due to the remains of the organic residues and the beginning of the crystallization of some inorganic phases. In contrast the XRPD data from the sample fired at 900°C (Figure 4.4) shows the presence of a pure crystalline phase of cubic $Y_2O_3:Eu^{3+}$. XRPD data from the 600°C sample (Figure 4.2) showed very little evidence of crystalline phases with broad background peaks again suggestive of much amorphous material with just some small amounts of an unidentified crystalline phase. The XRPD data of the 700°C, 800°C temperatures not presented showed intermediate behaviour. From this evidence firing temperatures of 650°C and 900°C were chosen for the studies presented in this thesis

4.3 Experimental production of phosphors by using----Micelle methods

The procedure used in this work was thus based on a method reported in the literature entitled “Facile self assembly of yttrium oxide and europium phosphor from solution using a sacrificial micelles phase [1].” This paper describes a method for preparing the red emitting phosphor $Y_2O_3:Eu^{3+}$ using a self assembling micelle mechanism. The resulting white powder has smaller sized particles than the commercial $Y_2O_3:Eu^{3+}$ phosphors and has luminescent properties comparable to commercial cathodoluminescent products at low exaction voltages. From the experiments set out in section 4.2.3, sets of experiments based on these were carried out at and fired at 650°C and 900°C. The following 36 samples were prepared in the synthesis of small particle yttrium oxide type phosphors from solution using a sacrificial micellar phase as a combustion fuel as follows where the rare earth metal chlorides were first formed in solution:

1. $[(Y, Eu)Cl_3]$ - $(C_{16}H_{33}NH_3Cl)$-6 experiments in the ratio of 1:1, 1:2, 1:3 with ethanol (3 fired at 900°C and 3 fired at 650°C).
2. $[(Y, Eu)Cl_3]$ - $(C_{16}H_{33}NH_3Cl)$-6 experiments in the ratio of

1:1, 1:2, 1:3 with methanol (3 at 900°C and 3 at 650°C).

3. [(Y, Eu)Cl_3] - ($C_{12}H_{25}NH_3Cl$)-6 experiments in the ratio of 1:1, 1:2, 1:3 with ethanol (3 at 900°C and 3 at 650°C).
4. [(Y, Eu)Cl_3] - ($C_{12}H_{25}NH_3C1$)-6 experiments in the ratio of 1:1, 1:2, 1:3 with methanol (3 at 900°C and 3 at 650°C).
5. [(Y, Eu)Cl_3] - ($C_8H_{17}NH_3Cl$)-6 experiments in the ratio of 1:1, 1:2, 1:3 with ethanol (3 at 900°C and 3 at 650°C).
6. [(Y, Eu)Cl_3] - ($C_8H_{17}NH_3Cl$)-6 experiments in the ratio of 1:1, 1:2, 1:3 with methanol (3 at 900°C and 3 at 650°C).

Next the experimental details of each of the above listed experiments are presented:-

4.4 Experiment 8. The materials prepared using- ($C_{16}H_{33}NH_3Cl$) with ethanol.

Preparations of [(Y, Eu)Cl_3] - ($C_{16}H_{33}NH_3Cl$)n (for n = 1, 2, 3) with ethanol based as follows:-

1. 1:1 solution of [(Y, Eu)Cl_3] - ($C_{16}H_{33}NH_3Cl$) was produced based on using 25 mL of $EuCl_3$ +25 mL of YCl_3 + 20 mL of ethanol (C_2H_5OH) +1.215 g of ($C_{16}H_{33}NH_3Cl$). The Micelles were = [(Y, Eu)Cl_3] - ($C_{16}H_{33}NH_3Cl$) present as a yellow soapy mass product.
2. 1:2 solution of [(Y, Eu)Cl_3] - ($C_{16}H_{33}NH_3Cl$) was produced based on using 25 mL of $EuCl_3$ +25 mL of YCl_3 + 20 mL of ethanol (C_2H_5OH) + 2.430 g of ($C_{16}H_{33}NH_3Cl$) Micelle = [(Y, Eu)Cl_3] - ($C_{16}H_{33}NH_3Cl$) results in a yellow soapy mass product.
3. 1:3 solution of [(Y, Eu)Cl_3] - ($C_{16}H_{33}NH_3Cl$) was produced based on using 25 mL of $EuCl_3$ +25 mL of YCl_3 + 20 mL of ethanol (C_2H_5OH) + 3.645 g of ($C_{16}H_{33}NH_3Cl$) Micelle = [(Y, Eu)Cl_3] - ($C_{16}H_{33}NH_3Cl$) results in a yellow soapy mass product.

The yellow soapy mass was washed with acetone and recrystallised from ethanol. The alkylammonium chlorides crystallized into thin soft laths. The solution was warmed to 85°C on a hot plate. The solution was allowed to boil at 100°C and then the yellow soapy mass changed to white solution. The solution volume was reduced till it became a viscous solution .3 samples with the material ratio 1:1, 1:2 and 1:3 of the viscous products were fired in a crucible in a furnace for 30 min at 650°C. The remaining 3 samples with the material ratio 1:1, 1:2 and 1:3 of the viscous product were fired in a crucible in a furnace for 30 min at 900°C. This allowed the combustion of the alkylammonium chains to form white powders. These white powders were the end products and their characterization and properties are reported in the following chapters.

4.4.1 Experiment 8a. The materials prepared using- ($C_{16}H_{33}NH_3Cl$) with methanol

Preparations of [(Y, Eu)Cl_3] - ($C_{16}H_{33}NH_3Cl$)n (for n = 1, 2, 3) with methanol based as follows:-

1. 1:1 solution of [(Y, Eu)Cl_3] - ($C_{16}H_{33}NH_3Cl$) was produced based on using 25 mL of $EuCl_3$ +25 mL of YCl_3 + 20 mL of methanol (CH_3OH) + 1.215 g of ($C_{16}H_{33}NH_3Cl$) Micelle = [(Y, Eu)Cl_3] - ($C_{16}H_{33}NH_3Cl$) results in a yellow soapy mass product.
2. 1:2 solution of [(Y, Eu)Cl_3] - ($C_{16}H_{33}NH_3Cl$) was produced based on using 25 mL of $EuCl_3$ +25 mL of YCl_3 + 20 mL of methanol (CH_3OH) + 2.430 g of ($C_{16}H_{33}NH_3Cl$) Micelle = [(Y, Eu)Cl_3] - ($C_{16}H_{33}NH_3Cl$) results in a yellow soapy mass product.
3. 1:3 solution of [(Y, Eu)Cl_3] - ($C_{16}H_{33}NH_3Cl$) was produced based on using 25 mL of $EuCl_3$ +25 mL of YCl_3 + 20 mL of methanol (CH_3OH) + 3.645 g of ($C_{16}H_{33}NH_3Cl$) Micelle = [(Y, Eu)Cl_3] - ($C_{16}H_{33}NH_3Cl$) results in a yellow soapy mass product.

The yellow soapy mass was washed with methanol and recrystallised from methanol. The alkylammonium chlorides crystallized into thin soft laths. The solution was warmed to 85°C on a hot plate. The solution continued to boil at 100°C and then the yellow soapy mass changed to white solution. The solution volume was reduced to a viscose solution. 3samples with the material ratio 1:1, 1:2 and 1:3 of the viscous product were fired in a crucible in a furnace for 30min at 650°C. The remains 3 samples with the material ratio 1:1, 1:2 and 1:3 of the viscous product were fired in a crucible in a furnace for 30min at 900°C, This allowed the combustion of the alkylammonium chains to form white powders. These white powders were the end products and their characterization and properties are reported in the following chapters.

4.5 Experiment 9. The materials prepared using- ($C_{12}H_{25}NH_3Cl$) with Ethanol

Preparations of [(Y, Eu)Cl_3] - ($C_{12}H_{25}NH_3Cl$)n (for n = 1, 2, 3) with ethanol based as follows:-

1. 1:1 solution of [(Y, Eu)Cl_3] - ($C_{12}H_{25}NH_3Cl$) was produced based on using 25 mL of $EuCl_3$ +25 mL of YCl_3 + 20 mL of ethanol (C_2H_5OH) + 1.215 g of ($C_{12}H_{25}NH_3Cl$) Micelle = [(Y, Eu)Cl_3] - ($C_{12}H_{25}NH_3Cl$) results in a yellow soapy mass product.
2. 1:2 solution of [(Y, Eu)Cl_3] - ($C_{12}H_{25}NH_3Cl$) was produced based on using 25 mL of $EuCl_3$ +25 mL of YCl_3 + 20 mL of ethanol (C_2H_5OH) + 2.430 g of ($C_{12}H_{25}NH_3Cl$) Micelle = [(Y, Eu)Cl_3] -($C_{12}H_{25}NH_3Cl$) results in a yellow soapy mass product.
3. 1:3 solution of [(Y, Eu)Cl_3] - ($C_{12}H_{25}NH_3Cl$) was produced based on using 25 mL of $EuCl_3$ +25 mL of YCl_3 + 20 mL of ethanol (C_2H_5OH) + 3.645 g of

($C_{12}H_{25}NH_3Cl$) Micelle = [(Y, Eu)Cl_3] - ($C_{12}H_{25}NH_3Cl$) results in a yellow soapy mass product.

The yellow soapy mass was washed with acetone and recrystallised from ethanol. The alkylammonium chlorides crystallized into thin soft laths. The solution was warmed to 85°C on a hot plate. The solution continued to boil at 100°C and then the yellow soapy mass changed to white solution. The solution volume was reduced to a viscose solution. 3 samples with the material ratio 1:1, 1:2 and 1:3 of the viscous product were fired in a crucible in a furnace for 30min at 650°C. The remains 3 samples with the material ratio 1:1, 1:2 and 1:3 of the viscous product were fired in a crucible in a furnace for 30min at 900°C, This allowed the combustion of the alkylammonium chains to form white powders. These white powders were the end products and their characterization and properties are reported in the following chapters.

4.5.1 Experiment 9a .The materials prepared using - ($C_{12}H_{25}NH_3Cl$) with Methanol

Preparations of [(Y, Eu)Cl_3] - ($C_{12}H_{25}NH_3Cl$) n (for n = 1, 2, 3) with methanol based as follows:-

1. 1:1 solution of [(Y, Eu)Cl_3] ($C_{12}H_{25}NH_3Cl$) was produced based on using 25 mL of $EuCl_3$ +25 mL of YCl_3 + 20 mL of methanol (CH_3OH) + 1.215 g of ($C_{12}H_{25}NH_3Cl$) Micelle = [(Y, Eu)Cl_3] - ($C_{12}H_{25}NH_3Cl$) results in a yellow soapy mass product.
2. 1:2 solution of [(Y, Eu)Cl_3] - ($C_{12}H_{25}NH_3Cl$) was produced based on using 25 mL of $EuCl_3$ +25 mL of YCl_3 + 20 mL of methanol (CH_3OH) + 2.430 g of ($C_{12}H_{25}NH_3Cl$) Micelle = [(Y, Eu)Cl_3] - ($C_{12}H_{25}NH_3Cl$) results in a yellow soapy mass product.
3. 1:3 solution of [(Y, Eu)Cl_3] - ($C_{12}H_{25}NH_3Cl$) was produced based on using 25 mL of $EuCl_3$ +25 mL of YCl_3 + 20 mL of methanol (CH_3OH) + 3.645 g of ($C_{12}H_{25}NH_3Cl$) Micelle = [(Y, Eu)Cl_3] - ($C_{12}H_{25}NH_3Cl$) results in a yellow soapy mass product.

The yellow soapy mass was washed with methanol and recrystallised from methanol. The alkylammonium chlorides crystallized into thin soft laths. The solution was warmed to 85°C on a hot plate. The solution continued to boil at 100°C and then the yellow soapy mass changed to white solution. The solution volume was reduced to a viscose solution. 3 samples with the material ratio 1:1, 1:2 and 1:3 of the viscous product were fired in a crucible in a furnace for 30 min at 650°C. The remains 3 samples with the material ratio 1:1, 1:2 and 1:3 of the viscous product were fired in a crucible in a furnace for 30 min at 900°C, This allowed the combustion of the alkylammonium chains to form white powders. These white powders were the end products and their characterization and properties are reported in the following chapters.

4.6 Experiment 10. The materials prepared using - ($C_8H_{17}NH_3Cl$) with Ethanol.

Preparations of [(Y, Eu)Cl_3] - ($C_8H_{17}NH_3Cl$)n (for n = 1, 2, 3) with ethanol based as follows:-

1. 1:1 solution of [(Y, Eu)Cl_3] -($C_8H_{17}NH_3Cl$) was produced based on using 25 mL of $EuCl_3$ +25 mL of YCl_3 + 20 mL of ethanol (C_2H_5OH) + 1.215g of ($C_8H_{17}NH_3Cl$) Micelle = [(Y, Eu)Cl_3] - ($C_8H_{17}NH_3Cl$) results in a yellow soapy mass product.
2. 1:2 solution of [(Y, Eu)Cl_3] - ($C_8H_{17}NH_3Cl$) was produced based on using 25mL of $EuCl_3$ +25 ml of YCl_3 + 20 mL of ethanol (C_2H_5OH) + 2.430g of ($C_8H_{17}NH_3Cl$) Micelle = [(Y, Eu)Cl_3] - ($C_8H_{17}NH_3Cl$) results in a yellow soapy mass product.
3. 1:3 solution of [(Y, Eu)Cl_3] - ($C_8H_{17}NH_3Cl$) was produced based on using 25mL of $EuCl_3$ +25 mL of YCl_3 + 20 mL of ethanol (C_2H_5OH) + 3.645g of ($C_8H_{17}NH_3Cl$) Micelle = [(Y, Eu)Cl_3] - ($C_8H_{17}NH_3Cl$) results in a yellow soapy mass product.

The yellow soapy mass was washed with acetone and recrystallised from ethanol. The alkylammonium chlorides crystallized into thin soft laths. The solution was warmed to 85°C on a hot plate. The solution continued to boil at 100°C and then the yellow soapy mass changed to white solution. The solution volume was reduced to a viscose solution. 3 samples with the material ratio 1:1, 1:2 and 1:3 of the viscous product were fired in a crucible in a furnace for 30min at 650°C. The remains 3 samples with the material ratio 1:1, 1:2 and 1:3 of the viscous product were fired in a crucible in a furnace for 30 min at 900°C, This allowed the combustion of the alkylammonium chains to form white powders. These white powders were the end products and their characterization and properties are reported in the following chapters.

4.6.1 Experiment 10a. The materials prepared using- ($C_8H_{17}NH_3Cl$) with Methanol.

Preparations of [(Y, Eu)Cl_3] - ($C_8H_{17}NH_3Cl$)n (for n = 1, 2, 3) with methanol based as follows:-

1. 1:1 solution of [(Y, Eu)Cl_3] - ($C_{16}H_{33}NH_3Cl$) was produced based on using 25mL of $EuCl_3$ +25 mL of YCl_3 + 20 mL of methanol (CH_3OH) + 1.215 g of ($C_8H_{17}NH_3Cl$) Micelle = [(Y, Eu)Cl_3] - ($C_8H_{17}NH_3Cl$) results in a yellow soapy mass product.
2. 1:2 solution of [(Y, Eu)Cl_3] - ($C_8H_{17}NH_3Cl$) was produced based on using 25mL of $EuCl_3$ +25 mL of YCl_3+ 20 mL of methanol (CH_3OH) + 2.430g of ($C_8H_{17}NH_3Cl$) Micelle = [(Y, Eu)Cl_3] - ($C_8H_{17}NH_3Cl$) results in a yellow soapy mass product.
3. 1:3 solution of [(Y, Eu)Cl_3] - ($C_8H_{17}NH_3Cl$) was produced based on using 25mL of $EuCl_3$ +25 mL of YCl_3 + 20 mL of methanol (CH_3OH) + 3.645 g of ($C_8H_{17}NH_3Cl$) Micelle = [(Y, Eu)Cl_3] - ($C_8H_{17}NH_3Cl$) results in a yellow soapy mass product.

The yellow soapy mass was washed with methanol and recrystallised from methanol. The alkylammonium chlorides crystallized into thin soft laths. The solution was warmed to 85°C on a hot plate. The solution continued to boil at 100°C and then the yellow soapy mass changed to white solution. The solution volume was reduced to a viscose solution. 3 samples with the material ratio 1:1, 1:2 and 1:3 of the viscous product were fired in a crucible in a furnace for 30min at 650°C. The remains 3 samples with the material ratio 1:1, 1:2 and 1:3 of the viscous product were fired in a crucible in a furnace for 30 min at 900°C. This allowed the combustion of the alkylammonium chains to form white powders. These white powders were the end products and their characterization and properties are reported in the following chapters.

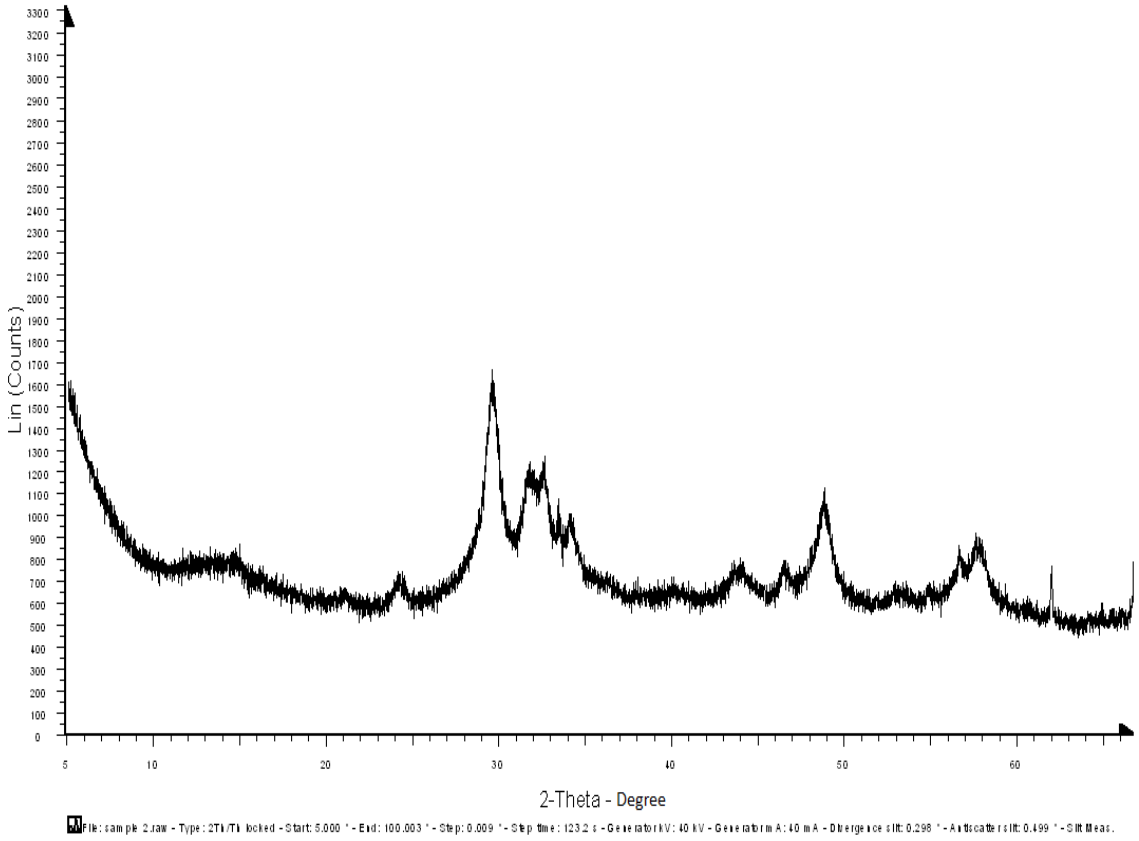

Figure 4.1 XRD of $C_{12}H_{25}NH_3Cl$ prepared from ethanol and than fired at 500°C.

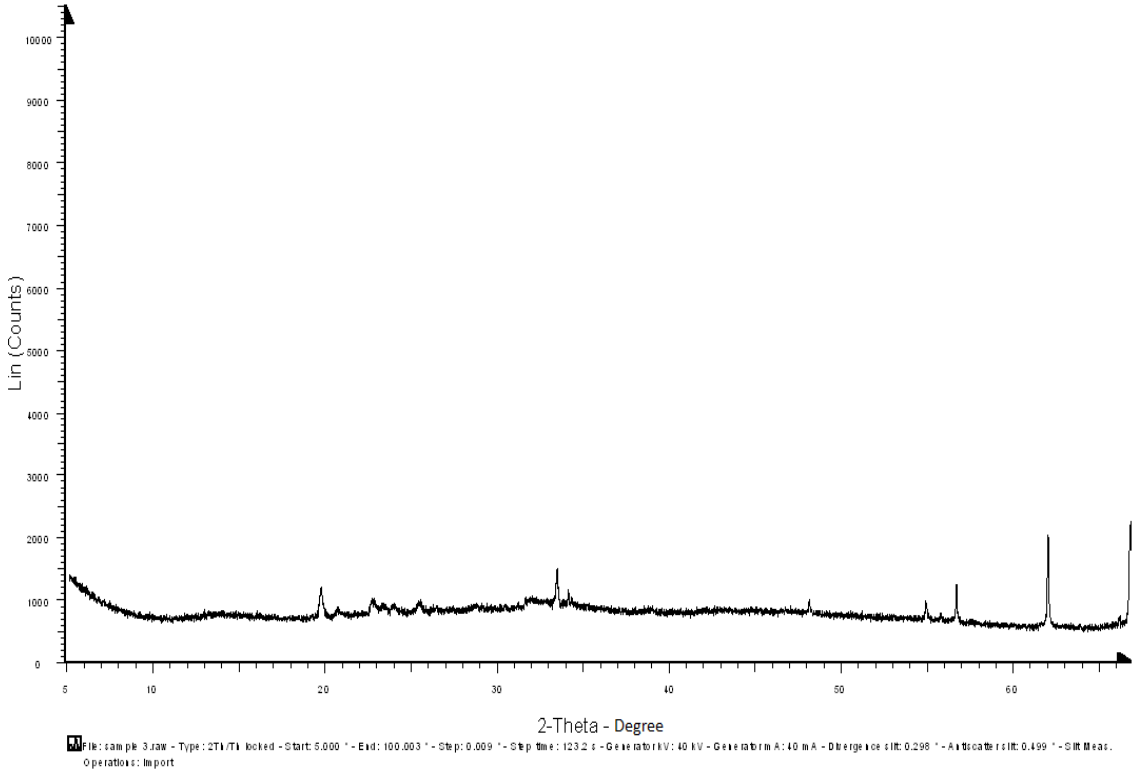

Figure 4.2 XRD of $C_{12}H_{25}NH_3Cl$ prepared from ethanol and than fired at 600°C.

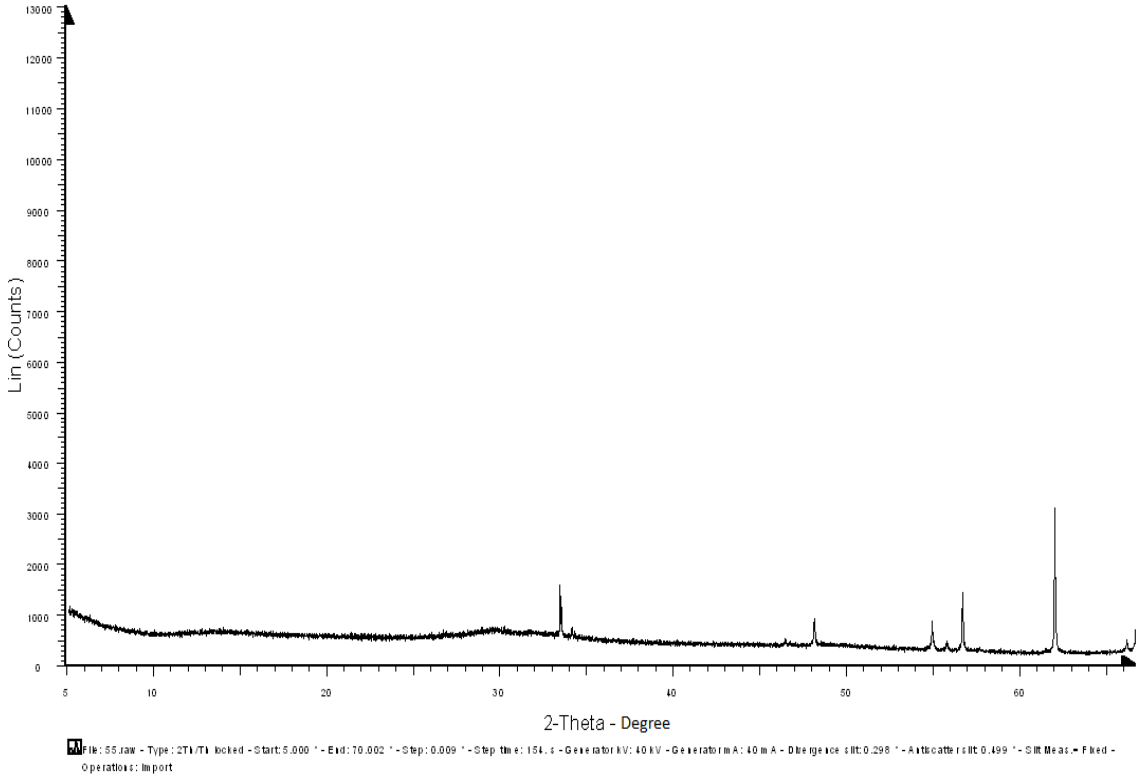

Figure 4.3 XRD of $C_{12}H_{25}NH_3Cl$ prepared from ethanol and than fired at 800°C.

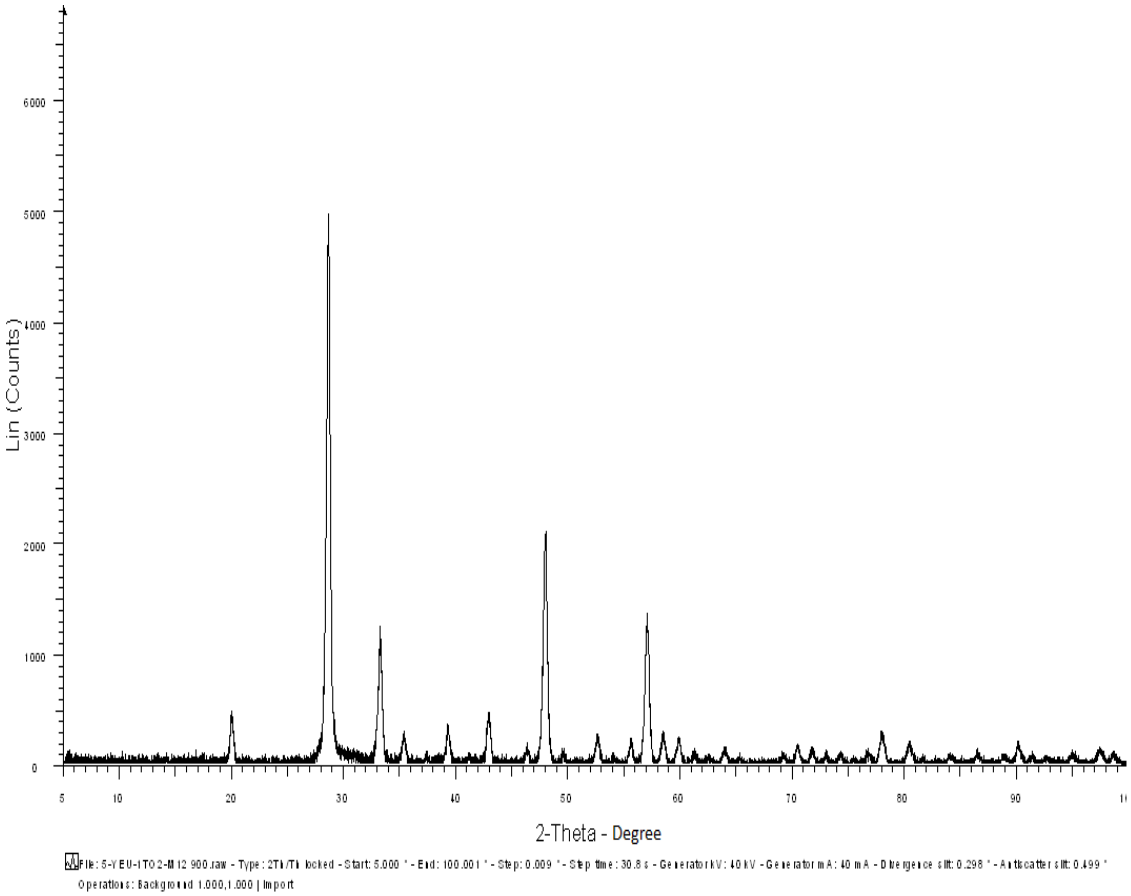

Figure 4.4 XRD of $C_{12}H_{25}NH_3Cl$ prepared from ethanol and than fired at 900°C.

References

[1] T.Ireland and J.Silver.”Facile self-assembly of yttrium oxide europium phosphor from Solution using a sacrificial Micellar phase”. Journal of the Electrochemical Society. 2, 1, 52-54, 1999.

[2] J. Silver. R. Withnall, K. Saltoun, T.G. Ireland and G.R. Fern. “A Study of Small Particle Yttrium Oxide Type Phosphors prepared from Solution using a Sacrificial Micellar Phase as a Combustion Fuel.” Proceedings of the 22nd International Conference on Raman Spectroscopy, (Boston, USA, August 8-13th August 2010).

Chapter Five

5.0 $Y_2O_3:Eu^{3+}$ phosphors from the [(Y, Eu)Cl_3] - ($C_{16}H_{33}NH_3Cl$) precursor materials

5.1 Introduction

Over the last fifteen years there has been continual interest on the synthesis and properties of phosphors made up of sub micrometer sized particles [1-20]. Our group and others have published widely on the urea homogeneous precipitation method of preparing the cubic $Y_2O_3:Eu^{3+}$ phosphor [2-18]. One of the problems with making such sub micrometer sized particles is that during annealing of the precursor particles at high temperatures (often necessary for good crystallite quality and hence emission properties) the particles tend to sinter. One way to partially alleviate this problem is to synthesise the particles as rapidly as possible at a high temperature. A method that has been explored for this purpose is combustion synthesis using an organic fuel that is ignited when a crucible or other vessel containing the phosphor precursors and the fuel is placed in a furnace that is already at 900°C. The fuel ignites and raises the temperature in the vessel very quickly. The first report [1] of facile self-assembly of the red emitting phosphor yttrium oxide europium ($Y_2O_3:Eu^{3+}$) from solution using a sacrificial micellar phase appeared in 1999. The micellar phase was assembled using the alkylammonium chloride salt ($C_{12}H_{25}NH_3Cl$) in an ethanolic solution. The resulting fine powder had smaller particles, ranging in size from 0.1 to 1.0 μm, than the commercial cubic $Y_2O_3:Eu^{3+}$ phosphor [1]. The results discussed in this chapter were obtained using a more sophisticated way to control the rate of crystallization of the phosphor particles. This was to vary the ratio of phosphor precursor to fuel ($C_{16}H_{33}NH_3Cl$). In theory the presence of more fuel around the phosphor precursor should facilitate/influence the combustion process and possibly lead to more crystalline products. In this chapter a longer chained alkylammonium hydrochloride ($C_{16}H_{33}NH_3Cl$) was used as fuel and now the affect of varying the ratio of this to the [(Y, Eu)Cl_3] precursor on the cathodeluminescence (CL) and photoluminescence (PL) properties of the resulting phosphors is discussed.

The following systems were studied;-

1. [Y,Eu]Cl_3 - ($C_{16}H_{33}NH_3Cl$) -6 experiments in the ratio of 1:1, 1:2, 1:3 with ethanol (3 samples fired at 650°C and 3 fired at 900°C).

2. [Y,Eu]Cl_3 - ($C_{16}H_{33}NH_3Cl$) -6 experiments in the ratio of 1:1, 1:2, 1:3 with methanol (3 samples fired at 650°C and 3 fired at 900°C).

Chapter 5 $Y_2O_3:Eu^{3+}$ phosphors from the [(Y, Eu) Cl_3]- ($C_{16}H_{33}NH_3Cl$)

5.2 Experimental

For the experimental technique the reader is referred to chapter 4 paragraph 4.4 experiments 8/8a. Preparations of [Y, Eu] Cl_3 - ($C_{16}H_{33}NH_3Cl$) n (for n = 1, 2, 3) were carried out with ethanol and methanol. The muffle furnaces used in the preparations though having chimneys for waste gases to pass through did not have air circulation other than the chimneys. The furnace used for the phosphor samples prepared from ethanol fired at 900°C samples (D, E and F) had a chimney with a diameter of 3 cm, whereas that used for the three repeat combustions samples 54, 55 and 56 had a diameter of 1 cm, and this is important in understanding the synthesis of monoclinic $Y_4O_5Cl:Eu^{3+}$ which is a fairly new phosphor. Attenuated total reflectance (ATR)-Fourier transform infrared (FTIR) spectra were obtained using a Perkin Elmer Spectrum One FTIR spectrometer. Raman spectroscopy was performed in order to probe the structure and composition of the lattices [21]. The spectra were obtained using a Horiba Jobin Yvon Labram HR spectrometer in conjunction with an Olympus BX40 microscope to facilitate the examination of particles of micrometre dimensions. The exciting radiation was provided by a helium-neon laser operating on the 632.8 nm line and the Raman scattered light was measured with a Peltier-cooled CCD detector after the Rayleigh line had been rejected by a notch filter (see chapter 3 paragraph 3.6). The crystalline phases of the products were determined by X-ray powder diffraction (XRPD) using a Bruker D8 Advance X-ray powder diffractometer fitted with a nickel-filtered copper source and a LynxEye™ silicon strip detector (for details see chapter 3 ref 32). Data were recorded from 5 to 100 2θ° at 20°C. The diffractometer was previously calibrated using an aluminium oxide line position standard from Bruker and LaB_6 NIST SRM 660a line profile standard. The emission of the nickel filtered Cu source and hence the instrumental line broadening was determined by fitting the NIST standard using Bruker Topas version 3. Phases in the combusted products were identified from the XRD patterns by peak search matching using the ICCD PDF-2 data files. The identifiable phases were refined using Bruker Topas version 3. Their degree of disorder/order and their crystallite sizes were also studied [22]. Diffractograms were collected using the fired powders in a conventional holder, or mounted on an aluminium pin stub or on an aligned silicon substrate [23, 24].Field emission scanning electron microscopy (FESEM) was used to study the microstructure of the samples using a Zeiss Supra VP 35 instrument. The samples were mounted on carbon tabs attached to aluminium pin stubs and sputter coated with a thin conducting layer of gold. The PL excitation and emission spectra were obtained using a Bentham (Reading, UK) M300 programmable spectrophotometer equipped with a 1800 lines/mm grating with computer controlled wavelength scanning and

intensity data collection. The stepping motor and sine drive allow wavelength scanning to be completely controlled from a remote stepping drive unit (SMD3B). Samples for excitation and emission were contained inside an in-built sealed chamber connected to the M300 monochromator via a fibre-optic bundle. The CL measurement data and spectra were undertaken using a high-vacuum (5×10^{-7} Torr) chamber with a Kimball Physics Inc. (Walton, USA), model EGPS-7 electron gun. The CL luminance measurements were obtained by means of a Jeti spectroradiometer (Specbos 1201, Jeti Technische Instrument GmbH, Jena, Germany). The phosphor screens were excited with electron beam energies from 1000 to 5000V, and emission currents from 1.1 to 9.8μA/cm^2, with an electron beam spot size of 9 mm for defocused measurements and 1.41 mm for the focussed measurements. For some of the samples, CL emission and excitation spectra were obtained using the Bentham system previously described except that the fibre optic bundle was disconnected from the in-built sealed chamber and attached to a telescope (TEL 301D).For the CL luminance measurements and spectra of the prepared samples phosphor screens were prepared in the following manner. After cleaning the aluminium pin stubs in an ultrasonic bath containing ethanol, followed by drying in an oven at a temperature of 100°C they were weighed. A stub was then placed in an electrochemical cell containing an ultrasonically dispersed solution of the phosphor powder (0.5g), in an electrolyte solution of magnesium nitrate (0.075g/L) and isopropanol (50ml). The stub was positioned with its flat surface forming a meniscus with the surface of the phosphor/electrolyte solution and also acting as an electrode, the counter electrode being a strip of magnesium ribbon. A field of 300V was applied facilitating the coating of the stub by electrode position. This procedure was repeated until all the stubs were coated with 3mg (±0.1mg) of phosphor. After drying the stubs at 100°C they were introduced into the vacuum chamber for CL measurements.

5.3. Results and Discussion

5.3.1. Appearance of Products prepared with methanol and ethanol at temperatures of 650°C.

5.3.1.1 Sample appearance:- Products (samples) prepared with methanol and ethanol at a temperature of 650°C were observed to be light grey in colour, where as the samples prepared at 900°C were all white powders. Under 254nm excitation the samples prepared at 650°C displayed a weak red luminescence which was in contrast to the strong red luminescence from the samples prepared at 900°C that is

characteristic of the Eu^{3+} ion in cubic Y_2O_3. The strongest red luminescence comes from 1:3 material sample ratios.

5.3.1.2 SEM Studies: - Firstly the samples prepared from methanol and ethanol at 650°C. In Figure 5.1 FESEM micrographs of $Y_2O_3:Eu^{3+}$ phosphor samples annealed at 650°C prepared from metal chloride to alkylammonium chloride ratios of 1:1 (a and b), 1:2 (c and d) and 1:3 (e and f) in methanol are presented. It can be seen that a number of morphological forms are present, the variety of these forms increase with higher alkylammonium chloride (micelle) concentration. This is evident from the images of the material formed from the 1:1 ratios in Figure 5.1a and b where large straw-like sheets are shown to be formed from intergrowths of thin needles that have dimensions of approximately 20 to 30nm in width by 200nm in length. The material prepared from the 1:2 ratios presented in Figure 5.1 c and d have needles that have formed into slightly rounded structures. Progressing to the final SEMs in Figure 5.1 of the material prepared from the 1:3 ratios; they show the micelles have left behind evidence of their existence as tubules; these structures have assembled into large lamellar sheets that in these images are two structural units in thickness. The spherical, tubular and lamellar structures display remnant micellar morphologies, although they are much larger in dimensions than those that are commonly associated with micelles. Nevertheless it is obvious that the samples heated to 650°C retain morphological structures that were caused by the organic sheaths that formed around their inorganic precursors in the original methanolic solutions. It can be seen in Figure 5.1(b and d) that the crystallites are all small with one or more dimensions less than 50nm. In Figure 5.2A and 5.2B, FESEM micrographs of samples annealed at 650°C prepared from metal chloride to alkylammonium chloride ratios of 1:1 (a and b), 1:2 (c and d) and 1:3 (e and f) in ethanol are presented. Again it can be seen that a number of morphological forms are present, and again the variety of these forms increase with higher alkylammonium chloride (micelle) concentration. This is evident from the images of the material formed from the 1:1 ratios in Figure 5.2a and b where large straw-like sheets are shown to be formed from intergrowths of thin needles that have dimensions of approximately 20 to 30nm in width by 200nm in length. Progressing to the final SEMs in Figure 5.2B of the material prepared from the 1:3 ratios; they also show the micelles have left behind evidence of their existence as tubules; these Structures have assembled into large lamellar sheets that in these images are two structural units in thickness similar to those observed in Figure 5.1.

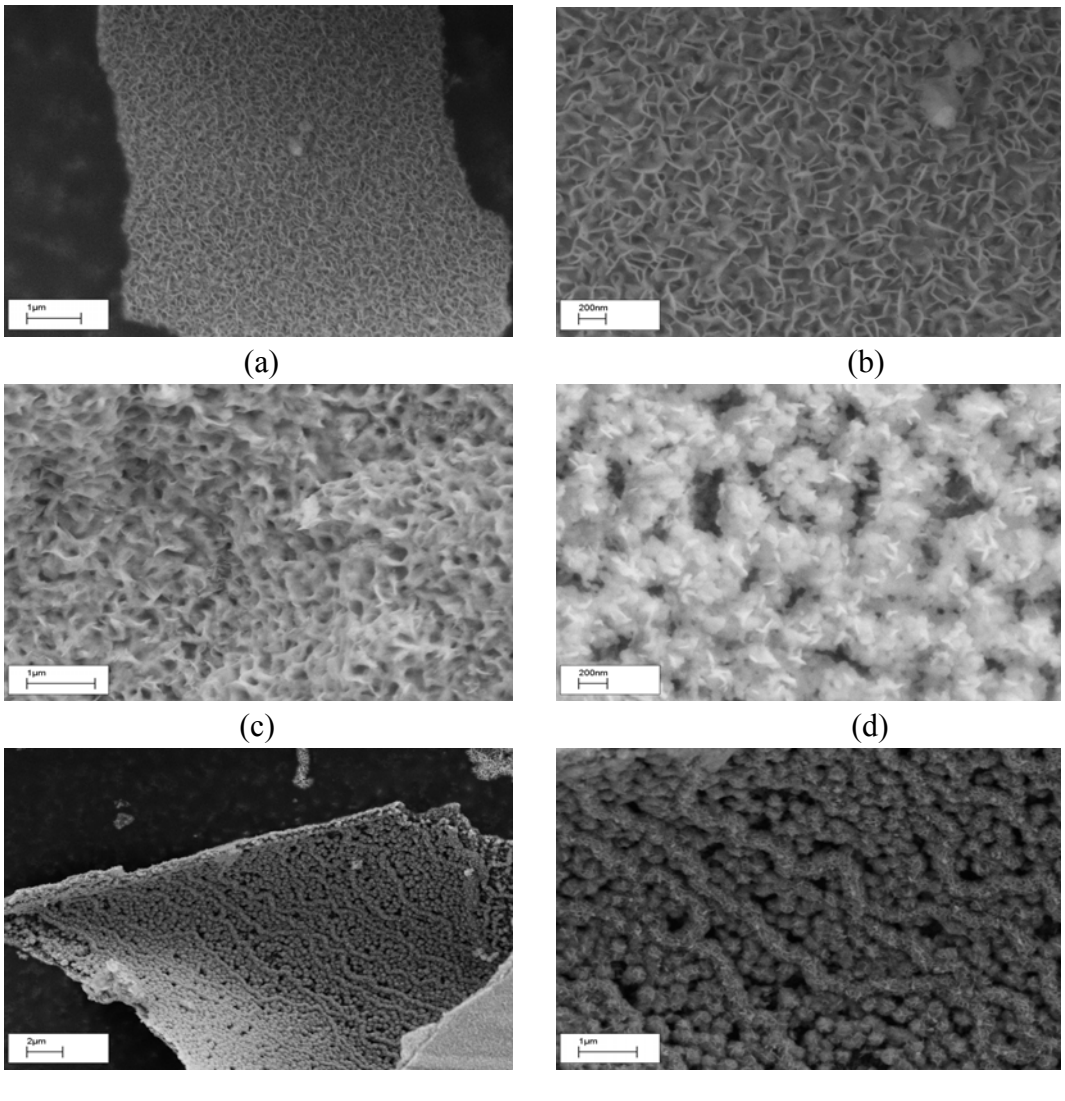

Figure 5.1 FESEM micrographs of phosphor samples fired at 650°C prepared from methanol at metal ion to alkylammonium chloride ratios of (a and b) 1:1, (c and d) 1:2, (e and f) 1:3, In a, c and f the bar is 1μm, and in b and d it is 200nm and in e it is 2 μm.

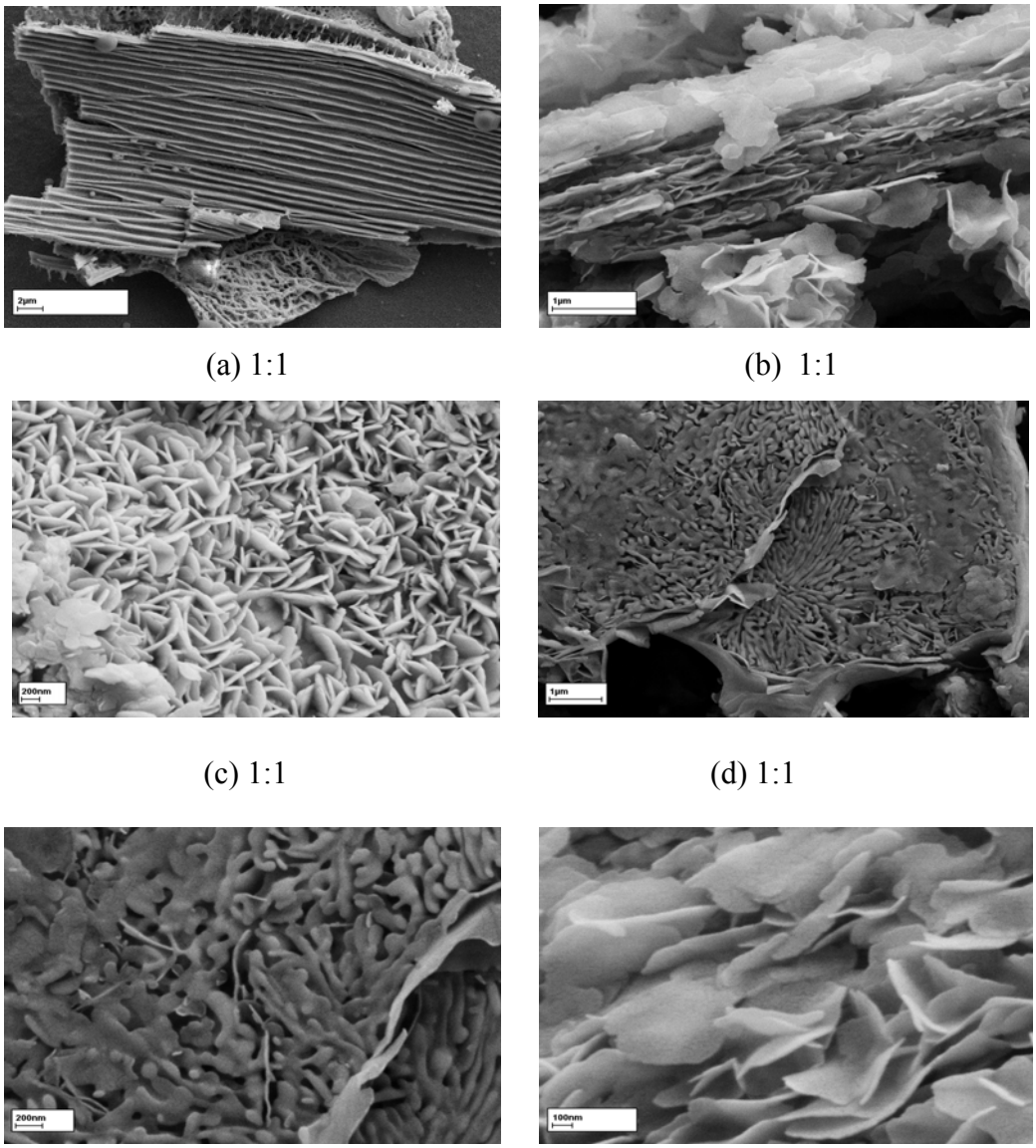

(a) 1:1 (b) 1:1

(c) 1:1 (d) 1:1

(e) 1:1 (f) 1:1

Figure 5.2A FESEM micrographs of phosphor samples fired at 650°C prepared from ethanol at metal ion to alkylammonium chloride ratios of:- (a,b,c,d,e, and f.) 1:1.In a, the bar is 2 µm, in b and d it is1µm, in c and e it is 200nm and in f it is 100nm.

Structures have assembled into large lamellar sheets that in these images are two structural units in thickness similar to those observed in Figure 5.1. In many of the SEMs presented in Figures 5.2A and 5.2B it can be seen that there is evidence of structures where the surfaces appear to be smooth suggesting they neared meltdown this is thought to be due to the presence of ethanol rather than methanol (see Figure 5.1) driving the surface temperature higher during the synthesis. It is only a surface

effect as the XRPD data (see below) show no evidence for the high temperature cubic $Y_2O_3:Eu^{3+}$ phase.

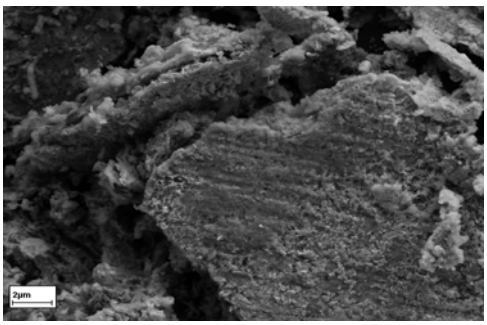

(g) 1:2

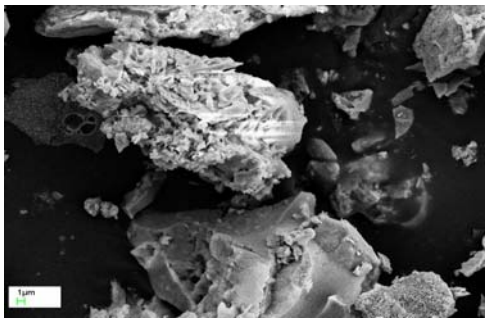

(h) 1:2

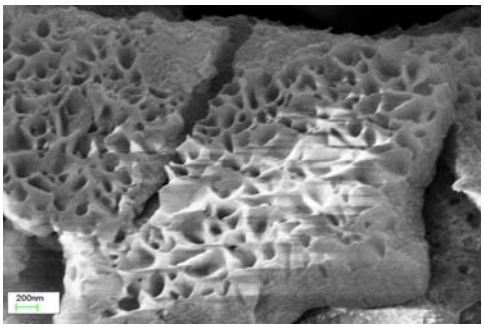

(i)1:2

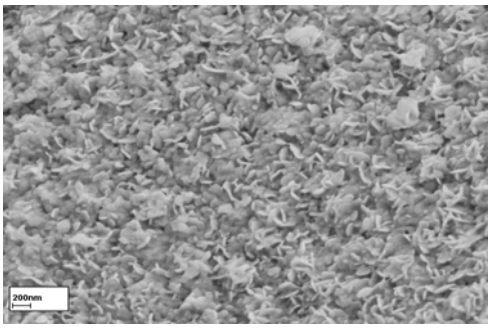

(j) 1:3

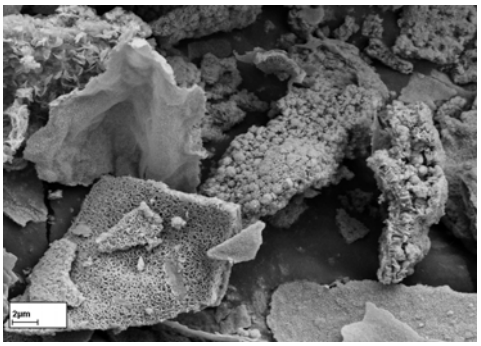

(k) 1: 3

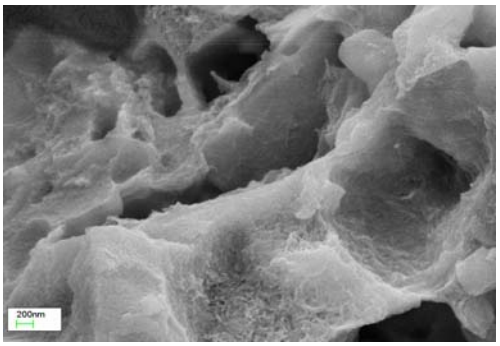

(l) 1:3

Figure 5.2B FESEM micrographs of phosphor samples fired at 650°C prepared from ethanol at metal ion to alkylammonium chloride ratios of:- (g,h and i) 1:2 and (j, k and l) 1:3. In h the bar is 1µm, in i, j and l it is 200nm. In g and k it is 2 µm.

5.3.2 Sample structures (from XRPD data):-

The XRPD diffractograms of the samples that were produced under the 650°C conditions from the methanolic solutions (1:1, 1:2 and 1:3 ratios) are shown in Figures 5.3a-c. At first sight they point to the presence of a large amount of amorphous material. However, it is clear from transmission electron microscopy that the samples contain a large amount of crystalline material of 1-5 nm dimensions. Tetragonal YOCl was considered as a candidate material for the product; since these were carried out thermogravimetric analysis of YCl_3 to show that it decomposes to tetragonal YOCl when heated in air at 650°C which is also consistent with the literature (see section 5.4.5 Thermal methods). However, fits of the XRPD data for the samples produced from metal ion to alkylammonium chloride ratios of 1:1, 1:2 and 1:3 clearly indicated that the products were not tetragonal YOCl [25,26], but were nanocrystalline rhombohedral YOCl [27] instead (see Figures 5.3a-c). The experimental XRPD diffractograms are shown by the grey traces, which are superimposed on the fits, shown by a solid black line, in each case. The residuals of a subtraction of the fit from the experimental data are given below the superimposed fit/data traces in each case. The fits of the XRPD diffractograms for the products resulting from the 1:1 and 1:3 metal ion to alkylammonium chloride ratios (see Figures 5.3a and 5.3c) give crystallite sizes of 1.0 and 0.9 nm, respectively. It is apparent that the very broad reflections in these diffractograms arise from extremely small crystallite sizes of the rhombohedral YOCl. The diffractograms obtained from the product of the combustion of the precursor having a 1:2 metal ion to alkylammonium chloride ratios (see Figures 5.3b) also exhibits sharper reflections at 2θ values of 10.3 and 35.4°. A Pawley fit of this diffractograms (see Figure 5.3b) indicates the presence of rhombohedral YOCl with two different average nanocrystallites sizes, one (43 wt. %) having a very small dimension of 1.5 nm giving rise to very broad reflections and the other (57 wt. %) having a larger dimension of 27.9 nm giving rise to sharper reflections. Broadening of lines in an XRPD diffractograms to a similar extent was reported previously for ZnS: Mn quantum dots and the crystallite sizes were reported to be 1.5 nm from fitting the XRPD data [28]. There was no evidence for cubic $Y_2O_3:Eu^{3+}$ in these data. In the samples prepared from ethanol (Figure 5.4) there is evidence of different crystalline phases from that prepared from methanol, and again there is evidence of amorphous material. Again there was no evidence for cubic $Y_2O_3:Eu^{3+}$ in these XRPD plots. The data in fact fit two phases of YOCl and there is evidence for a third material that is found in more abundance in the material fired at 900°C (see further on in this chapter) which is $Y_4O_5Cl_2$ see Table 5.1. All of these chloride containing phases were unexpected and will be discussed in detail further on in this chapter.

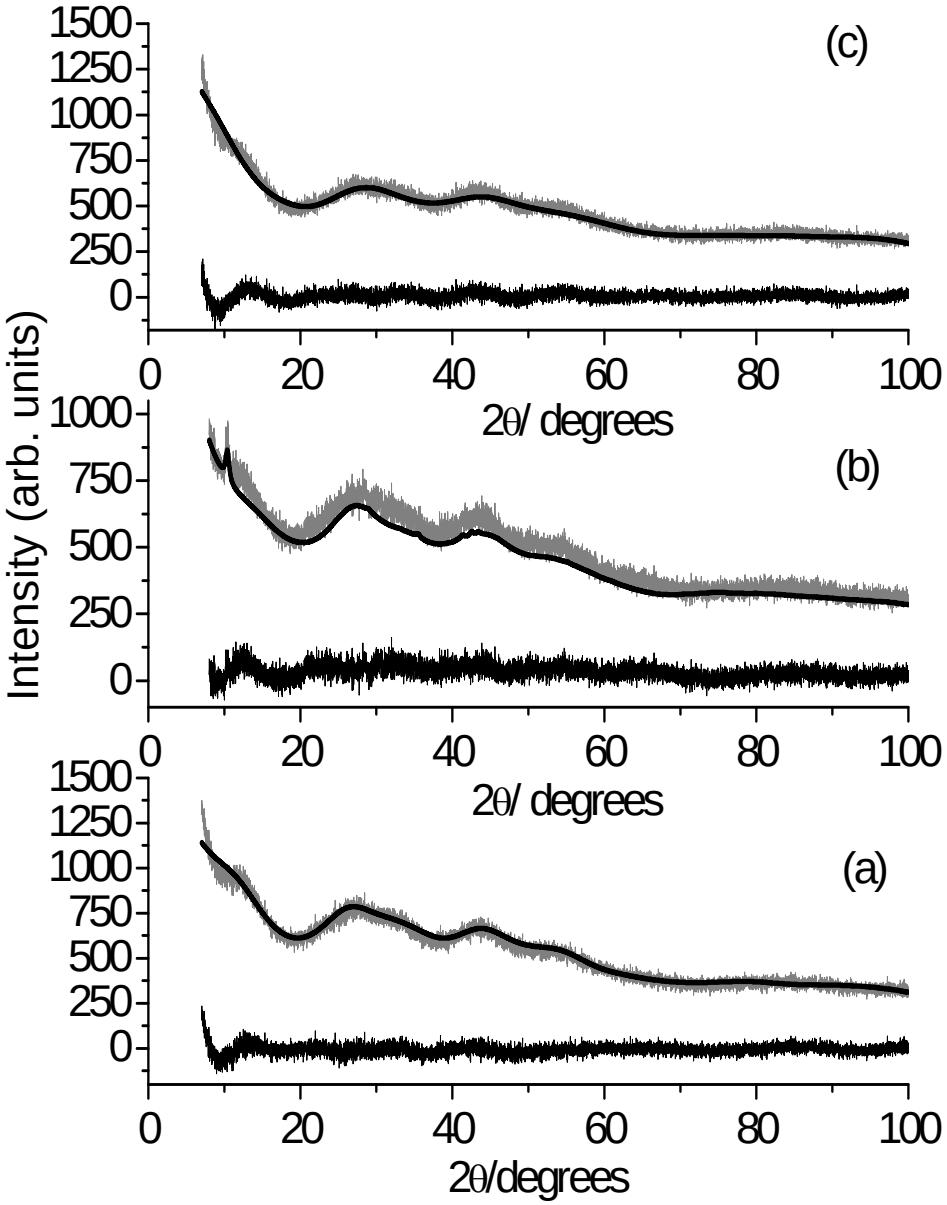

Figure 5.3 XRPD diffractograms of the [Y,Eu]Cl_3 - ($C_{16}H_{33}NH_3Cl$) samples annealed at 650°C, metal ion to alkylammonium chloride ratios: (a) 1:1, (b) 1:2, and (c) 1:3 all prepared from methanolic solution.

Chapter 5 $Y_2O_3:Eu^{3+}$ phosphors from the $[(Y, Eu)\ Cl_3]$- $(C_{16}H_{33}NH_3Cl)$

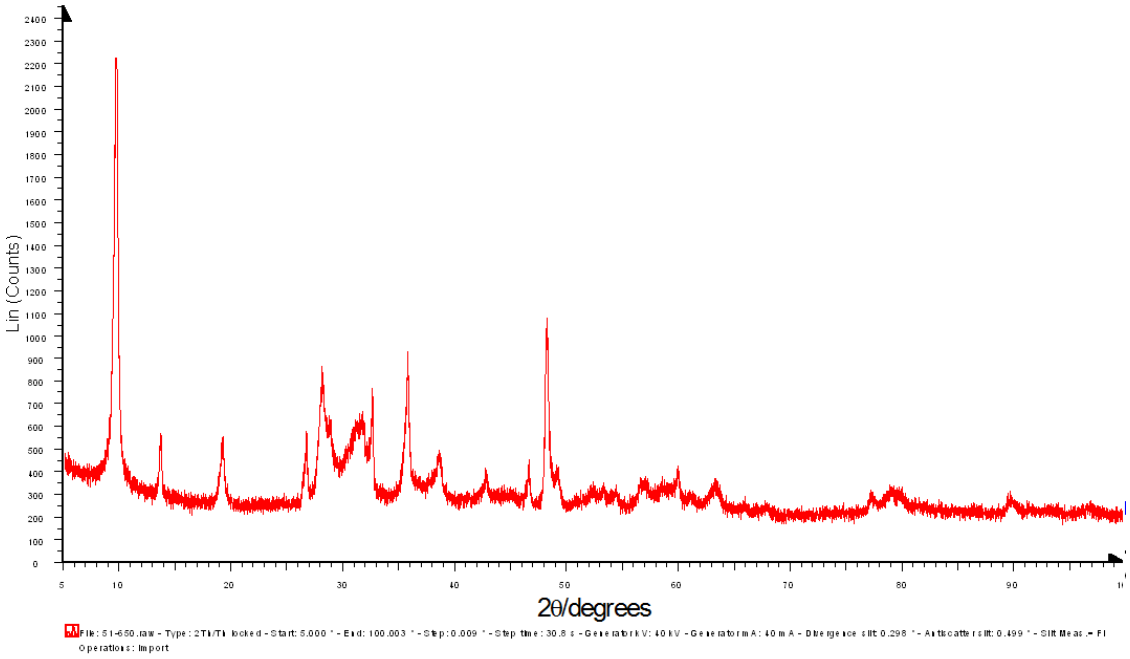

Sample 51

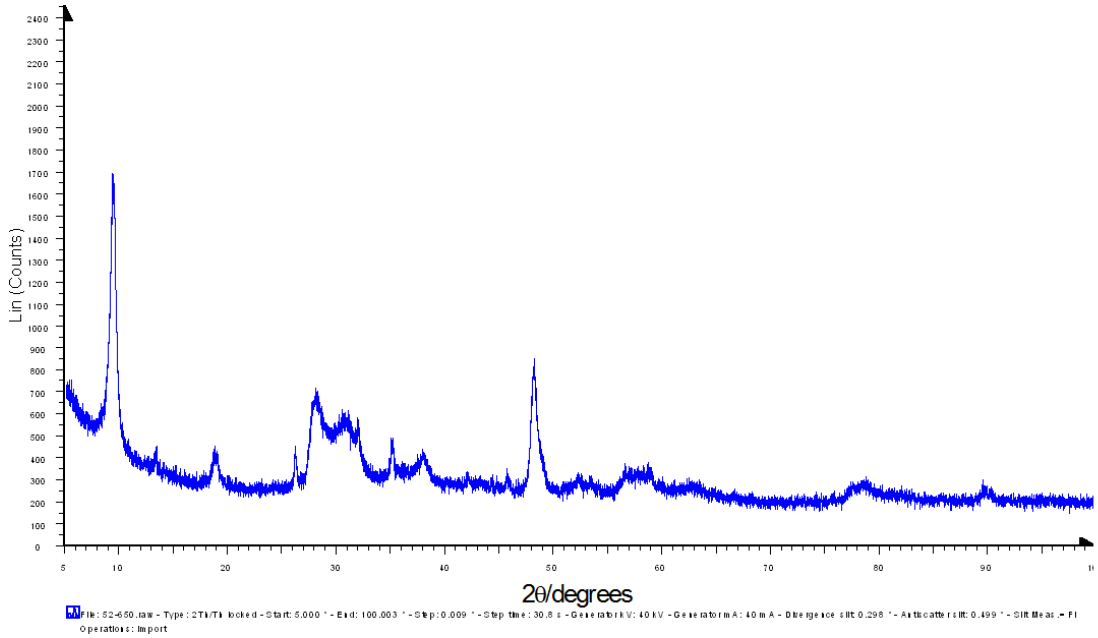

Sample 52

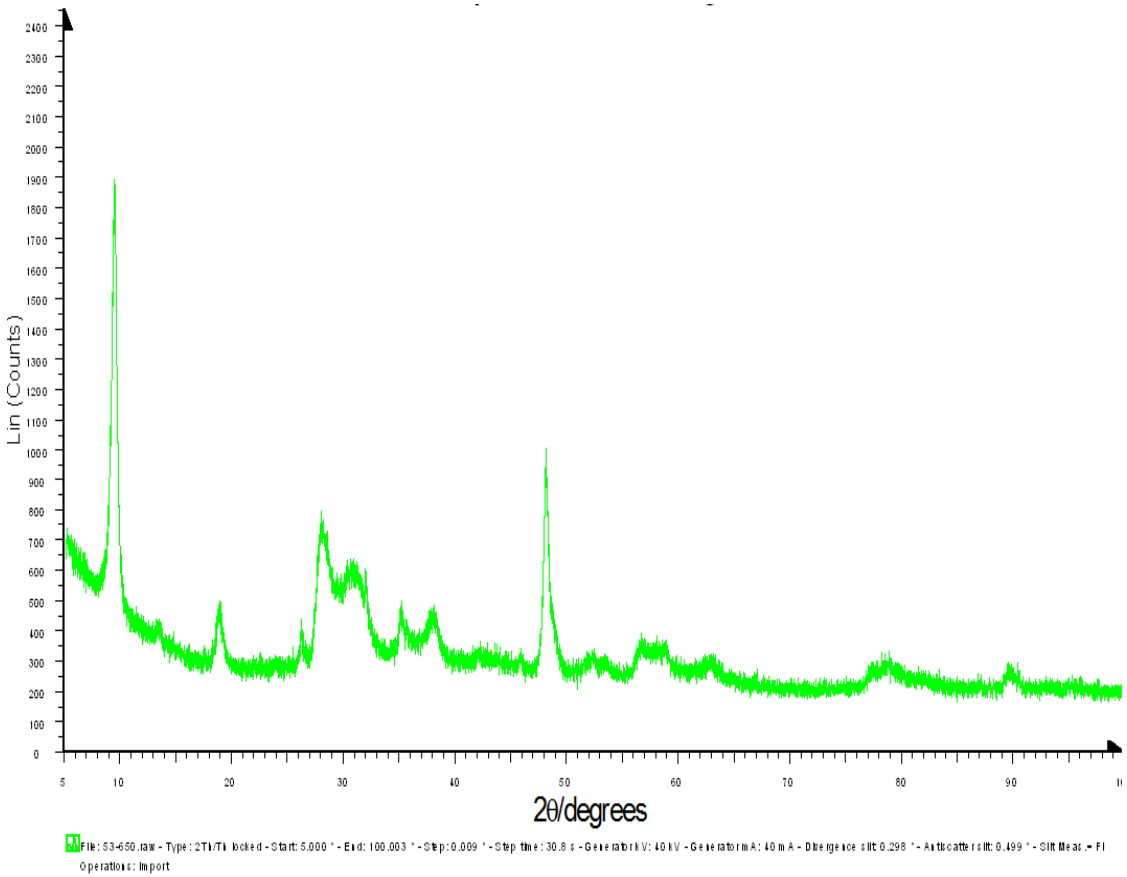

Sample 53

Figure 5.4 XRPD diffractograms of the samples [Y,Eu]Cl_3 - ($C_{16}H_{33}NH_3Cl$) annealed at 650°C, prepared from ethanolic solution, metal ion to alkylammonium chloride ratios; 1:1 (red), 1:2 (blue) and 1:3 (green).

Table 5.1 Cell parameters for the yttrium oxy chloride phases found in the materials fired at 650°C prepared from ethanol.

	1:1	1:2	1:3
Yttrium oxide chloride YOCl P4/nmm	a= 3.90533(35)(Å) c= 6.5983(10) (Å)	a= 3.87830(84)(Å) c= 6.36665(Å)	a= 3.8777069 (Å) c= 6.3869142 (Å)
Yttrium oxide chloride YOCl R-3m	a= 3.78237(59)(Å) c= 28.0580(34)(Å)	a= 3.72307(Å) c=28.04235(Å)	a= 3.7693671(Å) c= 28.0829709(Å)
$Y_4O_5Cl_2$ Phase	a= 6.5148(11)(Å) b= 6.3856(10)(Å) c=14.5917(27)(Å) beta= 96.000(15)	a= 6.50651(Å) b= 6.36498 (Å) c= 14.51618(Å) beta= 96.1856	a= 6.5269740(Å) b= 6.3742656(Å) c=14.5525525(Å) beta= 96.08302
Yttrium oxide chloride YOCl P4/nmm [25]	a= 3.903(2) c= 6.597 (4)		
Yttrium oxide chloride YOCl P4/nmm [26]	a= 3.900(2) c= 6.604(2)		
Yttrium oxide chloride YOCl R-3m [27]	a= 3.7895 (5) c= 28.03 (1)		

5.3.3 Photoluminescent Spectra: - The PL excitation and emission spectra of the samples prepared at 650°C from methanolic solutions using 1:1, 1:2 and 1:3 ratio products are displayed in Figure 5.5. They support the XRPD data; they have similar spectral features of varying intensities yet they are different to that of cubic $Y_2O_3:Eu^{3+}$. The excitation spectra of all the above products have low intensity with the strong, broad Eu^{3+} - O^{2-} charge transfer band observed around 250nm in cubic $Y_2O_3:Eu^{3+}$ being particularly weak, the bands at 395 and 462nm are other prominent features in

these excitation spectra. In the very weak emission spectra of these samples, the strong, sharp emission band at 611nm in cubic $Y_2O_3:Eu^{3+}$ due to the $^5D_o \rightarrow {}^7F_2$ transition is observed only in the spectrum of the 1:1 ratio sample, and is absent for the higher ratio samples where a broader band centred at approximately 615nm is seen. Also absent in all three samples are the set of emission peaks with a maximum at 709nm due to the $^5D_o \rightarrow {}^7F_4$ of the Eu^{3+} ion in cubic Y_2O_3. The ratio of the bands around 630nm and 700nm compared to those in figure 5.6 below are in agreement with the different crystalline phases present in Figures 5.3 and 5.4. The predominant emission bands in Figure 5.6B are located around 630.5 nm and are shape and more intense than those in Figure 5.5b. This value agrees well with literature values for YOCl [28, 29, 30]

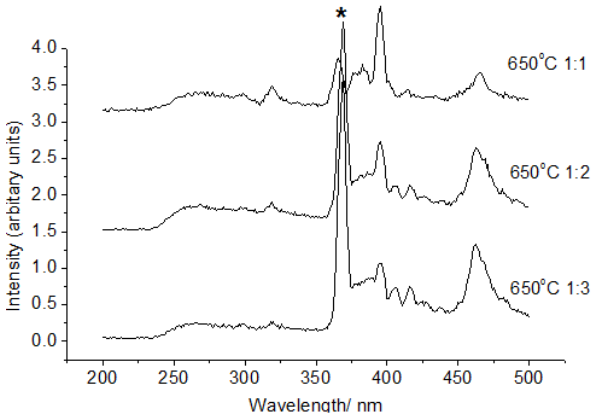

(a)

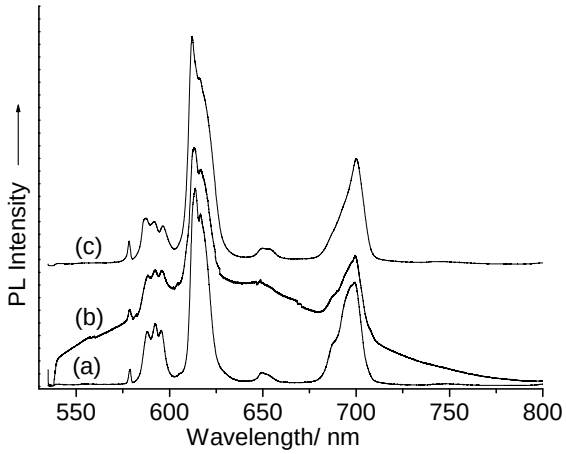

(b)

Figure 5.5 **(**a) Photoluminescent excitation spectra obtained by monitoring the emission at 615 nm, and (b) emission spectra of the 650°C samples from methanolic solution, excitation wavelength 254nm.

In Figures 5.6A and 5.6B the PL excitation and emission spectra of the samples prepared at 650°C using 1:1, 1:2 and 1:3 ratio products prepared in ethanol are displayed. They support the XRPD data; their excitation spectra are all similar and are different to those in Figure 5.5 in addition their emission spectra manifest similar features with some simplification in the 1:2 and 1:3 ratio products. However in all cases the emission spectra in Figure 5.6 manifest much sharper lines than those in Figure 5.5 As these spectra originate near the surfaces of the material they may hold a clue to the surface phase that was seen to be present in the SEMs in Figure 5.2. There are some small peaks around 611 in all three emission spectra in Figure 5.6 which may indicate the presence of a small amount of cubic $Y_2O_3:Eu^{3+}$. As stated above the differences between Figures 5.5 and 5.6 are in agreement with the different crystalline phases present in Figures 5.3 and 5.4. The predominant emission bands in Figure 5.6B are located around 620.5 nm, and the intensities of the emissions in this area are much greater than those around 700nm, this is again in keeping with the presence of $Y_4O_5Cl_2$.

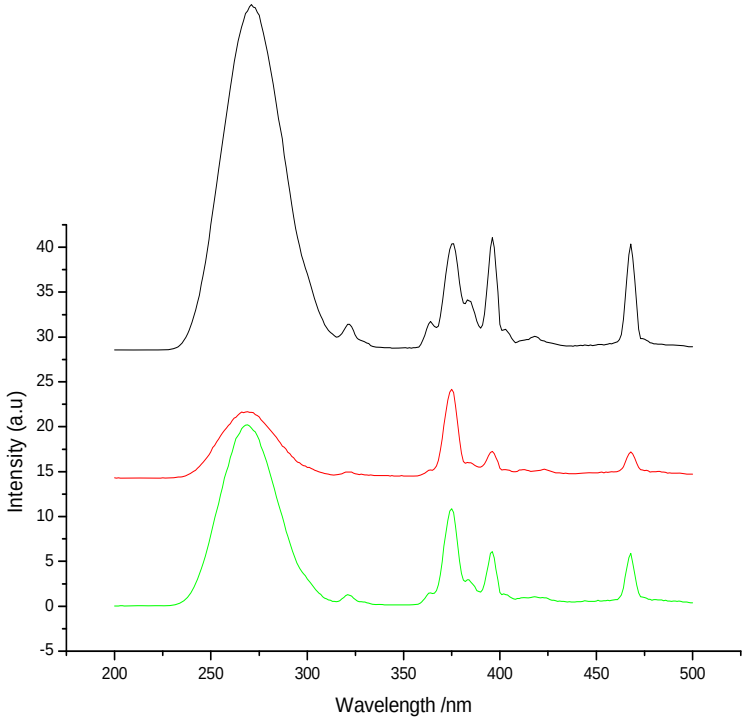

Figure 5.6A An overlay of the photoluminescent excitation spectra of the 650°C samples prepared from ethanolic solution obtained by monitoring the emission at 615 nm. Excitation spectra 1:1 (Black) Top, 1:2 (Red), and 1:3 (Green) (monitored at 627nm).

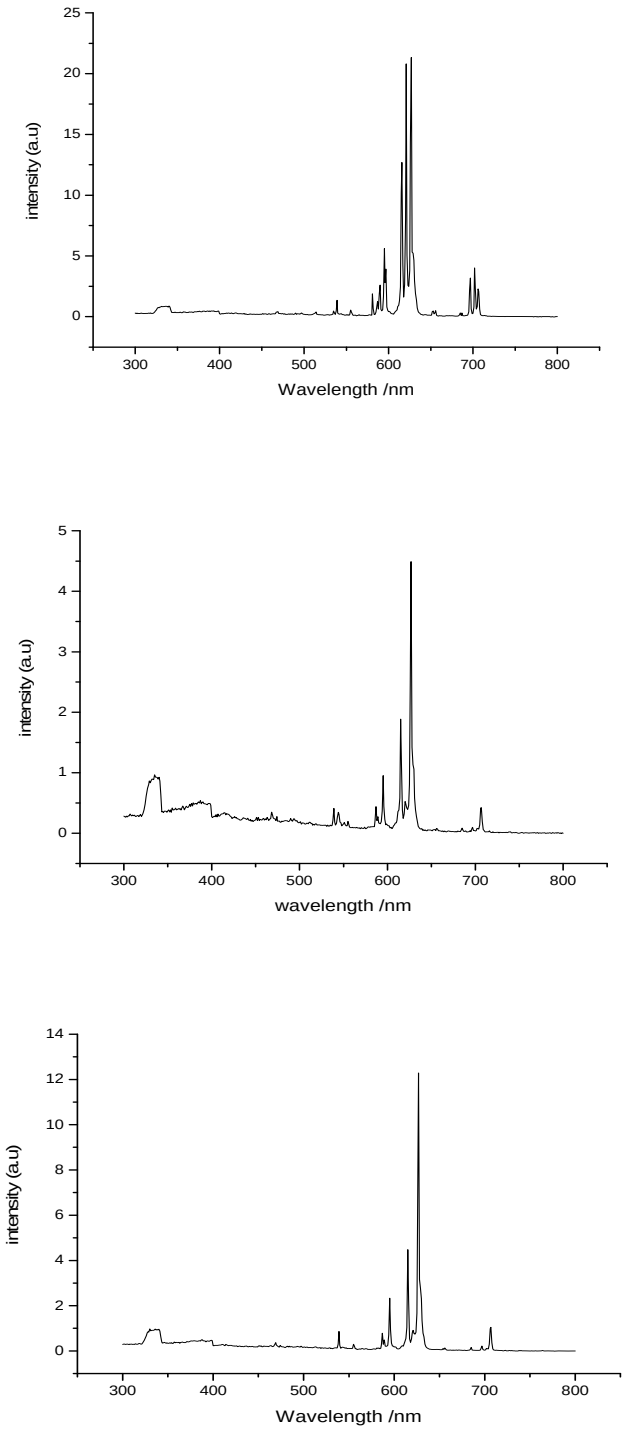

Figure 5.6B Photoluminescent emission spectra of the 650°C samples prepared from ethanolic solution, emission spectra 1:1 (Top), 1:2 (Centre), 1:3 (Bottom). Excitation wavelength 254nm.

5.3.4 Cathodoluminescence Spectra:-

The CL (5000V, emission current 9.6μA) spectra of the samples prepared from methanolic solution at 650°C using the products produced from the 1:1, 1:2 and 1:3 ratios, presented in figure 5.7 are shown to be different with the 1:3 products being closest to that of the cubic phase using defocused and focussed electron beams respectively. The CL data are the only data that show convincing evidence of the presence of cubic phase material in the samples fired at 650°C. This could be due to the high sensitivity of Cl to cubic Y_2O_3, but it is also more likely that nanoparticles of a precursor phase convert to cubic Y_2O_3 in the electron beam, (that is, the electron beam has sufficient energy to convert these particles into the cubic phase). The sample prepared from the 1:3 reactant ratios showed almost complete conversion to the cubic phase, on account of this sample containing more fuel (a larger proportion of alkylammonium cations) and was probably close to complete conversion to the cubic structure even when fired at 650°C.These observations can be rationalised by a transformation from YCl_3 to Y_2O_3 proceeding via mixed oxychloride species having an increasing O:Cl stiochometric ratio, as shown in equation (1):

$$YCl_3 \rightarrow \text{“YOCl”} \rightarrow \text{“2YOCl.}Y_2O_3\text{”} \rightarrow \text{“YOCl.}Y_2O_3\text{”} \rightarrow Y_2O_3 \qquad (1)$$

Clearly, the higher the combustion temperature, the greater the O:Cl stoichiometry of the products, as the transformation shown by equation (1) proceeds. This explains why the sample prepared from the 1:3 reactant ratios showed almost complete conversion to cubic Y_2O_3, since this sample contained more fuel (a larger proportion of alkylammonium cations) thus enabling a higher combustion temperature to be attained. This transformation from YCl_3 to Y_2O_3 is consistent with literature reports of rare earth oxychloride species that have identical stoichiometries to the intermediates shown in equation (1). In fact, the “YOCl” species has been reported as a compound crystallising in both PbFCl and YOF-type structures [31, 32]. Furthermore, both $Y_4O_5Cl_2$ (≡ “2YOCl.Y_2O_3”) [33] and Y_3O_4Cl (≡“YOCl.Y_2O_3”) [34, 35] have also been reported. The Cl (5000V, emission current 9.6μA) spectra of the samples prepared from ethanol at 650°C using the products produced from the 1:1, 1:2 and 1:3 ratios are presented in Figures 5.8A and B. The spectra obtained using the focussed beam are all simplified compared to the defocused beam and in all three cases there is a little evidence of the cubic phase being formed in the beam.

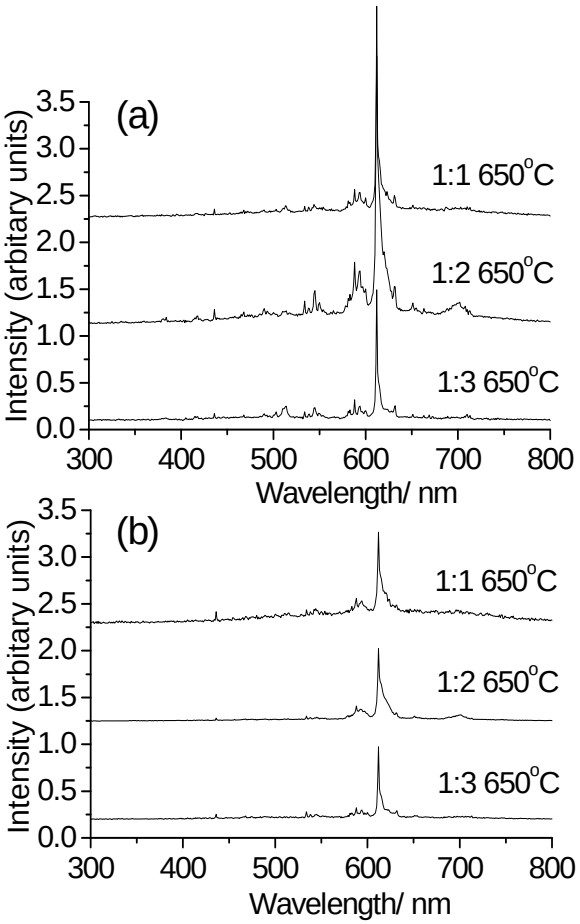

Figure 5.7 Cathodoluminescent spectra of the 650°C samples prepared from methanol: (a) defocused beam and (b) focused beam.

This may be due to formation of some cubic $Y_2O_3:Eu^{3+}$ in the focused electron beam. Again as in the methanol samples (Figure 5.7) the Cl data are the only data that show convincing evidence of the presence of cubic phase material in the samples fired at 650°C. Again this may mean that the Cl is more sensitive to the cubic phase or may be due to the conversion of the samples to cubic in the electron beam. Again this is because the samples are made up of very small particles of a precursor phase to that of the cubic $Y_2O_3:Eu^{3+}$ phosphor and the electron beam having sufficient energy to convert these particles into the cubic phase. The fact that the defocused beam results are similar to those of the photoluminescent emission spectra is in keeping with the presence of YOCl.

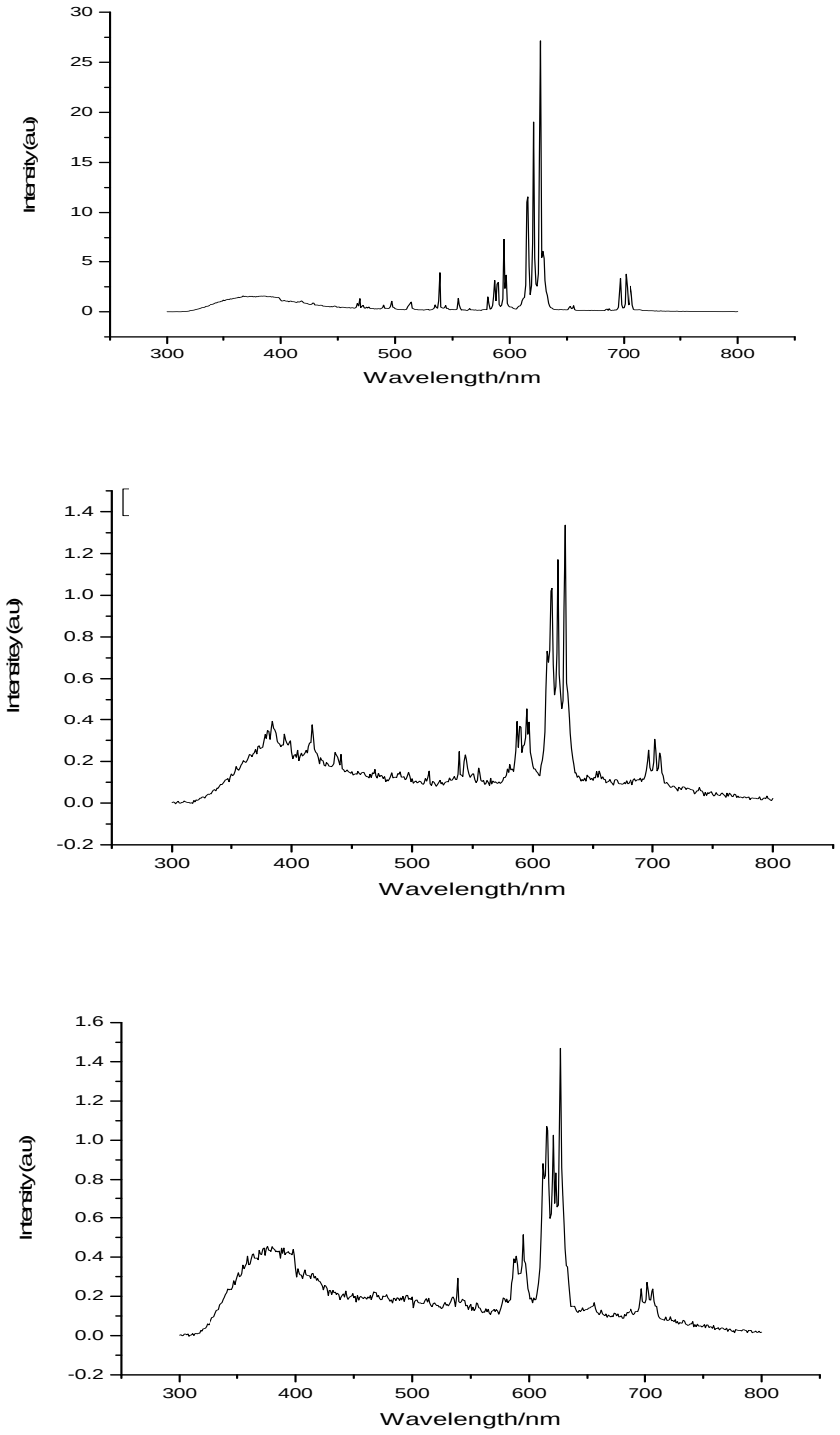

Figure 5.8A Cathodoluminescent spectra of the 650°C samples prepared from ethanolic solution; defocused beam, 1:1 (Top), 1:2 (Centre), 1:3(Bottom), at 5000V and 50uA.

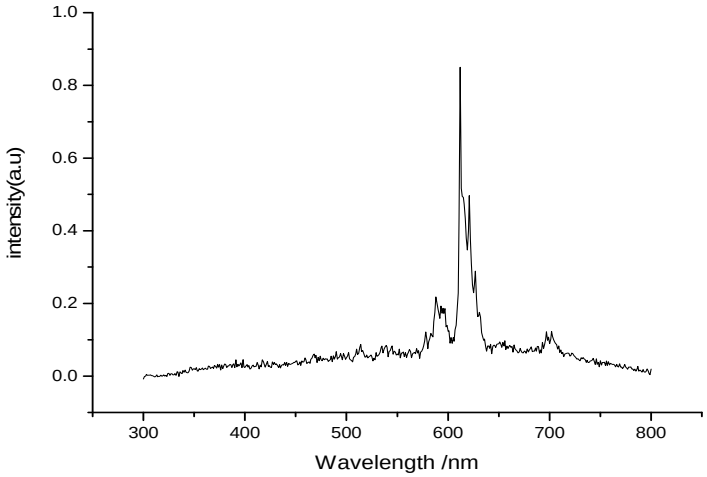

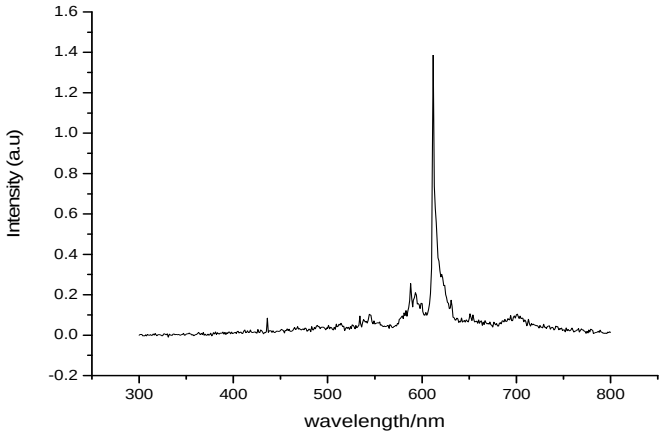

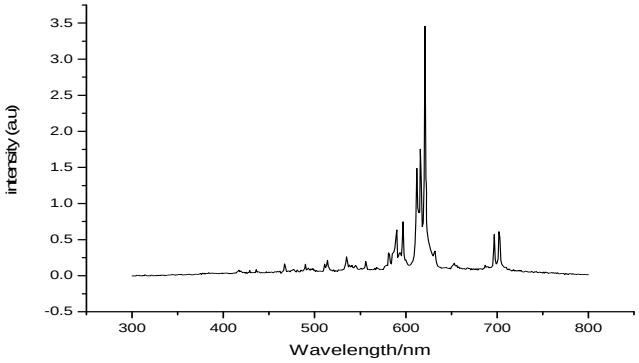

Figure 5.8B Cathodoluminescent spectra of the 650°C samples prepared from ethanolic solution; Focused beam, 1:1 (Top), 1:2 (Centre), 1:3 (Bottom) at 5000V and 50uA.

5.3.5 FTIR Spectra: - The FTIR spectral assignments of the samples prepared from ethanol and methanol at 650°C are summarised in Table 5.2, all show the presence of bands that can only be ascribed to the presence of metal hydroxycarbonate. Firstly for the samples prepared from methanolic solution at 650°C. Figures 5.9, 5.10A, 5.10B and 5.10C present FTIR spectra of these samples in the 3600 to 700 cm^{-1} range; the broad band observed in the region of 3600-3000 cm^{-1} is assigned to the O-H symmetric and antisymmetric stretching vibrations of water. The band observed at 1626 cm^{-1} is assigned to the bending vibration of water and the bands at 1515 and 1393 cm^{-1} are attributed to C-O antisymmetric stretching vibrations of CO_3^{2-} anions [36]. Furthermore, the weak band at 1092 cm^{-1} is assigned to a symmetric C-O stretching vibration of the CO_3^{2-} anions [37]. The inhomogeneous broadening of the various vibrational bands in the spectra of these samples is due to the disorder within the lattices when the products are formed at 650°C. It is not possible to identify bands due to Y-Cl stretching vibrations in these FTIR spectra as they are expected to appear below the low wavenumber cut-off at ca. 700 cm^{-1}. The FTIR spectra of the samples (from the methanolic solutions) prepared at 650°C show the presence of bands that are ascribed to a mixture of $Y_{0.98}Eu_{0.02}(OH)CO_3$ and unidentified chlorine containing species. The basic europium doped yttrium carbonate, $Y_{0.98}Eu_{0.02}$ $(OH)CO_3$, could have been formed from the surface reaction of YCl_3 with H_2O and CO_2 produced from the combustion of the alkylammonium cations, according to reactions (2) and (3).

$$2YCl_3 + 3H_2O \rightarrow (Y_{0.98}Eu_{0.02})_2O_3 + 6HCl \qquad (2)$$

$$(Y_{0.98}Eu_{0.02})_2O_3 + 2CO_2 + H_2O \rightarrow 2Y_{0.98}Eu_{0.02}(OH)CO_3, \qquad (3)$$

The most reasonable explanation taking into account also the SEM and XRD evidence is that the reactions (2) and (3) take place only on the surface and that this basic carbonate forms a crust over the YOCl nanoparticles. Thus as $Y_{0.95}Eu_{0.05}(OH)CO_3$ was reported to lose most of its hydroxide to give $(Y_{0.95}Eu_{0.05})_2O(CO_3)_2$ and $(Y_{0.95}Eu_{0.05})_2O_2CO_3$ when it was calcined at 550°C for 1 h in a muffle furnace [38], it is likely that a similar decomposition occurred, albeit incompletely only in the crust, under the rapid combustion conditions at a set temperature of 650°C in the present work.

Table 5.2 Materials prepared at 650°C

Wavenumber/cm^{-1}		
3600-3000	(m)	ν (O-H)
1626	(w)	δ (O-H)
1515	(m)	ν_{as} (CO_3^{2-})
1393	(s)	ν_{as} (CO_3^{2-})
1092	(w)	δ (O-H)
~760	(w shoulder on cut-off)	δ (CO_3^{2-})

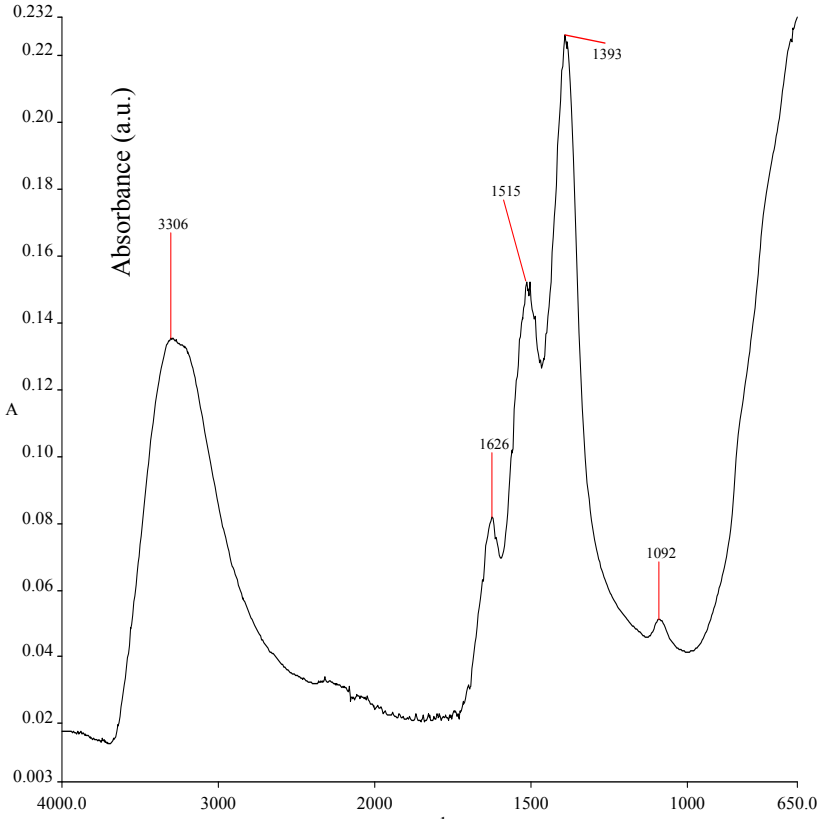

Wavenumber (cm^{-1})
(a)

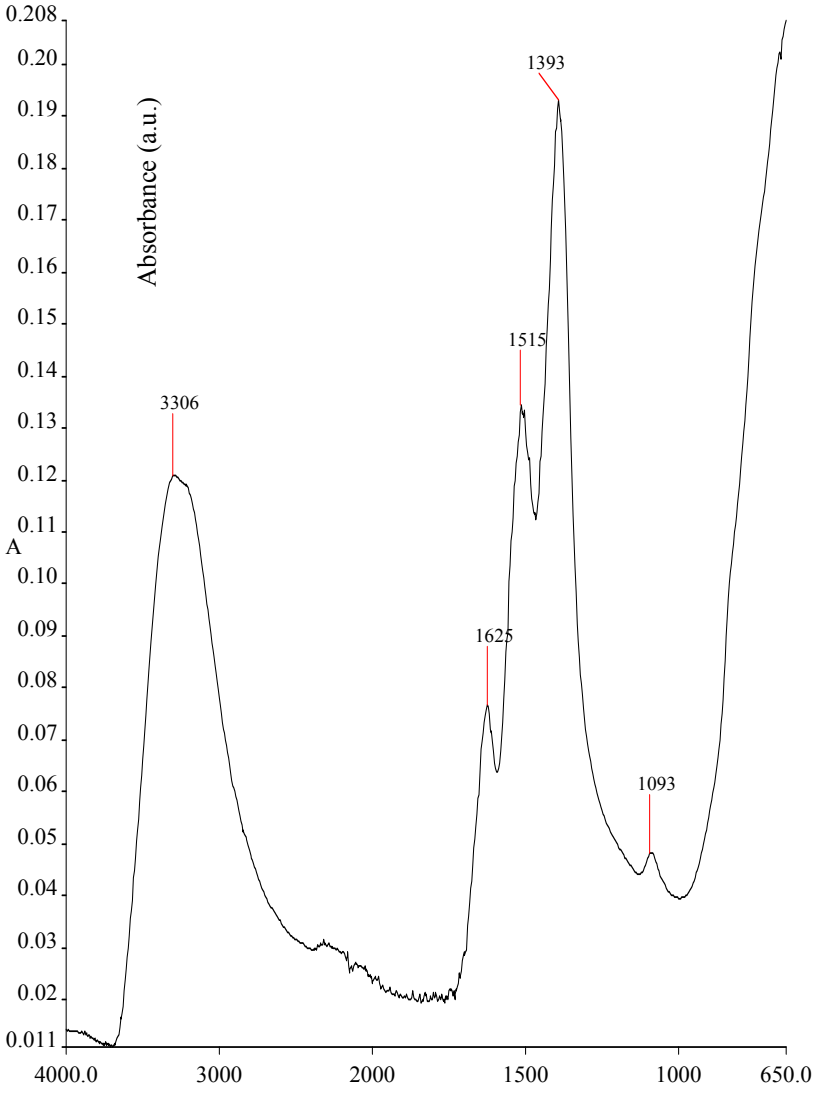
Absorbance (a.u.)
A
0.208
0.20
0.19
0.18
0.17
0.16
0.15
0.14
0.13
0.12
0.11
0.10
0.09
0.08
0.07
0.06
0.05
0.04
0.03
0.02
0.011
3306
1393
1515
1625
1093
4000.0
3000
2000
1500
1000
650.0
Wavenumber (cm-1)

(b)

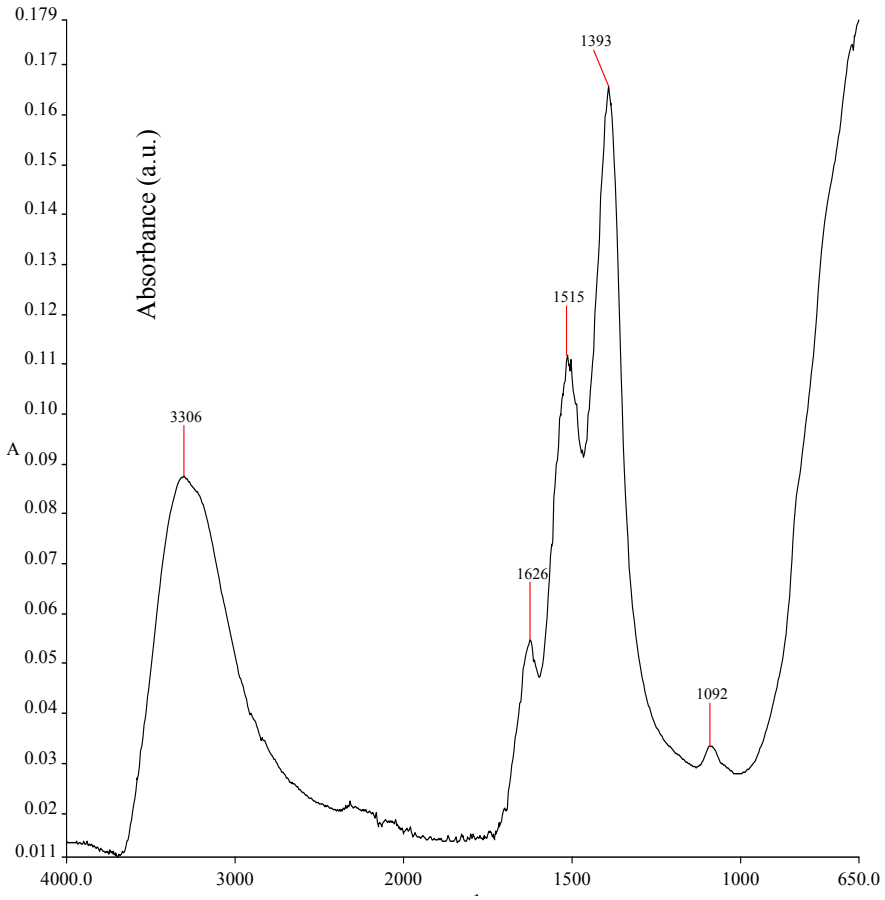

(c)

Figure 5.9 FTIR spectra of the [Y,Eu]Cl_3 - ($C_{16}H_{33}NH_3Cl$) samples prepared from methanol with metal ion to alkylammonium chloride ratios: (a) 1:1, (b) 1:2 and (c) 1:3. (In KBr discs) fired at 650°C.

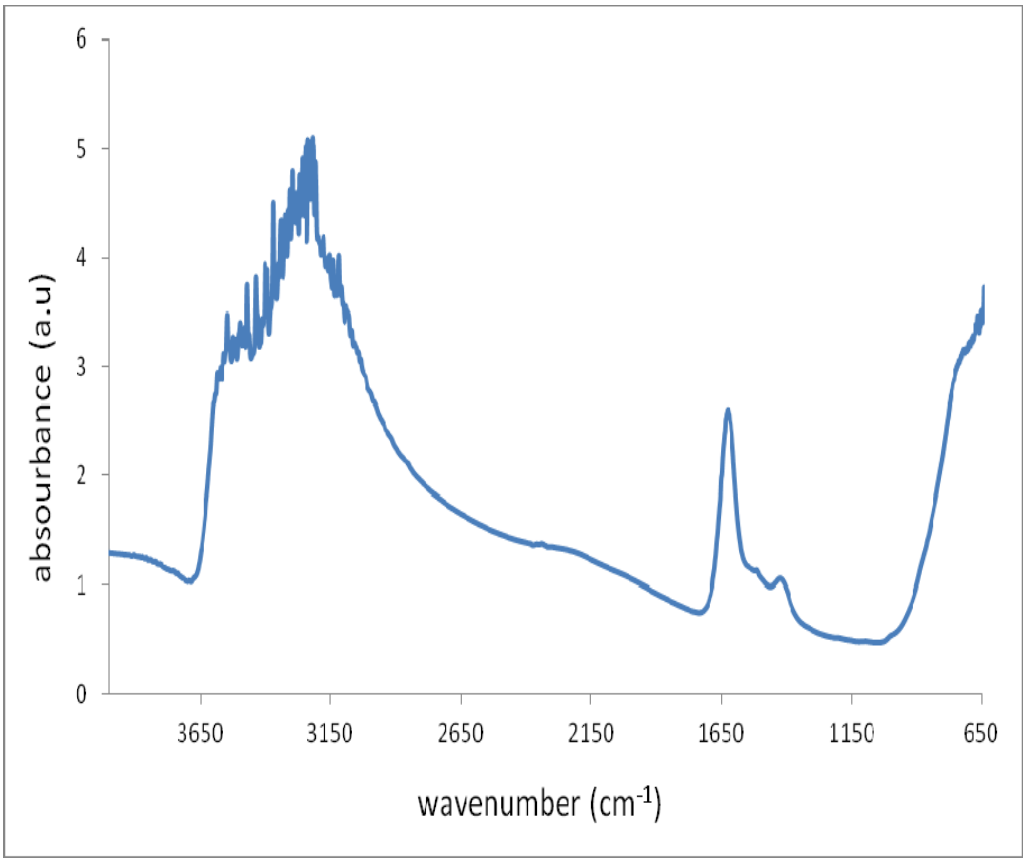
absourbance (a.u)
0
1
2
3
4
5
6
3650
3150
2650
2150
1650
1150
650
wavenumber (cm-1)

(a)

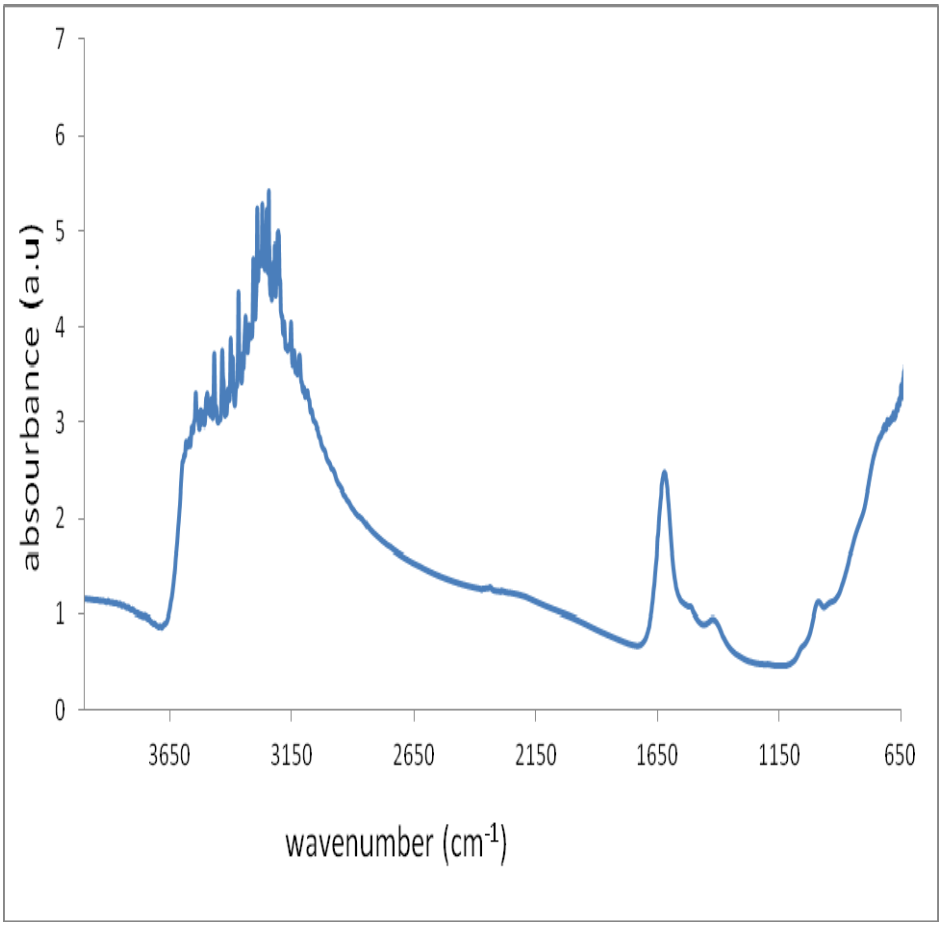
absourbance (a.u)
0
1
2
3
4
5
6
7
3650
3150
2650
2150
1650
1150
650
wavenumber (cm-1)

(b)

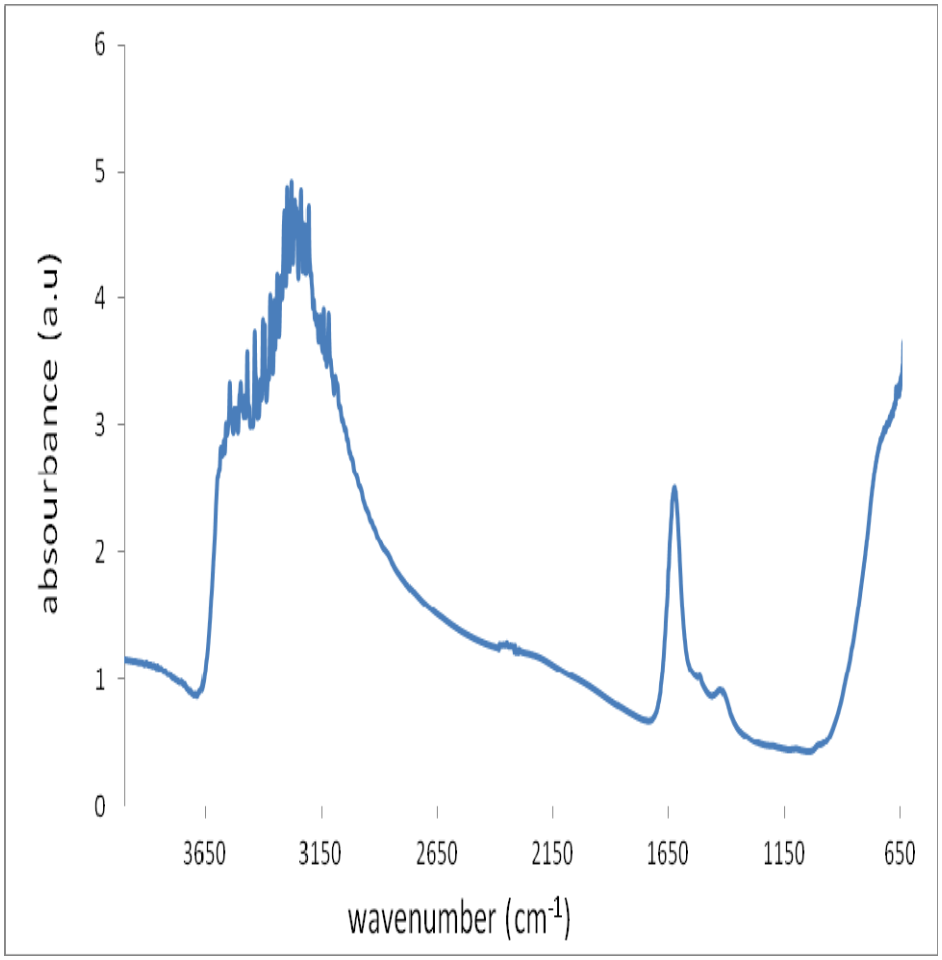

(c)

Figure 5.10A FTIR spectra of the $[Y,Eu]Cl_3$ - $(C_{16}H_{33}NH_3Cl)$ samples prepared from ethanol, with metal ion to alkylammonium chloride ratios 1:1 (a), 1:2 (b) and 1:3 (c).(In KBr discs) fired at 650°C.

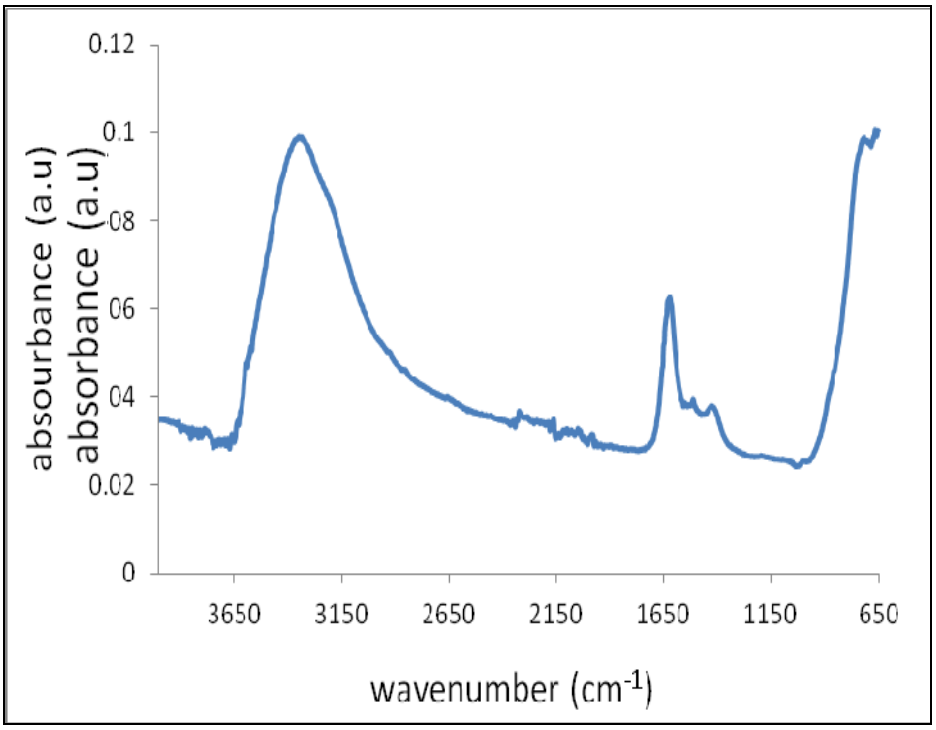
absourbance (a.u)
absorbance (a.u)
0.12
0.1
08
06
04
0.02
0
3650
3150
2650
2150
1650
1150
650
wavenumber (cm-1)

(a)

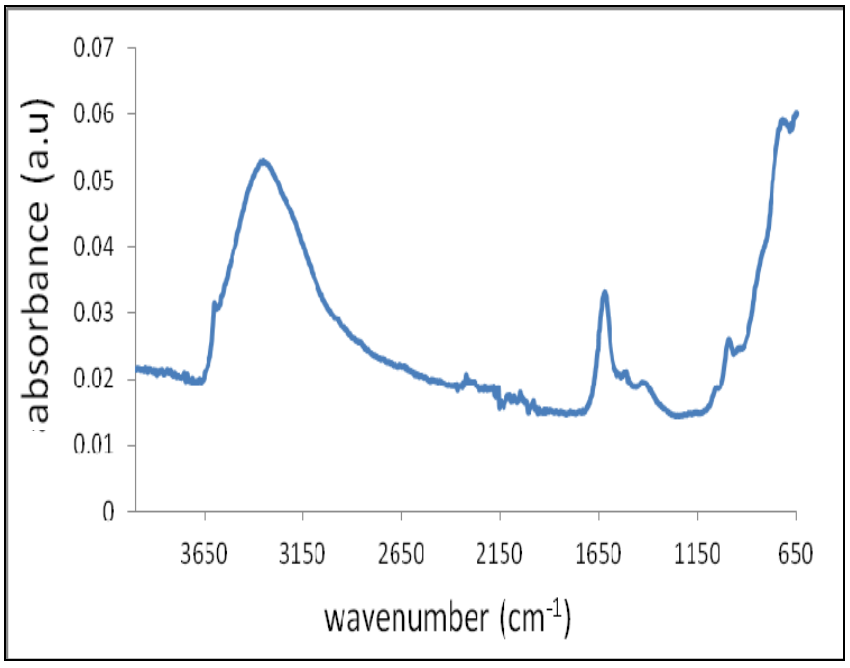
absorbance (a.u)
0.07
0.06
0.05
0.04
0.03
0.02
0.01
0
3650
3150
2650
2150
1650
1150
650
wavenumber (cm-1)

(b)

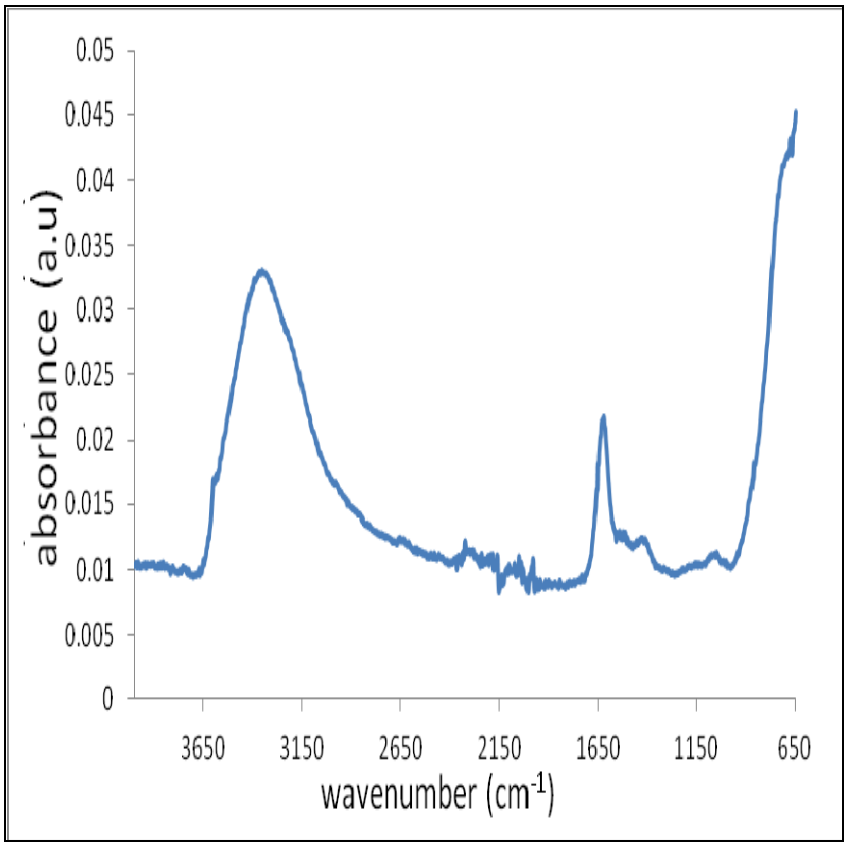

(c)

Figure 5.10B ATR, spectra of the [Y,Eu]Cl_3 - ($C_{16}H_{33}NH_3Cl$) samples prepared from ethanol with metal ion to alkylammonium chloride ratios 1:1 (a), 1:2 (b) and 1:3 (c). Fired at 650°C.

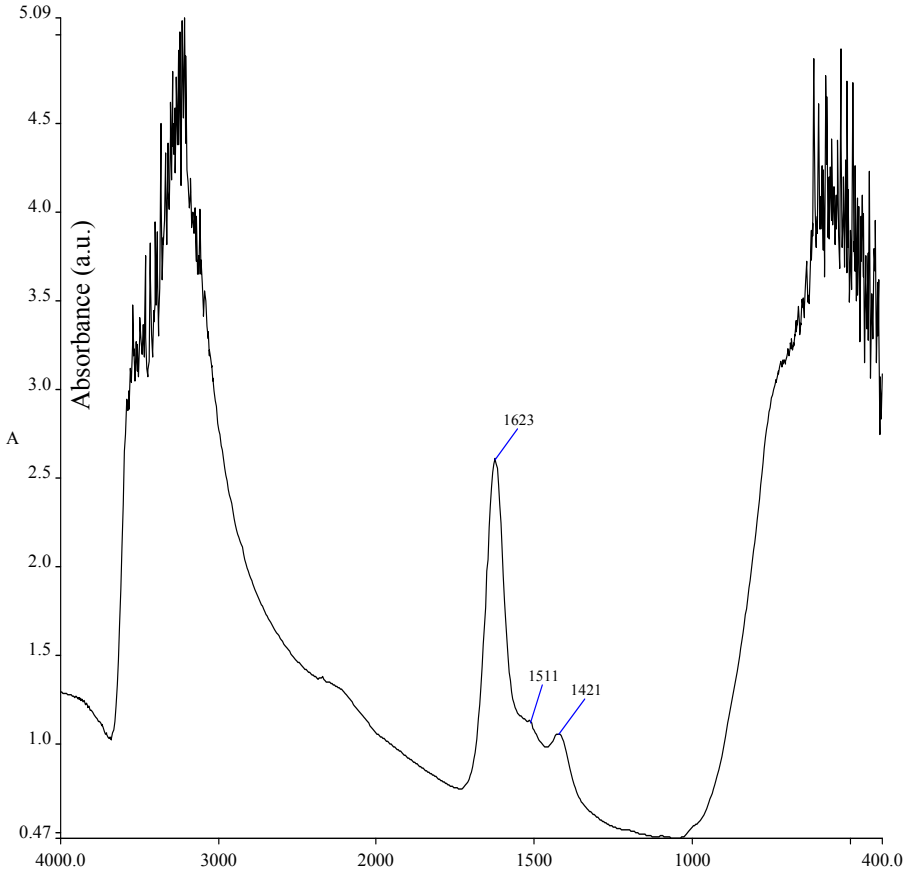
5.09
4.5
4.0
3.5
3.0
2.5
2.0
1.5
1.0
0.47
A
Absorbance (a.u.)
1623
1511
1421
4000.0
3000
2000
1500
1000
400.0
Wavenumber (cm-1)

(a)

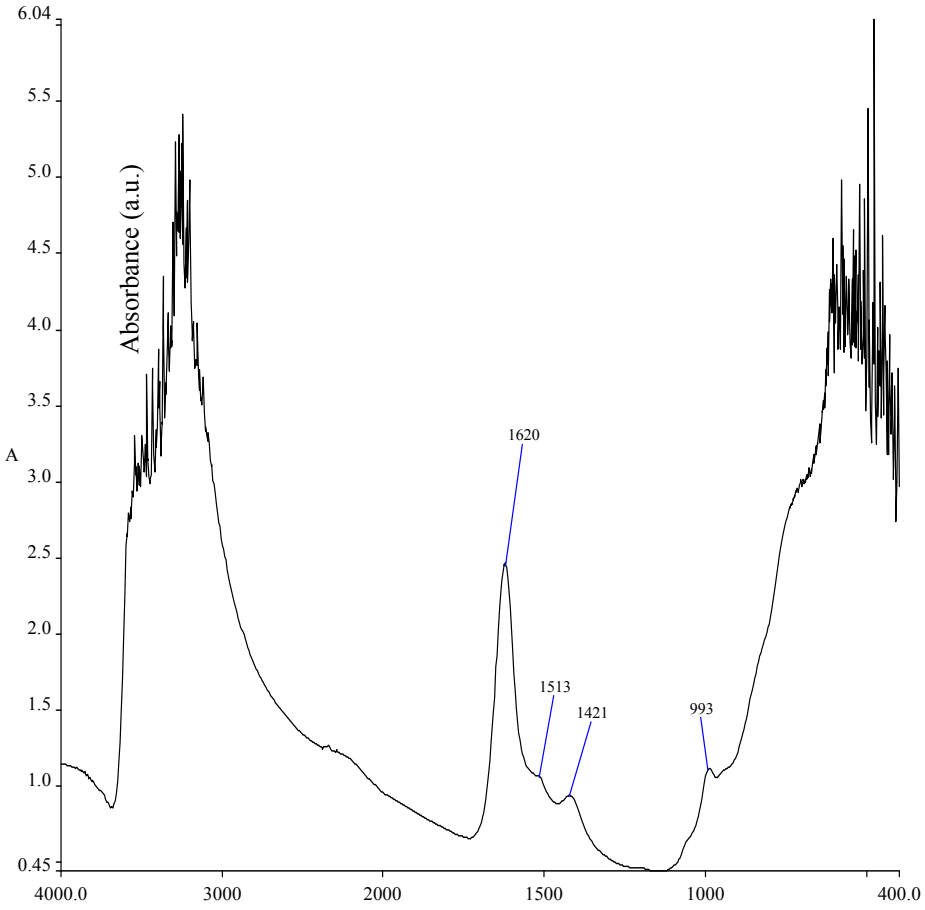
Absorbance (a.u.)
A
6.04
5.5
5.0
4.5
4.0
3.5
3.0
2.5
2.0
1.5
1.0
0.45
4000.0
3000
2000
1500
1000
400.0
1620
1513
1421
993
Wavenumber (cm-1)

(b)

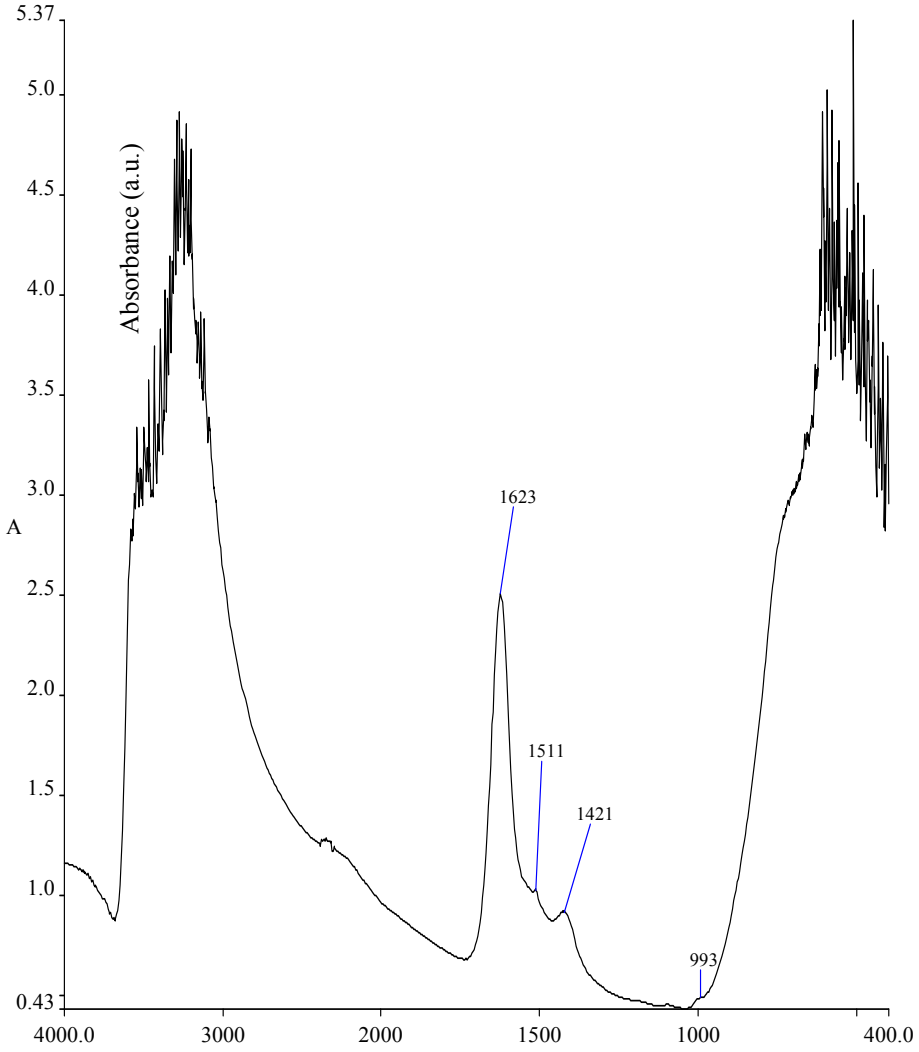

(c)

Figure 5.10C FTIR spectra of the [Y,Eu]Cl_3 - ($C_{16}H_{33}NH_3Cl$) samples prepared from ethanol with metal ion to alkylammonium chloride ratios 1:1 (a), 1:2 (b) and 1:3 (c).((In a KBr discs). Fired at 650°C.

The FTIR spectra of the materials prepared from ethanol all show bands that are indicative of the presence of carbonate ions. These techniques are sensitive to the surfaces of the materials and indicate that the particle surfaces have reacted with CO_2 to form carbonate phases.

5.3.6 Raman spectral studies: - Raman spectra of the samples annealed at 650 and 900°C for the 1:1 and 1:3 ratios are shown in Figure 5.11. In Figure 5.11 (a) and (b) are the 650°C spectra that show there was not any significant residual chloride ions present. As can be seen from the Raman spectra shown in Figure 5.11, a strong Raman band at 377 cm^{-1} (arrowed in Figure 5.11) is absent when the phosphor nanoparticles are fired at 650°C (see Figure 5.11 a and b), but appears when the phosphor nanoparticles are fired at 900°C (see Figure 5.11 c and d). This band is due to the cubic phase of Y_2O_3: Eu [37, 39-44]. In addition, a number of other strong bands also appear in Figures 5.11 (c and d); these are due to the photoluminescence of the Y_2O_3:Eu phosphors under 632.8 nm excitation.

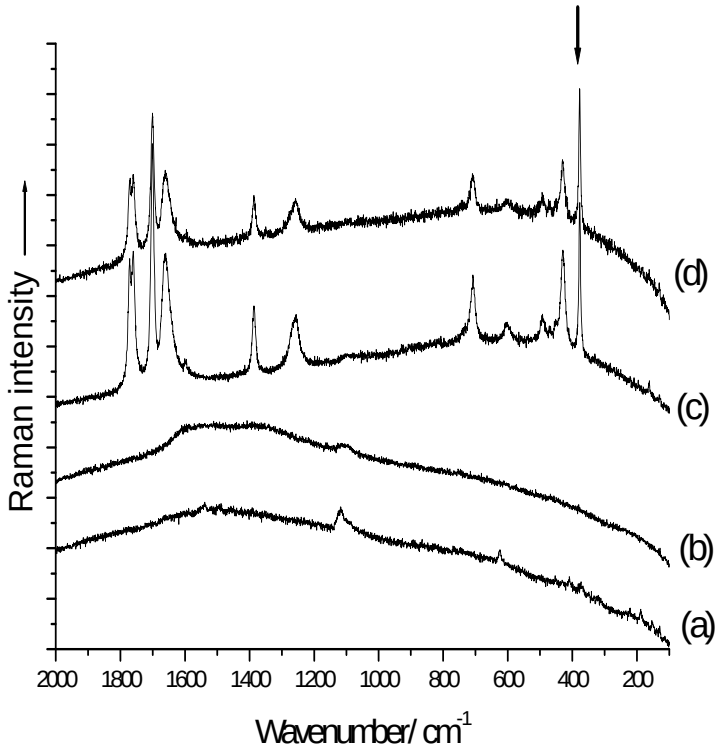

Figure 5.11 Raman spectra of phosphor samples prepared from methanol at metal ion to alkylammonium chloride ratios of:- (a) 1:1, (b) 1:3 both annealed at 650°C, (c) 1:1 and (d) 1:3 both annealed at 900°C. The exciting wavelength was equal to 632.8 nm.

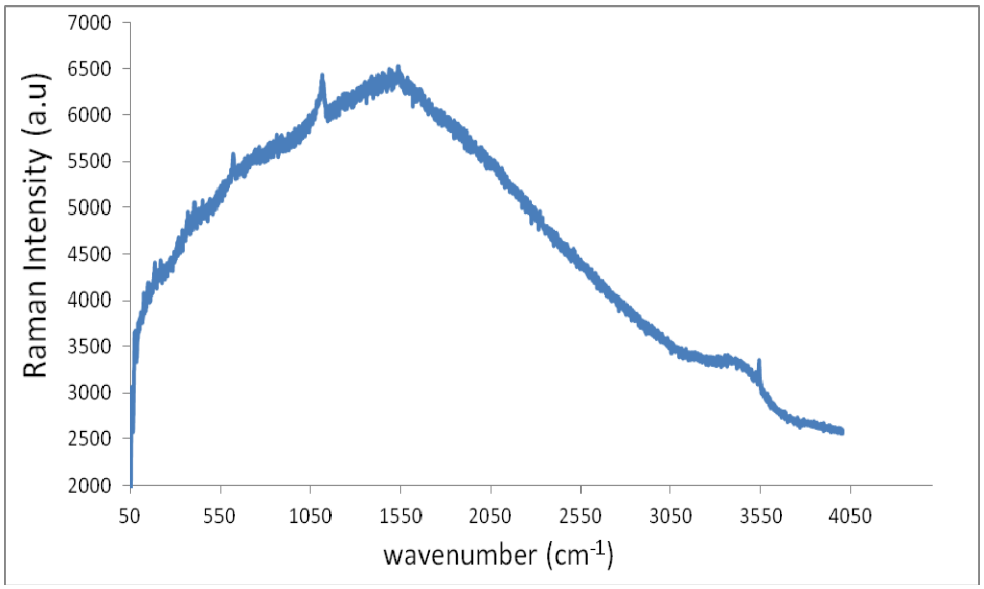

1:1 650°C - (a)

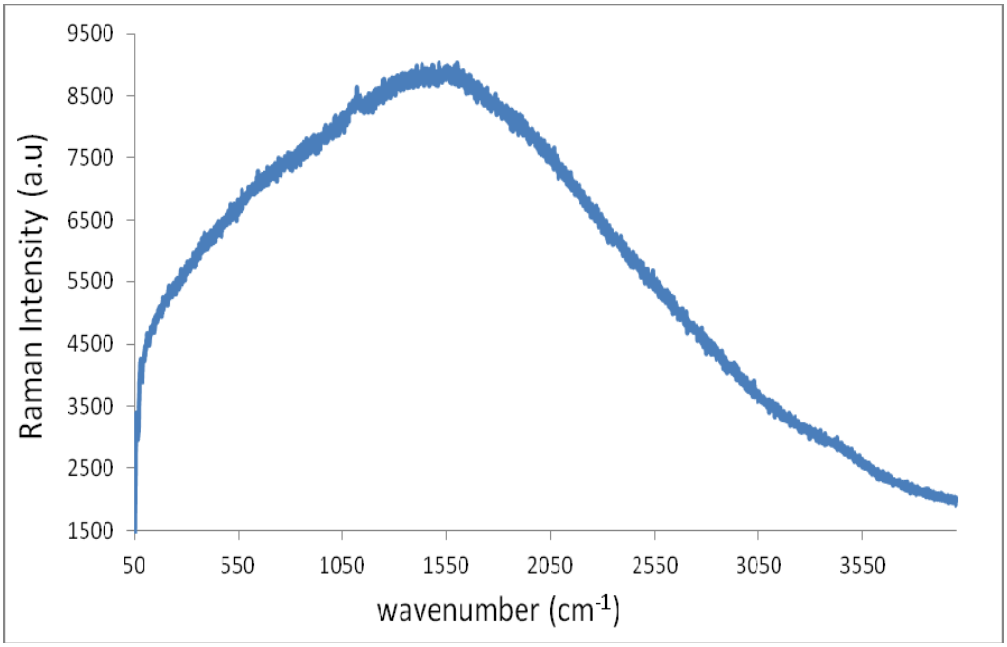

1:2 650°C - (b)

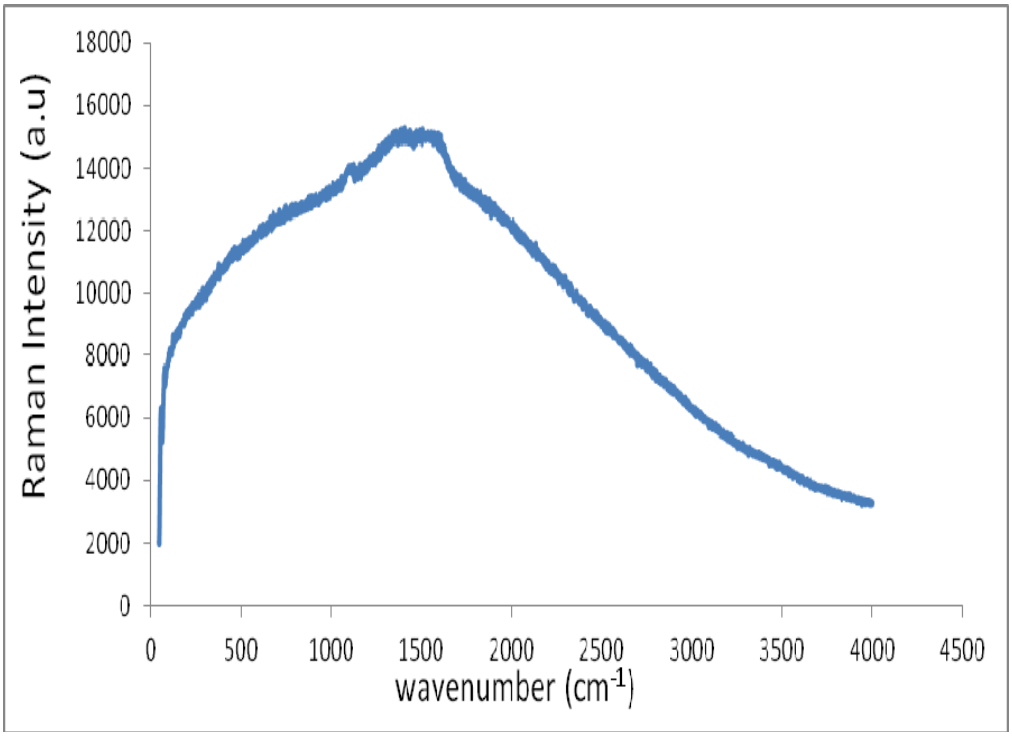

1:3 650°C- (c)

Figure 5.12A Raman spectra of phosphor samples prepared from ethanol at metal ion to alkylammonium chloride ratios of: - (a) 1:1, (b) 1:2 (c) 1:3, annealed at 650°C. The exciting wavelength was equal to 632.8 nm.

In the Raman spectra shown in Figure 5.12A, the strong Raman band at 377 cm^{-1} (arrowed in Figure 5.11) is absent when the phosphor nanoparticles prepared from ethanol were fired at 650°C. However there are some Raman bands in the 1:1 materials in common in Figures 5.11(a) and 5.12A, whereas only one of these bands is apparent in Figures 5.11(b), 5.12A(b) and 5.12A(c). In Figures 5.12B (a) and (c) the Raman spectra show features in common. Unfortunately a good Raman spectrum could not be obtained from Figure5.12B(c).The best of these latter three spectra is presented in Figure 5.12B(a). This spectrum is repeated in figure 34 and is more conveniently discussed there in section 5.4.8.

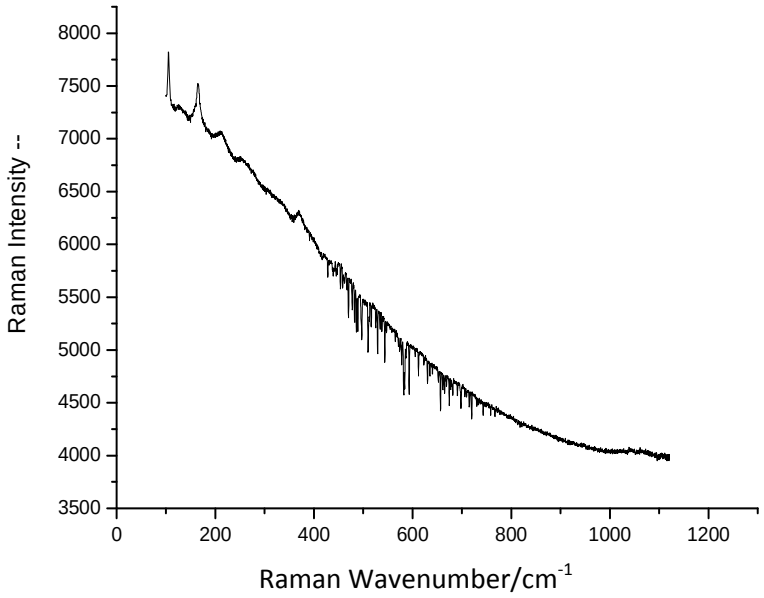
Raman Intensity --
Raman Wavenumber/cm-1
8000
7500
7000
6500
6000
5500
5000
4500
4000
3500
0
200
400
600
800
1000
1200

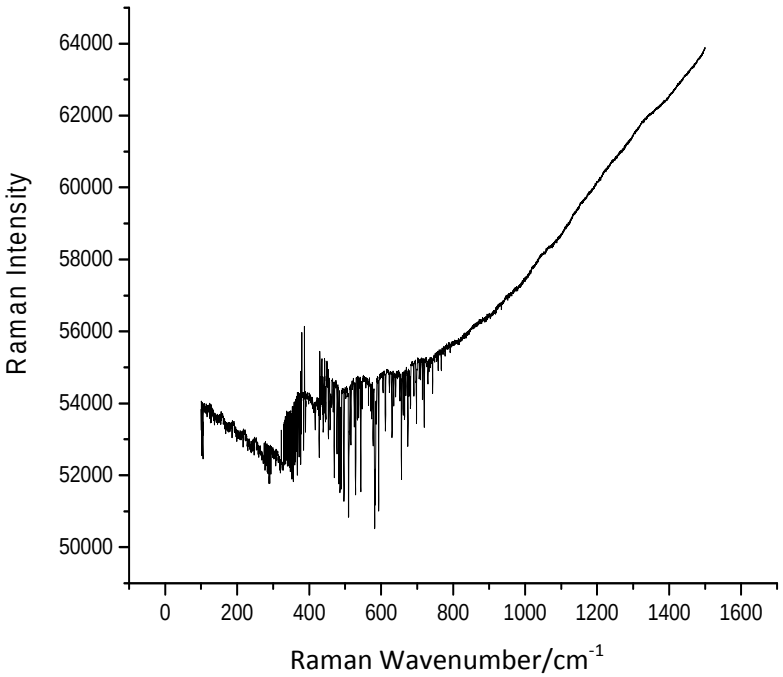
Raman Intensity
Raman Wavenumber/cm-1
64000
62000
60000
58000
56000
54000
52000
50000
0
200
400
600
800
1000
1200
1400
1600

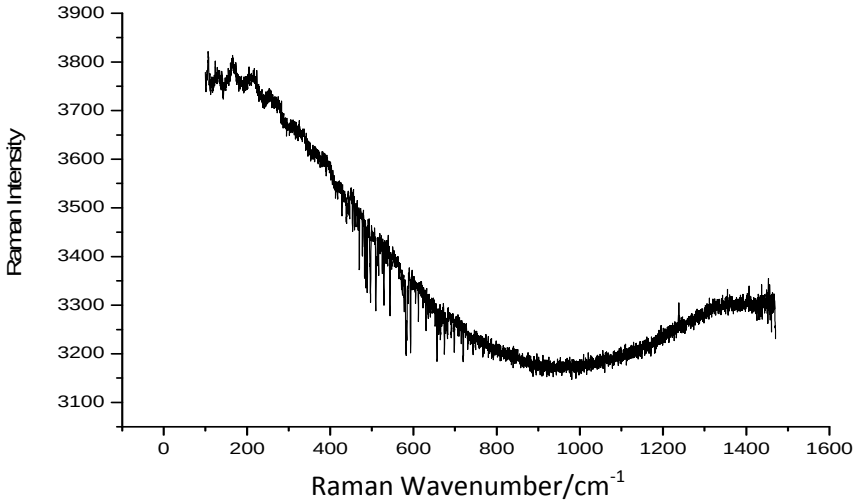

Figure 5.12B Raman spectra of phosphor samples prepared at metal ion to alkylammonium chloride ratios of: - (a) 1:1, (51), (b) 1:2 (-52) and (c) 1:3 (53) from ethanolic solution then annealed at 650°C. The exciting wavelength was equal to 1064 nm.

5.3.7 Conclusions so far:- It is clear from these results so far that the presence of the combustion fuel in the samples prepared at 650°C was insufficient to raise the temperature high enough to form the cubic $Y_2O_3:Eu^{3+}$ phase or that the furnace temperature was insufficient. All the 650 °C FTIR spectra are similar, although the emission spectra do indicate that for the higher fuel ratios that a greater degree of order is found. The samples prepared from both methanol and ethanol are consistent with the presence of chloride containing phases; predominantly there is evidence for YOCl.

5.4 Studies on the samples produced at 900°C

5.4.1 Appearance of products prepared with methanol and ethanol at a temperature of 900°C.

5.4.1.1 SEM Studies: - The phosphor samples annealed at 900°C are now discussed. In Figure 5.13 SEM micrographs of phosphor samples prepared from methanol solutions then fired at 900°C at metal chloride to alkylammonium chloride ratios of 1:1 (a and b), 1:2 (c and d) and 1:3 (e and f) are presented. It is interesting to note that the same morphological forms and the individual crystallites of the 650°C 1:1 and 1:2 samples are present in the 900°C 1:1 sample and the remnant micellar forms of the 650°C 1:3 sample are present in the higher temperature 1:2 sample. The 900°C 1:3 sample is shown to have undergone sintering that has eliminated some of the fine remnant micellar structures, therefore the higher temperature and metal chloride to fuel

ratio has been sufficient to raise the temperature significantly. However even in firing temperatures in excess of 900°C the samples retain morphologies that were either imposed on them by the original micellar environments their inorganic precursors form in, or that were derived from those original environments.

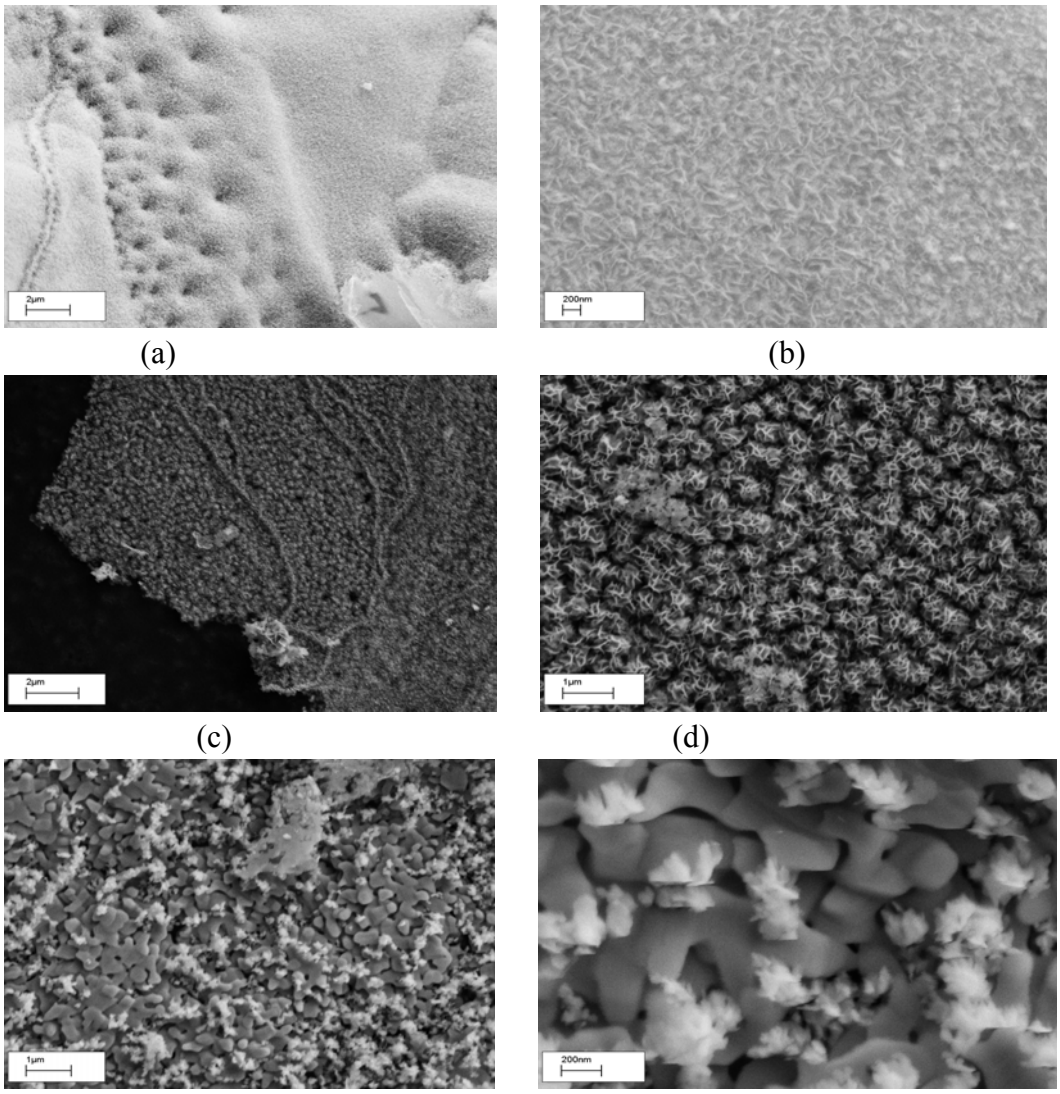

Figure 5.13 FESEM micrographs of phosphor samples prepared from methanol solutions then fired at 900°C prepared at metal chloride to alkylammonium chloride ratios of (a and b) 1:1, (c and d) 1:2, and (e and f) 1:3, In d and e the bar is 1µm, and in b and f it is 200nm and in a and c it is 2 µm.

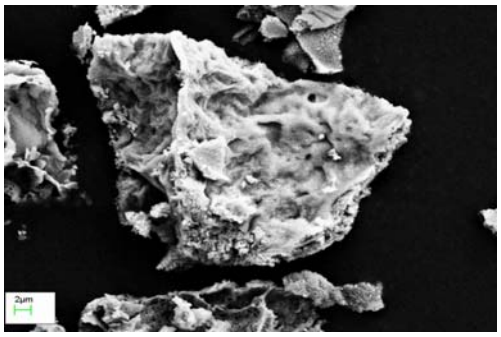

1:1-D (Bar = 2μm)

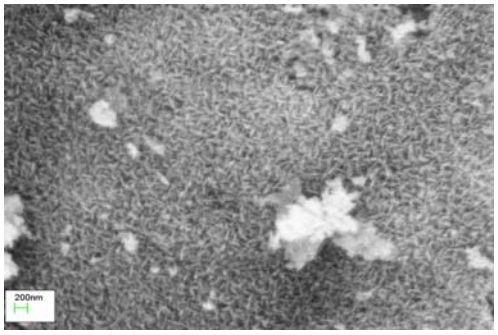

1:1-D (Bar = 200nm)

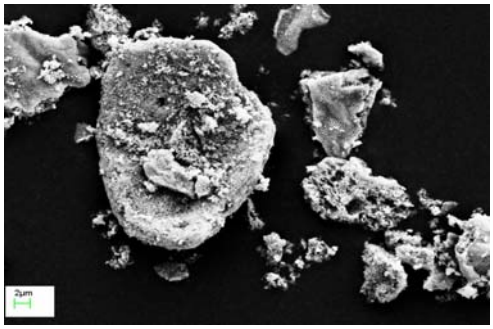

1:2-E (Bar = 2μm)

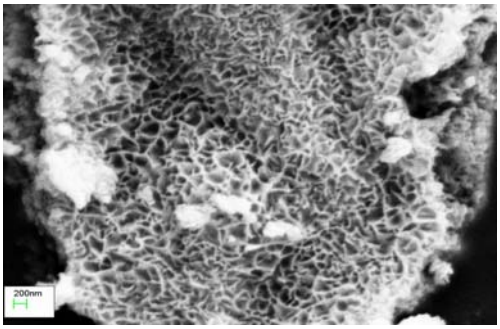

1:2-E (Bar = 200nm)

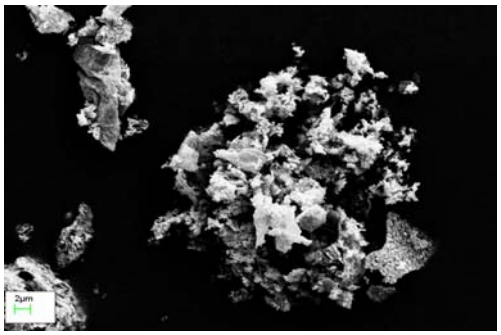

1:3-F (Bar = 2μm)

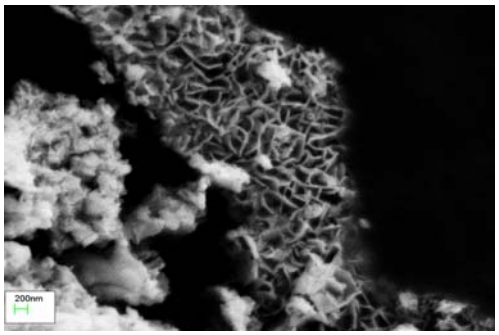

1:3-F (Bar = 200nm)

Figure 5.14-A Samples D, E, F- 900°C with ethanol**.** FESEM micrographs of phosphor samples fired at 900°C prepared from ethanol solutions then fired. Metal chloride to alkylammonium chloride ratios of: 1:1-D, 1:2-E and 1:3-F;

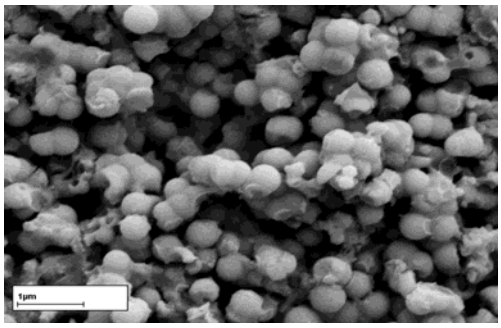

1:1-54 (bar = 1μm)

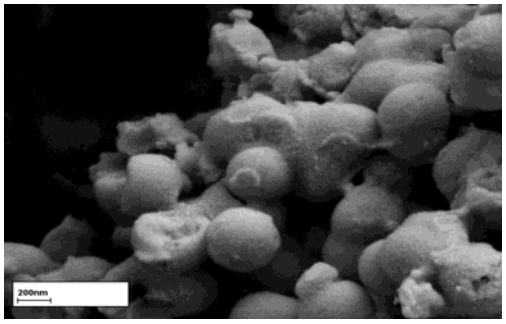

1:1-54 (bar = 200nm)

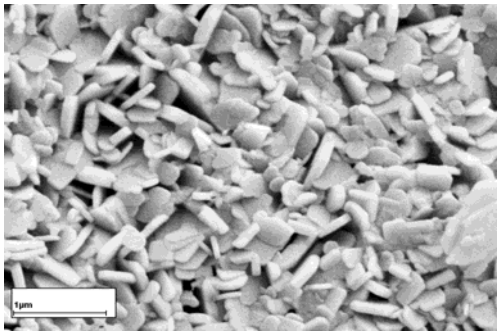

1:2-55 (bar = 1μm)

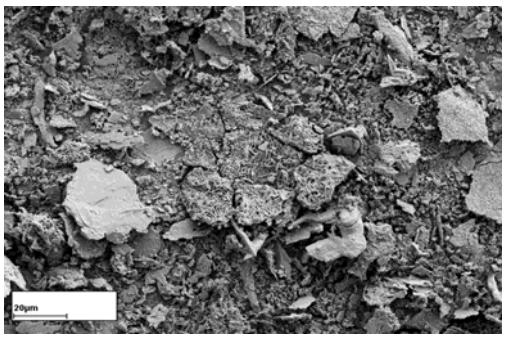

1:2-55 (bar = 20μm)

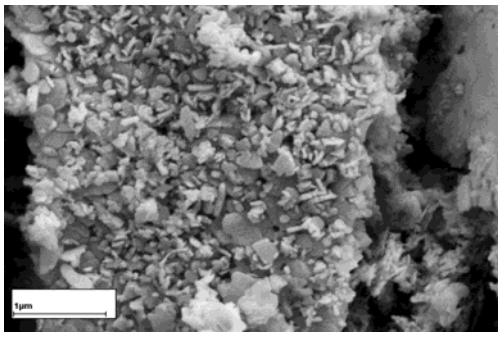

1:3-56 (bar = 1μm)

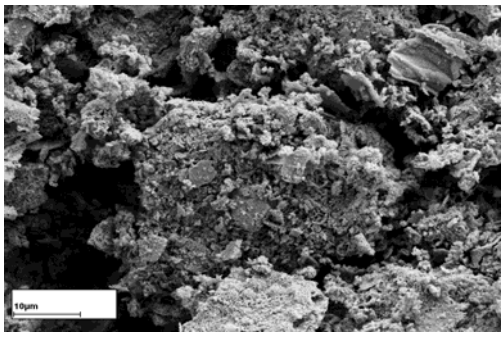

1:3-56 (bar = 10μm)

Figure 5.14-B Samples 54, 55, 56 - 900°C with ethanol. FESEM micrographs of phosphor samples fired at 900°C prepared from ethanol solutions then fired at metal chloride to alkylammonium chloride ratios of: 1:1-54, 1:2 -55 and 1:3-56.

In Figure 5.14A SEM micrographs of phosphor samples prepared from ethanol solutions then fired at 900°C at metal chloride to alkylammonium chloride ratios of 1:1, 1:2 and 1:3 are presented. All of these three samples were prepared in a muffle furnace with a wide chimney 3cm diameter. In these samples the SEMs show small sub micron crystals that form as two dimensional sheets suggesting that they were formed from the two dimensional extended micelle sheets.

The three samples presented in figure 5.14B were prepared in a different muffle furnace with a much narrower chimney (1 cm diameter). In the SEMs in figure 5.14B of the 1:1 sample there are many ovoid type shapes that may have originated from micellular interiors. In the higher ratio samples there is much evidence of crystal forms though they are often arranged in sheets again possibly showing their regrowth from micellular two and three dimensional structures. The 900°C 1:3 sample is shown to have undergone sintering that has eliminated some of the fine remnant micellular structures, therefore the higher temperature and metal chloride to fuel ratio has been sufficient to raise the temperature significantly compared to the 650°C samples.

5.4.2 Sample structures (from XRPD data):- All the samples that were produced under the 900°C conditions from methanol solution showed the presence of crystalline material and all showed a similar XRPD (see Figure 5.15) pattern identified as cubic $Y_2O_3:Eu^{3+}$. [PDF 251011], as exemplified by the diffractograms of the 1:1, 1:2 and 1:3 samples which are shown in Figure 5.8. The reflection lines exhibited by these diffractograms can be indexed to a pure cubic Y_2O_3 phase belonging to space group Ia3 (No. 206) with Z = 16 and a lattice parameter of a = 10.604 Å [45]. Samples prepared from the 1:1, 1:2 and 1:3 ratios all contained cubic Y_2O_3 with Lorentzian average crystallite sizes of 60 nm, 34 nm and 60 nm respectively.

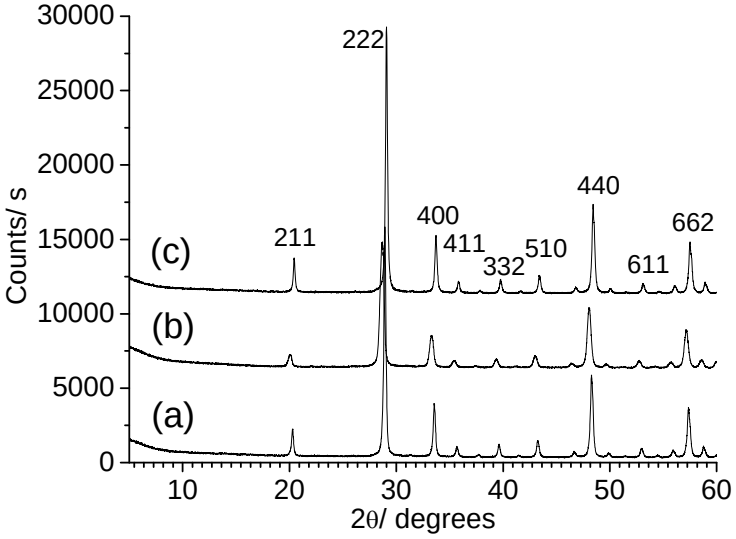

Figure 5.15 XRD diffractograms of the samples [Y,Eu]Cl_3 - ($C_{16}H_{33}NH_3Cl$) prepared from methanolic solution then fired/annealed at 900°C; metal ion to alkylammonium chloride ratios: (a) 1:1, (b) 1:2, and (c) 1:3.

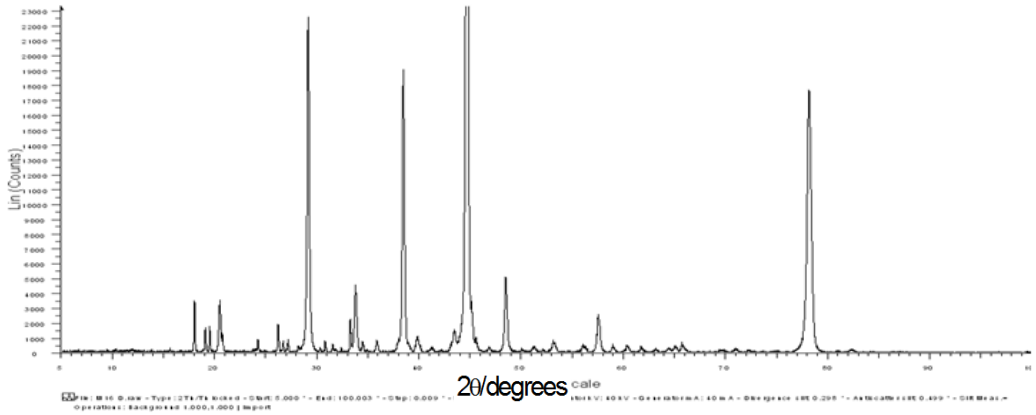

1:1 (D on Aluminium stub),

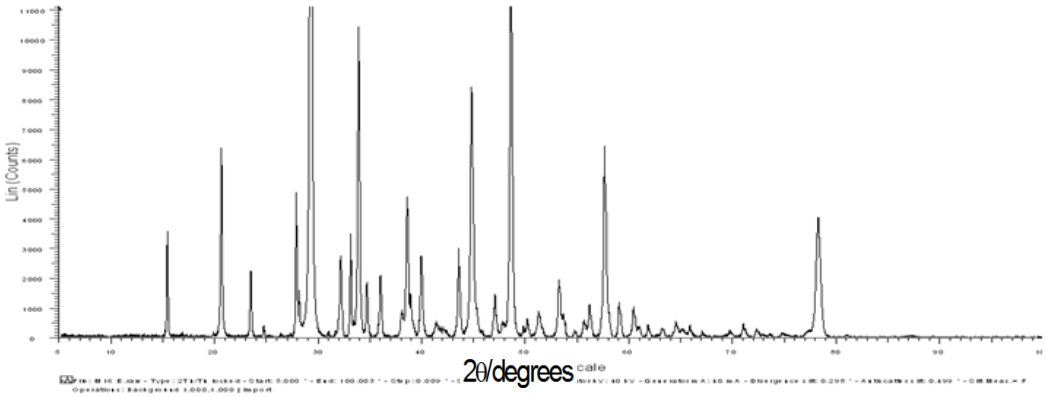

1:2 (E on Aluminium stub),

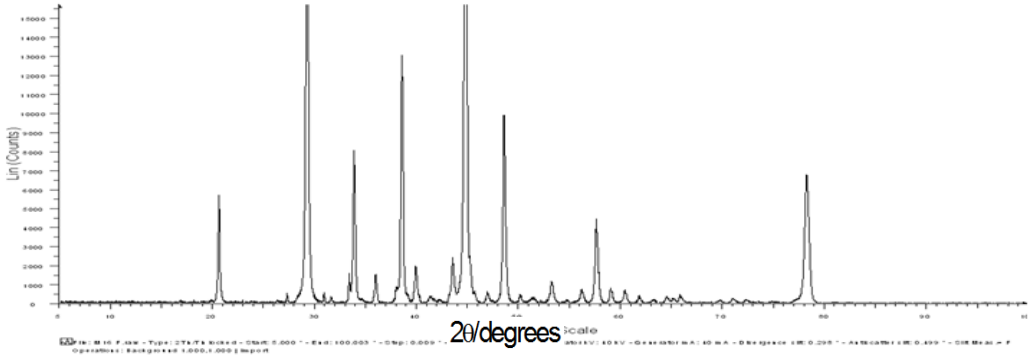

1:3 (F on Aluminium stub).

Figure 5.16A XRD diffractograms of the samples [Y,Eu]Cl_3 - ($C_{16}H_{33}NH_3Cl$) prepared from ethanolic solution then fired/annealed at 900°C, metal ion to alkylammonium chloride ratios.1:1(D on Aluminium stub), 1:2 (E on Aluminium stub),1:3 (F on Aluminium stub).

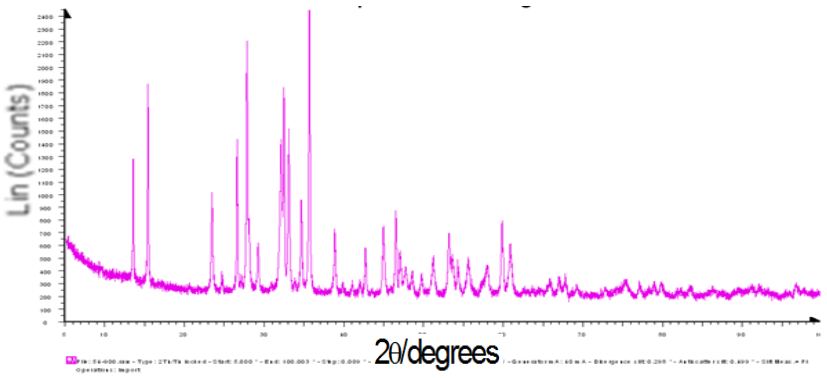

1:1-54

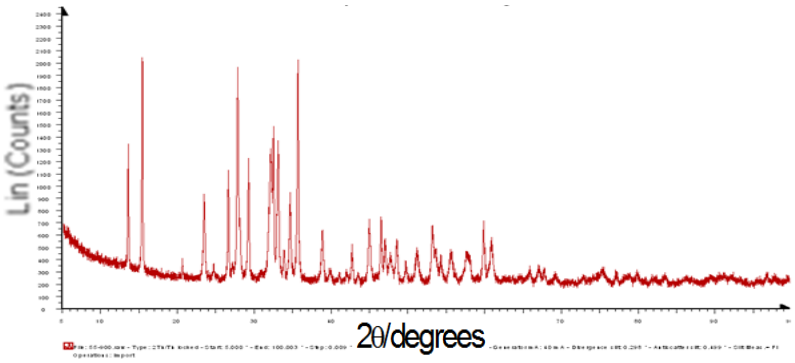

1:2-55

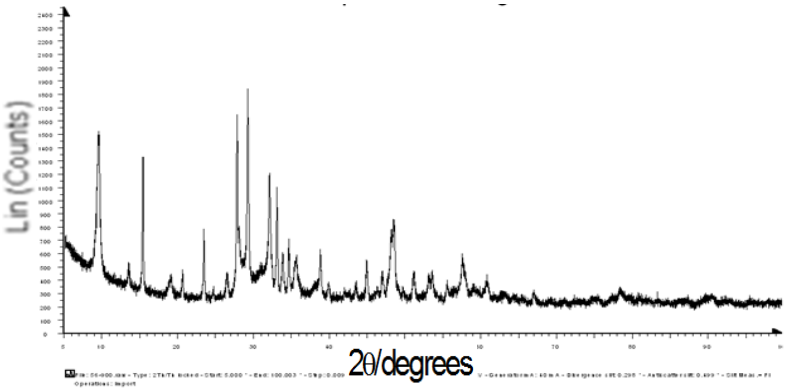

1:3-56

Figure 5.16B XRPD diffractograms of the samples [Y,Eu]Cl_3 - ($C_{16}H_{33}NH_3Cl$) prepared from ethanol then fired/annealed at 900°C, metal ion to alkylammonium chloride ratios.1:1(54 purple), 1:2 (55 brown),1:3 (56 Black).

All the samples that were produced under the 900°C conditions from ethanol solution showed the presence of crystalline material and five had XRPD data that gave evidence for a new phosphor lattice (see Figures 5.16 A and 5.16 B) and Table 3. Surprisingly the main phase (99%) was identified as monoclinic $Y_4O_5Cl_2:Eu^{3+}$ in Figure 5.16B. Samples prepared from the 1:1, 1:2 and 1:3 ratios all contained monoclinic $Y_4O_5Cl_2:Eu^{3+}$ with Lorentzian average crystallite sizes of 72nm, 72nm and 59nm respectively. Two of the samples (the 1:1 and 1:2) that are presented in Figure 5.16A also show the monoclinic $Y_4O_5Cl_2:Eu^{3+}$ phase but the third sample (1:3) shows mainly cubic $Y_2O_3:Eu^{3+}$, though there is evidence for a cell given in table 3 but not further identified. The monoclinic $Y_4O_5Cl_2:Eu^{3+}$ phosphor has chloride in the lattice and this was verified using EDAX analysis in the scanning electron microscope. (See below).

Table 5.3 Cell parameters for the yttrium oxychloride phase $Y_4O_5Cl_2:Eu^{3+}$ found in the materials fired at 900°C prepared from ethanol.

Samples No.	a (Å)	b (Å)	c (Å)	beta (°)
54	6.51176(37)	6.41143(43)	14.4398(12)	97.5634(59)
55	6.51631(42)	6.41342(50)	14.4456(14)	97.5503(68)
56	6.51991(86)	6.41543(99)	14.4620(27)	97.594(12)
D	6.50879(31)	6.40040(25)	14.43148(48)	97.6026(36)
E	6.48878(71)	6.39493(73)	14.3631(24)	97.581(13)
F	5.38125(29)	4.48996(39)	11.02517(72)	99.6964(65)

5.4.3 EDX analysis of the samples prepared from ethanol

The EDAX analysis traces for the samples prepared from ethanol are presented in figures 5.17A and 5.17B below. Chloride was detected by EDAX in sample 1:1-D in the powder, but not on the powder on the stub. The amount in the powder was small so it may have been undetectable on the stub. Samples 1:2-E and 1:3-F showed the presence of chloride in all locations but relatively more was detected on the powders.

In samples 1:1-54, 1:2-55 and 1:3-56 the amount of chloride is obviously greater in keeping with the finding that these samples contained much more of the monoclinic $Y_4O_5Cl_2:Eu^{3+}$.

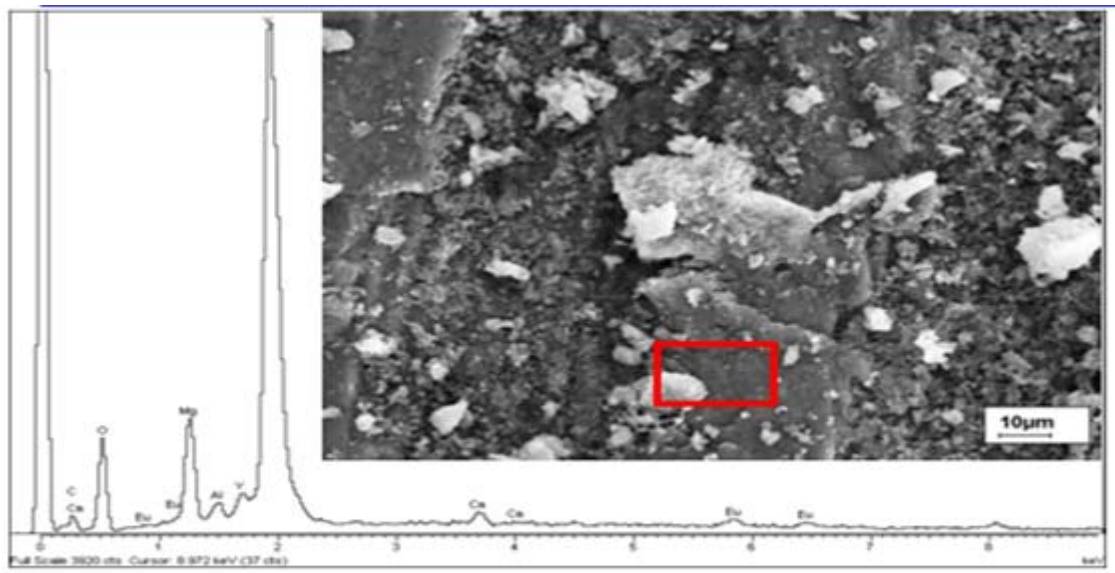

Edge stub

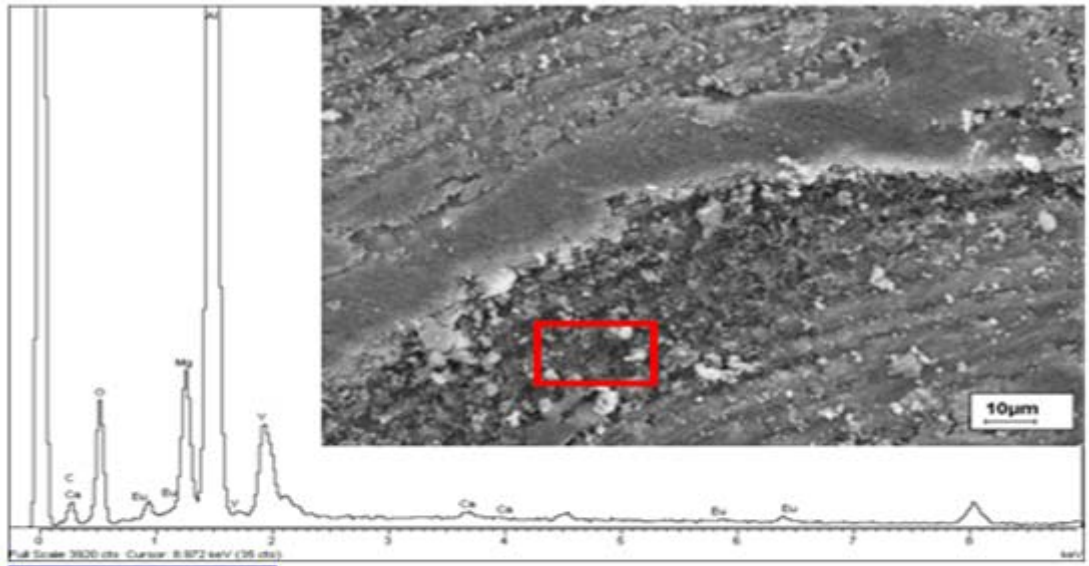

Centre stub

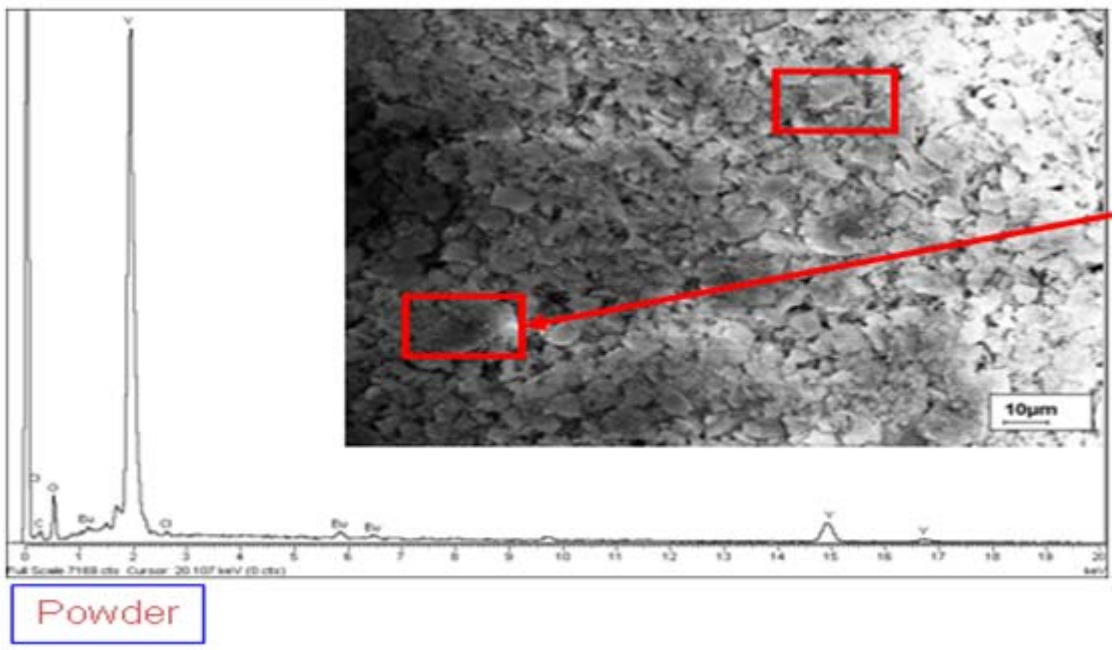

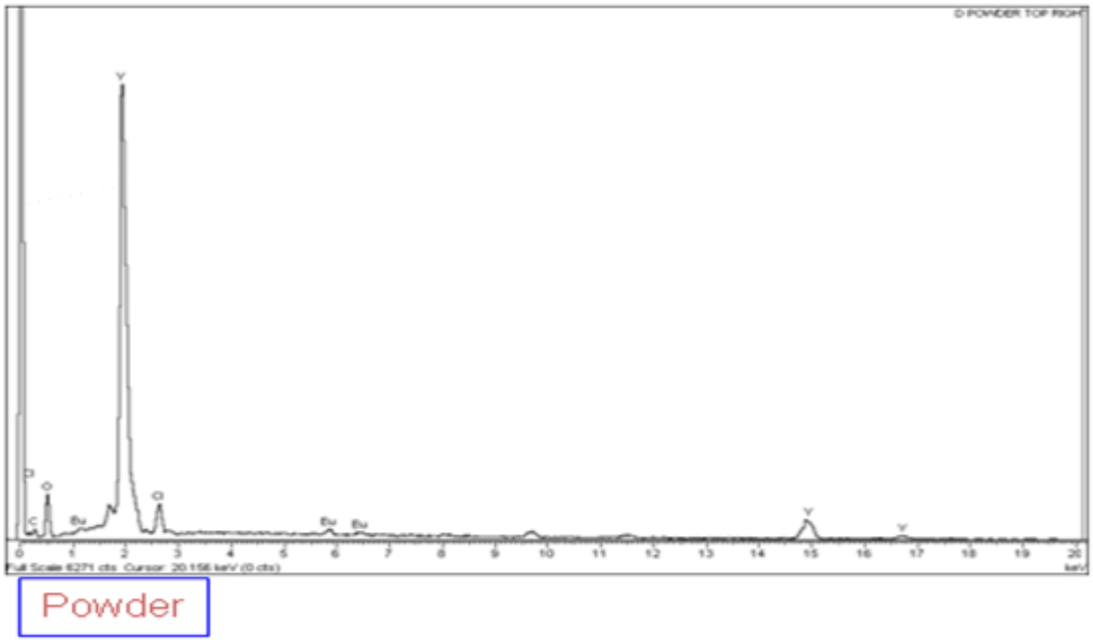

1:1-D

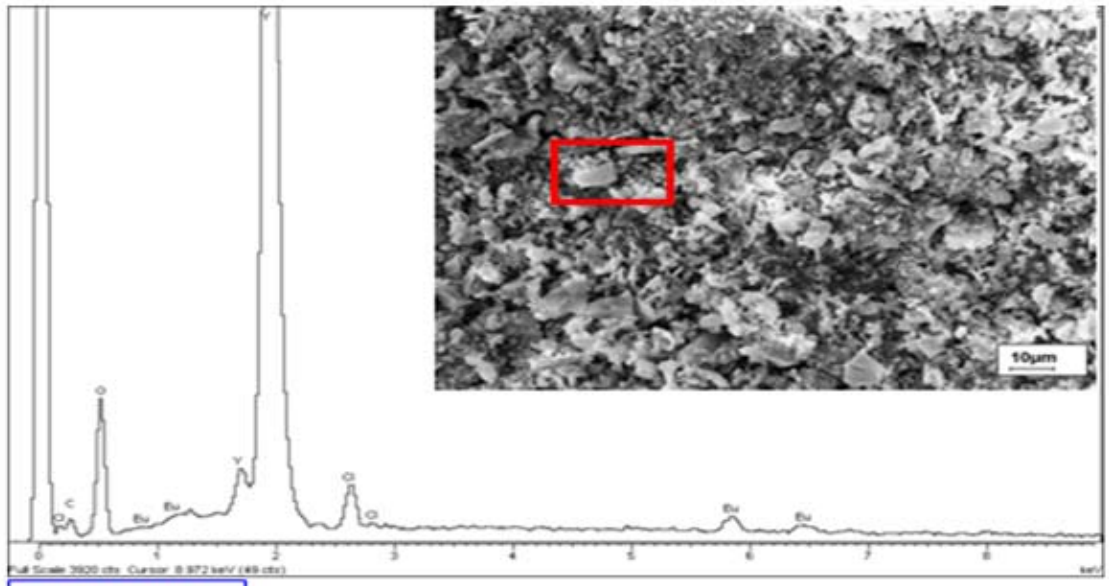

Edge stub

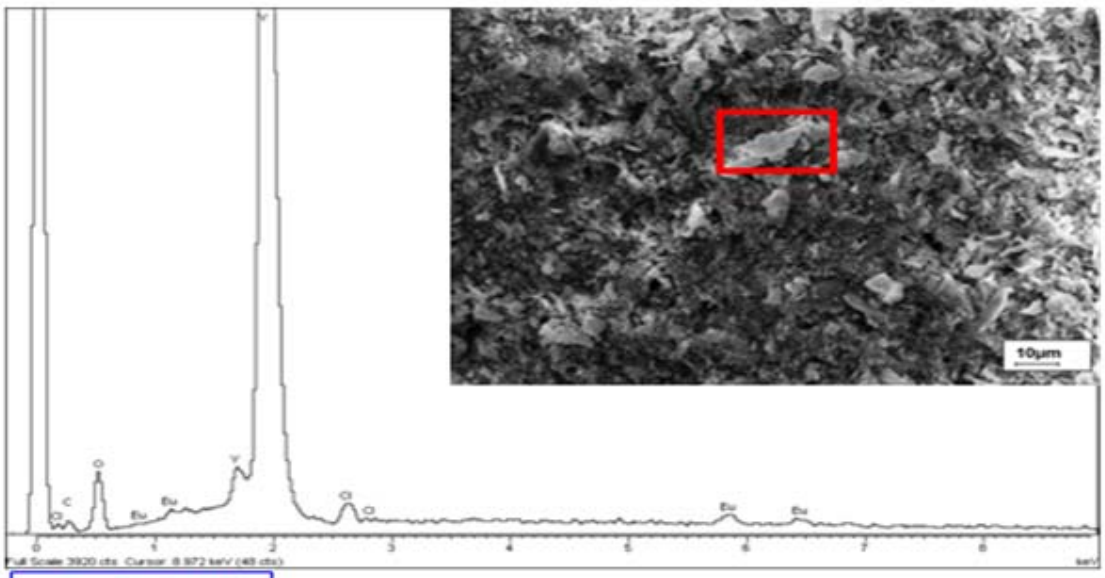

Centre stub

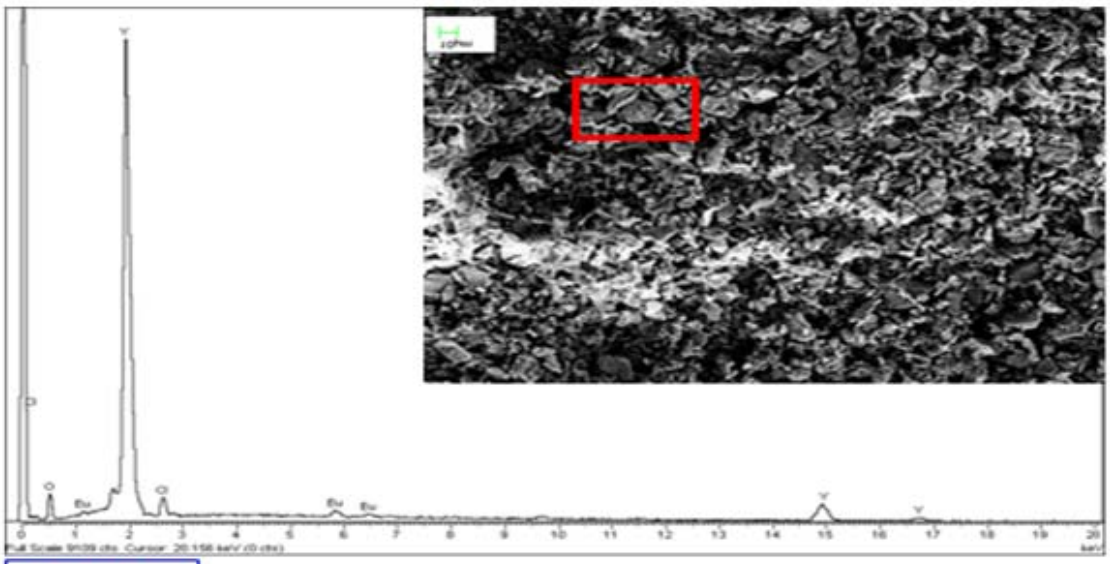

1:2-E

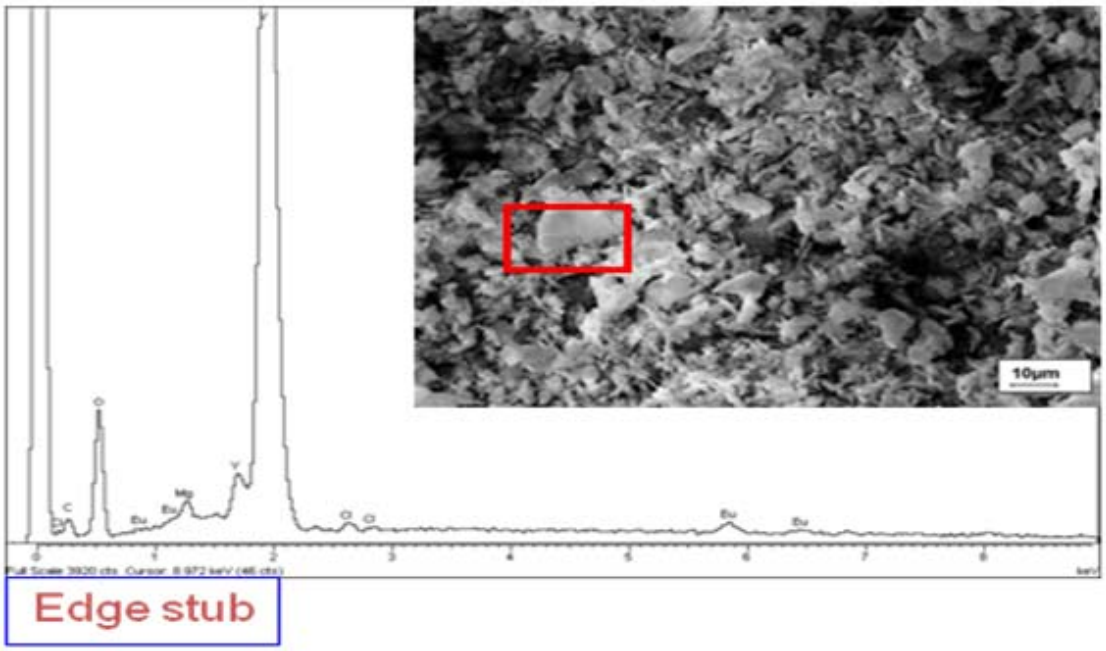

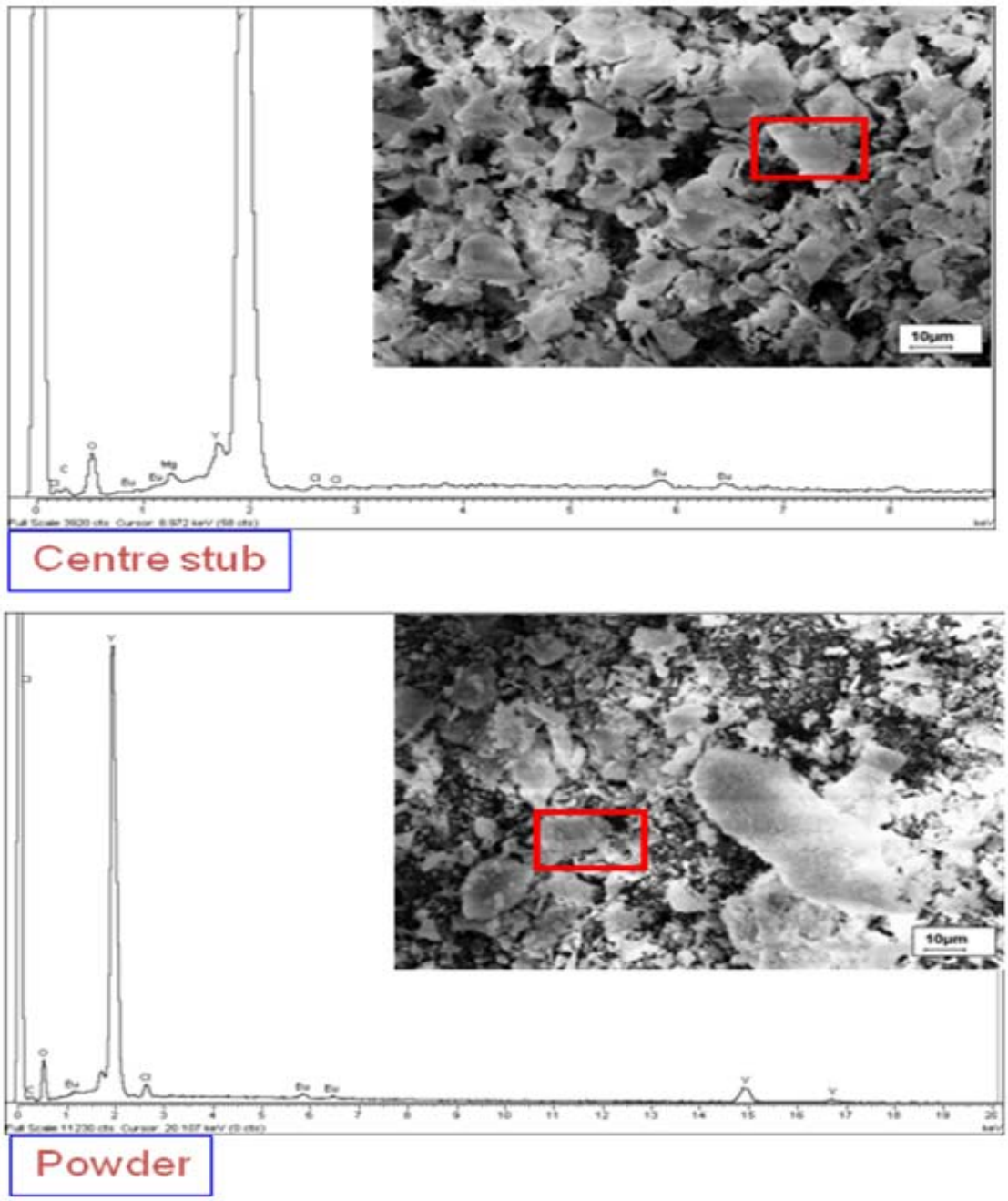

1:3-F

Figure 5.17A Combined SEM + EDX of the samples prepared from ethanolic solution then fired/-annealed at 900°C, metal ion to alkylammonium chloride ratios. 1:1- D, 1:2-E and 1:3-F. (the red boxes show the areas that were analysed).

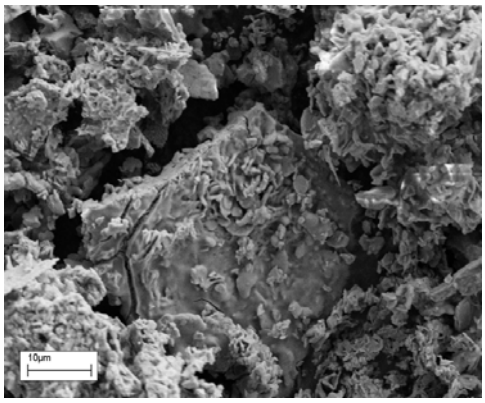

1:1-54 (bar = 10µm)

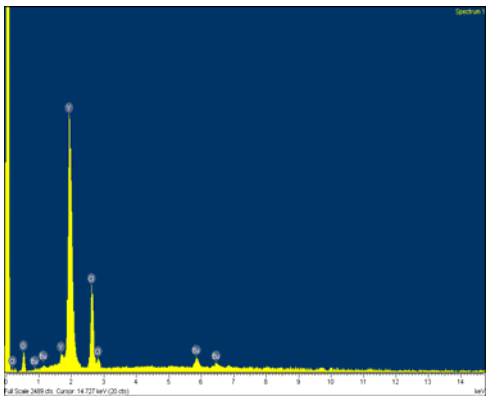

1:1 54-EDAX

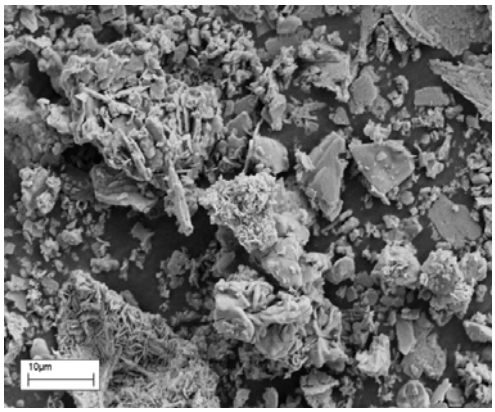

1:2-55 (bar = 10µm)

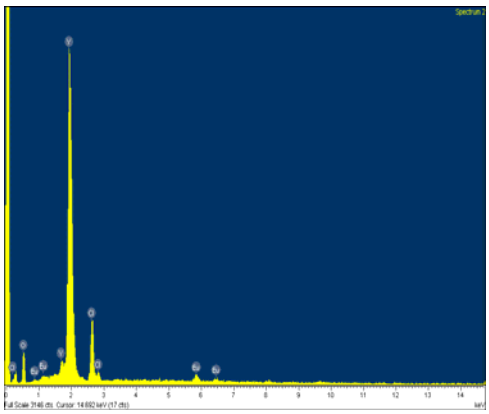

1:2 55-EDAX

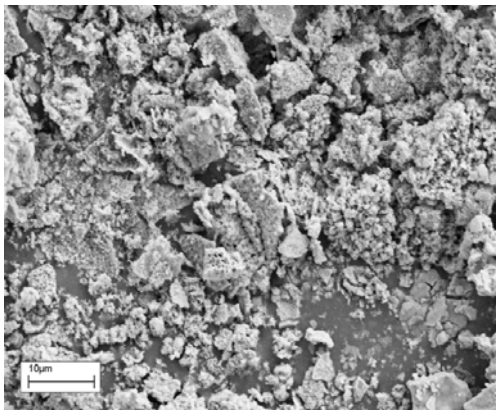

1:3-56 (bar = 10µm)

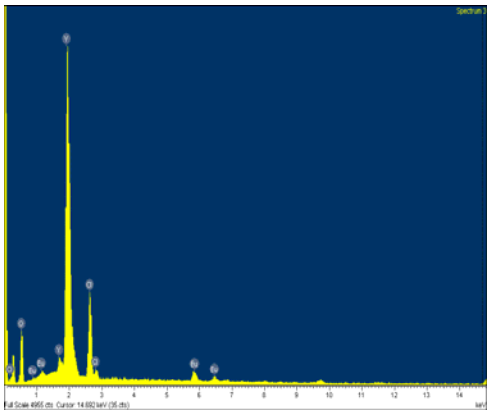

1:3 56-EDAX

Figure 5.17 B Combined SEM + EDX of the samples prepared from ethanolic solution then fired/-annealed at 900°C, metal ion to alkylammonium chloride ratios. 1:1-54, 1:2-55 and 1:3-56.

5.4.4 Photoluminescent Spectra:- All the PL emission spectra of the samples made from methanol are typical of cubic $Y_2O_3:Eu^{3+}$, as are the excitation spectra. Typical excitation and emission spectra are presented in Figure 18 for the 1:1, 1:2 and 1:3 900°C samples.

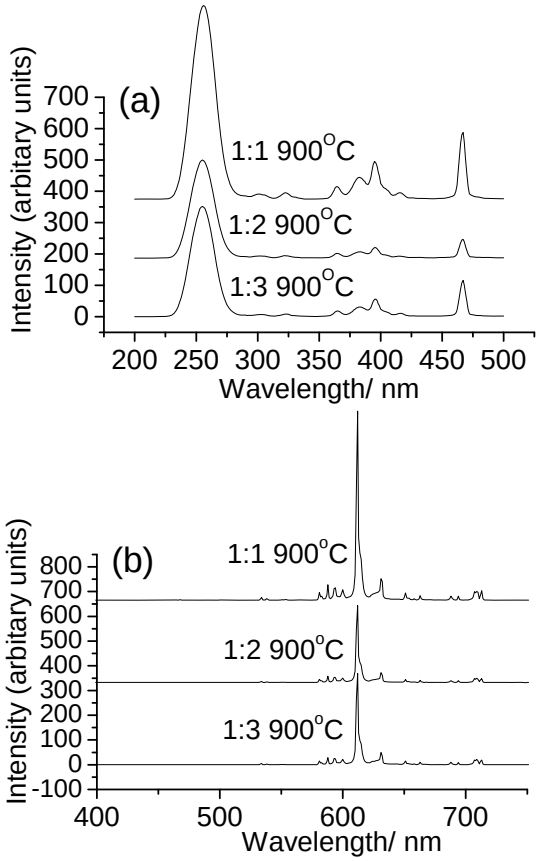

Figure 5.18 (a) Photoluminescent excitation spectra obtained by monitoring the emission at 611nm, and 5.18 (b) emission spectra of the 900°C samples from methanolic solution, excitation wavelength 254nm.

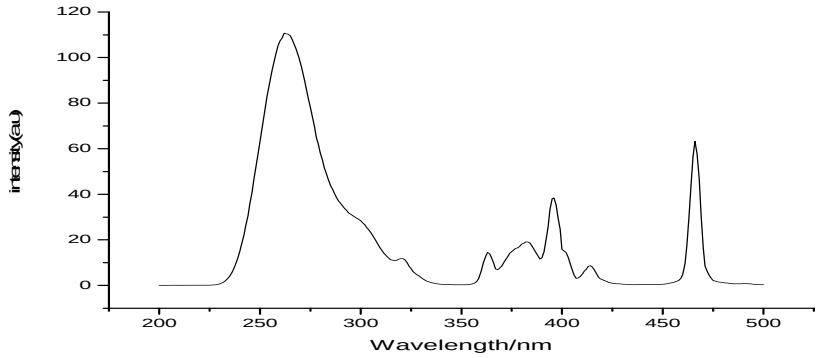

(a-54)

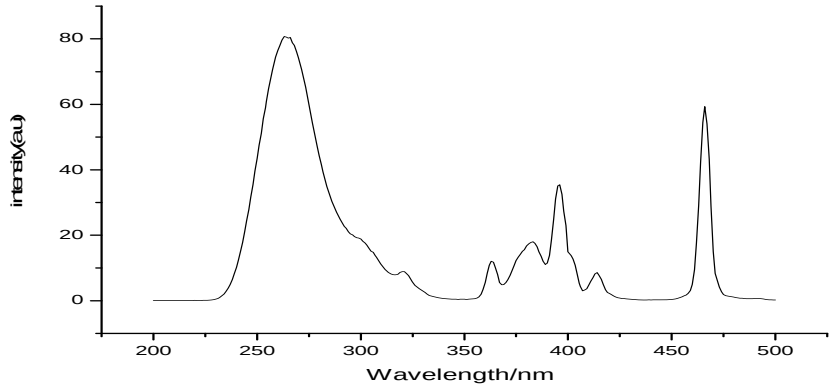

(b-55)

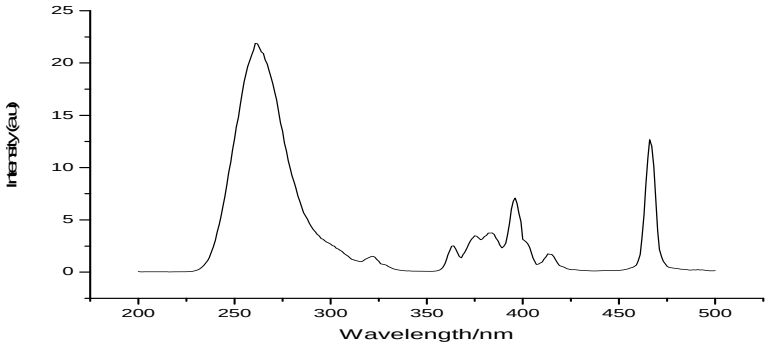

(c-56)

Figure 5.19 A Photoluminescent excitation, spectra of the samples fired at 900°C prepared from ethanolic solution. Excitation spectra 1:1(a-54), 1:2(b-55), 1:3 (c-56). Excitation monitored at 623 nm.

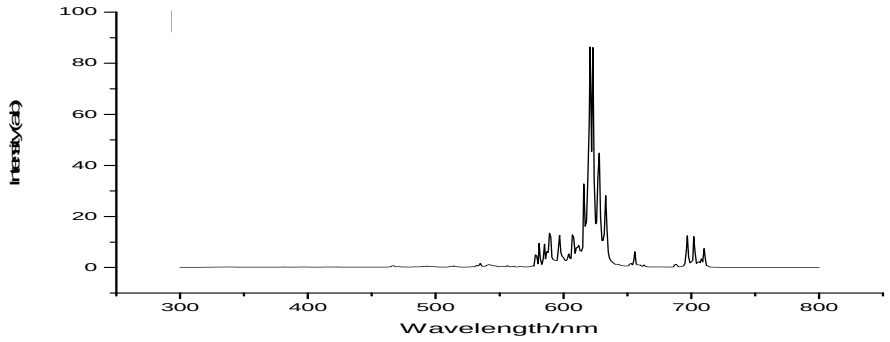

(a-54)

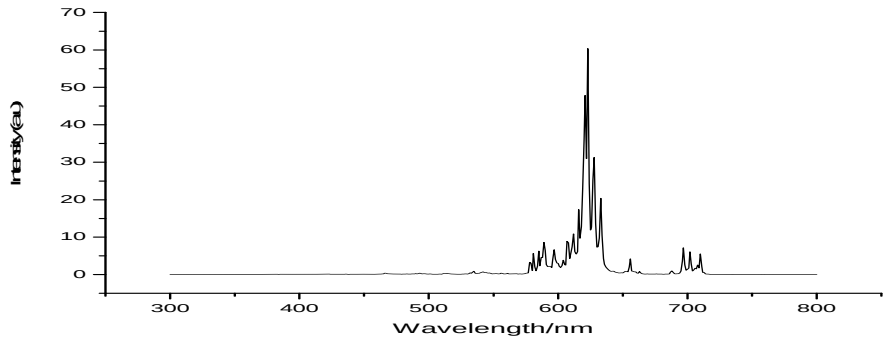

(b-55)

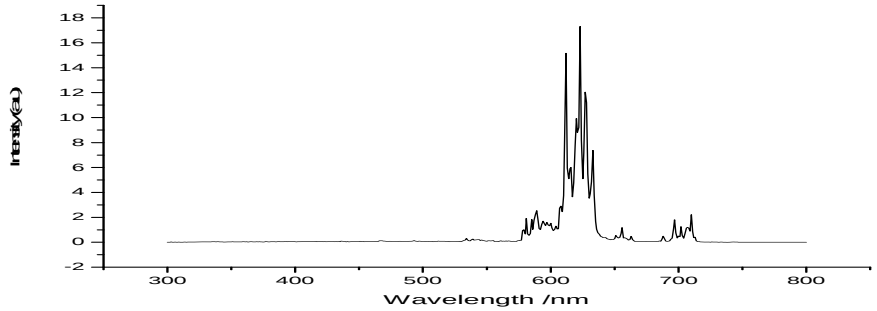

(c-56)

Figure 5.19B Photoluminescent emission, spectra of the samples fired at 900°C prepared from ethanolic solution. Emission spectra 1:1-54 (a), 1:2-55 (b), 1:3-56 (c). Excitation wavelength 254nm.

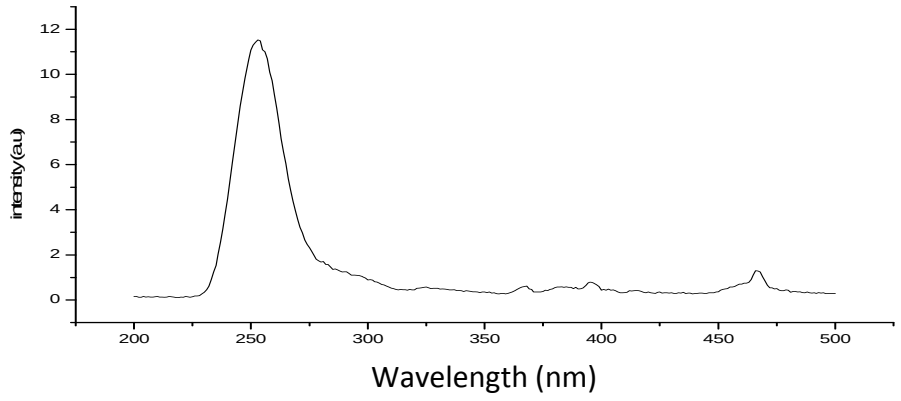

(D)

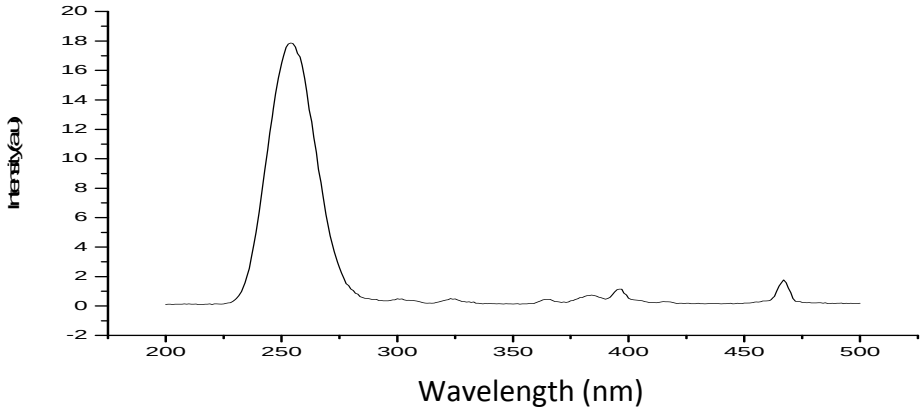

(E)

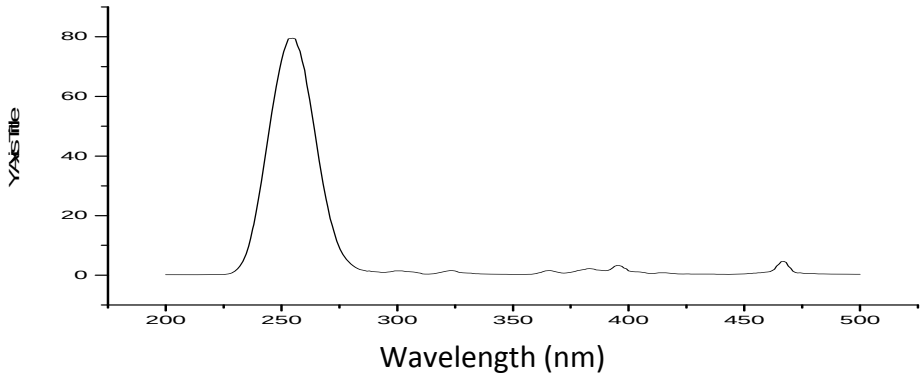

(F)

Figure 5.19C Photoluminescent excitation, spectra of the 900°C samples prepared from ethanolic solution. Excitation graphs 1:1 (D), 1:2 (E), 1:3 (F). Excitation monitored at 611 nm. Excitation wavelength 254nm.

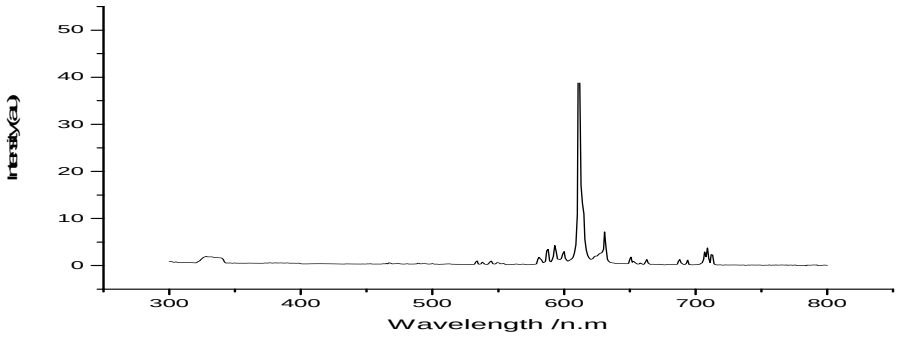

(D)

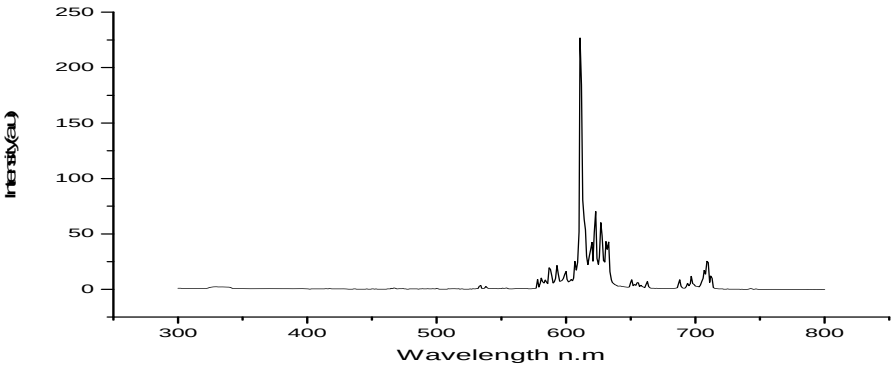

(E)

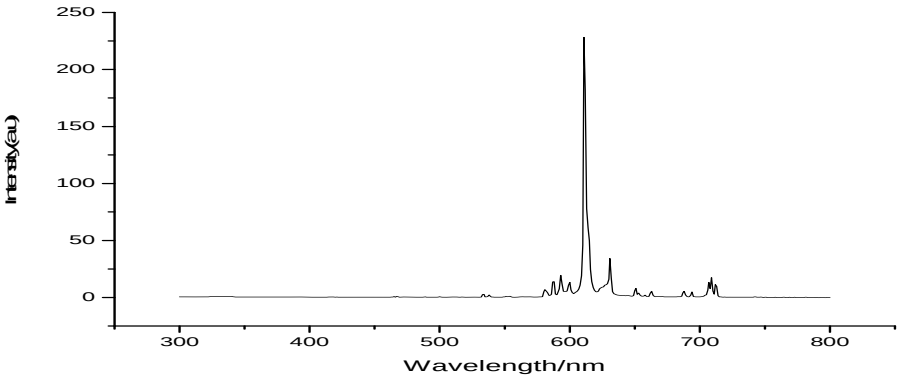

(F)

Figure 5.19D Photoluminescent emission, spectra of the 900°C samples prepared from ethanolic solution. Emission graphs 1:1 (D), 1:2 (E), 1:3 (F).Excitation monitored at 611 nm. Excitation wavelength 254nm.

Typical excitation and emission spectra are presented in Figures 5.19A 5.19B 5.19Cand5. 19D for the 1:1, 1:2 and 1:3 900°C samples prepared from ethanol solutions. From the above five of the samples made from ethanol contain monoclinic $Y_4O_5Cl_2:Eu^{3+}$. All the PL emission spectra of these samples of monoclinic $Y_4O_5Cl_2:Eu^{3+}$ and are clearly different from those of cubic $Y_2O_3:Eu^{3+}$ (compare Figure 5.18), as are the excitation spectra. In the case of the excitation spectra the relative intensities of the excitation bands of those prepared from the ethanolic solutions are very different to those prepared from the methanolic solution (see Figures 5.18 and 5.19A). All the spectra in Figure 5.19A have a shoulder on the main band (centered around 255nm on). The shoulder in the spectra in Figure 5.19A is clearly a more intense version of the 300nm centred band in Figure 5.18. In the samples D, E and F Figure 5.19C only sample D shows this shoulder. The emission spectra in Figures 5.19B and 5.19D are also very different those prepared from the methanolic solutions all contain more bands than those of Figure 5.18. This clearly reflects the different amounts of monoclinic $Y_4O_5Cl_2:Eu^{3+}$ present in the samples prepared from ethanol compared to the amounts of cubic $Y_2O_3:Eu^{3+}$ present.

5.4.5 Thermal Methods

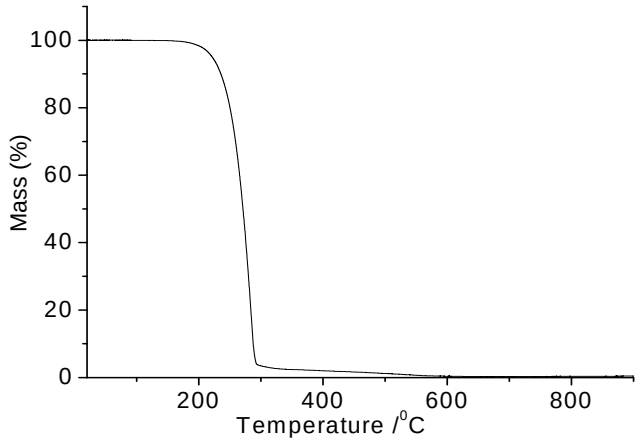

Figure. 5.20 TGA trace of the alkyl ammonium salt, $[C_{16}H_{33}NH_3]^+ Cl^-$ heated in air at a rate of 10°C per min.

Chapter 5 $Y_2O_3:Eu^{3+}$ phosphors from the $[(Y, Eu)\ Cl_3]$- $(C_{16}H_{33}NH_3Cl)$

The thermogravimetric analysis of the $[C_{16}H_{33}NH_3]^+\ Cl^-$ alkyl ammonium salt in air is shown in Figure 5.20 over the temperature range of room temperature to 900°C using a heating rate of 10°C/min. The mass loss is greater than 95% when the temperature is increased to 300°C and confirms that the alkyl ammonium salt has completely decomposed before the temperature reaches 650°C. This is consistent with the samples prepared from ethanolic solution and heated to 650°C, as is made evident by the XRD diffractograms shown in Figures 5.16A and 5.16B, being mixed yttrium/europium oxychloride species without the presence of any organic residue from the alkyl ammonium salt. Furthermore, it has been reported that $YCl_3.6H_2O$ decomposes to YOCl between 375 and 450°C [46], although it is possible that further transformation to $Y_4O_5Cl_2$ (≡ "$2YOCl.Y_2O_3$") and/or Y_3O_4Cl (≡ "$YOCl.Y_2O_3$") could occur, according to Equation 1, when the samples are prepared at 650°C.

So in figure it is apparent that the alkylammonium chains decompose into the gases CO_2, H_2O (steam) and NH_3, between the temperatures of 190°C and 250°C. So this process can now be identified in the more complex TGA data of the phosphor precursor materials.

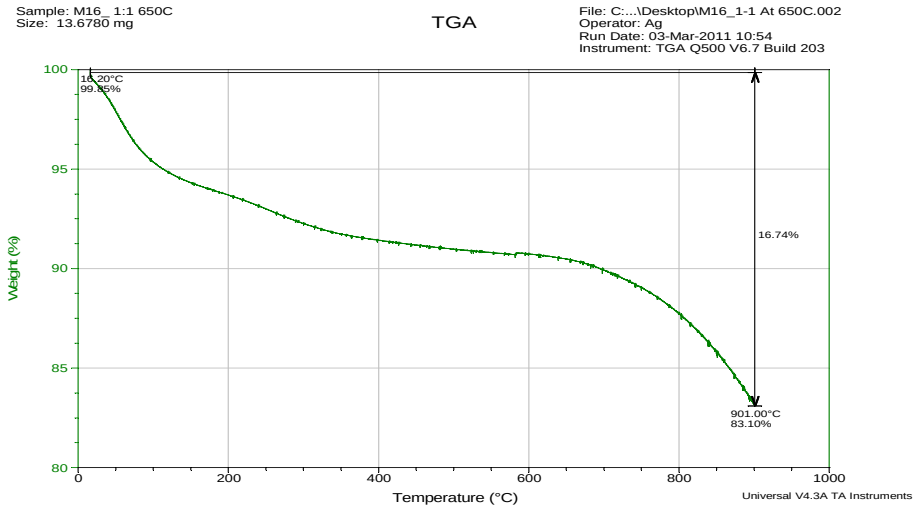

Figure 5.21 TGA trace of the 1:1 sample pre- fired at 650°C prepared from ethanolic solution (ran in air).

In Figure 5.21 the TGA of the 1:1 sample first fired at 650°C prepared from ethanolic solution (ran in air) is presented. It is apparent that there is evidence of some residual alkylammonium chains between 220°C and 300°C even after the combustion at 650°C. In fact the chains account for around 2% of the total mass of this sample. There is also evidence for some water from the initial wieght loss of around 5% up to 100°C.There is an additional weight loss of around 1.5% between 300°C and 600°C. Finally above 600°C there is a further weight loss of 8.8% of the original weight. If the weight at 600°C after remaining water and organics are removed is taken as 100%. Then the final weight loss becomes 9.56%. This weight loss may be due to either carbonates decomposing to oxide and CO_2 gas (see discussion in 5.3.5), or to chloride being replaced by oxide. As shown below it is most likely due to Cl being replaced by oxide. In fact if YOCl reacts with water vapour we would expect Y_2O_3 as:-

$$2YOCl + H_2O = Y_2O_3 + 2HCl \qquad \text{equation 4}$$

With a weight loss from the solid of 13.86%. However if the reaction was:-

$$4YOCl + H_2O = Y_4O_5Cl_2 + 2HCl \qquad \text{equation 5}$$

Then the weight loss would be 9.39% which is closer to the observed value for equation 5.

The third possibility is that shown in equation 6

$$Y_4O_5Cl_2 + H_2O = 2Y_2O_3 + 2HCl \qquad \text{equation 6}$$

Here the weight loss would be 10.82% which is not as close as that from equation 5 However from this data we cannot rule out that some carbonate decomposition has occurred on the surface of the particles and this could be the weight loss that occurs from 100°C to 600°C rather than being all due to residual alkylammonium chains.
In Figure 5.22 the TGA of the 1:2 sample first fired at 650°C prepared from ethanolic solution (ran in air) is presented. It is apparent that there is again evidence of either some residual alkylammonium chains or some carbonate decomposition. between 100°C and 600°C In fact this account for around 4% of the total mass of this sample as in Figure 5.21.

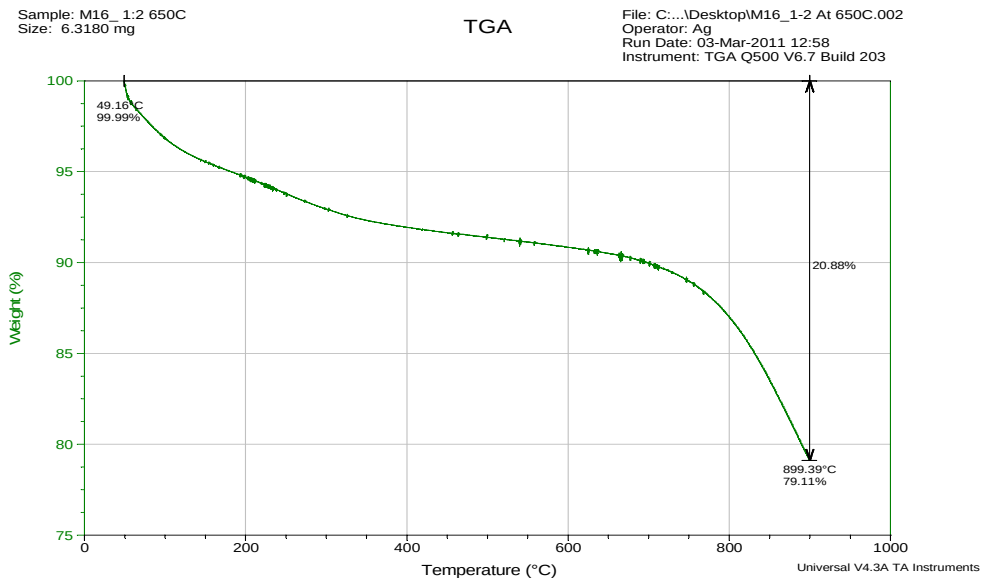

Figure 5.22 TGA trace of the 1:2 sample first fired at 650°C prepared from ethanolic solution (ran in air).

There is also evidence for some water from the initial wieght loss of around 4% up to 100°C. Finally above 600°C there is a further weight loss of 12% of the original weight. If the weight at 600°C after remaining water and organics are removed is taken as 100%. Then the final weight loss becomes 13.73% which is close to the value for equation 4.This weight loss is most likely to be due to chloride being replaced by oxide. In Figure 5.23 the TGA of the 1:3 sample first fired at 650°C prepared from ethanolic solution (ran in air) is presented. It is apparent that there is again evidence of some residual alkylammonium chains and or carbonate between 100°C and 600°C. In fact the chains again account for around 5% of the total mass of this sample as in Figure 5.21. There is also evidence for some water from the initial wieght loss of around 4% up to 100°C. Finally above 600°C there is a further weight loss of 9% of the original weight. If the weight at 600°C after remaining water and organics are removed is taken as 100%. Then the weight loss would be 9.8%. This weight loss is most likely to be due to chloride being replaced by oxide as in equation 6. To sum up the information from Figures 5.21,5.22 and 5.23 it is apparent that even combustion synthesis at 650°C leaves either some alkylammonium chain residues unconsumed and some surface carbonate that forms on cooling and standing .

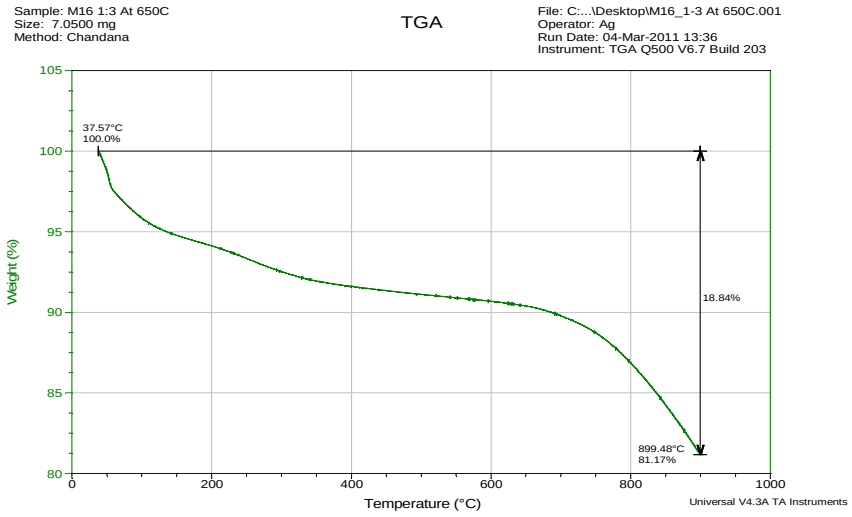

Figure 5.23 TGA trace of the 1:3 sample first fired at 650°C prepared from ethanolic solution (ran in air).

In addition these samples have either picked up water after cooling or reacted with steam produced in the combustion synthesis. If the weight loses above 600 °C are compared to the percentage of the remaining weight before this wieght loss, but after the water, the alkylammonium chain and or the carbonate loss, we can derive values of 90,44%, 86.27% and 90.2% of the final solid wieght above this temperature. Then if we assume the final product is Y_2O_3 then the values are not too far from the 89.18% we would have expected if the product above 600°C was predominantly $Y_4O_5Cl_2$. This would then have reacted with air to form the Y_2O_3. In Figure 5.24 the TGA of the 1:1 sample first fired at 900°C prepared from ethanolic solution (ran in air) is presented. It is apparent that there is again evidence of some residual alkylammonium chains or carbonate even after the combustion at 900°C. In fact the chains again account for around 2% of the total mass of this sample as in Figure 5.21. The carbonate may have been formed on the crystal surfaces after the samples cooled. There is also evidence for some water from the initial wieght loss of around 2% up to 100°C. Finally above 600°C there is a further weight loss 8.5% of the original weight. If the weight at 600°C after remaining water and organics are removed is taken as 100%. Then the final weight loss becomes 8.94%.

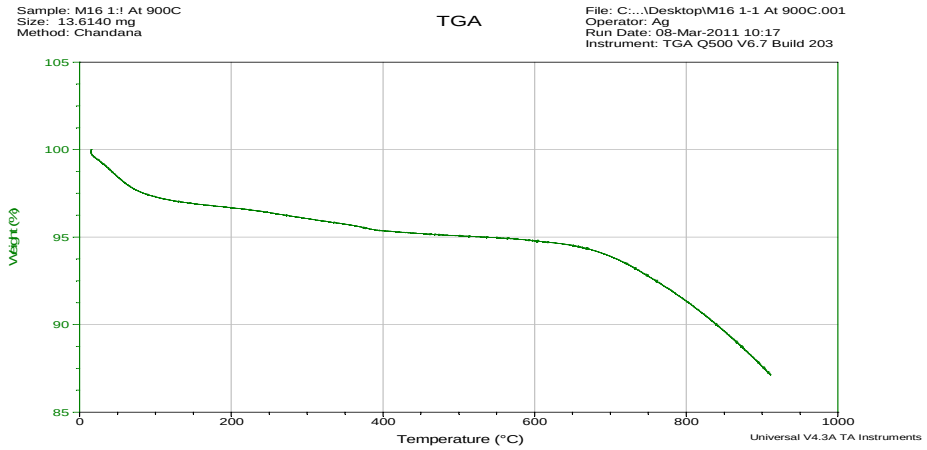

Figure 5.24 TGA trace of the 1:1 sample first fired at 900°C prepared from ethanolic solution (ran in air).

If the final product from the first firing was $Y_4O_5Cl_2$ and this is converted to Y_2O_3 then:-

$$Y_4O_5Cl_2 + H_2O = 2Y_2O_3 + 2HCl \qquad \text{equation 6}$$

a weight loss of 9.39% would be expected. So the experimental weight loss is close to the value for equation 6. This weight loss is most likely to be due to chloride being replaced by oxide when heated in air.

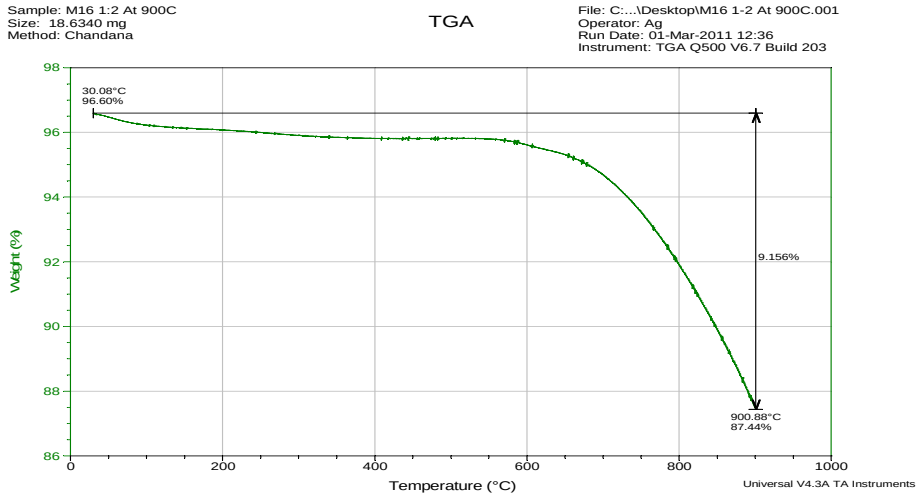

Figure 5.25 .TGA trace of the 1:2 sample first fired at 900°C prepared from ethanolic solution (ran in air).

In Figure 5.25 the TGA of the 1:2 sample first fired at 900°C prepared from ethanolic solution (ran in air) is presented. Here there is very little evidence of some residual alkylammonium chains even after the combustion at 900°C. In fact here the chains again account for less than 1% of the total mass of this sample as in Figure 5.21. There is also little evidence for water from the initial wieght loss of less than 1% up to 100°C. Finally above 600°C there is a further weight loss of 8.16% of the original weight. If the weight at 400°C after remaining water and organics are removed is taken as 100%. Then the final weight loss becomes 8.51%. If the final product from the first firing was $Y_4O_5Cl_2$ and this is converted to Y_2O_3 then from equation 6 a weight loss of 9.39% would be expected. So the experimental weight loss is less close to the value for equation 6, however it is not out of range completely. This weight loss is most likely to be due to chloride being replaced by oxide.

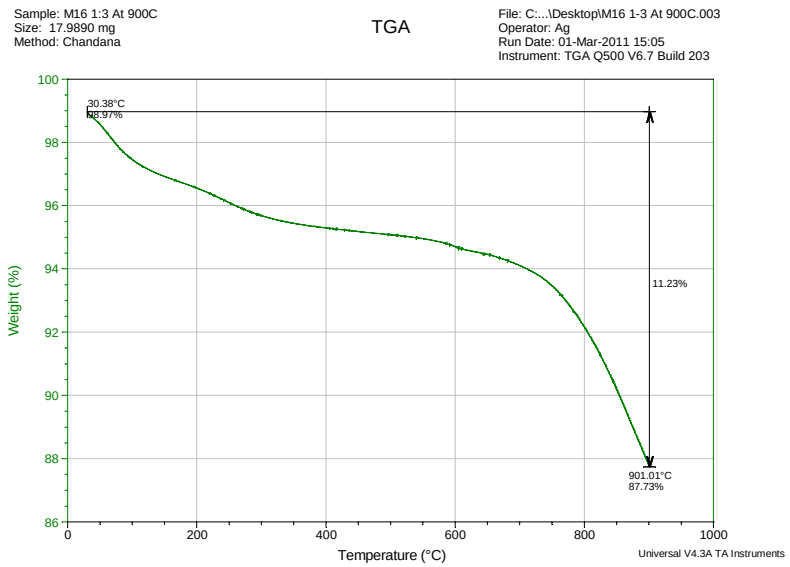

Figure 5.26 TGA trace of the 1:3 sample first fired at 900°C prepared from ethanolic solution (ran in air).

In Figure 5.26 the TGA of the 1:3 sample first fired at 900°C prepared from ethanolic solution (ran in air) is presented. It is apparent that there is again evidence of some residual alkylammonium chains even after the combustion at 900°C. In fact the chains again account for around 1.75% of the total mass of this sample as in Figure 5.21. There is also evidence for some water from the initial wieght loss of around 1.75% up to 100°C. Finally above 600°C there is a further weight loss of around 7.00% of the original weight. If the weight at 600°C after remaining water and organics are removed is taken as 100%. Then the final weight loss becomes 7.3%. If the final product from the first firing was $Y_4O_5Cl_2$ and this is converted to Y_2O_3 then from equation 6 a weight loss of 9.39% would be expected. So the experimental weight loss is less close to the value for equation 6, however it is not out of range completely. This weight loss

is most likely to be due to chloride being replaced by oxide. To sum up the information from Figures 5.24, 5.25 and 5.26 it is apparent that even combustion synthesis at 900°C leaves some alkylammonium chain or more likely carbonate residues unconsumed. In addition these samples have either picked up water after cooling or reacted with steam produced in the combustion synthesis. If the weight loses above 600 °C are compared to the percentage of the remaining weight before this wieght loss, but after the water and alkylammonium chain loss, we can derive values of 91.06%, 91.45%, and 93.7% of the final solid wieght above this temperature. Then again if we assume the final product is Y_2O_3 then the values are not too far from the 90.61% we would have expected if the product above 600°C was predominantly $Y_4O_5Cl_2$. This would then have reacted with air to form the Y_2O_3.

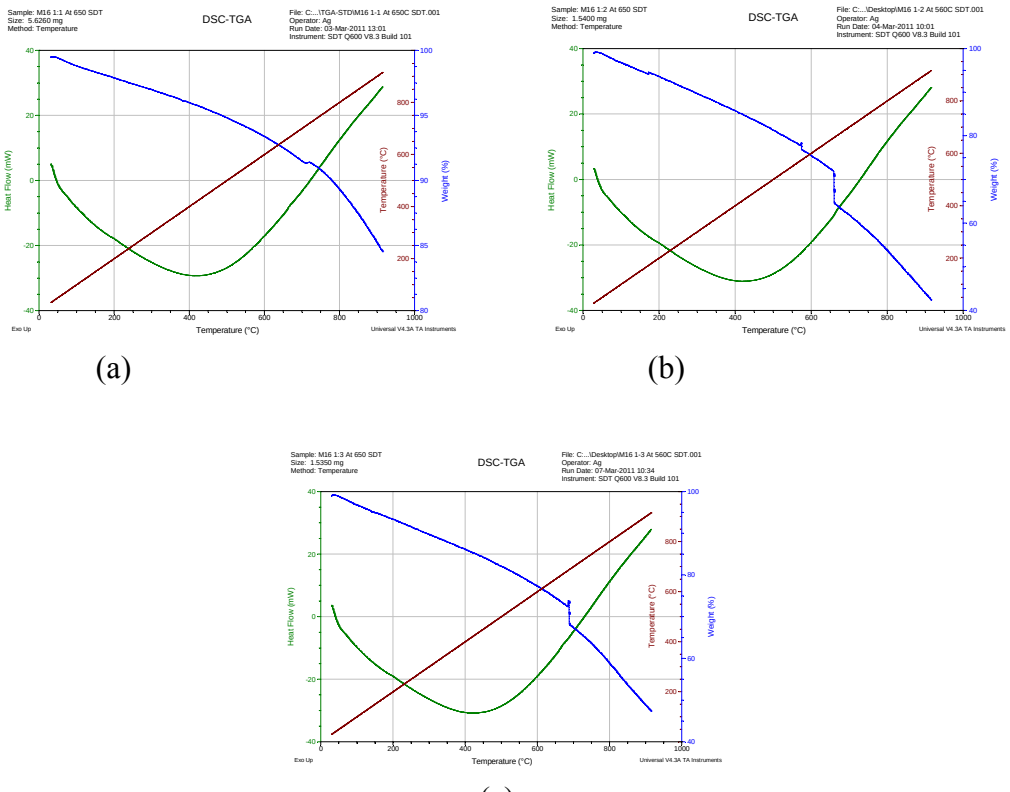

Figure 5.27 DSC/TGA traces of the (a)1:1, (b) 1:2 and (c) 1:3 samples first fired at 650°C prepared from methanolic solution (ran in air).

The green curves in Figure 5.27 show that the loss of water and the combustion of the remaining alkylammonium chains and or carbon dioxide release in all three samples that underwent combustion at 650°Care associated with heat loss and are therefore exothermic process, whereas between 400°C and 600°C there is a change over where the weight loss is due to an exothermic process in keeping with chloride being

replacedoxide as the Y_2O_3 forms and crystallizes.The blue curves in Figure 5.27 show overall wieght loss and give similar results to the TGA data presented above, but these curves are not as detailed as the previous TGA curves. The brown diagonal lines show the even regular temperature change.

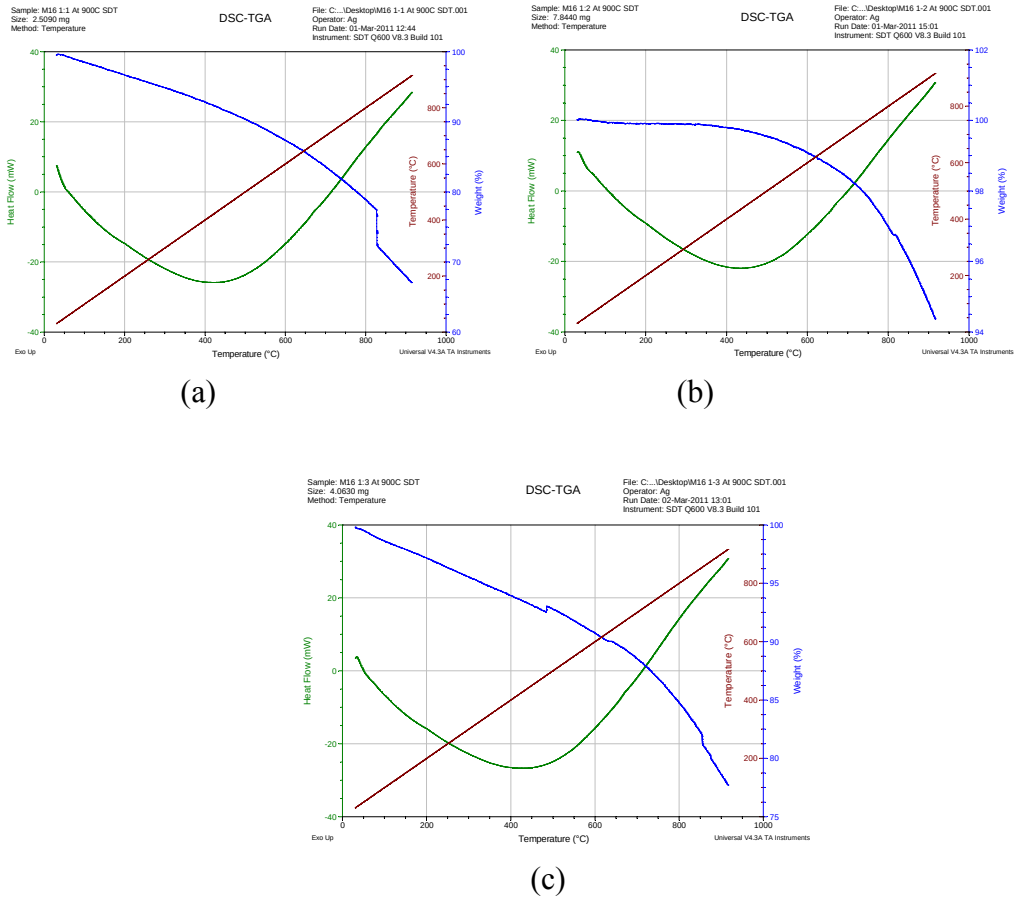

Figure 5.28 DSC/TGA traces of the (a)1:1, (b) 1:2 and (c) 1:3 samples first fired at 900°C prepared from methanolic solution (ran in air).

The green curves in Figure 5.28 show that the loss of water and the combustion of the remaining alkylammonium chains and or carbon dioxide release (carbonate conversion to oxide) in all three samples that underwent combustion at 900°C are associated with heat loss and are therefore exothermic process, whereas between 400°C and 600°C there is again a changeover where the weight loss is due to an exothermic process in keeping with chloride being replaced by oxide as the Y_2O_3 forms and crystallizes.

The blue curves in Figure 5.28 show overall wieght loss and give similar results to the TGA data presented above, but these curves are not as detailed as the TGA curves. The brown diagonal lines show the even regular temperature change.

5.4.6 Discussion of results so far presented on samples prepared at 900°C

At this point it is worth exploring why the samples prepared at 900°C from ethanol are different from those prepared from methanol. First it should be stated that all the preparations were performed twice so the findings are repeatable. The difference in the methanol and ethanol samples is only the solvent, however as the solvents were not totally removed as they were only left in air for 24h before firing the samples still contained solvent when they were fired. Hence there was more carbon content in the ethanol samples on firing and this would have formed extra carbon dioxide. This gas is heavier than air and may have displaced excess oxygen from the vicinity of the crucible. Hence there was not enough oxygen in the furnace to convert all the way to the cubic $Y_2O_3:Eu^{3+}$ and hence only partial oxidation took place to form monoclinic $Y_4O_5Cl_2:Eu^{3+}$. As explained in the experimental section 5.2 the muffle furnaces used in the preparations though having chimneys for waste gases to pass through did not have air circulation other than the chimneys. The furnace used for the phosphor samples prepared from ethanol fired at 900°C samples (D, E and F) had a chimney with a diameter of 3 cm, whereas that used for the three repeat combustions samples 54, 55 and 56 had a diameter of 1 cm. The latter fact of the narrower chimney combined with the extra fuel in the ethanolic samples means that the CO_2 produced did not pass up the chimney well and deprived the reaction of oxygen thus limiting the oxidation. This is important in understanding the synthesis of monoclinic $Y_4O_5Cl:Eu^{3+}$ which is a phosphor that has only been reported twice in the literature [33, 46]. However as the monoclinic $Y_4O_5Cl_2:Eu^{3+}$ was prepared as nanoparticles they proved to be very unstable to some experimental investigations as will be apparent in the following sections.

5.4.7 Cathodoluminescence Spectra

The Cl (5000V, emission current 9.6μA) defocused and focused spectra of the products are shown in Figures 5.29 and 5.30. Those in Figure 5.29 of the samples prepared from methanol are all similar and typical of cubic$Y_2O_3:Eu^{3+}$. Those prepared from ethanol (see Figure 5.30) are all similar to the corresponding photoluminescent spectra and in addition to the presence of cubic $Y_2O_3:Eu^{3+}$ shows other material is also present. These spectra have similarities to those seen in Figures 5.19A, 5.19B and 5.19D and are indicative of $Y_4O_5Cl_2$. However during the further Cl studies we noticed subtle changes in these spectra as a function of applied voltage and beam current.

.

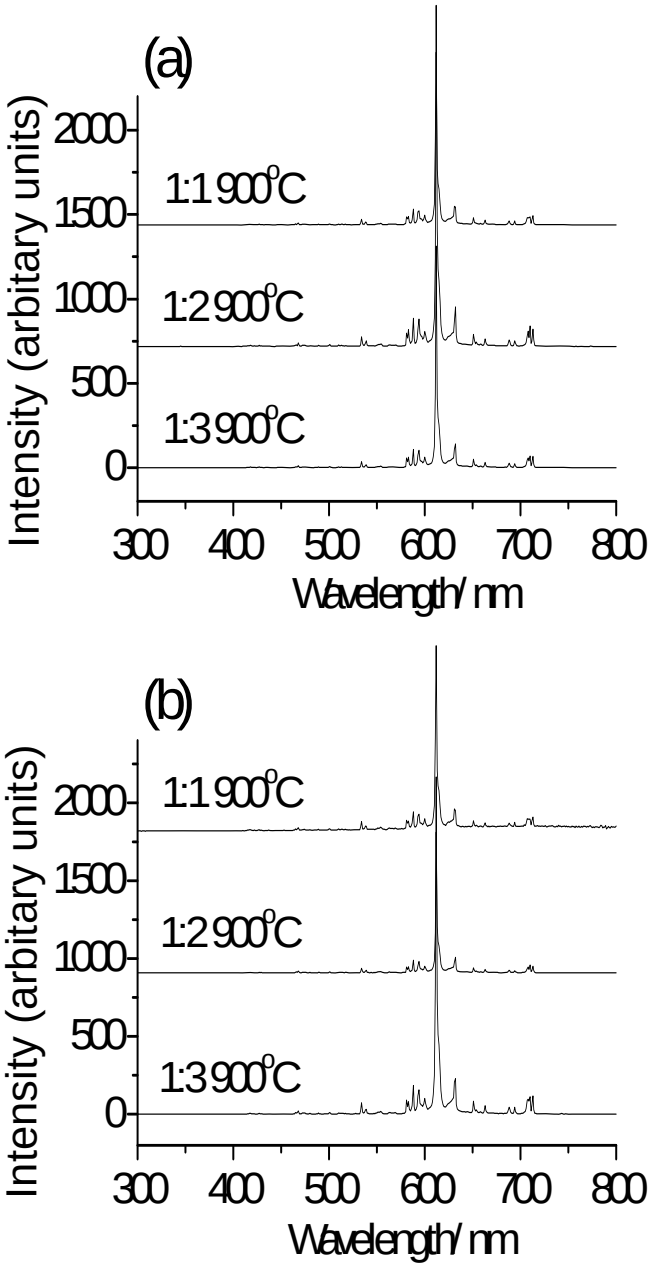

Figure 5.29 Cathodoluminescent spectra of the 900°C samples (prepared from methanolic solution): (a) focused beam and (b) defocused beam. At 5000V/50uA.

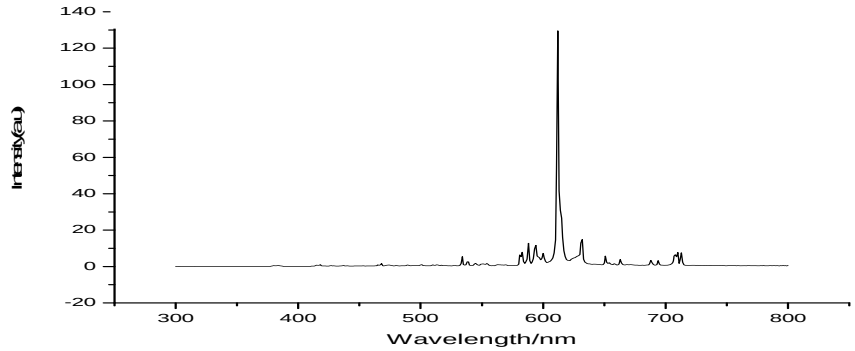

1:1 (D)

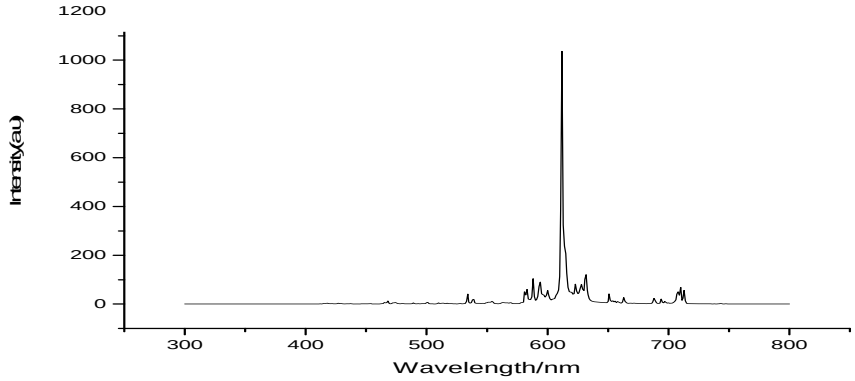

1:2 (E)

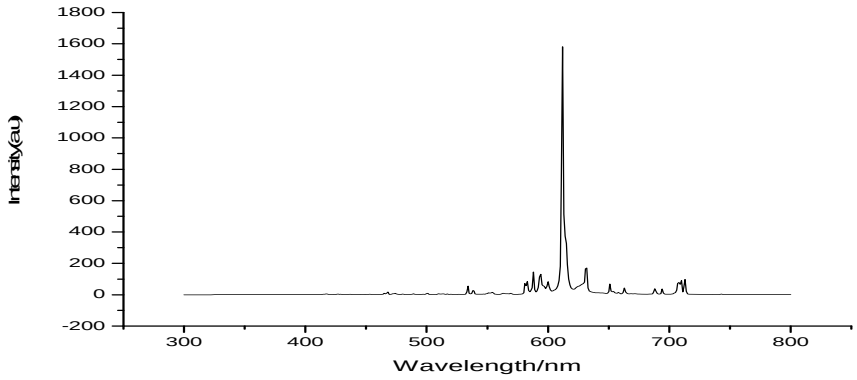

1:3 (F)

Figure 5.30A Cathodoluminescent spectra of the 900°C samples prepared from ethanolic solution, Defocused beam. Samples 1:1 (D), 1:2 (E), and 1:3 (F) at 5000V/50uA.

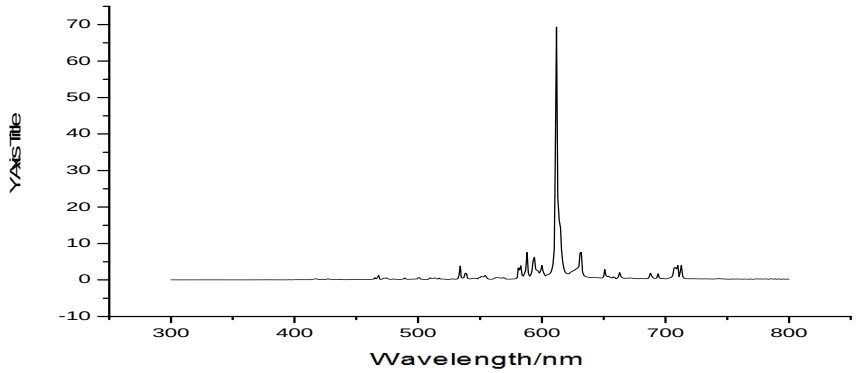

1:1 (D)

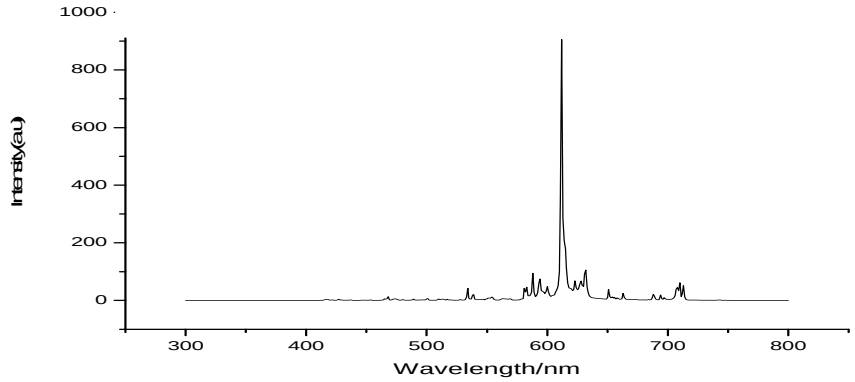

1: 2 (E)

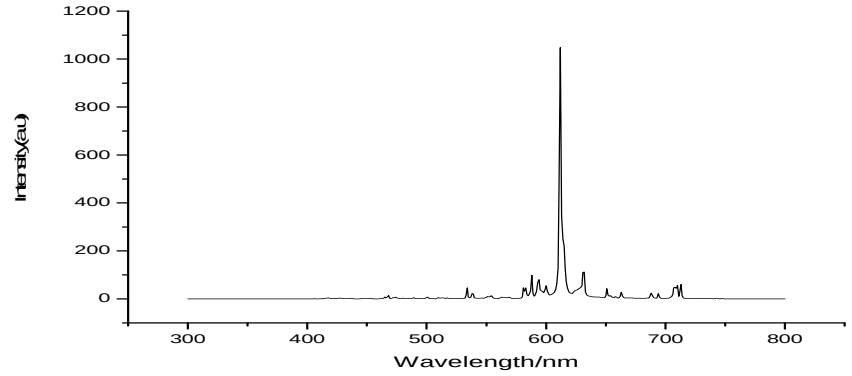

1:3 (F)

Figure 5.30B Cathodoluminescent spectra of the 900°C samples prepared from ethanolic solution, focused beam. Samples 1:1(D), 1:2 (E) and 1:3 (F) at 5000V/50uA.
Cl spectra for samples 54, 55, 56 Ethanol base defocused at5000V/50uA

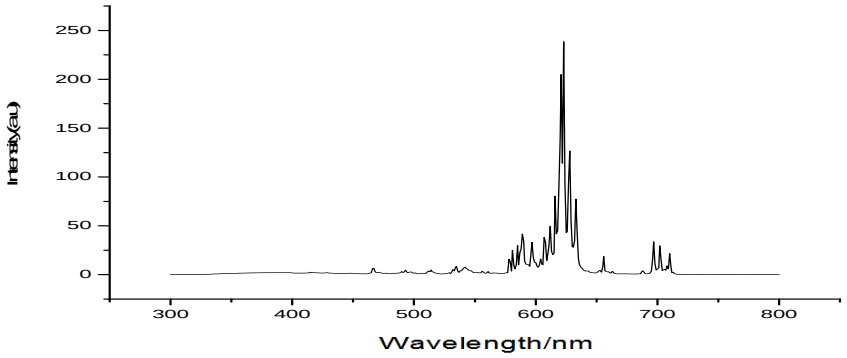

1:1 (a-54)

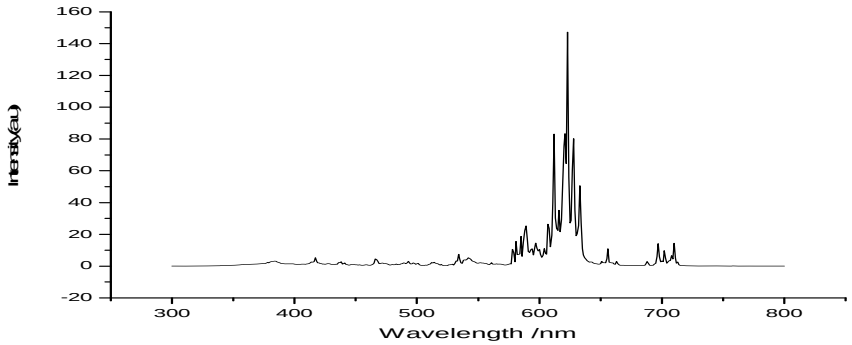

1:2 (b-55)

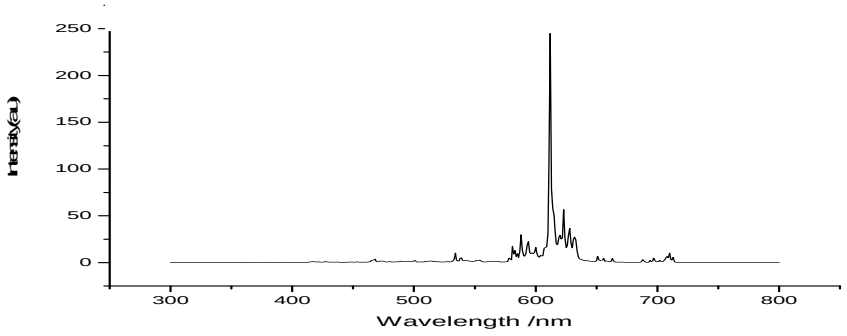

1:3 (c-56)

Figure 5.31 Cathodoluminescent spectra of the 900°C samples prepared from ethanolic solution, Defocused beam. Defocused 1:1 (a-54), 1:2 (b-55), and 1:3 (c-56), at 5000V/50uA.

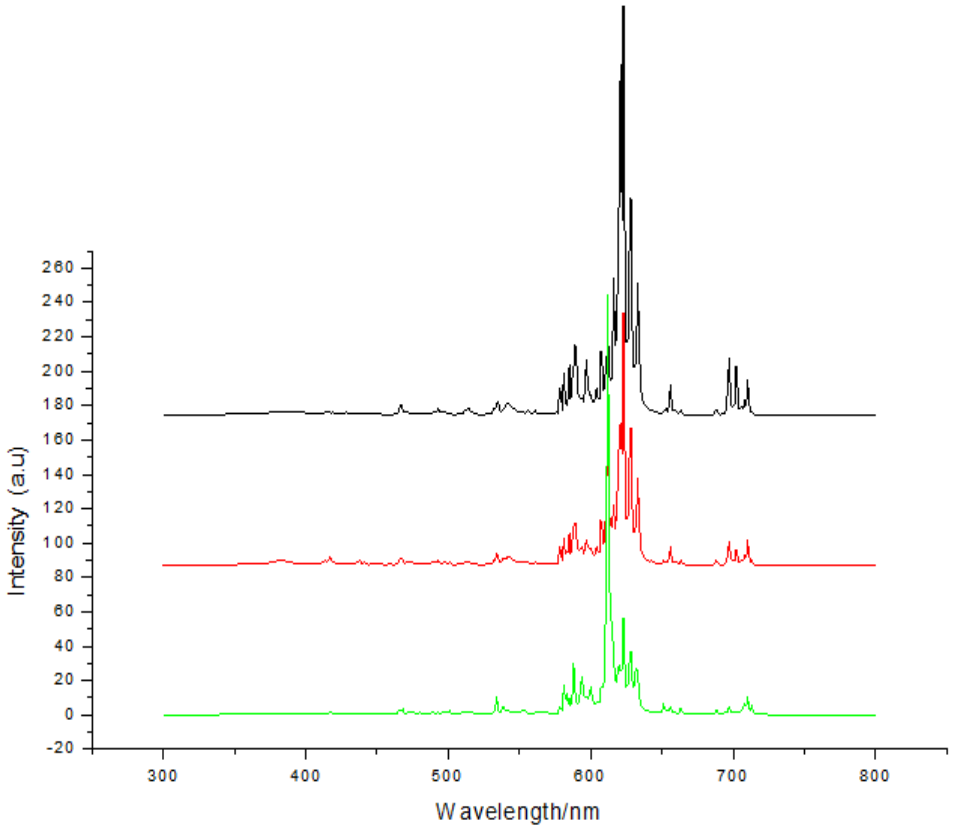

Figure 5.32 Cathodoluminescent spectra of the 900°C samples prepared from ethanolic solution, Defocused beam. Defocused overlay 1:1(a-54) Black, 1:2(b-55) Red, 1:3(c-56) Green, bottom at 5000V/50uA.

5.4.8 The Raman spectra of the samples prepared from methanol annealed at 900°C for the 1:1 and 1:3 ratios (previously shown in Figure 5.11/5.12 (c) and (d)) display the strong Raman band at 377 nm (arrowed) which was absent in the spectra of the low temperature treated samples (a and b) and is due to cubic Y_2O_3:Eu. Cubic Y_2O_3Eu is predicted to have twenty two first order Raman active modes [37, 39-44]. Raman spectroscopy has been previously used to determine the temperature at which $Y_2O_3:Eu^{3+}$ phosphor samples crystallize from hydroxycarbonate precursors [14]. The intensity of the cubic Y_2O_3 band at 377 cm^{-1} is correlated to the degree of crystallinity of the $Y_2O_3:Eu^{3+}$ phosphor powders. Figures 5.33 and 5.34(a) show a Raman spectrum of the 1:1 molar ratio prepared from ethanol after combustion at 650°C. The bands at 107 and 167 cm^{-1} are assigned to a rhombohedral disordered SmSI-PbFCl type YOCl phase [47]. The Raman spectrum of the 1:1 molar ratio prepared from ethanol after combustion at 900°C is presented in Figure 5.34(b) exhibits bands at 160, 215, 260, 375 and 526 cm^{-1}, which can be assigned to the tetragonal form of YOCl by comparison to a Raman spectrum of a pure sample of this compound

(see Figure 5.34(c). Additional bands in the spectrum shown in Figure 5.34(b) are due to other products of the combustion reaction at 900°C. All the samples prepared from ethanol annealed at 900°C for the 1:1 1:2 and 1:3 ratios (see Figure 5.34) show evidence of the sharp due to the cubic phase of Y_2O_3: Eu^{3+} though only a small amount of this phase is present. The additional number of other strong bands that appear in these spectra Figures 5.34 and 5.35 are probably due to the $Y_4O_5Cl:Eu^{3+}$ phosphor. The other bands seen for these materials presented in Figure 5.36 are due to the photoluminescence of the $Y_4O_5Cl:Eu^{3+}$ phosphor under 632.8 nm excitation. Thus a spin off from the main thrust of this work is that nanocrystallites of tetragonal and rhombohedral forms of YOCl having dimensions in the range of 1-100 nm have been prepared by a novel templating method involving the use of alkylamine hydrochlorides. This work demonstrates that the structure of the YOCl product is dependent on the firing conditions, the rhombohedral and tetragonal types being formed at nominal combustion temperatures of 650 and 900°C, respectively.

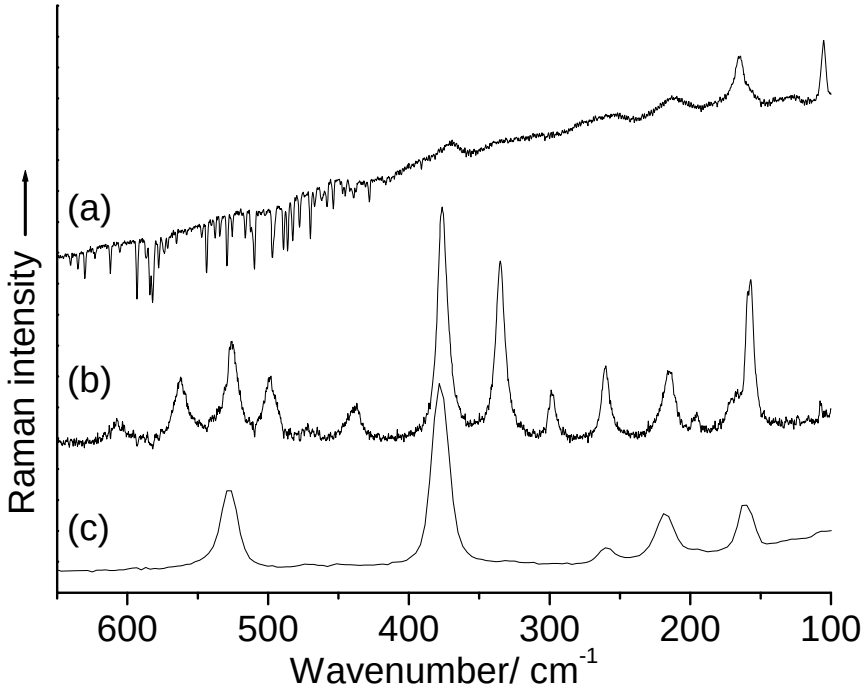

Figure 5.33 The Raman spectra of (a) the 1:1 molar ratio prepared from ethanol after combustion at 650°C,(b) the spectrum of the 1:1 molar ratio prepared from ethanol after combustion at 900°C; (c) a reference sample of the tetragonal form of YOCl. The exciting wavelength was equal to 1064 nm.

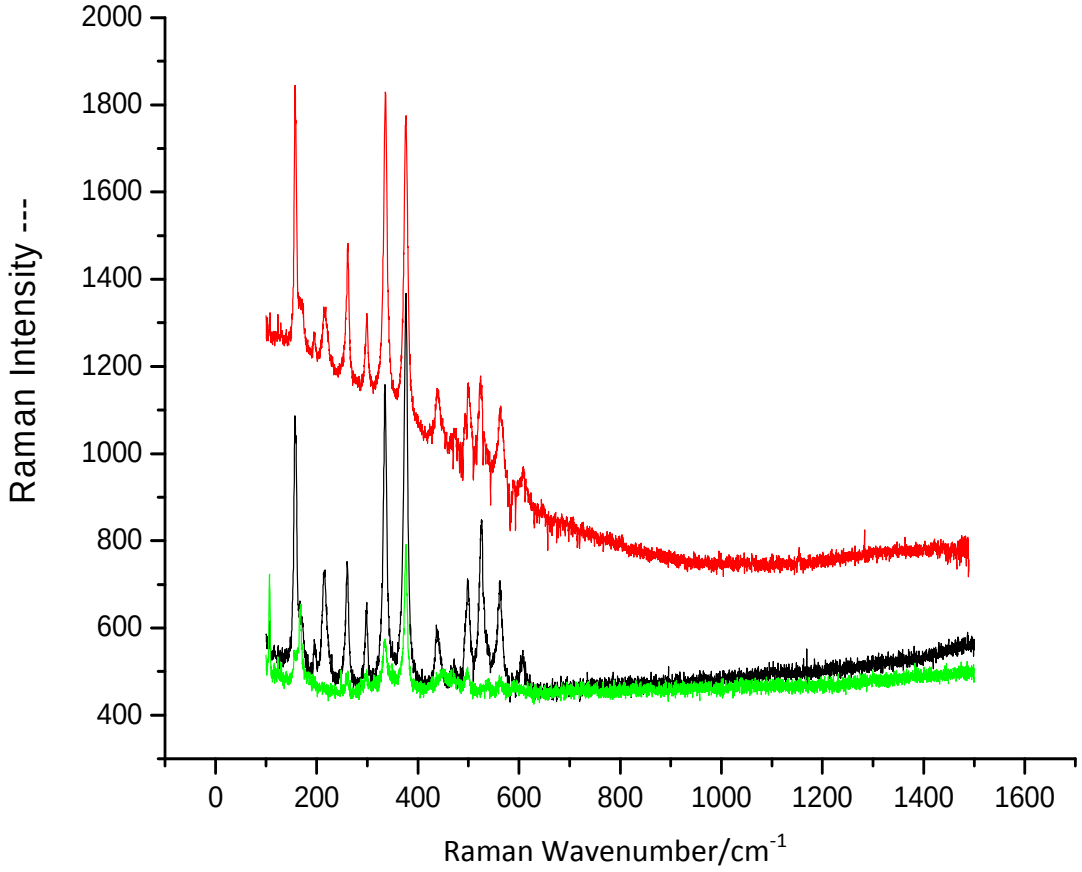

Figure 5.34 The Raman spectra of the 1:1 molar ratio prepared from ethanol (in black) same spectrum given in Figure 5.34(b) after combustion at 650°C; the spectrum of the 1:2 molar ratio prepared from ethanol after combustion at 900°C (in red); the spectrum of the 1:3 molar ratio prepared from ethanol after combustion at 900°C (in green). The exciting wavelength was equal to 1064 nm.

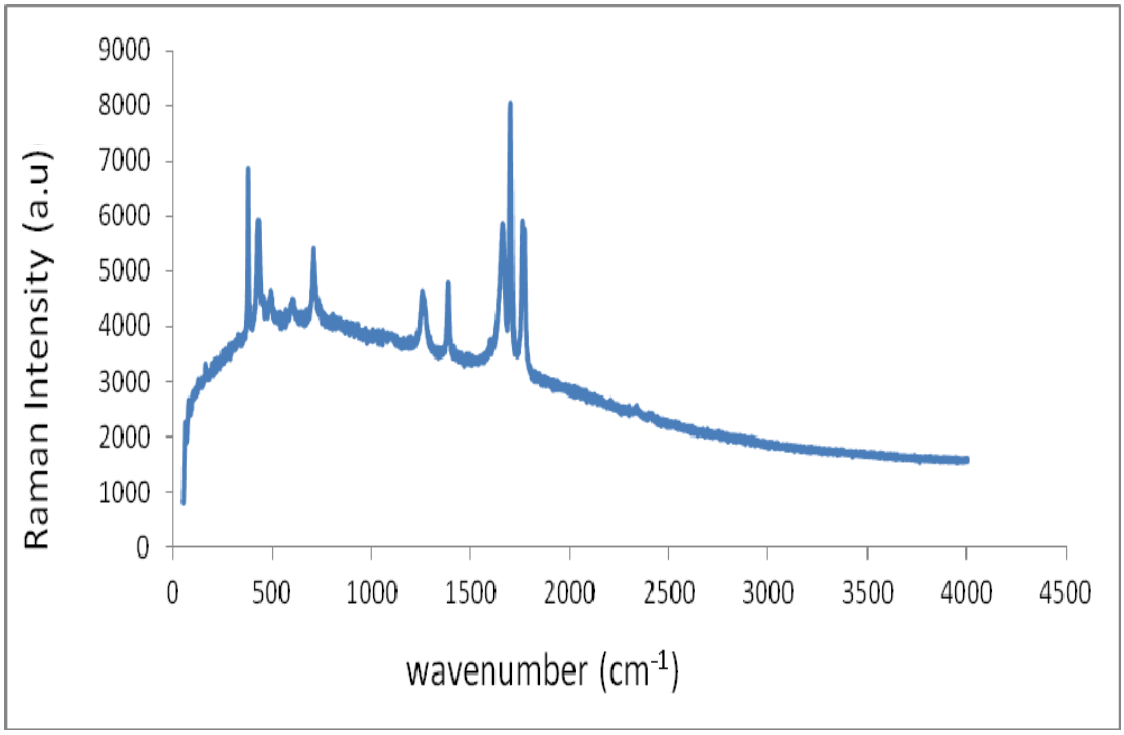
Raman Intensity (a.u)
9000
8000
7000
6000
5000
4000
3000
2000
1000
0
0
500
1000
1500
2000
2500
3000
3500
4000
4500
wavenumber (cm-1)

1:1 (D)

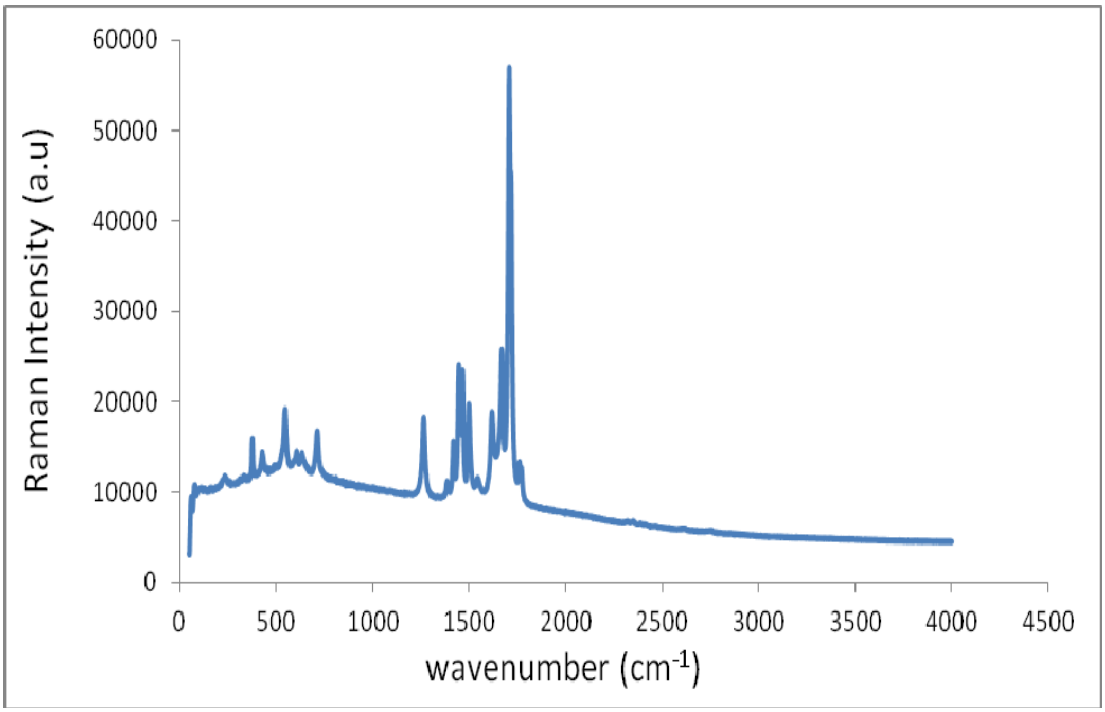
Raman Intensity (a.u)
60000
50000
40000
30000
20000
10000
0
0
500
1000
1500
2000
2500
3000
3500
4000
4500
wavenumber (cm-1)

1:2 (E)

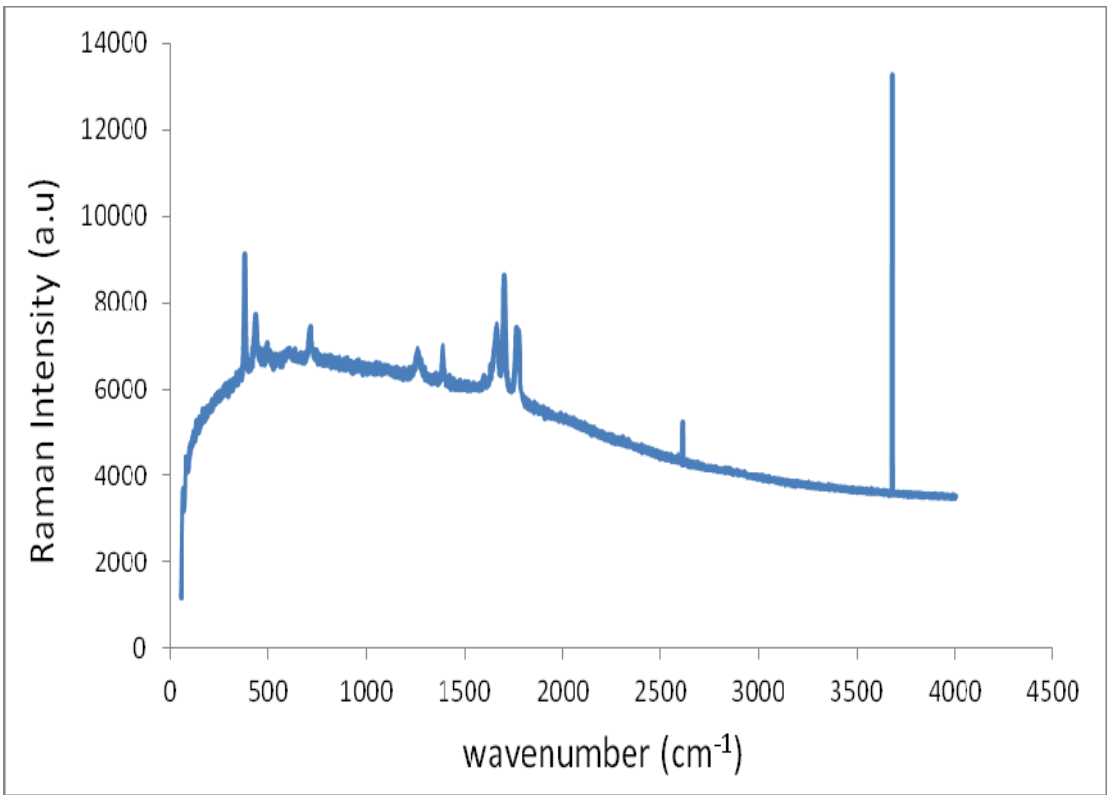

Figure 5.35 The Raman spectra of the (D) 1:1 molar ratio prepared from ethanol after combustion at 900°C; the spectrum of the (E) 1:2 molar ratio prepared from ethanol after combustion at 900°C ; the spectrum of the (F) 1:3 molar ratio prepared from ethanol after combustion at 900°C. The exciting wavelength was equal to 632.8 nm.

5.4.9 FTIR Spectra: The FTIR spectra from the samples prepared from methanolic solutions fired at 900°C are summarised in Table 5.4 and in Figure 5.36 and a comparison with the FTIR spectra of Figure 5.9 indicates that they are substantially different. Moreover, the positions of the basic yttrium carbonate (yttrium hydroxycarbonate) bands in the spectra of Figure 5.36 are in excellent agreement with those reported in the spectra of basic carbonates [(Y,Eu)$OHCO_3.H_2O$] precipitated by adding ammonium carbonate precipitating reagent to a homogeneous yttrium and europium chloride solution [48]. This finding will be explained below.The strong doublet with peaks at 1515 and 1403 cm^{-1} is assigned to the antisymmetric C-O stretching vibration of the CO_3^{2-} anion of the hydroxycarbonate, and the broad band in the 3600 to 3000 cm^{-1} region is assigned to the O-H stretching vibration. The only other noteworthy feature in these spectra is a weak band at 844 cm^{-1}, which appears at

the same wavenumber location as that reported in the spectra of basic carbonates precipitated by adding ammonium carbonate precipitating reagent to a homogeneous yttrium and europium chloride solution [48]. This band is assigned to the out of plane bending vibration of the CO_3^{2-} anion [36].It is clear from these results that the combustion fuel that was present in the samples in conjunction with the higher annealing temperature (900°C) was sufficient to raise the combustion temperature for nanometer sized crystallites of the cubic $Y_2O_3:Eu^{3+}$ phase to form in the materials prepared from methanol. As has been mentioned in the foregoing, the infrared spectra show bands which are due to the presence of yttrium hydroxycarbonate. This can be formed from the reaction of the surfaces of the nanometre sized particles of $Y_2O_3:Eu^{3+}$ with atmospheric CO_2 and H_2O at room temperature. In this work the nanometre sized particles of $Y_2O_3:Eu^{3+}$ were formed from the rapid combustion of a methanolic precursor gel containing $C_{16}H_{33}NH_3Cl$ and $YCl_3:Eu^{3+}$ at a set temperature of 900°C according to reaction (1). $Y_{0.98}Eu_{0.02}(OH)CO_3$ would not have formed via reaction (2) under these conditions, because it is unstable at 900°C; however, it is formed on the surfaces of the $(Y_{0.98}Eu_{0.02})_2O_3$ nanoparticles at room temperature due to reaction with atmospheric CO_2 and H_2O.In the past we have prepared larger nanometer sized particles of the metal oxide by the hydrothermal decomposition of urea facilitating the homogeneous precipitation of spherical sub-micrometre europium-doped yttrium hydroxycarbonate phosphor precursor particles. It is useful to explain this latter method here to help to understand the infrared data obtained in this work. This method is dependent on the addition of, and hydrothermal decomposition of, urea in acid solution in the presence of metal salts that are soluble at acid pHs. The chemistry involved includes the following steps [18, 49- 50].

Aqueous decomposition of urea (<85 ºC, ~ pH 3) resulting in the following ions,

$$H_2NCONH_2 \rightarrow NH_4^+ + OCN^- \quad (7)$$

The resulting cyanate ion rapidly reacts thus,

$$OCN^- + 2H^+ + 2H_2O \rightarrow H_2CO_3 + NH_4^+ \quad (8)$$

In the presence of Y^{3+} and Eu^{3+} cations which are added as acid salts the solution pH drops to ~2.5. The urea is added and the resulting hydroxonium ions (H_3O^+) promote urea decomposition. The subsequent release of carbonate ions causes precipitation of the metal hydroxycarbonate phosphor precursor, once the concentration of reactants reaches supercritical saturation:

$$[(Y,Eu)OH(H_2O)_x]^{2+} + H_2CO_3 \rightarrow [(Y,Eu)OHCO_3.yH_2O] + (x-y)H_2O + 2H^+ \quad (9)$$

Careful firing of the precursor particles allows their spherical morphology to be partially maintained in the resulting phosphor particles. This method for the preparation of cubic $Y_2O_3:Eu^{3+}$ has previously been reported for the dopant concentration range from 0.2 mole fraction to $1x10^{-3}$ mole fraction Eu^{3+} both by ourselves and others [3-18]. In the current work it has been shown that the surfaces of the $Y_2O_3:Eu^{3+}$ nanoparticles react with atmospheric CO_2 and H_2O to form [(Y,Eu)$OHCO_3$] at room temperature. This indicates that, although cubic $Y_2O_3:Eu^{3+}$ can be formed by firing yttrium/europium hydroxycarbonate at temperatures higher than ca. 700°C, the reverse transformation occurs on the surfaces of $Y_2O_3:Eu^{3+}$ nanoparticles in air at room temperature.This shows that cubic $Y_2O_3:Eu^{3+}$ is thermodynamically unstable in the presence of carbon dioxide and water vapour and reverts to the metal hydroxylcarbonate precursor.

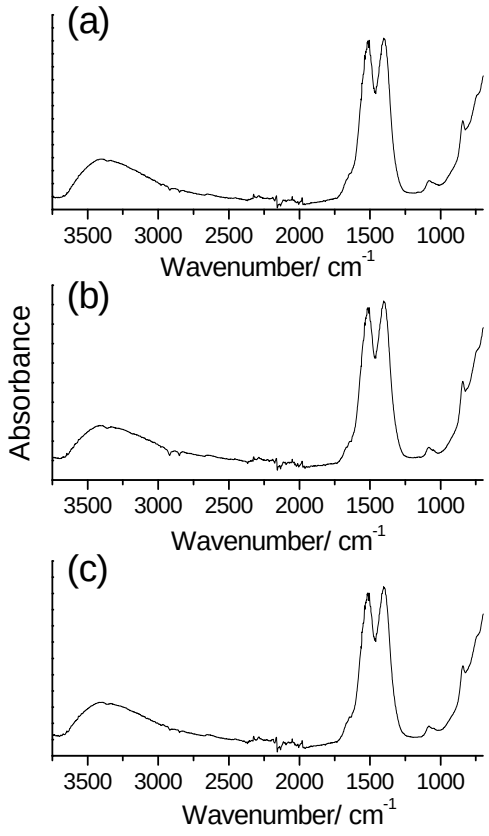

Figure 5.36 FTIR spectra of the samples fired at 900°C prepared from methanolic solution with metal ion to alkylammonium chloride ratios: (a) 1:1, (b) 1:2 and (c) 1:3 in KBr discs.

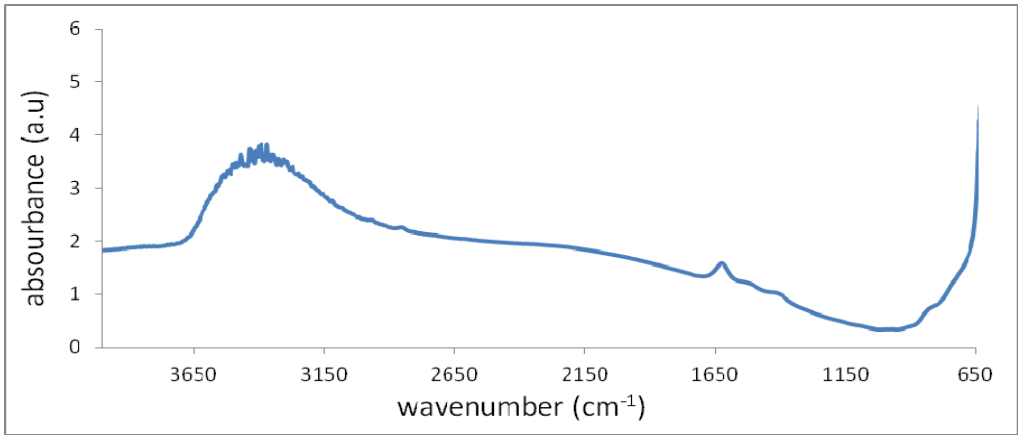

(a)

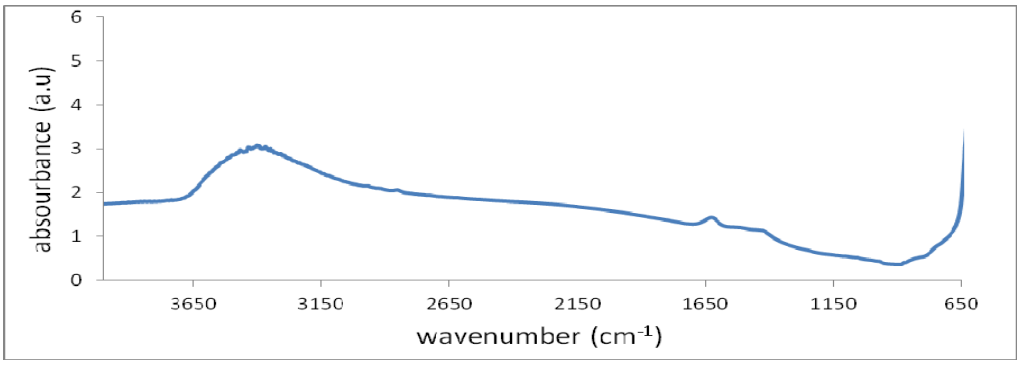

(b)

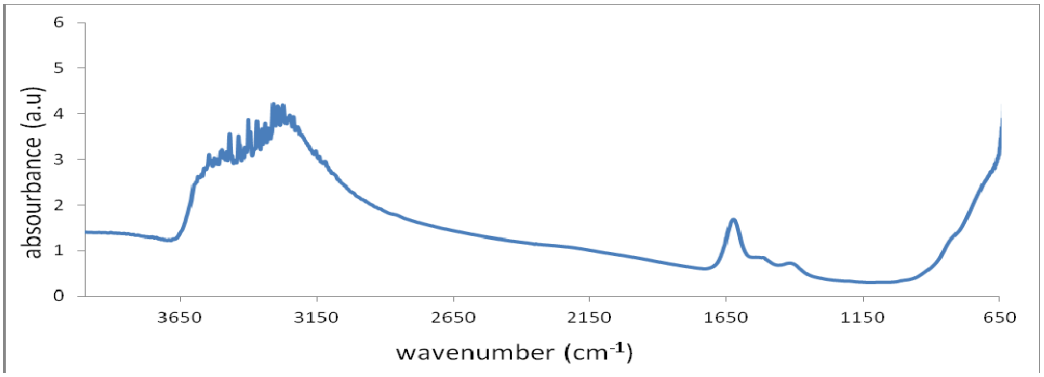

(c)

Figure 5.37 FTIR spectra of the samples fired at 900°C prepared from ethanolic solution with metal ion to alkylammonium chloride ratios: (a) 1:1,-54 (b) 1:2 -55 and -56(c) 1:3 in KBr discs.

Table 5.4 Materials prepared at 900°C

Wavenumber/cm^{-1}		
3600-3000	*(m)*	ν (O-H)
	(m)	ν_s (O-H)
1633	*(shoulder)*	δ (O-H)
1515	*(s)*	ν_{as} (CO_3^{2-})
1403	*(s)*	ν_{as} (CO_3^{2-})
1082	*(w)*	δ (O-H)
844	*(w)*	δ (CO_3^{2-})

The FTIR spectra from the samples prepared from ethanolic solutions fired at 900°C are summarised in Table 5.4 and in Figures 5.37 and 5.38 and a comparison with the FTIR spectra of Figure 5.36 indicates that they are substantially different from those prepared from the methanolic solutions as expected from the fact that here the carbonate has grown on the surface of monoclinic $Y_4O_5Cl_2:Eu^{3+}$ and not cubic $Y_2O_3:Eu^{3+}$. The samples in Figure 5.38 are taken in KBr discs. It was also observed that bands due to metal hydroxycarbonates of some kind in the infrared spectra of the monoclinic $Y_4O_5Cl_2:Eu^{3+}$ nanoparticles were present. These bands are in different positions to those found in bulk [(Y, Eu)$OHCO_3.H_2O$], and are explained as arising from the spontaneous reaction of the surface of the nanometer sized particles of the monoclinic $Y_4O_5Cl_2:Eu^{3+}$ with atmospheric CO_2 and water vapour. This indicates that nanometre sized particles of the monoclinic $Y_4O_5Cl_2:Eu^{3+}$ are also thermodynamically unstable in the atmosphere and must be protected against such back reactions.

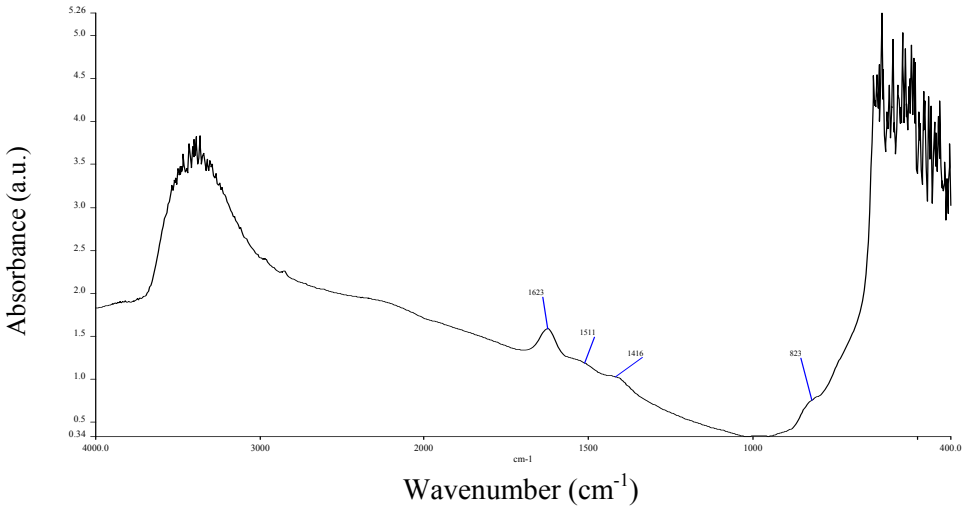

(a)

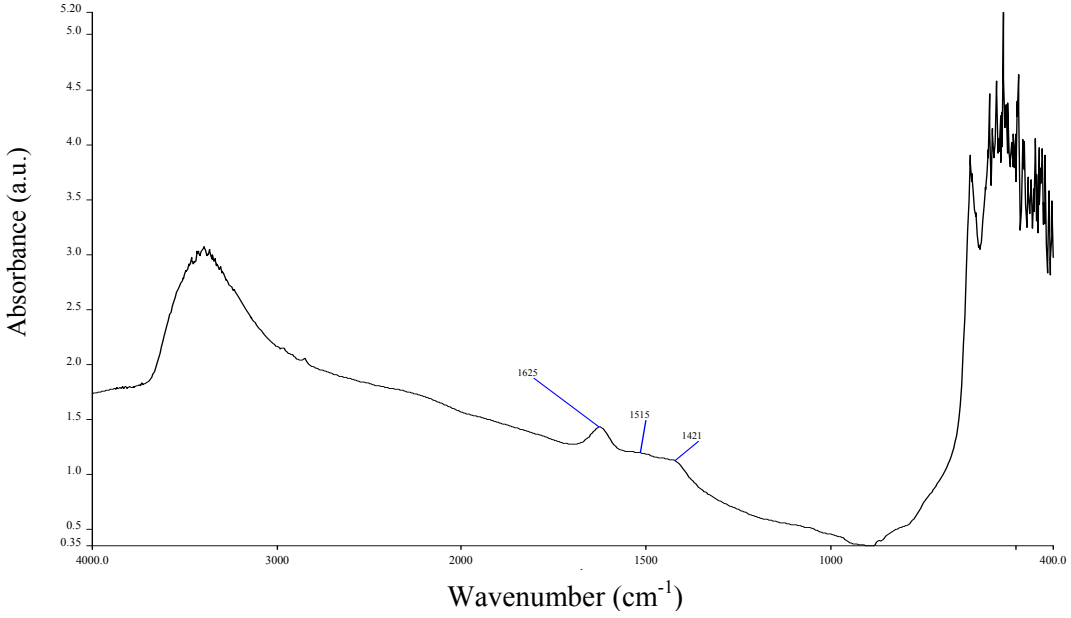

(b)

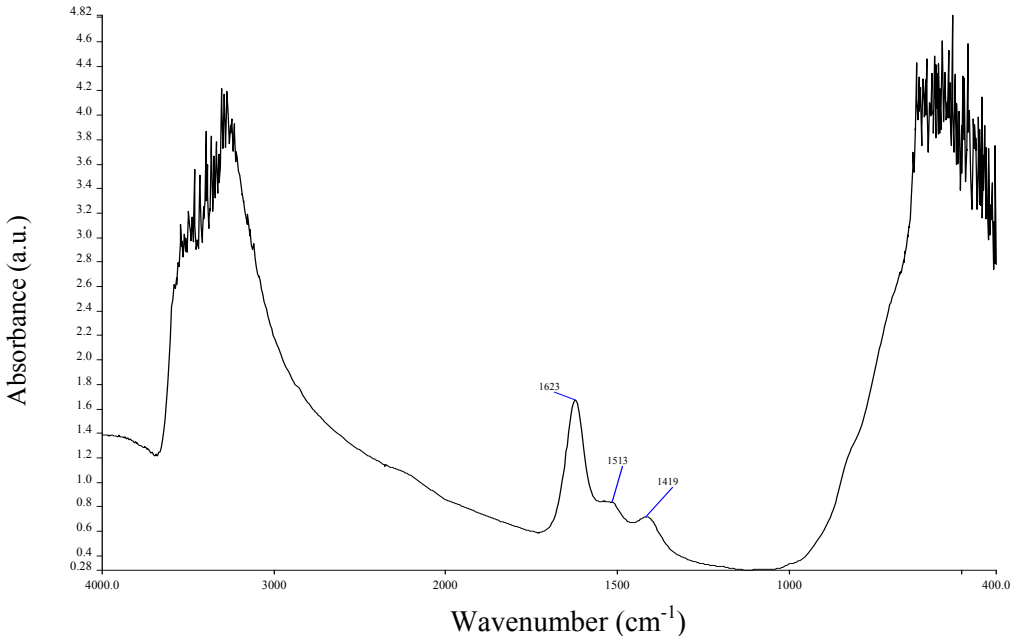

(c)

Figure 5.38 FTIR spectra of the samples fired at 900°C prepared from ethanolic solution with metal ion to alkylammonium chloride ratios: (a) 1:1-D, (b) 1:2-E and (c) 1:3-F in KBr discs.

5.4.10 Conclusions

A number of conclusions can be drawn from the work reported herein firstly for the materials prepared from the methanolic solutions:-

1) It has been shown that nanometer sized particles of cubic $Y_2O_3:Eu^{3+}$ can be prepared from metal chloride precursors formed in micelles encapsulated by alkylammonium chains (the fuel) by using a combustion synthetic method at 900°C.
2) The method produces a range of morphologies that are influenced by the initial alkylammonium chloride concentration; in particular remnant micellar forms are present such as spheres, tubules, and macrolamellar sheets of these aforementioned forms.
3) Evidence of morphologies and particle size being controlled by the initial micellar structures was found in the materials fired at both 650°C and 900°C.
4) It is clear from this work that the combustion fuel which was present in the samples prepared at 650°C was insufficient to raise the temperature over 900°C for a long enough time period (if at all) for the cubic $Y_2O_3:Eu^{3+}$ phase to form.
5) Further we have characterised the nanometre sized phosphor particles and demonstrated that they manifest many of the properties (CL and PL spectral properties) of bulk cubic $Y_2O_3:Eu^{3+}$.
6) It was observed that bands due to metal hydroxycarbonate in the infrared spectra of the cubic $Y_2O_3:Eu^{3+}$ nanoparticles were present. These bands are similar in position to those found in bulk [(Y, Eu)$OHCO_3.H_2O$], and are explained as arising from the spontaneous reaction of the surface of the nanometer sized particles of cubic $Y_2O_3:Eu^{3+}$ with atmospheric CO_2 and water vapour. This indicates that nanometre sized particles of cubic $Y_2O_3:Eu^{3+}$ are thermodynamically unstable in the atmosphere and must be protected against such back reactions. This could be achieved with surface coatings.
7) The materials prepared from methanol at 650°C were shown to be the two forms of YOCl, and this was converted to cubic $Y_2O_3:Eu^{3+}$ at the higher temperature (over 900°C).
8) It should be remembered that the presence of the yttrium hydroyoxycarbonate layer protected the YOCl in the materials prepared at 650°C from further reaction with the atmosphere.

A number of conclusions can be drawn from the work reported herein firstly for the materials prepared from the ethanolic solutions:-

Chapter 5 $Y_2O_3:Eu^{3+}$ phosphors from the $[(Y, Eu)\ Cl_3]$- $(C_{16}H_{33}NH_3Cl)$

1) It has been shown that nanometer sized particles of monoclinic $Y_4O_5Cl_2:Eu^{3+}$ can be prepared from metal chloride precursors formed in micelles encapsulated by alkylammonium chains (the fuel) by using a combustion synthetic method at 900°C.
2) The method again produces a range of morphologies that are influenced by the initial alkylammonium chloride concentration; in particular remnant micellar forms are present such as spheres, tubules, and macrolamellar sheets of these aforementioned forms.
3) Again evidence of morphologies and particle size being controlled by the initial micellar structures was found in the materials fired at both 650°C and 900°C.
4) It is clear from this work that the combustion fuel which was present in the samples prepared at 650°C or indeed at 900°C was insufficient to raise the temperature over 900°C for a long enough time period for the cubic $Y_2O_3:Eu^{3+}$ phase to form in the presence of the excess CO_2 atmosphere..
5) It was also observed that bands due to metal hydroxycarbonate in the infrared spectra of the monoclinic $Y_4O_5Cl_2:Eu^{3+}$ nanoparticles were present. These bands are in different positions to those found in bulk $[(Y, Eu)OHCO_3.H_2O]$, and are explained as arising from the spontaneous reaction of the surface of the nanometer sized particles of the monoclinic $Y_4O_5Cl_2:Eu^{3+}$ with atmospheric CO_2 and water vapour. This indicates that nanometre sized particles of the monoclinic $Y_4O_5Cl_2:Eu^{3+}$ are also thermodynamically unstable in the atmosphere and must be protected against such back reactions. This could be achieved with surface coatings.
6) The materials prepared from ethanol at 650°C were shown to be the two forms of YOCl, and monoclinic $Y_4O_5Cl_2:Eu^{3+}$ this was converted to a more pure form of monoclinic $Y_4O_5Cl_2:Eu^{3+}$ at the higher temperature (over 900°C).
7) It should be remembered that the presence of the yttrium hydroyoxycarbonate type layer protected the monoclinic $Y_4O_5Cl_2:Eu^{3+}$ in the materials prepared at 900°C from further reaction with the atmosphere.

Finally from the findings of this work it would appear that the use of sacrificial organised organic structures for the incorporation of inorganic precursors offers great potential as a method to control the morphology and size of nanometre sized particles.

Chapter 5 $Y_2O_3:Eu^{3+}$ phosphors from the $[(Y, Eu)\ Cl_3]$- $(C_{16}H_{33}NH_3Cl)$

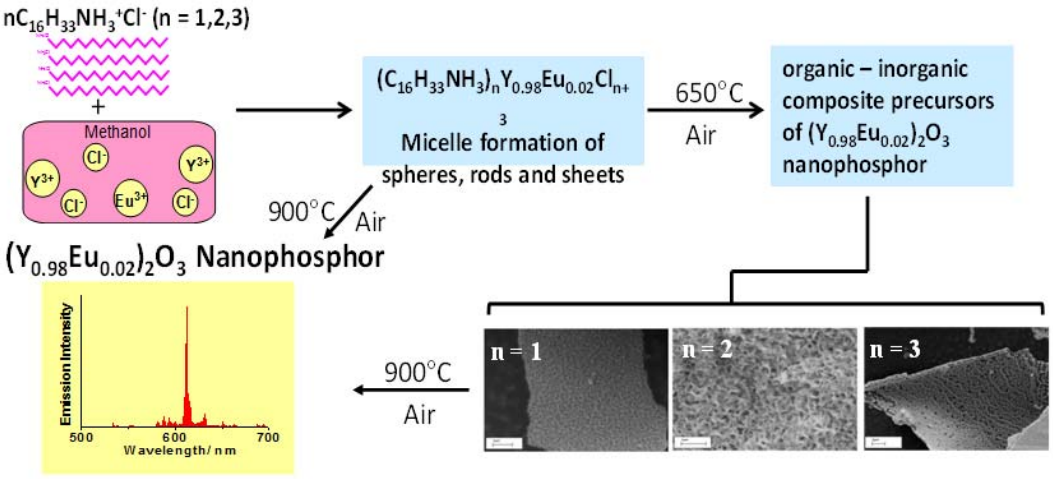

Figure 5.39 Chapter 5 summary

References

[1] T. Ireland and J.Silver."Facile self-assembly of yttrium oxide europium phosphor from Solution using a sacrificial Micellar phase". Journal of the Electrochemical Society. 2, 1.52-54, 1999.

[2] Y.Nishisu and M.Kobayashi. "Synthetic method for the production range of particle size for Y_2O_3:Eu." U.S. Patent 5,413.736-737, 1995.

[3] Y.D.Jiang, Z.L. Wang, F. Zhang, H.G. Paics and C.J. Summers."Spherical particles for high definition display screens". Journal Material. Res 13, 2950-2955, 1998.

[4] J.A.Cooper, H.G Paris, S.R.Stock, S.Yeng and C.J.Summers." Particle size effect on the crystal structure of Y_2O_3:Eu particles." Journal SID, 6. 163-164, 1998.

[5] A.Vecht, C.Gibbons, D.Davies, X.P.Jing, P.Marsh, T.G.Ireland, J.Silver, A. Newport and D. Barber."Engineering phosphors for field emission display." Journal Vac. Sci. Tech. B. 17, 750-751, 1999.

[6] X.P.Jing, T.G.Ireland, C.Gibbons, D.J.Barber, J.Silver, A.Vecht, G.Fern, P.Trogwa and D.C. Morton." Control of Y_2O_3:Eu spherical phosphor size ,assembly and properties." Journal of the Electrochemical Society 146. 4654-4656, 1999.

[7] M.I.Martinez-Rubio, T.G.Ireland, J.Silver, G.Fern, C.Gibbons and A.Vecht. " Effect on EDTA on controlling nucleation and morphology in the synthesis of ultrafine Y_2O_3:Eu phosphors Journal. Solid State Chem. Electrochem and Solid State Lett. 3. 446-448, 2000.

[8] A.Vecht, M.I.Martinez-Rubio, T.G.Ireland, J.Silver, G.Fern and C. Gibbons. "Factors effecting efficiency in submicron size phosphors for high definition display."SID '00 Digest, 31. 15-17, 2000.

[9] M.I.Martinez-Rubio, T.G.Ireland, J.Silver, G.Fern and M.J. Snowden. " Novel Method for the Synthesis of spherical particles of the Y_2O_3: Eu Phosphor Using a Copolymer Microgel of Nipam and Acrylic Acid". Langmuir 17, 7145-7149, 2001.

[10] J.Silver, M.I.Martinez-Rubio, T.G.Ireland, G.R Fern and R.Withnall.

"The effect of particle morphology and crystallite size on upconversion luminescence property of erbium and yttrium co-doped yttrium oxide." Journal. Phys. Chem. 105,948-950, 2001.

[11] J.Silver, R.Withnall, A. Newport, M.I.Martinez-Rubio, T.G.Ireland, P.J. Marsh and A.Vecht. "Yttrium up-converting phosphors Part-2 temperature depend up conversation luminescence SID '01 Digest .32**,** 756-759, 2001.

[12] J.Silver, M.I.Martinez-Rubio, T.G.Ireland, G.R Fern and R.Withnall. "Yttrium oxide up-converting phosphors Part-3, up conversation luminescence emission from europium doped yttrium. Journal. Phys.Chem, B. 105, 9107- 9110, 2001.

[13] M.I.Martinez-Rubio, T.G.Ireland, G.R.Fern, J.Silver and M.J.Snowden. " A synthetic method for the production of a range of Particle sizes for Y_2O_3 : Eu phosphors using a copolymer microgel of NIPAM." Journal of the Electrochemical Society. 149, 253-255, 2002.

[14] J.Silver, R.I. Galliano, G.R. Fern, T.G. Ireland and R. Withnall. "A novel synthesis of Y_2O_3 : Eu phosphor using carbon dioxide and Ammonia for high definition CRT."SID '02 Digest.33, 12-15, 2002.

[15] J.Silver, N. Wilstead. D.Nicholas and A.Vecht. "Rare earth element anti stock phosphors emission." SID '02 Digest.33, 388-390, 2002.

[16] J.Silver, M.I. Martinez-Rubio, S.Gebretensae, G.R.Fern, M.J.Snowden and R.Withnall. " Yttrium oxide up-conversion phosphors luminescence." SID '02 Digest.33, 393-395, 2002.

[17] J.Silver, M.I.Martinez-Rubio, T.G.Ireland, G.R Fern and R.Withnall. "Yttrium oxide up-conversion phosphors Part-4, up conversation luminescence emission from europium doped yttrium oxide under 632.8nm light excitation." Journal. Phys.Chem. B. 107,1548-1550, 2003.

[18] J.Silver, T.G. Ireland and R.Withnall." fine control of the doped level in cubic of Y_2O_3 : Eu phosphor."Journal. Electrochem. Soc. 151,66-89, 2004.

[19] M. Konaissmy, D. Jeyakumar, R. Jagannathan and M. Mohan." Energy transfer and upconversion luminescence property of Y_2O_3 : Eu phosphor."

Journal. Material. Res. Bull. 31. 1013-1016, 1996.

[20] P.Zhang, A.Navrotsky, B.Guo, I. Kennedy, A.N.Clark, C.Lesher and Q.Lui. "Direct calorimetric measurement of grain boundary and surface enthalpies in yttria-stabilized zirconia." Journal. Phys Chem. B. 112, 932-934, 2008.

[21] D.J.Gardiner and P.R.Graves."Practical Raman spectroscopy." Springer-Verlag. 30-40, 1989.

[22] L.S.DentGlasser." Crystallography and its Applications." Van Nostrand Reinhold Wokingham UK. 23-28, 1982.

[23] K.L. Chopra. "Thin Film Phenomena". McGraw-Hill New York. London .45-49, 1969.

[24] D.A Skoog and J. J Leary. "Principle of Instrumental Analysis". 4th Ed. Saunders College of publishing. London. 67-74, 1992.

[25] D.H.Templetoan and C.H.Dauben. "Crystal Structures of Rare Earth Oxychlorides." Journal American. Chem. Soc, 75. 6069-6070, 1953.

[26] W.H. Zachariasen. "Crystal chemical studies of the 5f-series of elements. XII. New compounds representing known structure types." Journal Acta Crystallographica, 2. 388-391, 1949.

[27] L.M.Seaverson and J.D.Corbet. "Synthesis and characterization of oxide interstitial derivatives of zirconium monochloride and monobromide." Journal Inorg.Chemistry, 22.3202-3210, 1983.

[28] A.S. Ethiraj, N. Hebalkar, S.K. Kulkarni, R. Pasricha, J. Urban, C. Dem, M. Schmitt, W. Kiefer, L.Weinhardt, S.Joshi, R. Fink, C. Heske, C.Kumpf and E. Umbach. Journal. Chem. Phys. 118, 8945-8953.2003.

[29] U. Rambabu, A. Mathur and S. Buddhudu." Fluorescence spectra of Eu^{3+} and Tb^{3+} - doped lanthanide oxychloride powder phosphors." Journal Mat. Chemical and Phys. 61, 156-162,1999.

[30] G.Blasse and A. Brill." Broad band UV excitation of Sm^{3+} -activated phosphors." Journal Phys. Lett. 23, 440-445, 1996.

[31] E. Garcia, J.D. Corbett, J.E. Ford and W.J. Vary." Stability of Rare-Earth Oxychloride Phases: Bond Valence Study." Journal Inorg. Chem. 24, 494- 496.1985.

[32] H.G. Brittain and G.Meyer." Luminescence and energy migration in Eu^{3+}-containing scheelites with different anions." Journal. Less Common Metals.126, 170-175,1986.

[33] L. Markovskii, E.Pesina, A.Omel'chenko and D. Kondrashev." The formation of $Y_2O_3Cl_2$."Russ, Journal Inorg Chem.14.10-11, 1969.

[34] S. Natansohn. "The synthesis and structure of rare-earth and indium tellurates, R2TeO6." Journal of Inorganic and Nuclear Chemistry. 30,3123-3125,1968.

[35] H.P. Beck, B. Naturforsch , B. Anorg." Low-temperature routes to new structures for yttrium, holmium, erbium, and thulium oxychlorides." Journal Chem Org. 32B,1015-1017,1977.

[36] N.B.Colthup, L.H. Daly and S.E.Wiberley. "Introduction to Infrared and Raman Spectroscopy," 3rd edition, Academic Press Ltd, London,1990.

[37] J.Silver and R.Withnall. "Probes of structural and electronic environments of phosphor activators." Journal Chem.104, 2833-2855, 2004.

[38] M.Tanaka, Y. Nishisu, M. Kobayashi, A.Kurita, H.Hanzawa and Y.Kanematsu." Optical characterization of spherical fine particles of glassy Eu^{3+} doped yttrium basic carbonates." Journal. Non-Crystalline Solids .318, 175-185, 2003.

[39] E.Husson, C. Proust, P. Gillet and J.P.Itié." Phase transition in yttrium oxide at high pressure studied by Raman spectroscopy." Journal Material. Res.34, 2085-2092, 1999.

[40] R.B.Hunt and R.G.Pappalardo." Fast excited-state relaxation of Eu-Eu pairs in commercial $Y_2O_3:Eu^{3+}$ phosphors." Journal. Lumin. 34, 133-146, 1985.

[41] G. Schaack and J.A. Köningstein." Phonon and electronic Raman spectra of cubic Rare earth-oxides and isomorphous yttrium oxide." Journal. Opt. Soc.American. 60, 1110-1115, 1970.

[42] W.B. White and V.G.Keramidas." Vibrational spectra of oxides with the C-type rare earth oxide structure." Journal Spectrochimica Acta part A.28, 501-509,1972.

[43] D. Bloor and J.R.Dean."Spectroscopy of rare earth oxide systems. I. Far infrared spectra of the rare earth sesquioxides, cerium dioxide And nonstoichiometric praseodymium and terbium oxides." Journal. Phys. C and Solid State Phys. 5, 1237-1252, 1972.

[44] Y.Repelin, C.Proust, E.Husson and J.M.Beny." Vibrational spectroscopy Of the C-form of yttrium oxide." Journal. Solid State Chem. 118, 163-169.1995.

[45] M.G. Paton and E.N. Maslen." Refinement of a crystal structure of Yttria nanocrystalline."Journal Acta Crystallographica. 19, 307-310, 1965.

[46] W.W.Wendlandt."The thermal decompostionof heavier rare earth metal Chloride hydrates." Journal of Inorganic and Nuclear Chemistry. 9,136-139,1959.

[47] R. Withnall, J. Silver, P.J. Marsh and G.R. Fern."Raman spectra of tetragonal and rhombohedral forms of YOCl." Journal Proc. ICORS XXIII,2012.

[48] L.Muresan, E.J.Popovici, R.Grecu and L.B.Tudoran." Studies on the synthesis of europium activated yttrium oxide by wet chemical method. 1. Influence of precursor quality on phosphor photoluminescence properties." Journal. Alloys and Compounds. 471, 421-427, 2009.

[49] B.Aiken, W.P.Hsu and E.Matijevic." Preparation and Properties of Monodispersed Colloidal Particles of Lanthanide Compounds: III, Yttrium (III) and Mixed Yttrium (III)/Cerium (III) Systems." Journal. American. Ceram. Soc. 71, 845-853, 1988.

[50] S.Sohn, Y. Kwon, Y. Kim and D. Kim." Synthesis and Characterization of near- monodisperse yttria particles by Homogeneous precipitation method Powder Technology." Journal of Solid State Chem. 142, 136-153, 2004.

Chapter Six

6 .0 $Y_2O_3:Eu^{3+}$ Materials from the [(Y, Eu) Cl_3] - ($C_{12}H_{25}NH_3CL$)

6.1 Introduction

In the last chapter the effect of looking at how [(Y,Eu)Cl_3] - ($C_{16}H_{33}NH_3Cl$) precursor materials led to different fired phosphors depending on firing conditions, atmosphere and whether the precursors were prepared from methanolic or ethanolic solutions was reported. Instead of just cubic $Y_2O_3:Eu^{3+}$ being formed it was found that in the reaction of [(Y,Eu)Cl_3]-($C_{16}H_{33}NH_3Cl$) two other phases:- $YOCl:Eu^{3+}$ and $Y_4O_5Cl_2$:-Eu^{3+} were also formed in the case of the materials prepared from ethanol. In this chapter the preparation of nanoparticles phosphors from [(Y, Eu) Cl_3] - ($C_{12}H_{25}NH_3Cl$).Are reported using similar preparative methods. The first report in this system was in 1999 [1]. Here again the aims of this work were motivated by widespread interest on the synthesis and properties of phosphors made up of highly crystalline sub micrometer sized particles. Our group and others have published widely on the urea homogeneous precipitation method of preparing the cubic $Y_2O_3:Eu^{3+}$ phosphor [2-19], however until this work we were never in a position to compare such methods to controlled combustion synthesis for making phosphor nanometre sized materials. In particular we were interested in the influence of the alkylammonium chain length of the precursor on the final products in the combustion synthesis. As stated in the introduction in chapter 5 "one of the problems with making such sub micrometer sized particles is that during annealing of the precursor particles at high temperatures (often necessary for good crystallite quality and hence emission properties) the particles tend to sinter." Again as in the previous chapter one way to partially alleviate this problem is to synthesise the particles as rapidly as possible at a high temperature. A method that has been explored for this purpose is combustion synthesis using an organic fuel that is ignited when a crucible or other vessel containing the phosphor precursors and the fuel is placed in a furnace that is already at 900°C. The fuel ignites and raises the temperature in the vessel very quickly.The facile self-assembly of the red emitting phosphor yttrium oxide europium ($Y_2O_3:Eu^{3+}$) from solution using a sacrificial micellar phase appeared in 1999 [1]. The micellar phase was assembled using the alkylammonium chloride salt ($C_{12}H_{25}NH_3Cl$) in an ethanolic solution. The resulting fine powder had smaller particles, ranging in size from 0.1 to 1.0 μm, than the commercial cubic $Y_2O_3:Eu^{3+}$ phosphor [1]. This chapter reports a reinvestigation of the earlier work as well as studies on making the precursors from methanol.

Chapter 6 $Y_2O_3:Eu^{3+}$ Materials from the $[(Y, Eu)\ Cl_3]$ - $(C_{12}H_{25}NH_3Cl)$

As in chapter 5 the results discussed in this chapter were obtained using a more sophisticated way to control the rate of crystallization of the phosphor particles. This was to vary the ratio of phosphor precursor to fuel. In theory the presence of more fuel around the phosphor precursor should facilitate/influence the combustion process and possibly lead to more crystalline products. Such influences were indeed observed in the last chapter. So in this chapter the dodecylalkylammonium hydrochloride chain ($C_{12}H_{25}NH_3Cl$) was used as fuel and now the affect of varying the ratio of this to the [(Y, Eu)$OHCO_3.H_2O$] precursor on the Cathodoluminescence (CL) and photoluminescence (PL) properties of the resulting phosphors is discussed.
The following systems were studied;-

1. $[Y,Eu]Cl_3$ - $(C_{12}H_{25}NH_3Cl)$-6 experiments in the ratio of 1:1, 1:2, 1:3with ethanol (3 fired at 650°C and 3 fired at 900°C).

2. $[Y,Eu]Cl_3$ - $(C_{12}H_{25}NH_3Cl)$-6 experiments in the ratio of 1:1, 1:2, 1:3with methanol (3 fired at 650°C and 3 fired at 900°C).

The temperatures 650°C and 900°C were chosen to be above the formation temperature of YOCl.

6.2 Experimental

For the experimental technique refer to chapter 4 paragraph 4.5 experiments 9/9a.
Preparations of $[(Y, Eu)\ Cl_3]$ - $(C_{12}H_{25}NH_3Cl)$ n (for n = 1, 2, 3) were carried out with materials prepared from methanolic and ethanolic solutions.Attenuated total reflectance (ATR)-Fourier transform infrared (FTIR) spectra were obtained using a Perkin Elmer Spectrum One FTIR spectrometer. This technique is used to study vibrational, rotational, and other low-frequency modes in a system. The crystalline phases of the products were determined by X-ray powder diffraction (XRPD) using a Bruker D8 Advance X-ray powder diffractometer. (See for detail to chapter 3 ref 3.2). XRPD studies have been used to identify the phases present in the combusted products synthesized in this work, and their degree of disorder/order and their crystallite sizes [10, 22]. Diffractograms were collected using the fired powders in a conventional holder, or mounted on aluminium pin stub or on an aligned silicon substrate. [6, 7, 23, 24] Field emission scanning electron microscopy (FESEM) was used to study the microstructure of the samples using a Zeiss Supra VP 35 instrument. The samples were mounted on carbon tabs attached to aluminium pin stubs and sputter coated with a thin conducting layer of gold.

The PL excitation and emission spectra were obtained using a Bentham (Reading, UK) M300 programmable grating monochromator photometer system with computer controlled wavelength scanning and intensity data collection, using in the visible region a 1800 lines/mm grating. The stepping motor and sine drive allows wavelength scanning to be completely controlled from a remote stepping drive unit (SMD3B). Sample excitation and collection was collected inside an in-built sealed chamber connected to the M300 monochromator via a fibre-optic bundle. The CL measurement data and spectra were undertaken using a high-vacuum chamber with a Kimball Physics Inc. (Walton, USA), model EGPS-7 electron gun. The CL luminance measurements were obtained by means of a Jeti spectroradiometer (Specbos 1201, Jeti Technische Instrument GmbH, and Jena, Germany). The phosphor screens were excited with electron beam energies from 1000 to 5000V, and emission currents from 1.1 to 9.8μA/cm^2, with an electron beam spot size of 9 mm for defocused measurements and 1.41 mm for the focussed measurements. For some of the samples, CL emission and excitation spectra were obtained using the Bentham system previously described except that the fibre optic bundle was disconnected from the in-built sealed chamber and attached to a telescope (TEL 301D).For the CL luminance measurements and spectra of the prepared samples phosphor screens were prepared in the following manner. After cleaning the aluminium pin stubs in an ultrasonic bath containing ethanol, followed by drying in an oven at a temperature of 100°C they were weighed. A stub was then placed in an electrochemical cell containing an ultrasonically dispersed solution of the phosphor powder (0.5g), in an electrolyte solution of magnesium nitrate (0.075g/L) and isopropanol (50ml). The stub was positioned with its flat surface forming a meniscus with the surface of the phosphor/electrolyte solution and acted as an electrode, the counter electrode being a strip of magnesium ribbon. A field of 300V was applied facilitating the coating of the stub by electrode position. This procedure was repeated till all the stubs were coated with 3mg (±0.01mg) of phosphor. After drying the stubs at 100°C they were introduced into the vacuum chamber for CL measurements.

6.3 Results and Discussion

6.3.1 Products prepared with methanol and ethanol at temperatures of 650°C.

6.3.1.1 Sample appearance: - Products (samples) prepared from precursors methanolic and ethanolic solutions were fired at a temperature of 650°C and observed to be light grey in colour, where as the samples prepared at 900°C were all white powders. Under 254nm excitation the samples prepared at 650°C displayed a weak red

luminescence which was in contrast to the strong red luminescence from the samples prepared at 900°C that is characteristic of the $Eu^{3=}$ ion in cubic Y_2O_3. The strongest red luminescence comes from 1:3 material sample ratios and at 900°C.

6.3.1.2 SEM Studies: Firstly the samples prepared from methanolic and ethanolic solutions and fired at a temperature of 650°C. In Figure 6.1 FESEM micrographs of samples annealed at 650°C prepared from metal chloride to alkylammonium chloride ratios of 1:1 (a, b, c and d), 1:2 (e and f) and 1:3 (g and h) in methanol are presented. It can be seen that a number of morphological forms are present, the variety of these forms increase with higher alkylammonium chloride (micelle) concentration in agreement with the findings in chapter 5.This is evident from the images of the material formed from the 1:1 ratios in Figure 6.1a, b, c and d where large straw-like sheets are shown to be formed from intergrowths of thin needles that have dimensions of proximately 20 to 30nm in width by 200nm in length. Also in Figure 6.1a there is evidence for the crystals forming clumps that suggest they originated from predominantly spherical micelles. The material prepared from the 1:2 ratios presented in Figures 6.1e and 6.1f show needles that have formed partially fused into sheets. Whereas the final SEMs in Figure 6.1g of the material prepared from the 1:3 ratios show the micelles have left behind evidence of their existence as tubules; these structures have assembled into large lamellar sheets that in these images are two structural units in thickness Figures 6.1g and 6.1h. The spherical, tubular and lamellar structures display remnant micellar morphologies, although they are much larger in dimensions than those that are commonly associated with micelles. It can be seen in Figure 6.1c that the crystallites are all small with one or more dimensions less than 50nm.

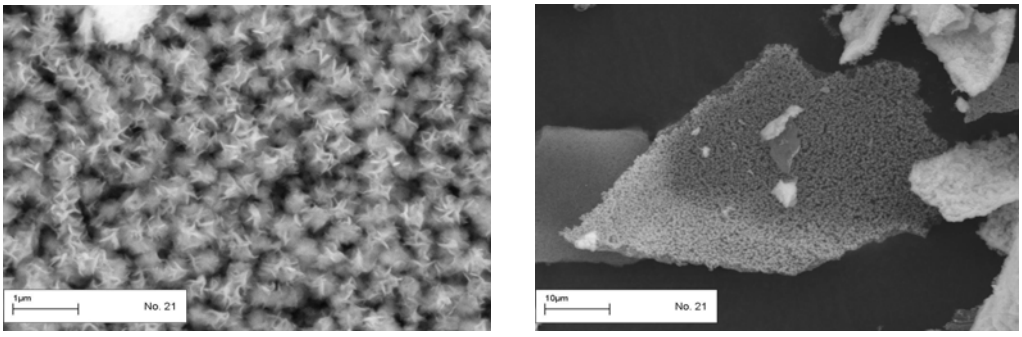

(a) (b)

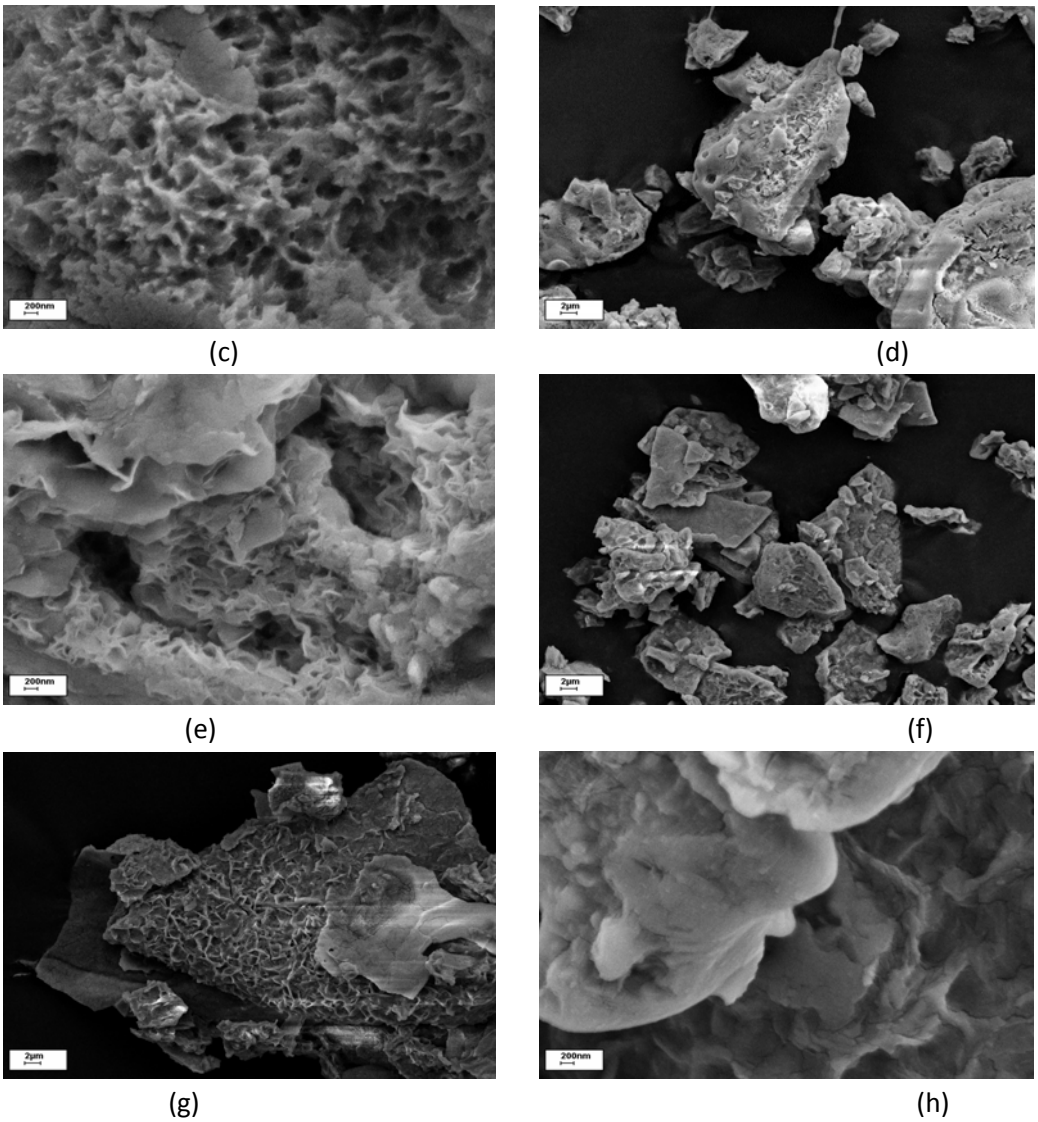

Figure 6.1 FESEM images of phosphor samples fired at 650°C from precursors prepared from methanolic solutions using metal chloride to alkylammonium chloride ratios of (a,b,c and d) 1:1, (e and f) 1:2, (g and h) 1:3. In (a), the bar is 1µm, in (c), (e) and (h) it is 200nm and in (d), (f) and (g) it is 2µm. In (b) the bar is 10µm.

In Figure 6.2 FESEM micrographs of samples annealed at 650°C prepared from metal chloride to alkylammonium chloride ratios of 1:1 (a and b), 1:2 (c and d) and 1:3 (e and f) in ethanol are presented. Again it can be seen that a number of morphological forms are present, and again the variety of these forms increase with higher alkylammonium chloride (micelle) concentration. This is evident from the images of the material formed from the 1:1 ratios in Figure 6.2 where the presence of some sheet like structures are apparent, and these are formed from fused smaller complex forms. These smaller forms are formed from intergrowths of thin needles that have dimensions up to 200nm in length. Progressing to the final SEMs in Figure 6.2 of the material prepared from the 1:3 ratios; they also show the micelles have left behind

evidence of their existence; these structures have assembled into large lamellar sheets that in these images are two structural units in thickness similar to those observed in Figure 6.1. In many of the SEMs presented in Figures 6.2 it can be seen that there is evidence of structures where the surfaces appear to be smooth suggesting they neared meltdown this is thought to be due to the presence of ethanol rather than methanol (see Figure 6.1) driving the surface temperature higher during the synthesis. It is only a surface effect as the XRPD data (see below) show no evidence for the high temperature cubic $Y_2O_3:Eu^{3+}$ phase.

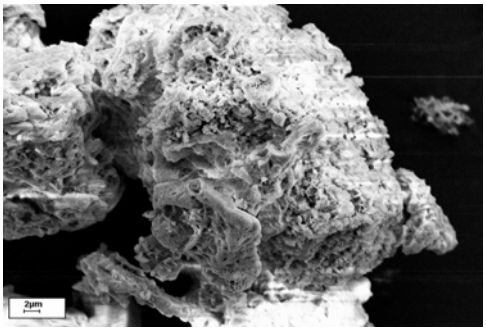

7 (a)

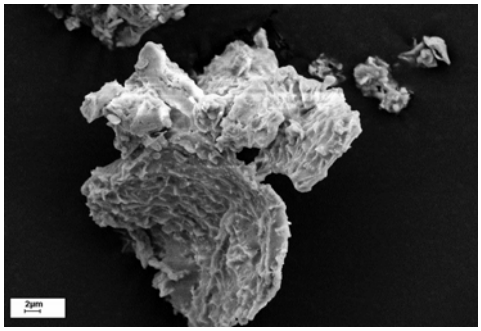

7 (b)

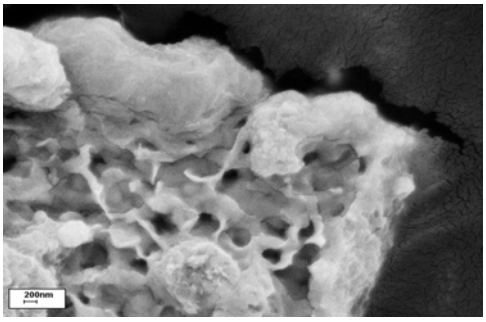

8 (c)

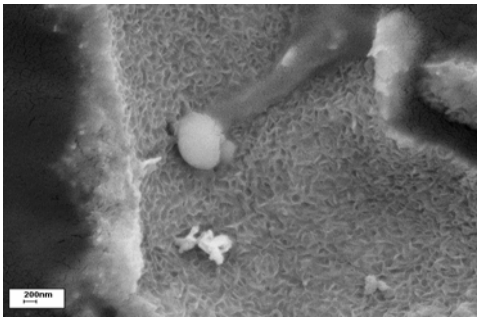

8 (d)

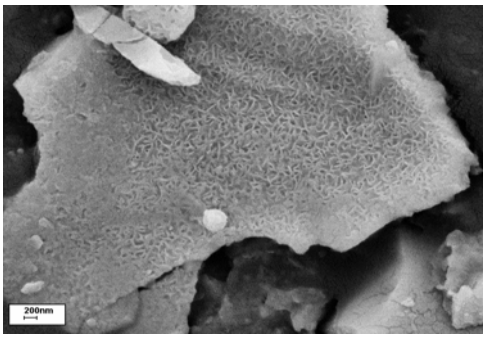

9(e)

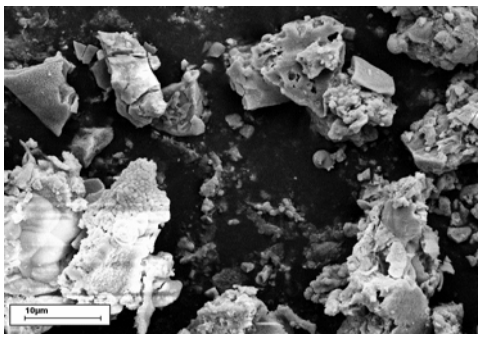

9 (f)

Figure 6.2 FESEM images of phosphor samples fired at 650°C from precursors prepared from ethanolic solutions using metal chloride to alkylammonium chloride ratios of (7a and 7b) 1:1, (8c and 8d) 1:2, (9e and 9f) 1:3 . In (7a and 7b), the bar is 2µm, and in (8c, 8d) and (9e) it is 200nm and in (9f), the bar is 10µm.

6.3.2 Studies on the samples produced at. 650°C

6.3.2.1 Sample structures (from XRPD data):- The XRPD Diffractograms of the samples prepared from methanolic solutions and fired at 650°C are shown in Figure 6.3; they contain evidence of the presence of very broad lines that would have previously been interpreted to indicate the presence of amorphous material with little or no crystalline material. However these results are very similar to those that were reported in chapter 5 for the materials made from methanolic solution and indicate the presence of $YOCl:Eu^{3+}$. There was no evidence for cubic $Y_2O_3:Eu^{3+}$ in these XRPD plots. The XRPD data of the samples prepared from the ethanolic solutions are presented in Figure 6.4 there is little evidence of anything different to those prepared from the methanolic solutions and are unlike those found in Chapter 5 for the same temperature range, The reason for the differences is most likely that the samples did not reach as high a temperature than that of the corresponding materials prepared from the $[(Y,Eu)Cl_3]$ - $(C_{16}H_{33}NH_3Cl)$ system and that this is a result of less fuel being available due to the shorter alkylammonium chains. Again there was no evidence for cubic $Y_2O_3:Eu^{3+}$ in these XRPD plots. In addition there is only evidence for the presence of $YOCl:Eu^{3+}$ unlike the findings for the $[(Y,Eu)Cl_3]$ - $(C_{16}H_{33}NH_3Cl)$ system prepared from ethanolic solutions.

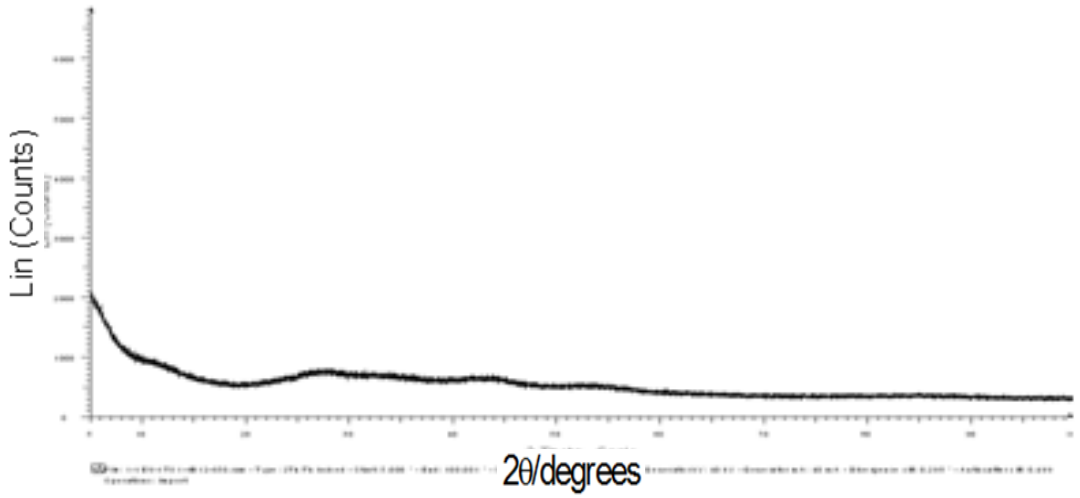

1:1 650°C methanol powder

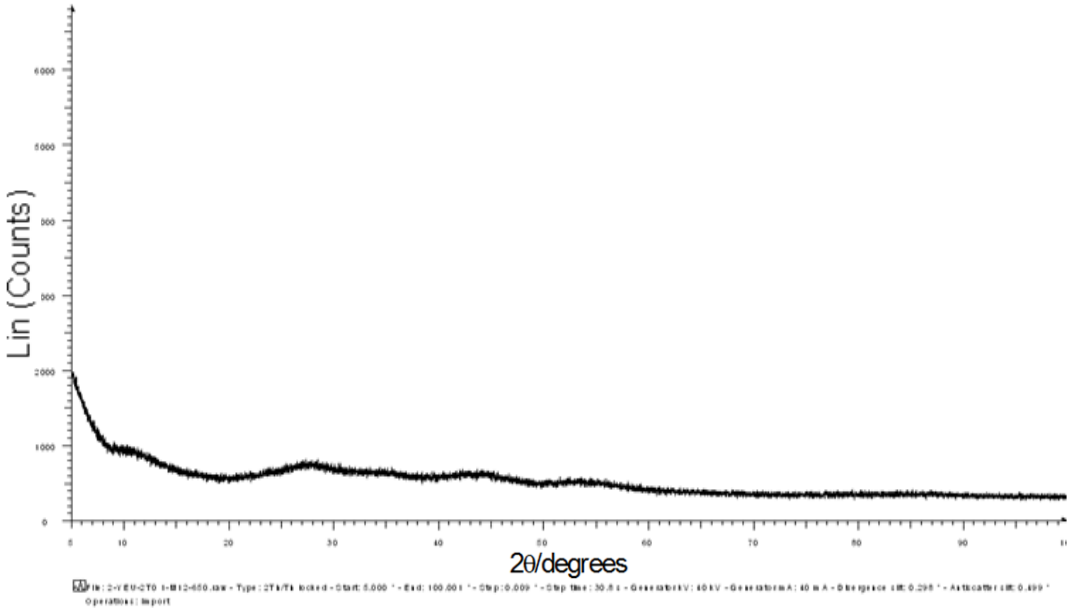

1:2 650°C methanol powder

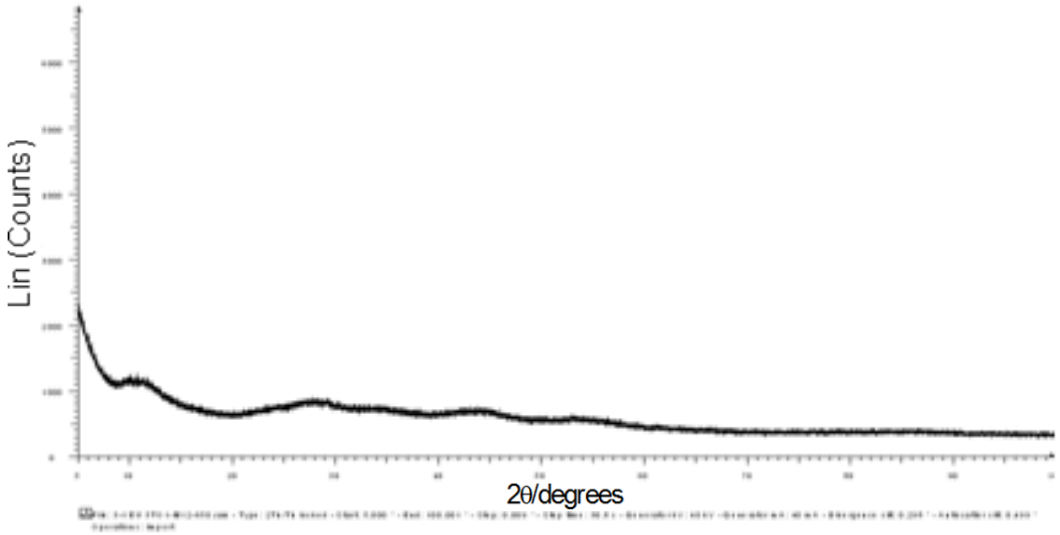

1:3 650°C methanol powders

Figure 6.3 XRPD diffractograms of the samples annealed at 650°C prepared from methanolic solutions, metal ion to alkylammonium chloride ratios; 1:1, 1:2 and 1:3.

Chapter 6 $Y_2O_3:Eu^{3+}$ Materials from the $[(Y, Eu)\ Cl_3]$ - $(C_{12}H_{25}NH_3Cl)$

Table 6.1 Cell parameters for the yttrium oxy chloride phases found in the materials fired at 650°C prepared from methanol.

	1:1	1:2	1:3
Yttrium oxide chloride YOCl R-3m -1 %	a= 4.861(34)(Å) c= 28.00(81)(Å) 30.3(36)	a= 5.000(35)(Å) c= 28.00(22)(Å) 6.13(65)	a = 5.000(18)(Å) c= 28.00(13)(Å) 13.03(71)
Yttrium oxide chloride YOCl R-3m -2 %	a= 4.114(11)(Å) c= 20.272(80)(Å) 69.7(36)	a= 4.175(13)(Å) c= 20.219(64)(Å) 93.87(65)	a= 4.197(11) (Å) c= 20.499(52)(Å) 86.97(71)
Yttrium oxide chloride YOCl P4/nmm [20]	a= 3.903 (2) c= 6.597 (4)		
Yttrium oxide chloride YOCl P4/nmm [21]	a= 3.900 (2) c= 6.604 (2)		
Yttrium oxide chloride YOCl R-3m [21a]	a= 3.7895 (5) c= 28.03 (1)		

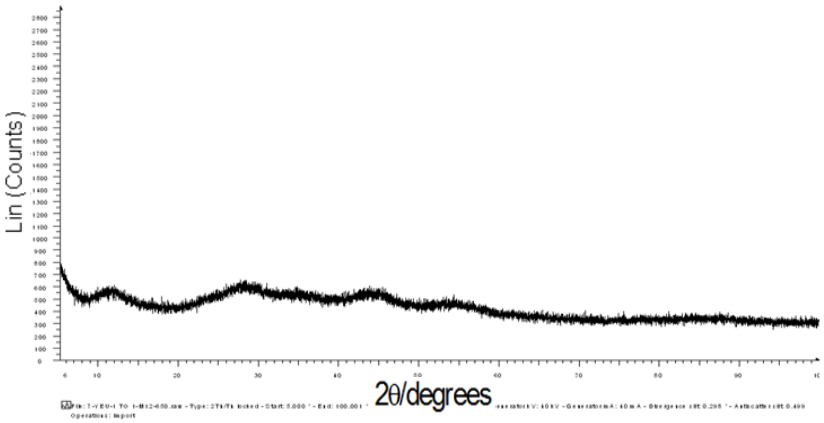

1:1 650°C ethanol powders

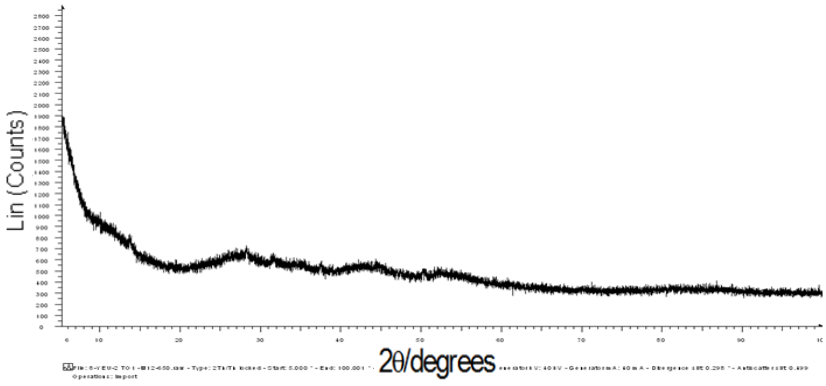

1:2 650°C ethanol powders

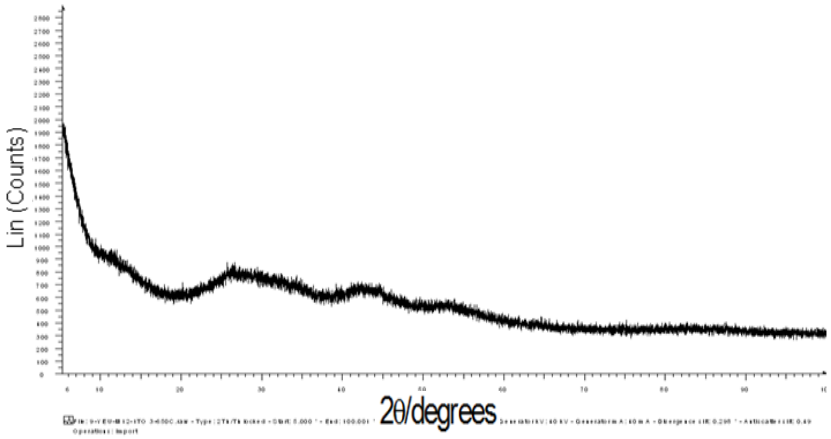

1:3 650°C ethanol powders

Figure 6.4 XRPD diffractograms of the samples annealed at 650°C prepared from ethanolic solutions, metal ion to alkylammonium chloride ratios: 1:1, 1:2 and 1:3.

Table 6.2 Cell parameters for the yttrium oxy chloride phases found in the materials fired at 650°C prepared from Ethanol.

	1:1	1:2	1:3
Yttrium oxide chloride YOCl R-3m -1 %	a= 4.347(20)(Å) c= 28.00(20)(Å) 2.32(22)	a=4.670(30)(Å) c=28.00(31)(Å) 12.2(15)	a =4.805(79)(Å) c= 28.00(60)(Å) 8.7(17)
Yttrium oxide chloride YOCl R-3m -2 %	a= 4.327(12) (Å) c=20.459(83)(Å) 97.68(22)	a=4.094(15)(Å) c= 20.81(12)(Å) 87.8(15)	a= 4.198(18) (Å) c=20.217(74)(Å) 91.3(17)
Yttrium oxide chloride YOCl P4/nmm [20]	a= 3.903 (2) c= 6.597 (4)		
Yttrium oxide chloride YOCl P4/nmm [21]	a= 3.900 (2) c= 6.604 (2)		
Yttrium oxide chloride YOCl R-3m [21a]	a= 3.7895 (5) c= 28.03 (1)		

6.3.3 Photoluminescent Spectra: The PL excitation and emission spectra of the samples prepared at 650°C using 1:1, 1:2 and 1:3 ratio precursor products prepared from methanolic solutions are displayed in Figure 6.5 and 6.6.Those for the samples prepared from ethanolic solutions are presented in figures 6.7 and 6.8. They support the XRPD data; they have similar spectral features of varying intensities yet they are different to that of cubic $Y_2O_3:Eu^{3+}$. In particular the excitation spectra of all the above products have peaks with weak absorption strength, an increase in the absorption bands intensity is seen for higher concentrations of alkylammonium chloride. All the emission and excitation spectra resemble those found for the methanolic solutions reported in chapter 5. The strong broad band observed at 254 nm in cubic $Y_2O_3:Eu^{3+}$ due to the Eu^{3+} - O^{2-} charge transfer transition is absent, although the usual lower intensity absorption lines due to the electronic transitions within the $4f^6$ configurations are present, some of which show a peak wavelength shift. The emission spectra of these samples are very weak, the strong sharp emission peak found at 611nm in cubic $Y_2O_3:Eu^{3+}$ due to the $^5D_o \rightarrow {}^7F_2$ transition is absent or the higher

ratio samples where a broader peak centred at approximately 615nm is seen. Also absent in all three samples are the set of emission peaks with a maximum at 709nm due to the $^5D_o \rightarrow {}^7F_4$ of the Eu^{3+} ion in cubic Y_2O_3.

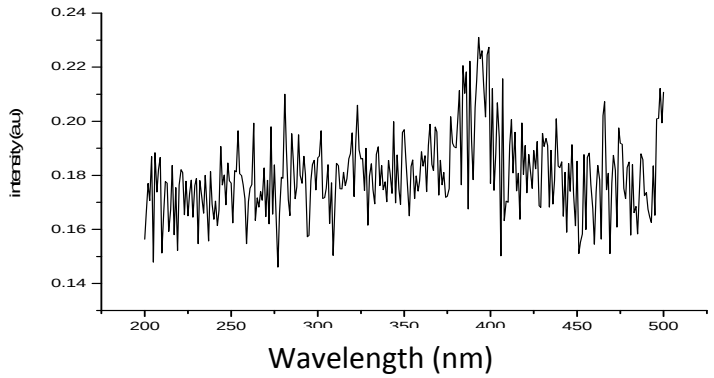

(a)

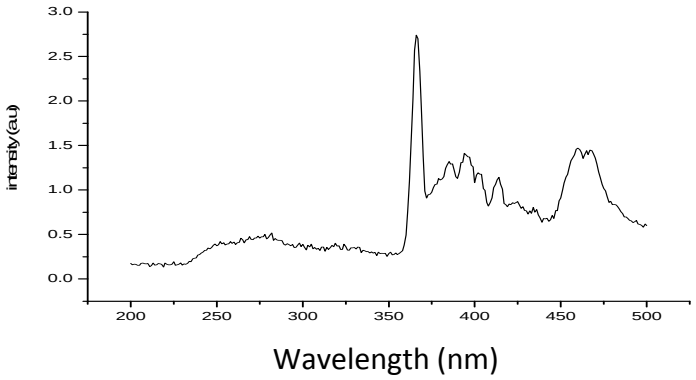

(b)

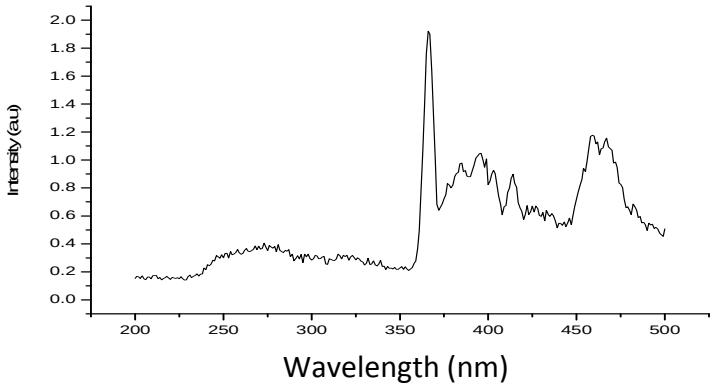

(c)

Figure 6.5 Photoluminescent excitation spectra of the samples prepared at 650°C from methanolic solution (a) 1:1, (b) 1:2 and (c) 1:3 ratio samples. Excitation monitored at 612nm.

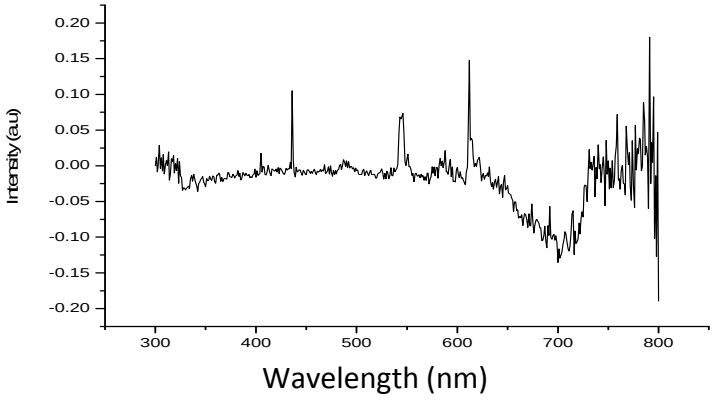

(a)

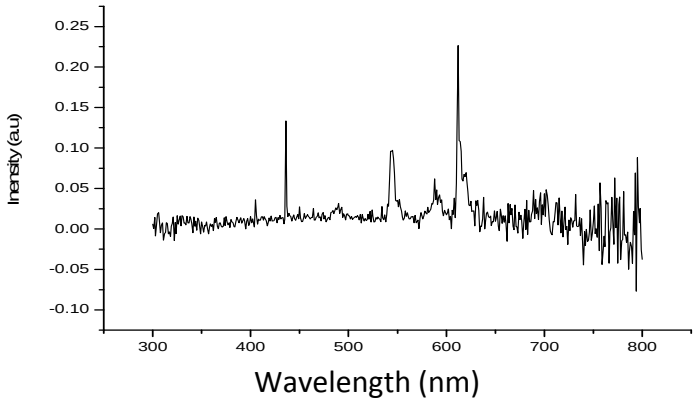

(b)

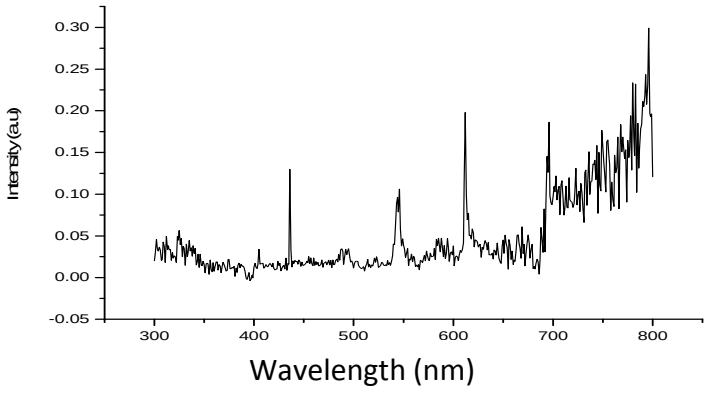

(c)

Figure 6.6 Photoluminescent emission spectra of the samples prepared at 650°C from methanolic solution (a) 1:1, (b) 1:2 and (c) 1:3 ratio samples (excitation wave length 254nm).

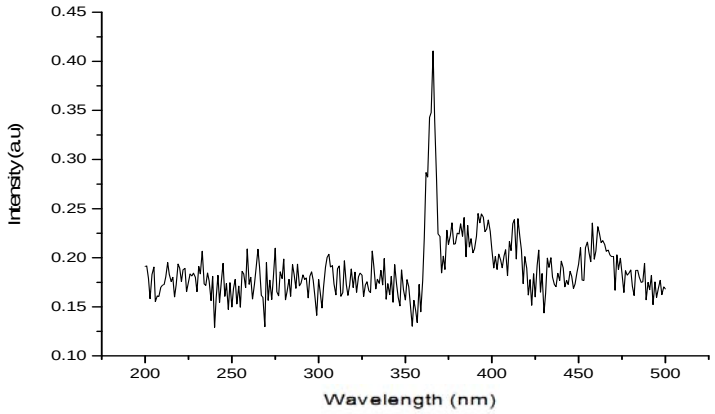

(a)

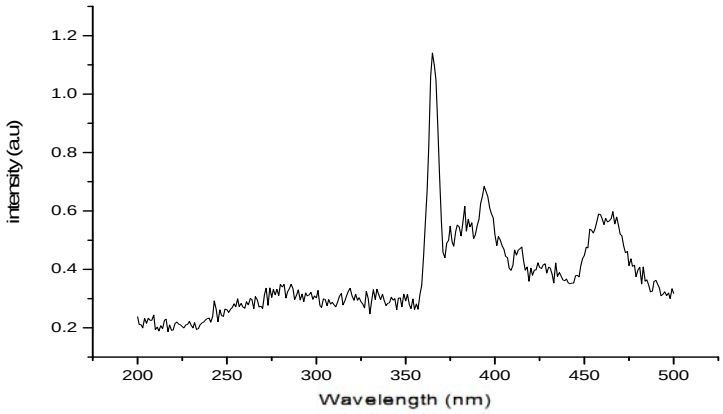

(b)

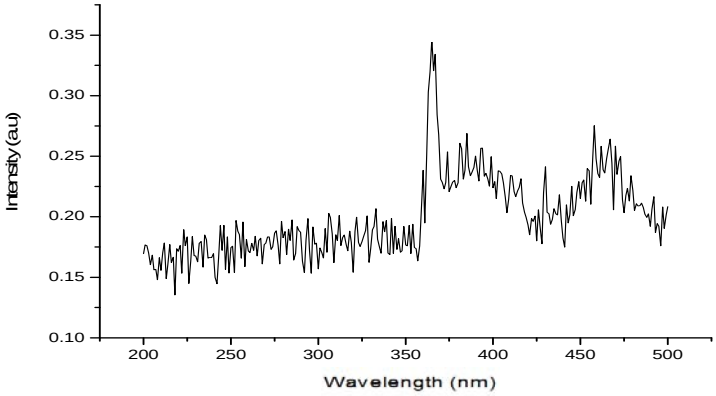

(c)

Figure 6.7 Photoluminescent excitation spectra of the samples prepared at 650°C from ethanolic solution (a) 1:1, (b) 1:2 and (c) 1:3 ratio samples. Excitation monitored at 612nm.

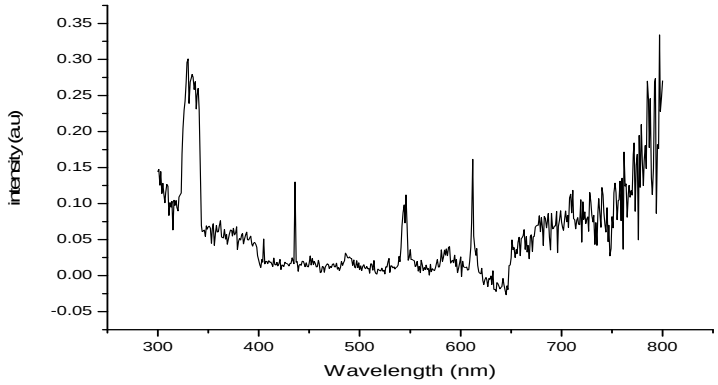

(a)

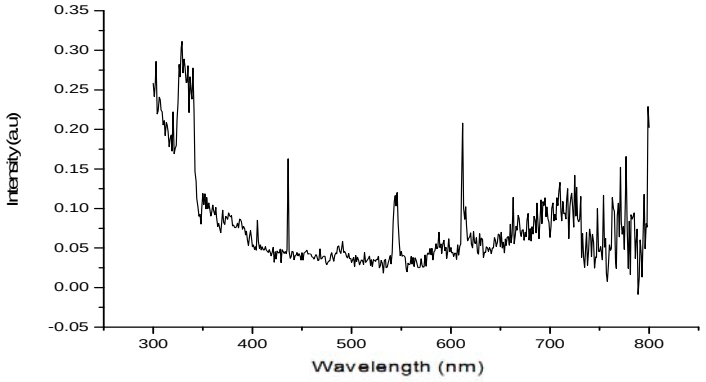

(b)

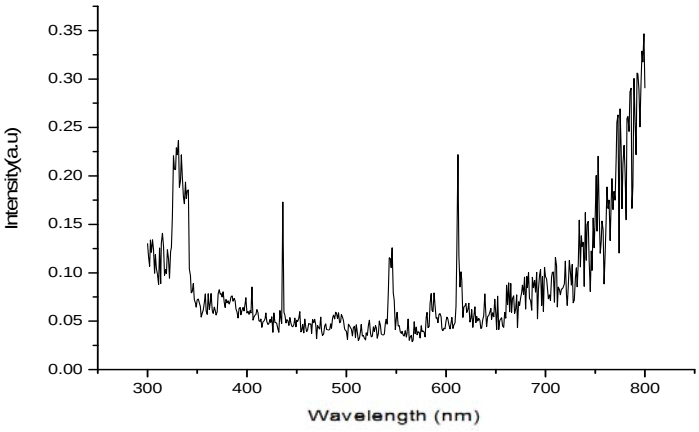

(c)

Figure 6.8A Photoluminescent emission spectra of the samples prepared at 650°C from ethanolic solution (a) 1:1, (b) 1:2 and (c) 1:3 ratio samples (excitation wave length 254nm).

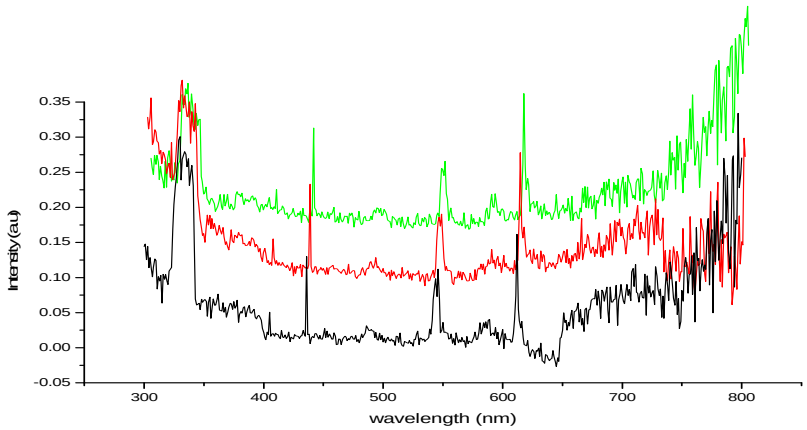

Figure 6.8B Photoluminescent emission spectra of the 650°C samples prepared from ethanolic solution overlaid (as in Figure 6. 8) 1:1 (bottom), 1:2 (Centre), 1:3 (top) (excitation wavelength 254nm.).

In Figure 6.7, 6.8A and 6.8B the PL excitation and emission spectra of the samples prepared at 650°C using 1:1, 1:2 and 1:3 ratio products prepared in ethanolic solution are displayed.They support the XRPD data; their excitation spectra are all very similar and are similar to those in Figures 6.5 and 6.6. This is different to the results found in chapter 6.5 where the results for the samples prepared from ethanol and methanol were different. Here for the samples prepared with the shorter chain length alkylammonium salt they are the same. There are some small peaks around 611 in all three emission spectra in Figure 6.6 and 6.8 which may indicate the presence of a small amount of cubic $Y_2O_3:Eu^{3+}$.

6.3.4 Cathodoluminescence Spectra: - The CL (5000V, emission current 50uA) spectra of the samples prepared from methanolic solution at 650°C using the products produced from the 1:1, 1:2 and 1:3 ratios, presented in Figures 6.9 and 6.10 are shown to be different with the 1:3 products being least closest to that of the cubic phase using defocused and focussed electron beams respectively. The CL data are the only data that show convincing evidence of the presence of cubic phase material in the samples fired at 650°C, and only for the 1:1 and 1; 2 samples the third sample the 1:3 is very weak. This is not because CL is more sensitive to the cubic phase but is in fact due to the conversion of the samples to cubic in the electron beam. This is because the samples are made up of very small particles of a precursor phase to that of the cubic $Y_2O_3:Eu^{3+}$ phosphor and the electron beam having sufficient energy to convert these particles into the cubic phase. The sample prepared from the 1:3 reactant ratios showed almost no conversion to the cubic phase.

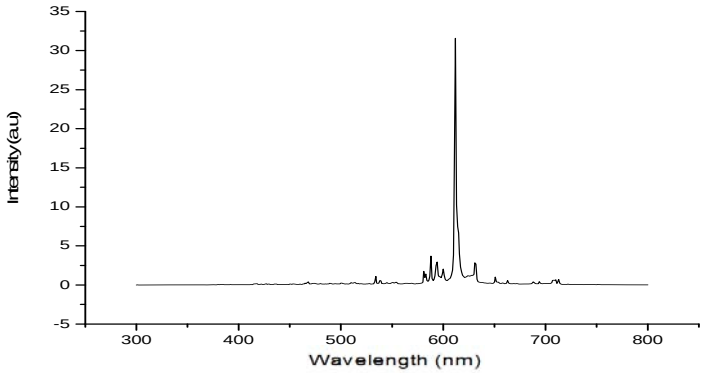

(a)

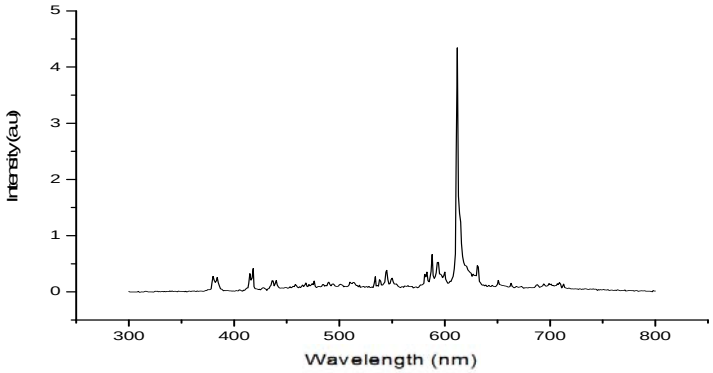

(b)

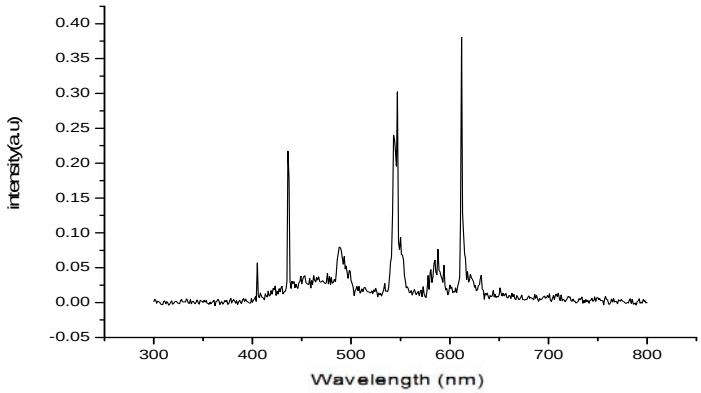

(c)

Figure 6.9 Cathodoluminescent spectra of the 650°C samples prepared from methanolic solution defocused beam.1:1 (a), 1:2 (b), 1:3 (c) at 5000V/50uA.

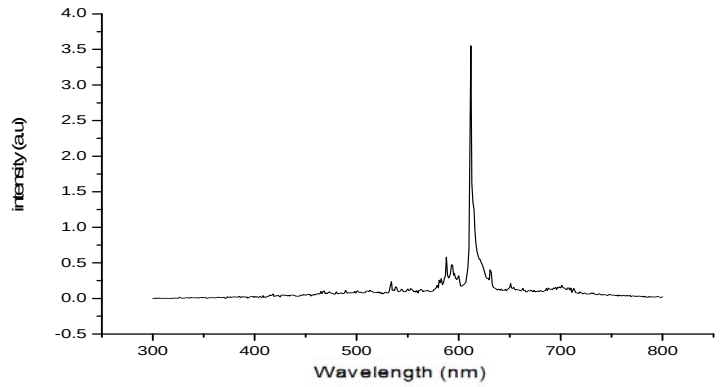

(a)

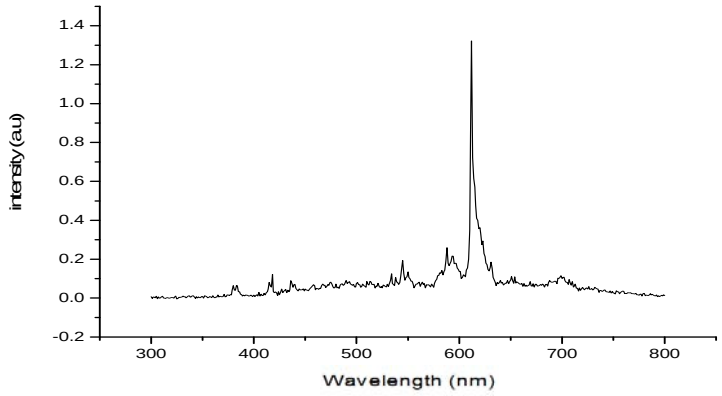

(b)

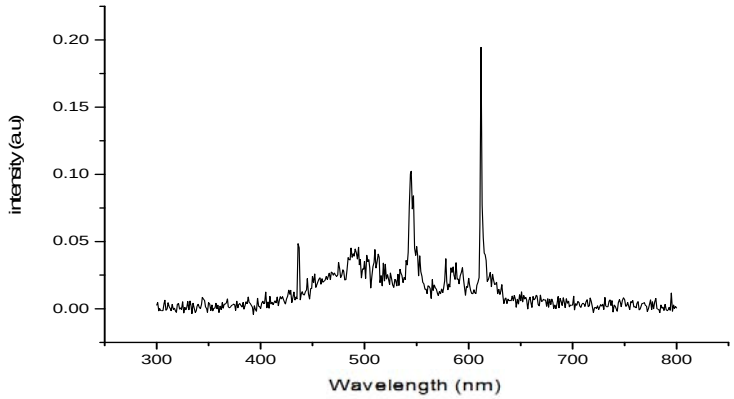

(c)

Figure 6.10 Cathodoluminescent spectra of the 650°C samples prepared from methanolic solution focused beam.1:1 (a), 1:2 (b), 1:3 (c) at 5000V/50uA.

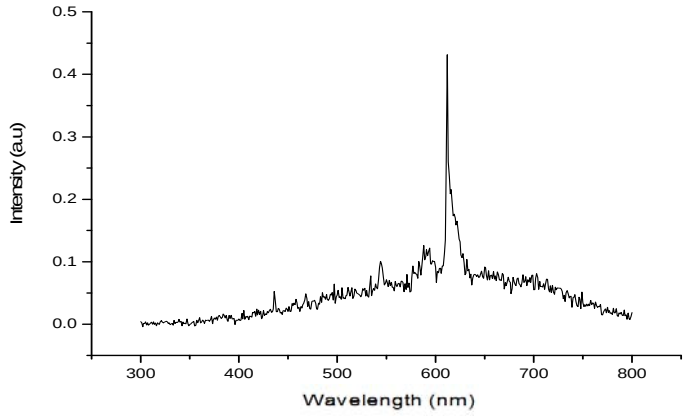

(a)

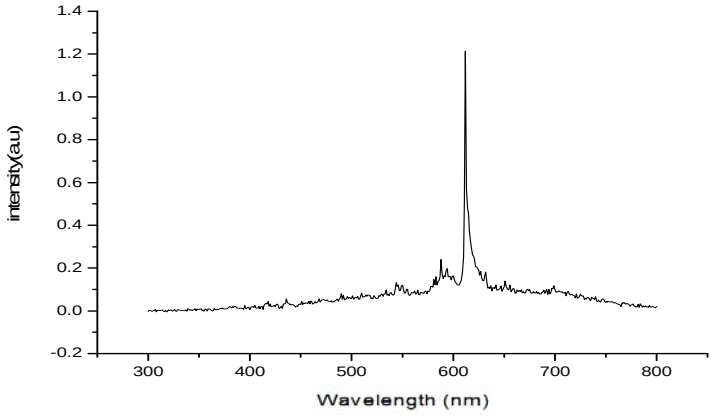

(b)

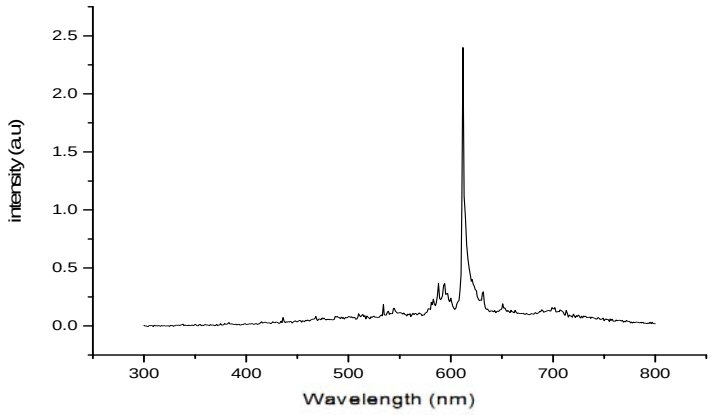

(c)

Figure 6.11 Cathodoluminescent spectra of the 650°C samples prepared from ethanolic solution defocused beam.1:1 (a), 1:2 (b), 1:3 (c) at 5000V/50uA.

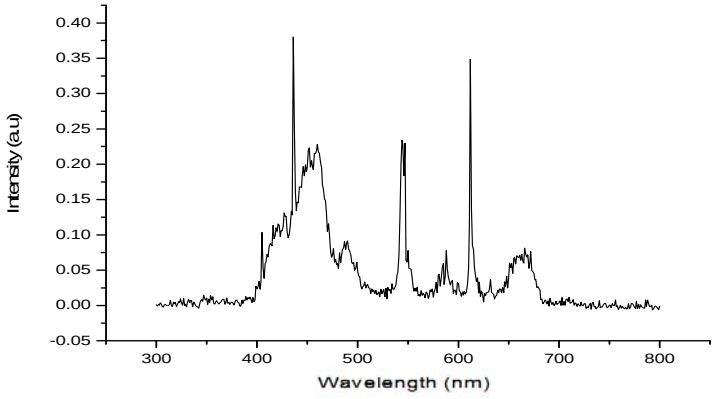

(a)

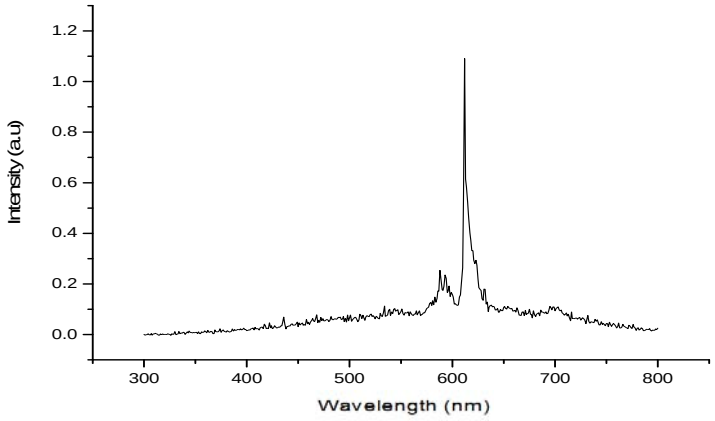

(b)

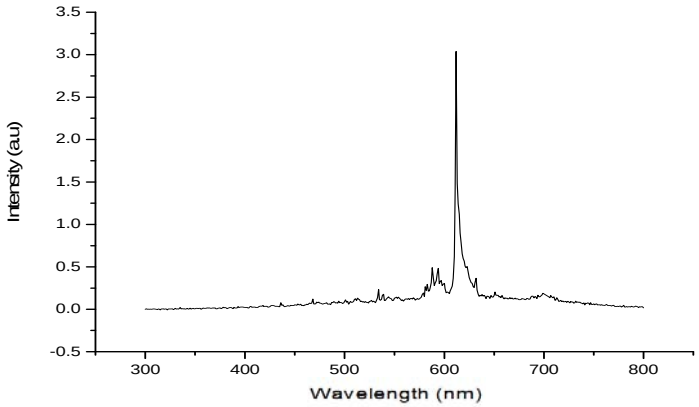

(c)

Figure 6.12 Cathodoluminescent spectra of the 650°C samples prepared from ethanolic solution focused beam.1:1 (a), 1:2 (b), 1:3 (c) at 5000V/50uA.

The CL (5000V, emission current 50uA) spectra of the samples prepared from ethanol at 650°C using the products produced from the 1:1, 1:2 and 1:3 ratios are presented in Figure 6.11 and 6.12. The spectra obtained using the defocused beam and then1:1 and 1:3 of the focused beam are all alike though that in Figure 6.11(a) is very weak and in all cases there is evidence of the cubic phase being formed in the beam. Surprisingly the 1:1 sample in the focused beam (see Figure 6.12(a)) shows no conversion to the cubic phase, although in the defocused beam some cubic was observed. This may be because the latter was over a much larger area of sample, and as stated before the data in Figure 6.11(a) are weak as seen in the curved background of the figure. Again as in the samples prepared from methanolic solution (Figures 6.9 and 6.10) the CL data are the only data that show convincing evidence of the presence of cubic phase material in the samples fired at 650°C. Again this is not because CL is more sensitive to the cubic phase but is in fact due to the conversion of the samples to cubic in the electron beam. Again this is because the samples are made up of very small particles of a precursor phase to that of the cubic $Y_2O_3:Eu^{3+}$ phosphor and the electron beam having sufficient energy to convert these particles into the cubic phase.

6.3.5 ATR-FTIR Spectra

The FTIR spectral assignments of the samples prepared from ethanolic and methanolic solution at 650°C are summarised in Table 6.3 and 6.4, all show the presence of bands that can only be ascribed to the presence of metal hydroxycarbonate. Firstly for the samples prepared from methanol at 650°C the FTIR spectra show the presence of bands that are ascribed to a mixture of $Y_{0.98}Eu_{0.02}(OH)CO_3$, $(Y_{0.98}Eu_{0.02})_2O(CO_3)_2$ and $(Y_{0.98}Eu_{0.02})_2O_2CO_3$. The basic europium doped yttrium carbonate, $Y_{0.98}Eu_{0.02}(OH)CO_3$, could have been formed from the surface reaction of YCl_3 with H_2O and CO_2 produced from the combustion of the alkylammonium cations.

$$2(Y,Eu)Cl_3 + 3H_2O \rightarrow (Y_{0.98}Eu_{0.02})_2O_3 + 6HCl \quad (6.1)$$
$$(Y_{0.98}Eu_{0.02})_2O_3 + 2CO_2 + H_2O \rightarrow 2Y_{0.98}Eu_{0.02}(OH)CO_3 \quad (6.2)$$

As $Y_{0.95}Eu_{0.05}(OH)CO_3$ was reported to lose most of its hydroxide to give $(Y_{0.95}Eu_{0.05})_2O(CO_3)_2$ and $(Y_{0.95}Eu_{0.05})_2O_2CO_3$ when it was calcined at 550°C for 1 hr in a muffle furnace [25], it is likely that a similar decomposition occurred, albeit incompletely, under the rapid combustion conditions at a set temperature of 650°C in the present work.

Figures 6.13 and 6.14 present ATR-FTIR spectra of these samples in the 3600 – 700 cm^{-1} range; the broad band observed in the region of 3600-2400 cm^{-1} is assigned to the

O-H stretching vibration of the hydroxycarbonate. The triplet of bands observed at 1633 cm^{-1}, 1522 and 1403 cm^{-1} is attributed to C-O stretching vibrations of CO_3^{2-} anions; the first component having some C=O character and the last two most likely being due to antisymmetric C-O stretching modes of CO_3^{2-} anions [26]. Furthermore, the weak band at 1092 cm^{-1} is assigned to a symmetric C-O stretching vibration of the CO_3^{2-} anions [27]. The inhomogeneous broadening of the various vibrational bands in the spectra of these samples is due to the disorder within the lattices when the products are formed at 650°C. It is not possible to identify bands due to Y-Cl stretching vibrations in these ATR-FTIR spectra as they are expected to appear below the low wavenumber cut-off at ca. 700 cm^{-1} of the ATR diamond crystal which was used for collecting the ATR-FTIR spectra (bands due to Y-Cl stretching vibrations would be expected to occur at lower wavenumber).

Table 6.3 Materials prepared from methanolic solutions at 650°C.

Wavenumber/cm^{-1}		
3600-2400	(m)	ν (O-H)
1633	(w)	δ (O-H)
1522	(m)	ν_{as} (CO_3^{2-})
1403	(s)	ν_{as} (CO_3^{2-})
1090	(w)	δ (O-H)
~759	(w shoulder on cut-off)	δ (CO_3^{2-})

Table 6.4 Materials prepared from ethanolic solutions at 650°C.

Wavenumber/cm^{-1}		
3600-2200	(m)	ν (O-H)
	(m)	ν_s (O-H)
1622	(shoulder)	δ (O-H)
1520	(s)	ν_{as} (CO_3^{2-})
1422	(s)	ν_{as} (CO_3^{2-})
1092	(w)	δ (O-H)
725	(w)	δ (CO_3^{2-})

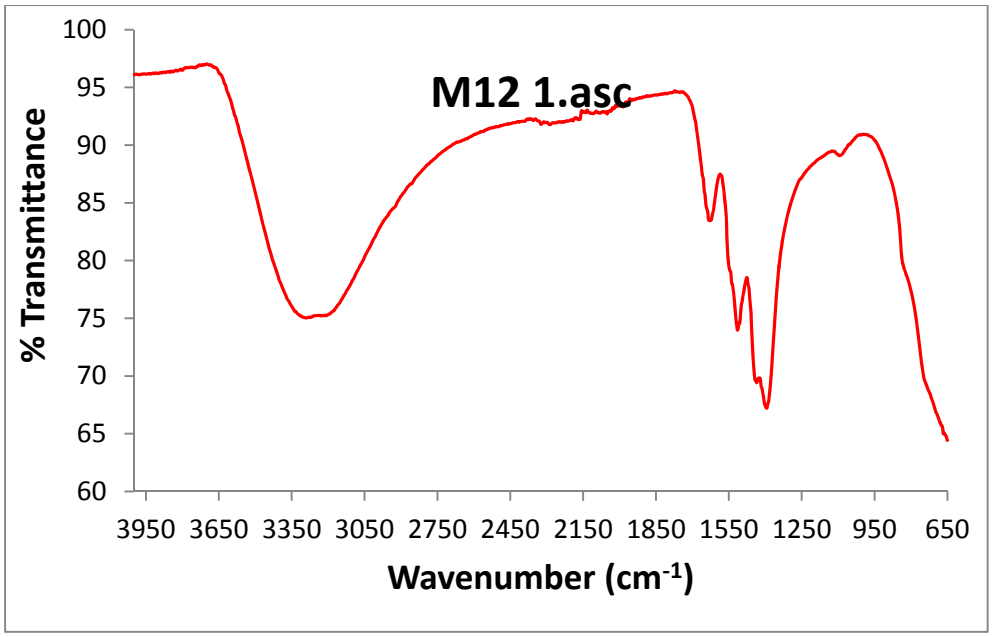
M12 1.asc
% Transmittance
100
95
90
85
80
75
70
65
60
3950 3650 3350 3050 2750 2450 2150 1850 1550 1250 950 650
Wavenumber (cm-1)

(a)

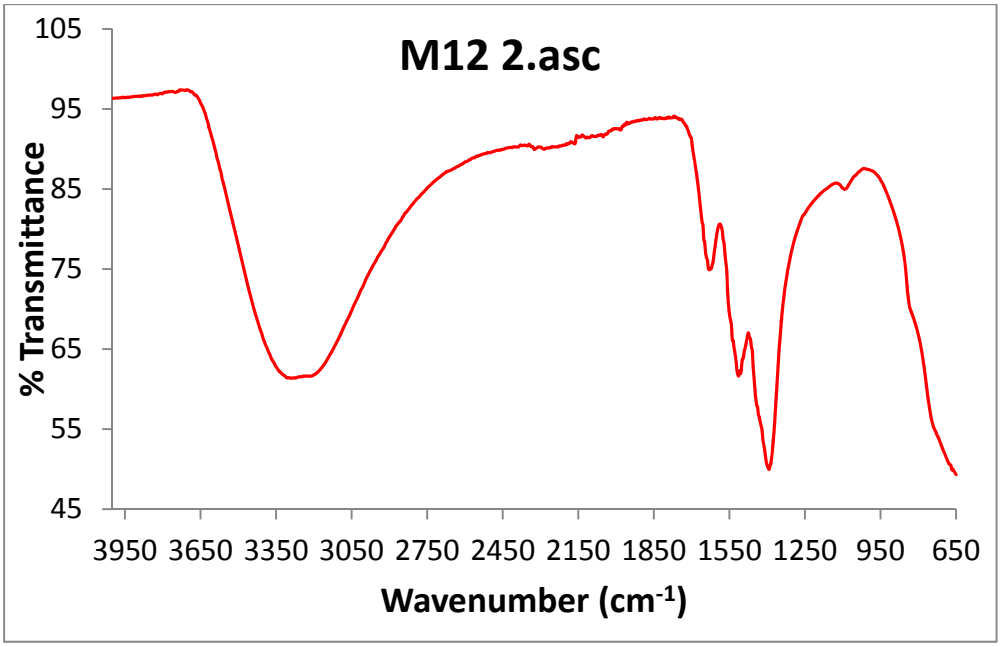
M12 2.asc
% Transmittance
105
95
85
75
65
55
45
3950 3650 3350 3050 2750 2450 2150 1850 1550 1250 950 650
Wavenumber (cm-1)

(b)

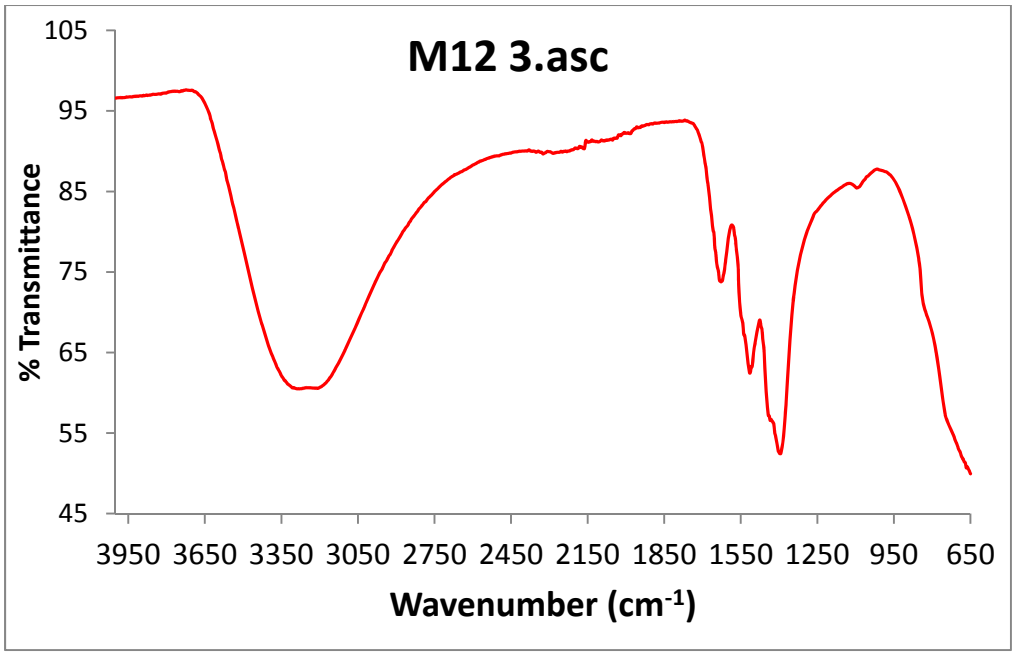

(c)

Figure 6.13 ATR spectra of the 650°C, samples a, b; c prepared from methanolic solution with metal ion to alkylammonium chloride ratios 1:1 (a), 1:2 (b) and 1:3 (c).

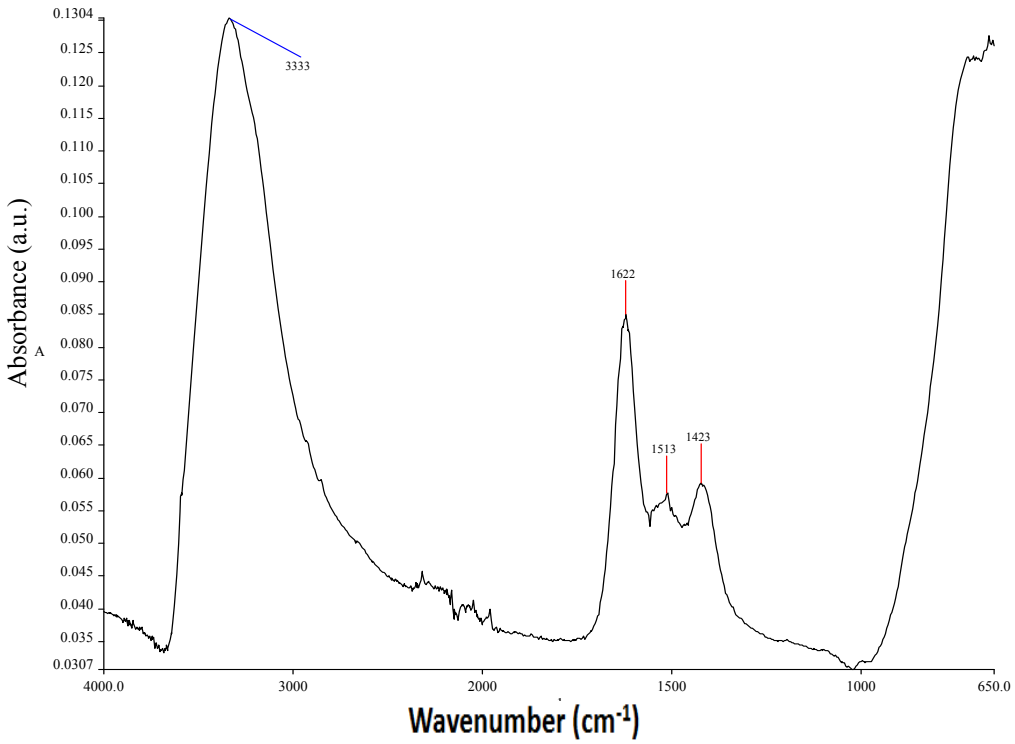

7

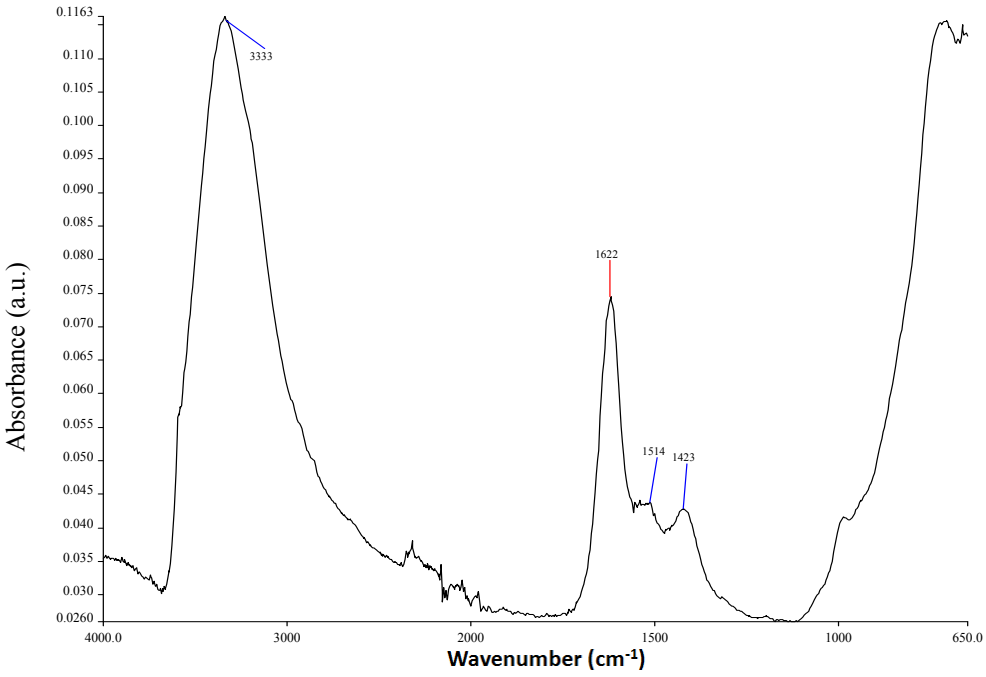

8

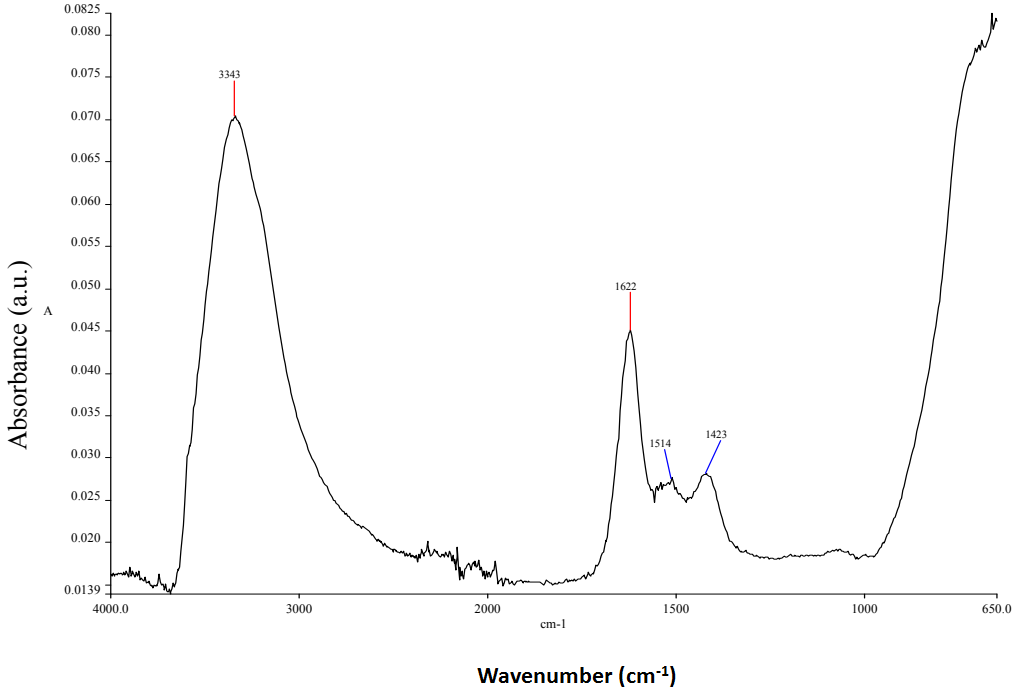

9

Figure 6.14 FTIR spectra of the 650°C, samples 7, 8, 9 prepared from ethanolic solution with Metal ion to alkylammonium chloride ratios 1:1 (7), 1:2 (8) and 1:3 (9) in KBr discs.

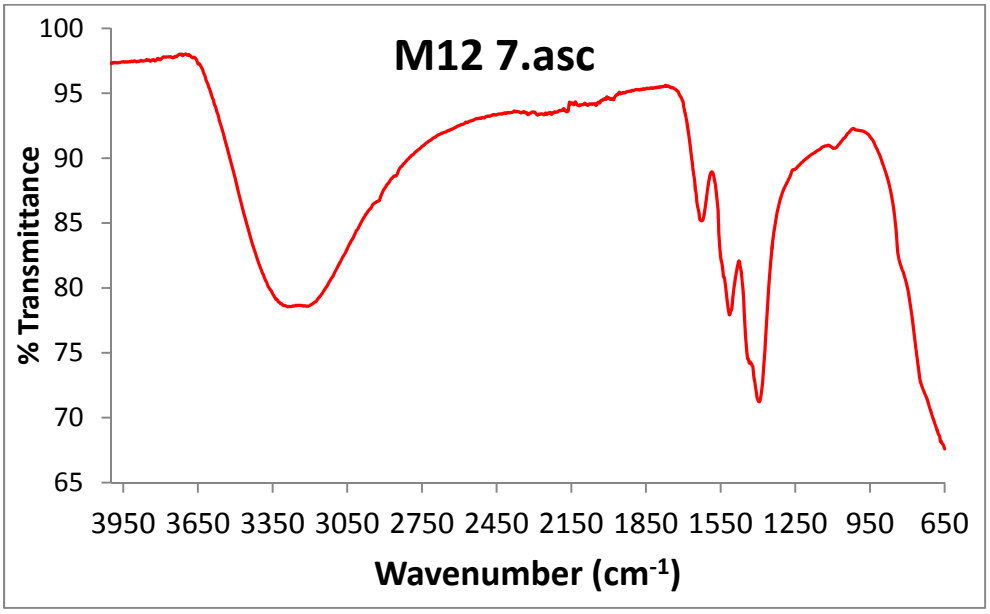
M12 7.asc
% Transmittance
100
95
90
85
80
75
70
65
3950 3650 3350 3050 2750 2450 2150 1850 1550 1250 950 650
Wavenumber (cm-1)

7

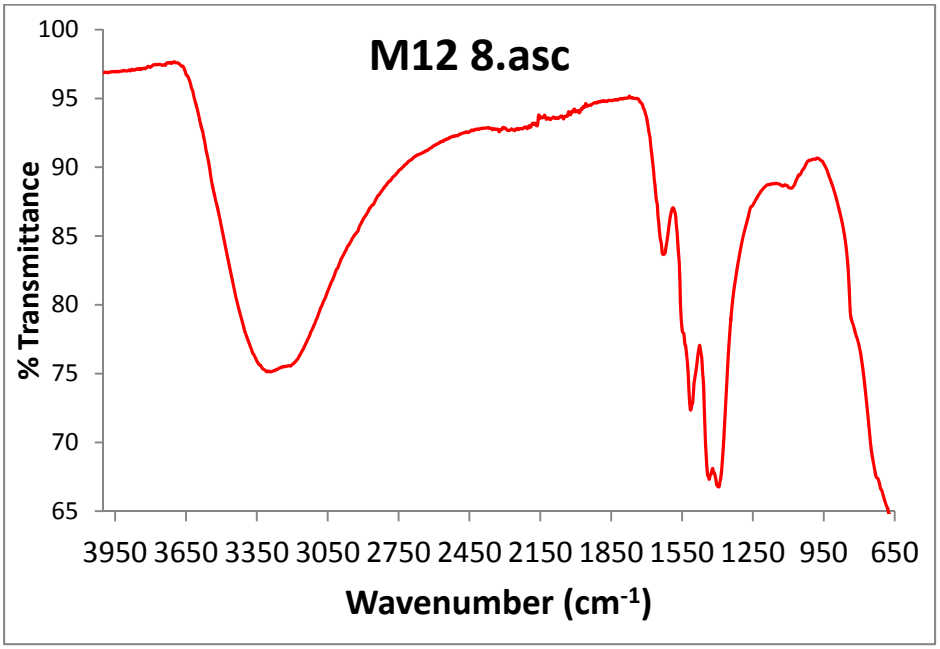
M12 8.asc
% Transmittance
100
95
90
85
80
75
70
65
3950 3650 3350 3050 2750 2450 2150 1850 1550 1250 950 650
Wavenumber (cm-1)

8

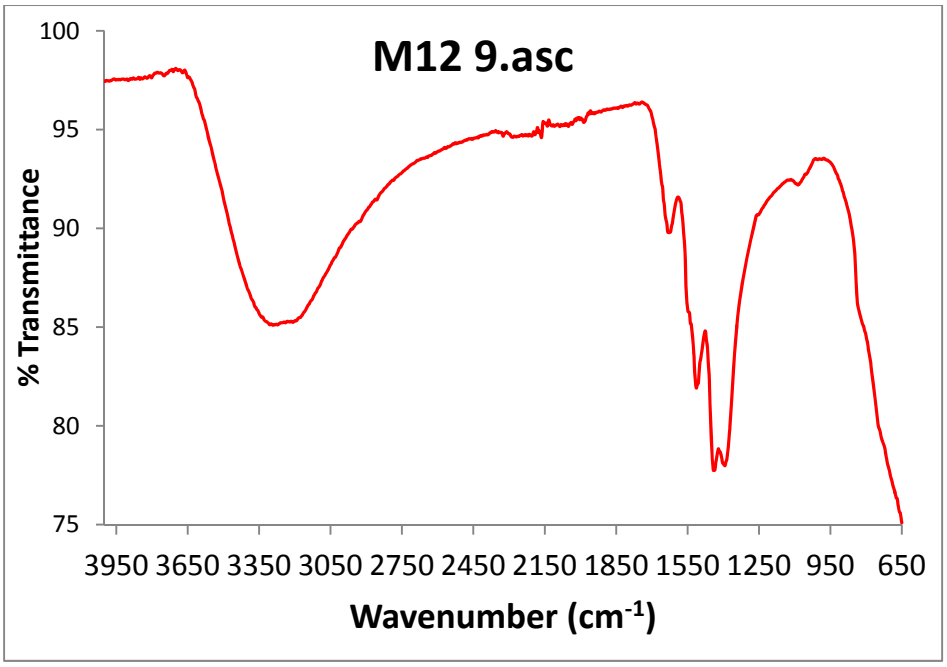

9

Figure 6.14A ATR spectra of the 650°C, samples 7, 8, 9 prepared from ethanolic solution with metal ion to alkylammonium chloride ratios 1:1 (7), 1:2 (8) and 1:3 (9).

6.3.6 Conclusions so far:- It is clear from these results so far that the presence of the combustion fuel in the samples prepared at 650°C was insufficient to raise the temperature high enough to form the cubic $Y_2O_3:Eu^{3+}$ phase or that the furnace temperature was insufficient. All the 650°C ATR-FTIR spectra are similar, although the emission spectra do indicate that for the higher fuel ratios that a greater degree of order is found. It is interesting that there is evidence for yttrium oxychloride doped with europium containing phases for the samples prepared from both methanolic and ethanolic solutions where the shorter chained alkylammonium salt has been used unlike the findings in Chapter 5.

6.4 Studies on the samples produced at. 900°C

6.4.1 Products prepared with methanol and ethanol at a temperature of 900°C.

Products (samples) prepared from precursors methanolic and ethanolic solutions were fired at a temperature of 900°C and observed to be all white powders in colour. Under 254nm excitation the samples prepared at 650°C displayed a weak red luminescence which was in contrast to the strong red luminescence from the samples prepared at

900°C that is characteristic of the Eu^{3+} ion in cubic Y_2O_3. The strongest red luminescence comes from 1:3 material sample ratios and at 900°C.

6.4.2 SEM Studies: - The phosphor samples annealed at 900°C are now discussed. In Figure 6.15 and 6.16 SEM micrographs of phosphor samples prepared from methanolic solutions then fired at 900°C at metal chloride to alkylammonium chloride ratios of Figure 6.15, 1:1 (a,b,c,k, and l), Figure 6.16, 1:2 (e,f and m) and Figure 6.17,1:3 (g,h,i,j,n,o and p) are presented.

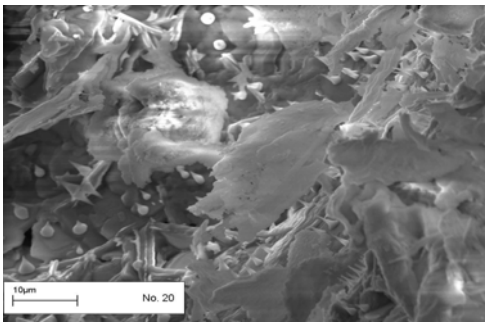

(a)

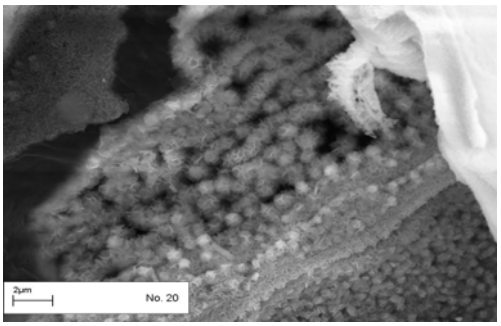

(b)

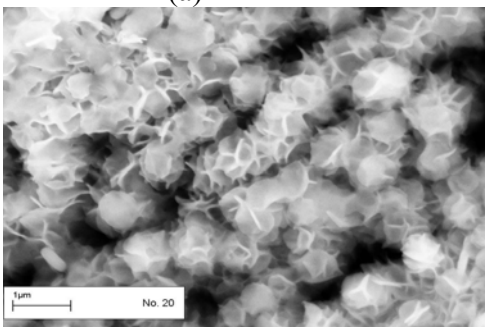

(c)

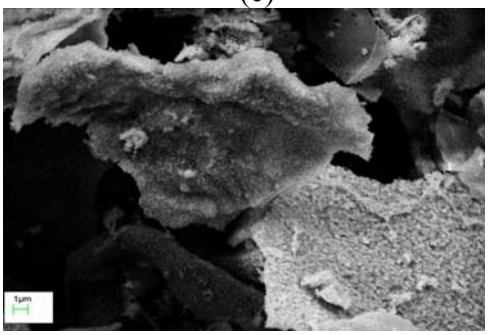

(k-4) 1:1

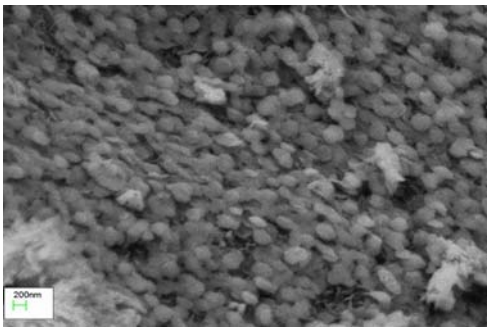

(l-4) 1:1

Figure 6.15 FESEM images of phosphor samples prepared from methanolic solutions then fired at 900°C using a metal chloride to alkylammonium chloride ratio of 1:1,a,b,c,k,l. In (a) the bar is 10 µm, in (b) the bar is 2µm, in (c and k) it is 1 µm, and in (l) it is 200 nm.

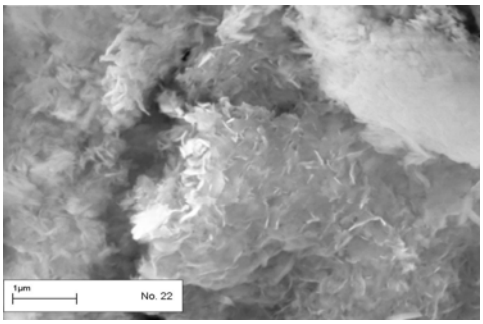

(e)

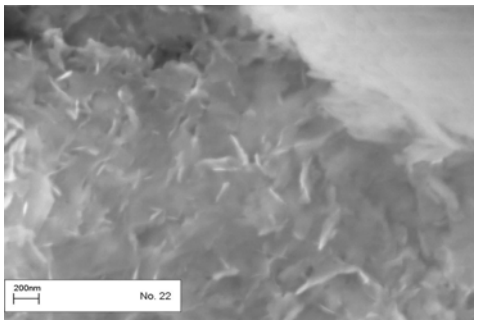

(f)

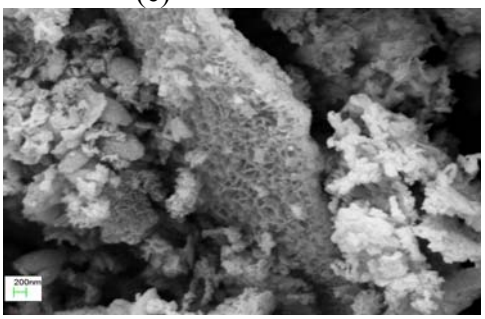

(g) 1:2

Figure 6.16 FESEM images of phosphor samples prepared from methanolic solutions then fired at 900°C using a metal chloride to alkylammonium chloride ratio of 1:2, e, f, and m. In (e) the bar is 1 μm, and in (f and g) it is 200 nm.

It is interesting to note that the same morphological forms and the individual crystallites of the 650°C 1:1 and 1:2 samples are present in the 900°C 1:1 sample and the remnant micellar forms of the 650°C 1:3 sample are present in the higher temperature 1:2 sample. The 900°C 1:3 sample is shown to have underg`one sintering that has eliminated some of the fine remnant micellar structures, therefore the higher temperature and metal chloride to fuel ratio has been sufficient to raise the temperature significantly.

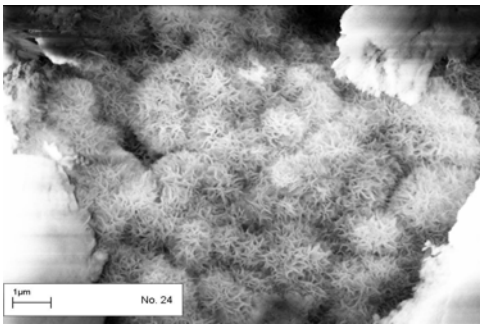

(g)

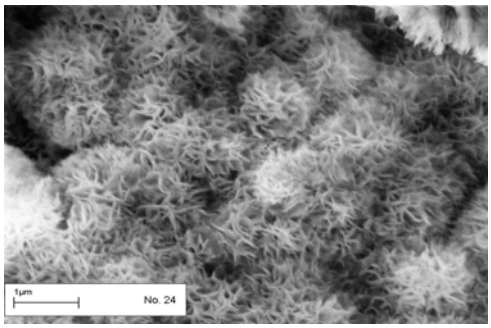

(h)

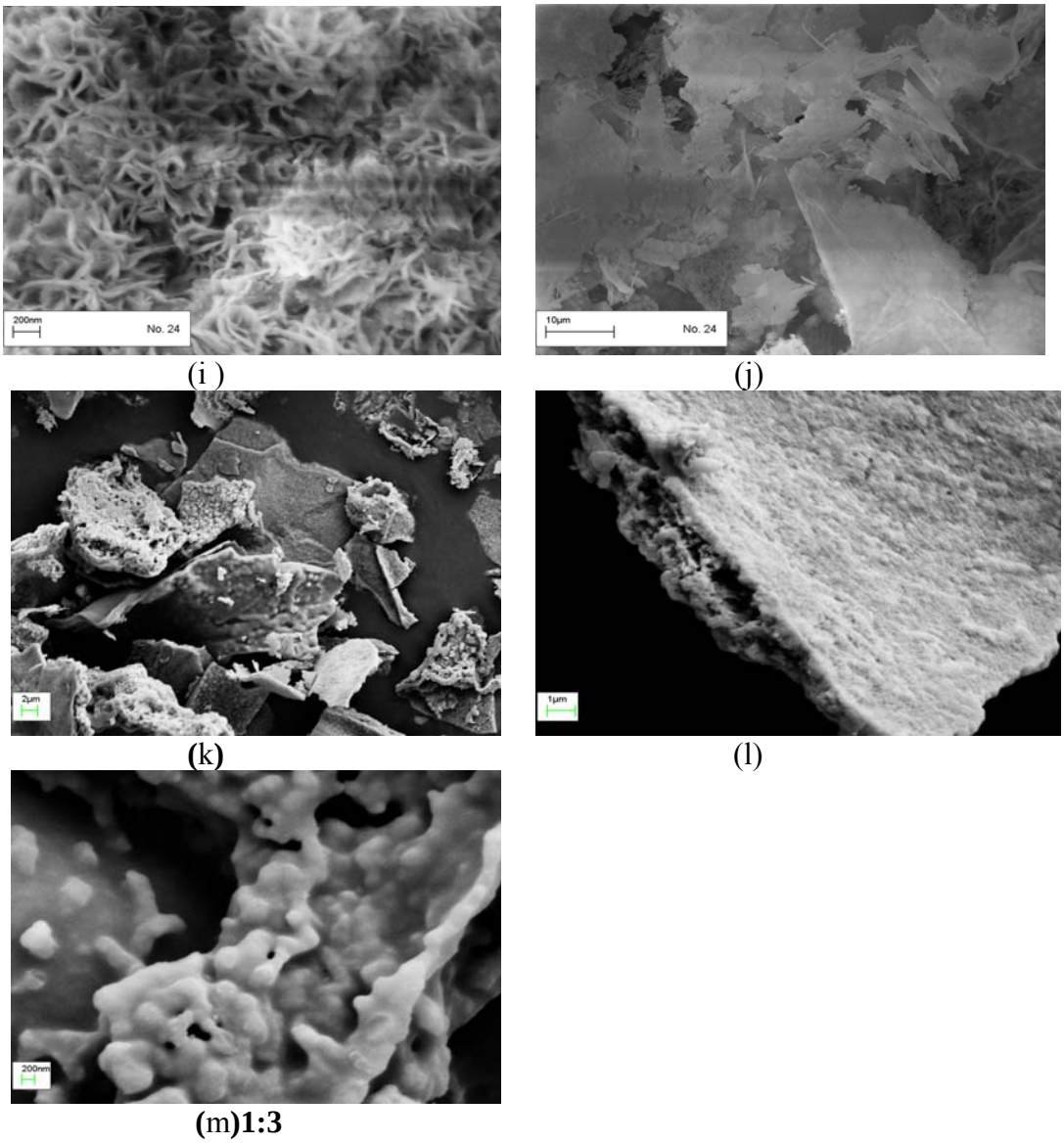

(i) (j)

(k**)** (l)

(m**)1:3**

Figure 6.17 FESEM images of phosphor samples prepared from methanolic solutions then fired at 900°C using a metal chloride to alkylammonium chloride ratio of 1:3, g,h,i,j,k,l,m. In (j) the bar is 10 µm, in (k) the bar is 2µm, in (g, h and l) it is 1 µm, and in (i and m) it is 200 nm.

Chapter 6 $Y_2O_3:Eu^{3+}$ Materials from the $[(Y, Eu)\ Cl_3]$ - $(C_{12}H_{25}NH_3Cl)$

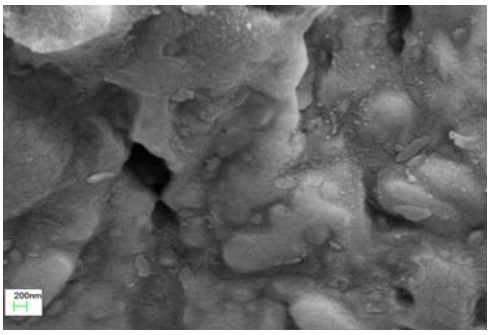

1:1-10-a

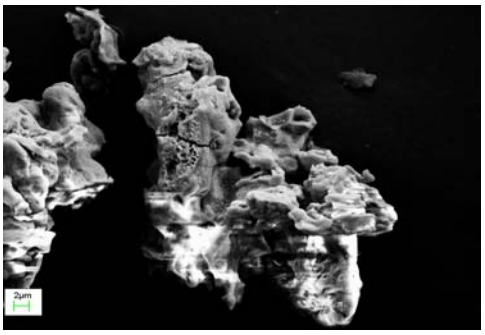

1:1-10-b

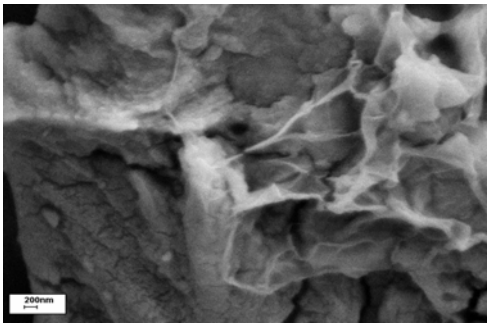

1:1-10 –c

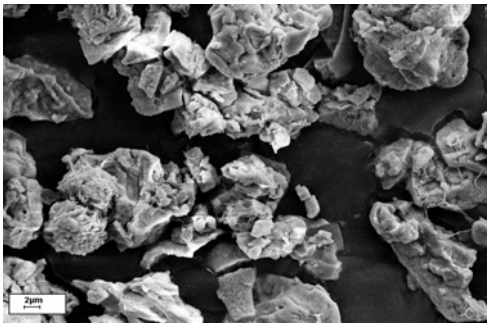

1:1 10-d

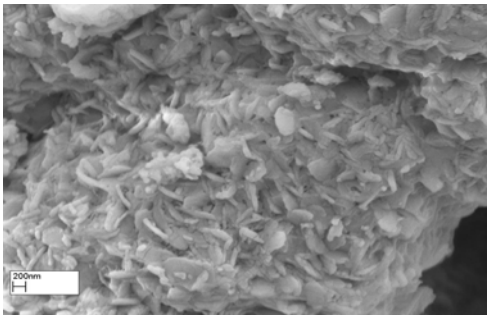

1:2 -11-e

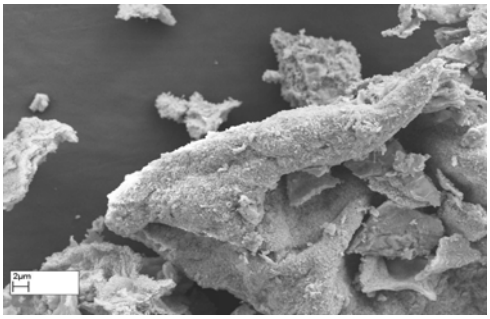

1:2 -11-f

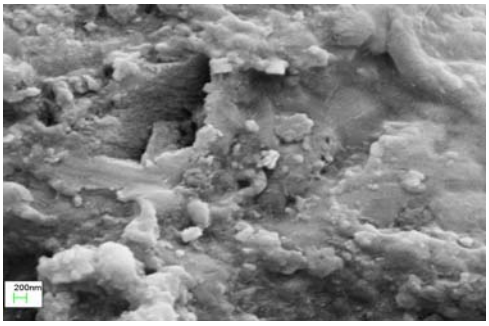

1:2-11-g

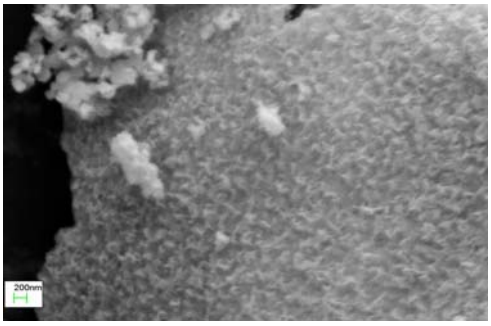

1:2 -11-h

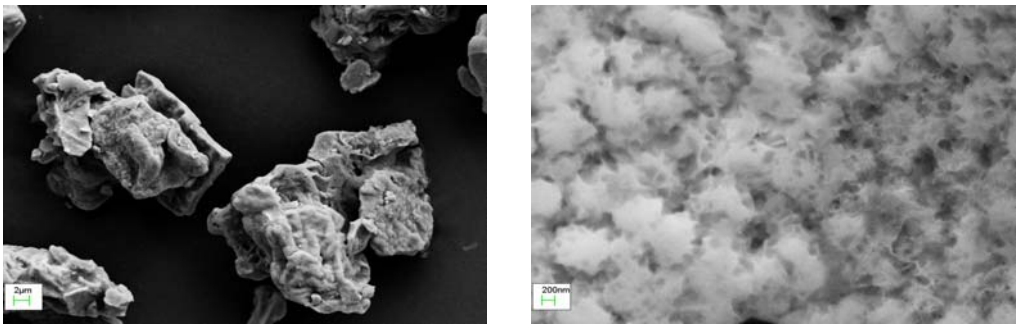

1:3- 12-i 1:3-12-j

Figure 6.18 FESEM images of phosphor samples prepared from ethanolic solutions then fired at 900°C prepared at metal chloride to alkylammonium chloride ratios of (10-a, b, c and d) 1:1. (11-e,f,g and h) 1:2 and (12-j and i) 1:3, In (b,d,f and i) the bar is 2µm, and in (a,c,e,g,h and j) it is 200nm.

In Figure 6.18 SEM micrographs of phosphor samples prepared from ethanolic solutions then fired at 900°C at metal chloride to alkylammonium chloride ratios of 1:1 (10-a,b,c and d), 1:2 (11-e,f,g and h) and 1:3 (12-j and i) are presented . All of these three samples were prepared in a muffle furnace with a wide chimney. In these samples the SEMs show small sub micron crystals that form as two dimensional sheets suggesting that they were formed from the two dimensional extended micelle sheets. Therefore the higher temperature and metal chloride to fuel ratio has been sufficient to raise the temperature significantly compared to the 650°C samples.

6.4.3 Sample structures (from XRPD data)

All the samples that were produced under the 900°C conditions from methanolic solution showed the presence of crystalline material and all showed a similar XRPD (see Figure 6.19) pattern identified as cubic $Y_2O_3:Eu^{3+}$. Samples prepared from the 1:1, 1:2 and 1:3 ratios all contained cubic Y_2O_3 with Lorentzian average crystallite sizes of 30.8 nm, 32.8 nm and 44.8 nm respectively. There were a few sharp lines in the 1:3 ratios that do not fit the cubic $Y_2O_3:Eu^{3+}$ and have not been fitted.

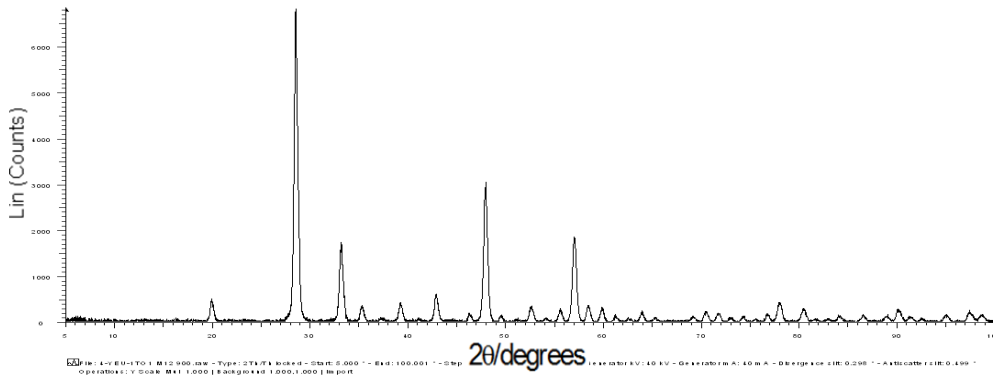

(a)

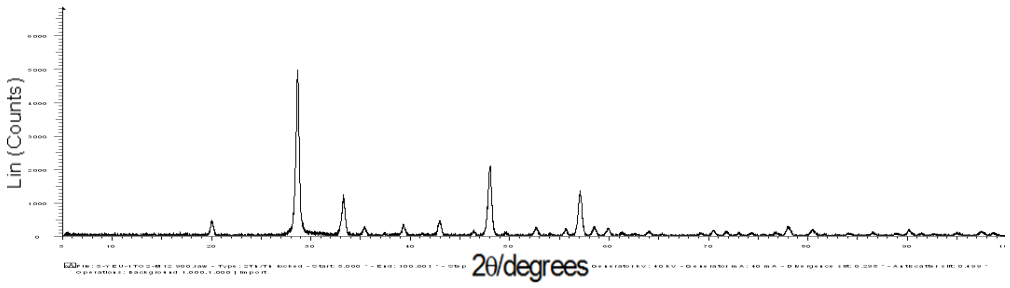

(b)

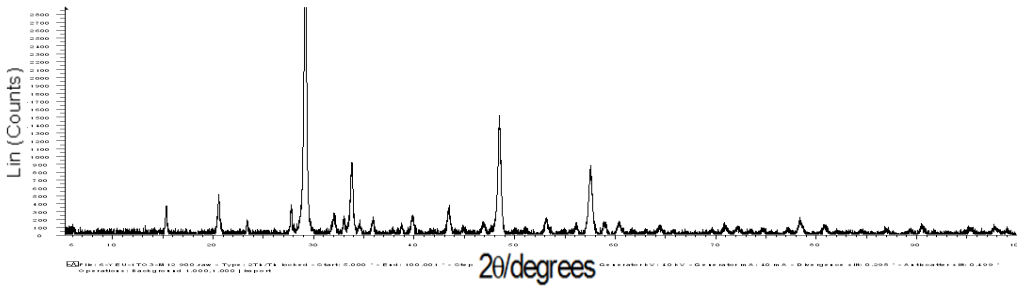

(c)

Figure 6.19 XRPD diffractograms of the samples prepared from methanolic solution then fired/annealed at 900°C, metal ion to alkylammonium chloride ratios: 1:1 (a), 1:2 (b) and 1:3 (c).

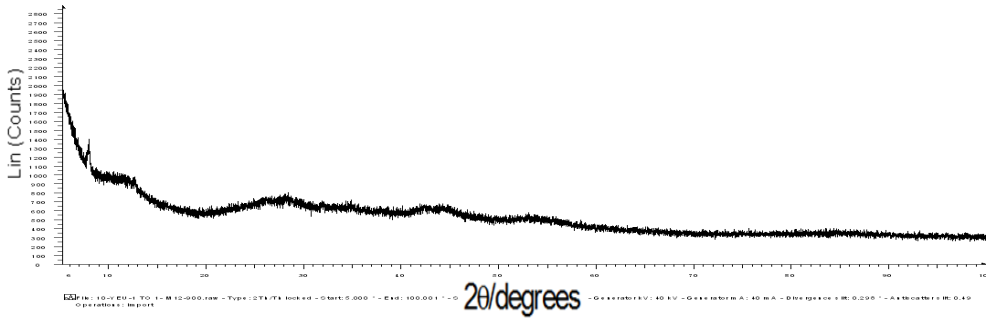

(a)

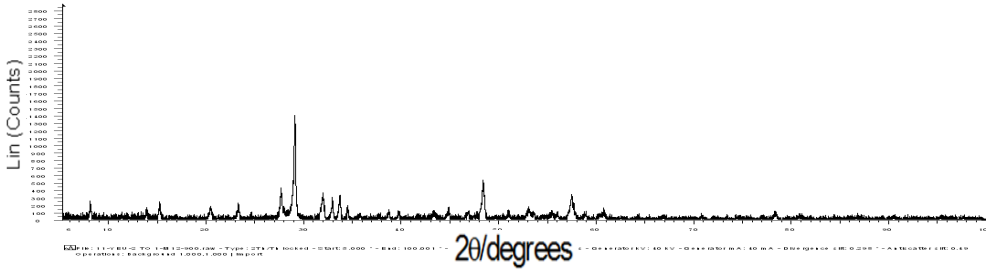

(b)

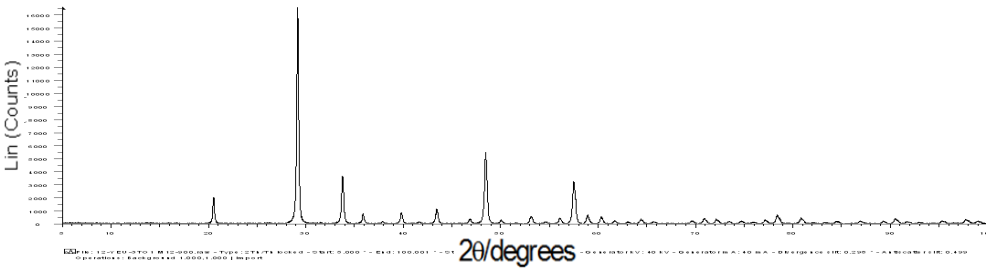

(c)

Figure 6.20 XRPD diffractograms of the samples prepared from ethanolic solution then fired/ Annealed at 900°C, metal ion to alkylammonium chloride ratios: 1:1 (a), 1:2 (b), 1:3 (c).

Chapter 6 $Y_2O_3:Eu^{3+}$ Materials from the $[(Y, Eu)\ Cl_3]$ - $(C_{12}H_{25}NH_3Cl)$

The samples that were produced under the 900°C conditions from ethanolic solution showed differing behaviour. The 1:1 sample had an XRPD pattern (see Figure 6.20 (a) that is typical of the presence of the material YOCl that found at 650°C. This must mean the temperature did not get high enough to change it to the cubic forn; this observation is in keeping with the glasslike structures observed in the SEM of this sample (see Figure 6.18 (a) to (d)). The 1:2 and 1:3 samples (see Figure 6.20 (b) and (c)) both showed the presence of crystalline material and in both cases the XRPD pattern was identified as cubic $Y_2O_3:Eu^{3+}$. However whereas for the 1:3 sample (figure 20(c) only cubic $Y_2O_3:Eu^{3+}$ was present in the case of the 1:2 sample a second crystalline phase was found. This phase was minor and not identified. The main phase was the cubic $Y_2O_3:Eu^{3+}$.These phases had Lorentzian average crystallite sizes of 60.59(20) nm1:3 and 58.50(14) nm 1:2 respectively.

Table 6.5
Cell parameters for the yttrium oxychloride phase $Y_2O_3:Eu^{3+}$ found in the materials fired at 900°C prepared from methanol and ethanol.

Methanol	a (Å)	a (Å)	c (Å)	Phase %
4 1:1	10.61210(40)			100
5 1:2	10.62168(27)			100
6 1:3	10.62231(35)			100
Ethanol				
10 1;1 phase 1*	R- 3m -1	5.000(26)	28.000(26)	11.78(97)
10 1:1phase 2*	R- 3m -2	34.185(15)	20.567(80)	88.22(97)
11 1;2	10.61901(89)			100
12 1:3	10.62109(11)			100

* These phases had very small crystallite sizes that were both less than 1nm. This is typical of this material (YOCl)

6.4.4. Photoluminescent Spectra

All the PL emission spectra of the samples made from methanolic solution are typical of cubic $Y_2O_3:Eu^{3+}$, as are the excitation spectra. Typical excitation and emission spectra are presented in Figures 6.21, 6.22, 6.23 and 6.24 for the 1:1, 1:2 and 1:3 900°C samples.

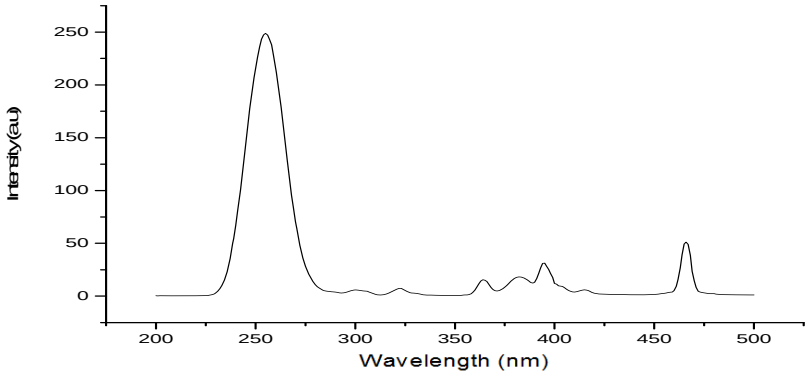

(a)

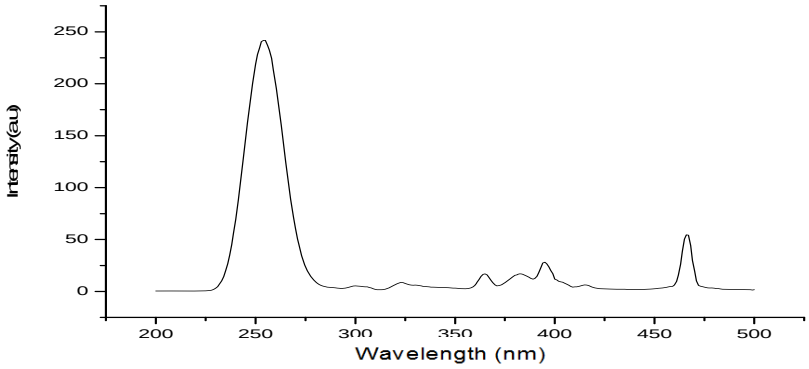

(b)

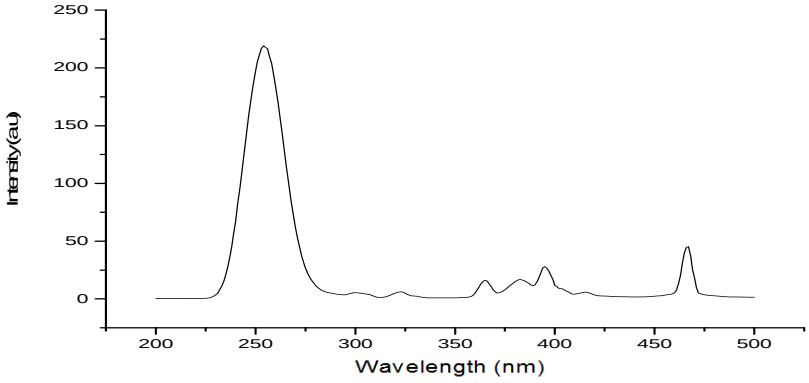

(c)

Figure 6.21 Photoluminescent excitation spectra of the 900°C samples prepared from methanolic solution. Excitation spectra (a) 1:1-4, (b)1:2-5, (c)1:3-6. Excitation monitored at 612 nm.

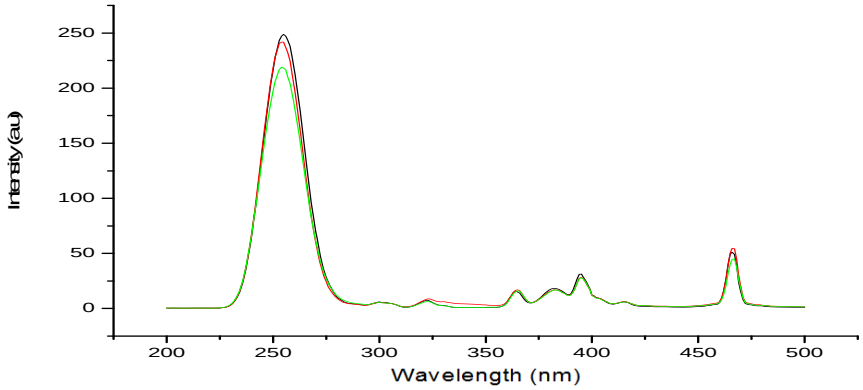

Figure 6.22 Overlay photoluminescent excitation spectra of the 900°C samples C-12 prepared from methanolic solution. Overlay excitation graphs 1:1-4-black-top, 1:2-5, red (mid), 1:3-6, green. Excitation monitored at 612 nm.

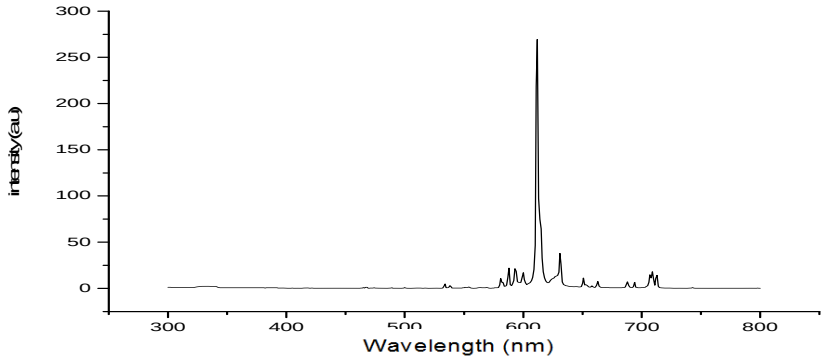

(a)

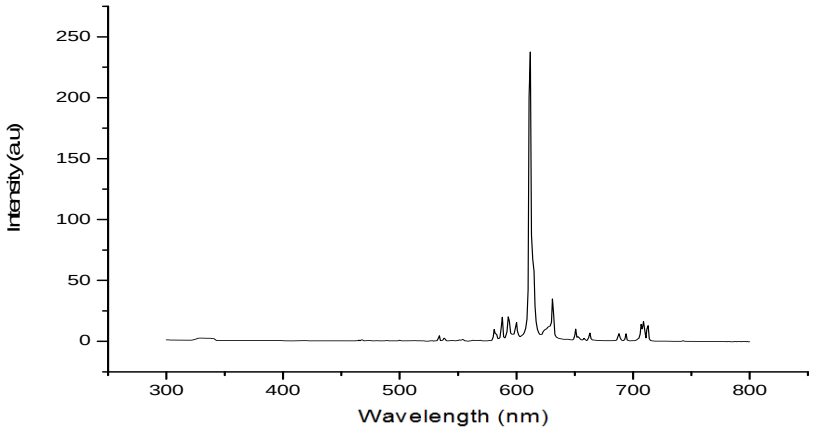

(b)

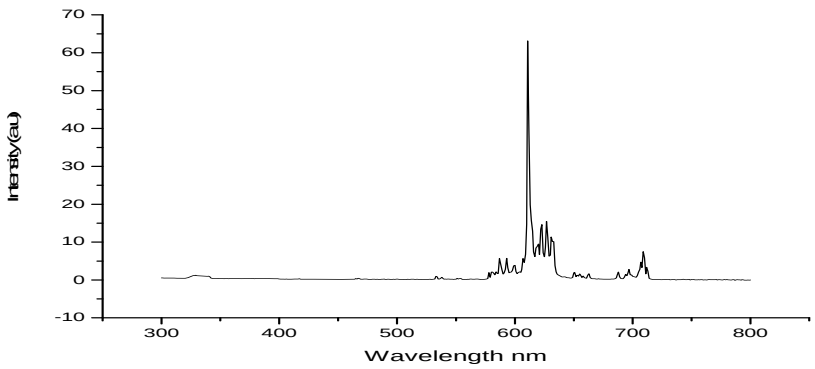

(c)

Figure 6.23 Photoluminescent emission spectra of the 900°C samples prepared from methanolic solution. Emission spectra (a)1:1-4,(b) 1:2-5, (c)1:3-6. Excitation wavelength 254nm.

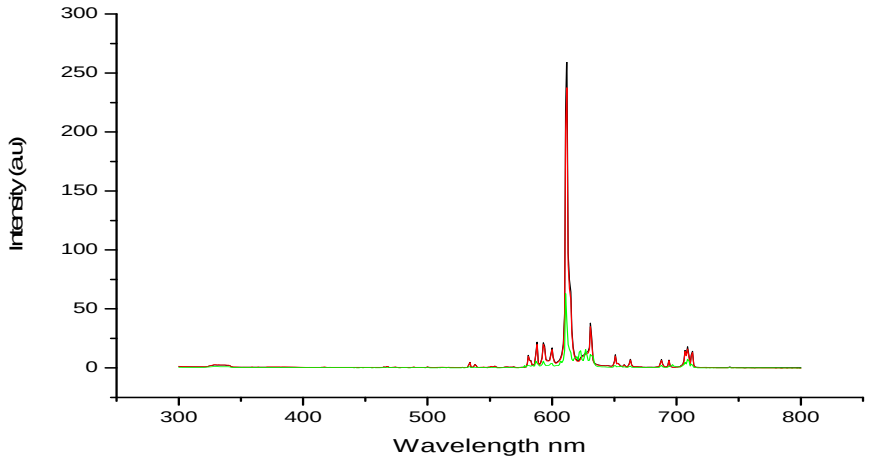

Figure 6.24 Overlay photoluminescent emission spectra of the 900°C samples C-12 prepared from methanolic solution. Overlay emission graphs 1:1-4, 1:2-5, 1:3-6 green. Excitation wavelength 254nm.

The PL emission spectra (Figure 6.25) of the samples made from ethanolic solution are not the same as those of those prepared from methanolic solution The 1:1 and 1:2 ratios are different from each other and differ from those in Figures 6.21 and 6.22 (those made from methanolic solution) where as that of the 1:3 ratio is much more typical of cubic $Y_2O_3:Eu^{3+}$, The PL excitation spectra (Figure 26) show a similar behaviour, with the 1:1 being the most out of line and very like the spectra of the same sample heated to 650°C, the 1:2 shows some changeover towards the cubic phase of $Y_2O_3:Eu^{3+}$ and the 1:3 material has an emission spectrum very like cubic $Y_2O_3:Eu^{3+}$. Clearly the materials prepared from ethanolic solution and fired at 900°C did not stay

at the temperature long enough to fully convert to the cubic phase, This was confirmed by refiring a portion of a 1:2 sample for sixty minutes at 900°C its emission spectrum is presented in Figure 6.27 it is clearly change compared to Figure 6.26 and is now fully cubic $Y_2O_3:Eu^{3+}$.

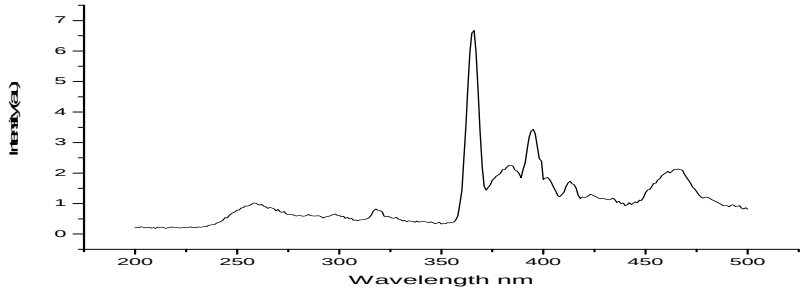

(a)

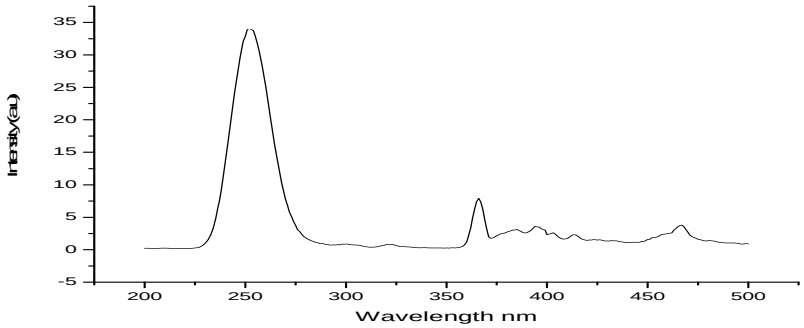

(b)

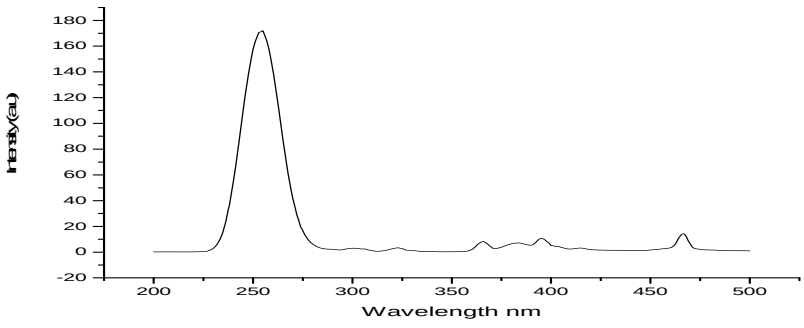

(c)

Figure 6.25 Photoluminescent excitation spectra of the 900°C samples prepared from ethanolic solution. Excitation spectra (top) (a) 1:1-10, (b) 1:2-11, (c) 1:3-12. Excitation monitored at 612 nm.

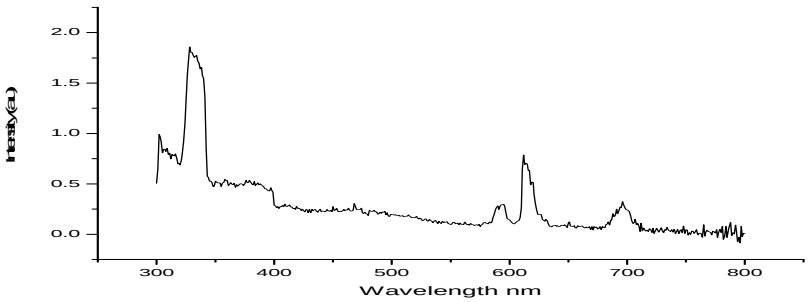

(a)

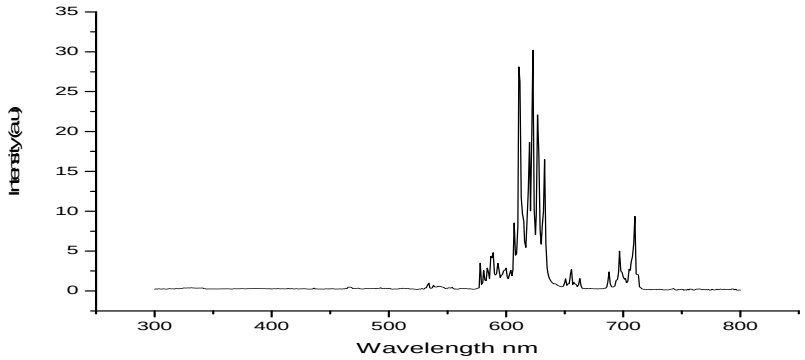

(b)

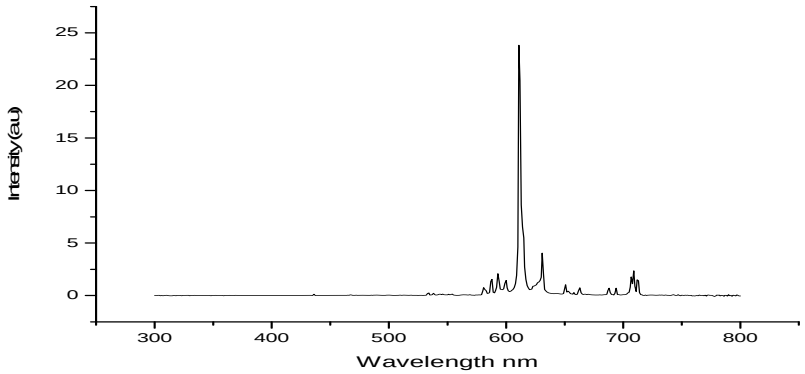

(c)

Figure 6.26 Photoluminescent emission spectra of the 900°C samples prepared from ethanolic solution. Emission spectra (a)1:1-10, (b)1:2-11, (c)1:3-12 . Excitation wavelength 254nm.

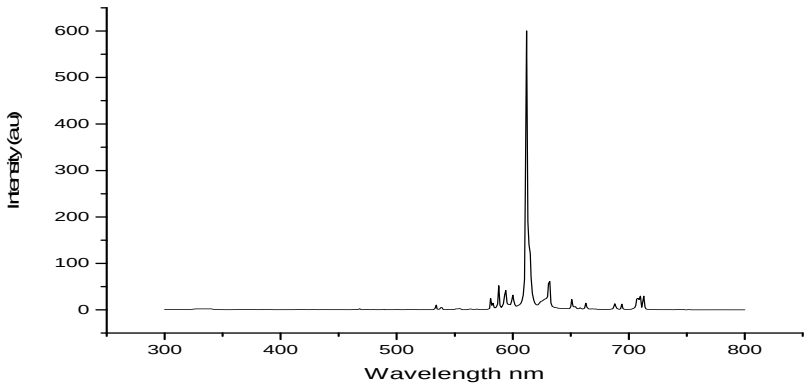

Figure 6.27 Photoluminescent emission spectrum of the (b) 1:2 -11 sample refired at 900°C for 60 min. Excitation wavelength 254nm.

At this point it is worth exploring why the samples prepared at 900°C from ethanolic solution are different from those prepared from methanolic solution. First it should be stated that all the preparations were performed twice so the findings are repeatable. The difference in the preparation of the samples is only the solvent. However as the solvents were not totally removed as they were only left in air for 24 h before firing the samples still contained solvent when they were fired. Hence there was more carbon content in the ethanolic samples on firing and this would have formed extra carbon dioxide. This gas is heavier than air and may have displaced excess oxygen from the vicinity of the crucible. Hence there was not enough oxygen in the furnace to convert all the way to the cubic $Y_2O_3:Eu^{3+}$ and hence only partial oxidation took place to form monoclinic $Y_4O_5Cl_2:Eu^{3+}$. Moreover as seen in the preceding chapter this excess carbon dioxide could react with the surface of the fired samples forming a carbonate rich layer and partially protecting the inner materials from full oxidation, So though the monoclinic $Y_4O_5Cl_2:Eu^{3+}$ was prepared as nanoparticles they proved to be stable only when the outer carbonate layer was intact and longer firing converted the material to cubic $Y_2O_3:Eu^{3+}$.

6.4.5. Cathodoluminescence Spectra The CL (5000V, emission current 9.6μA) defocused and focused spectra of the products prepared from the precursors originating in the methanolic solutions are shown in Figures 6.28, 6.29, 6.30 and 6.31; they are all similar and typical of cubic$Y_2O_3:Eu^{3+}$.

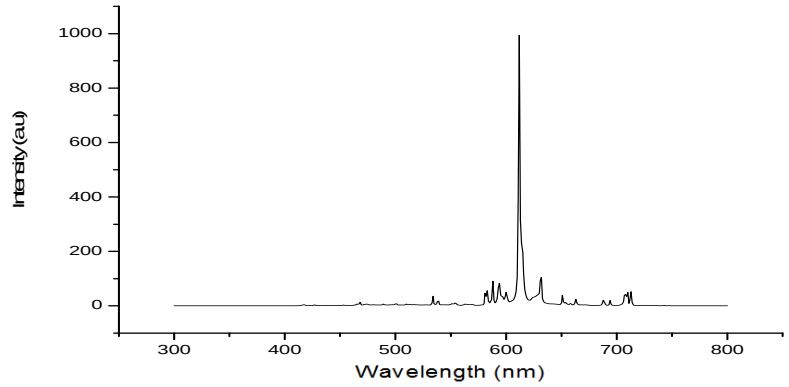

(a)

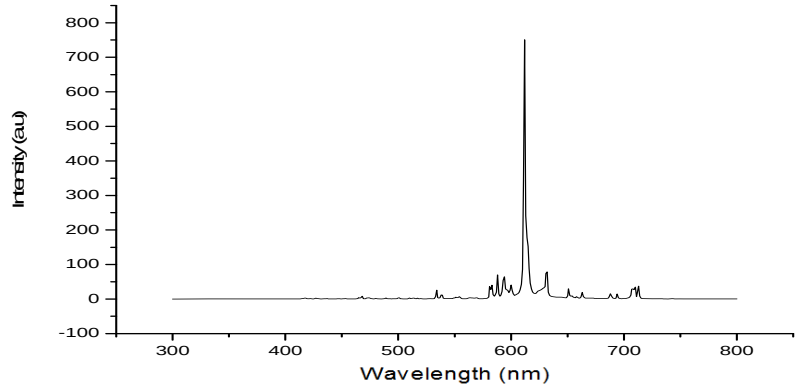

(b)

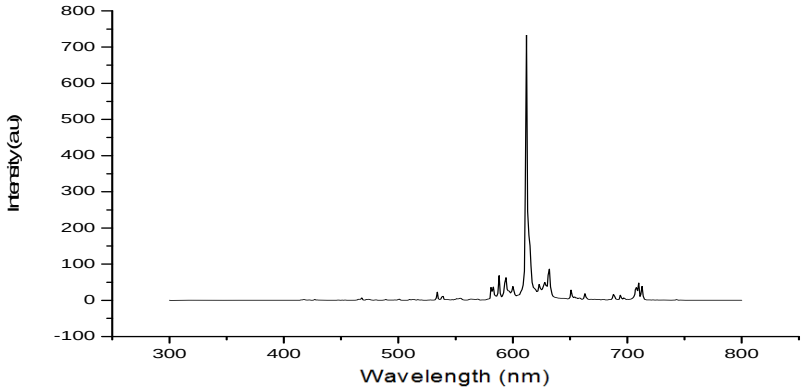

(c)

Figure 6.28 The CL defocused beam emission spectra for samples (a) 4-1:1, (b) 5-1:2 and (c) 6-1:3 prepared from methanolic solutions and fired/annealed at 900°C all three samples were excited using 5000V/50uA

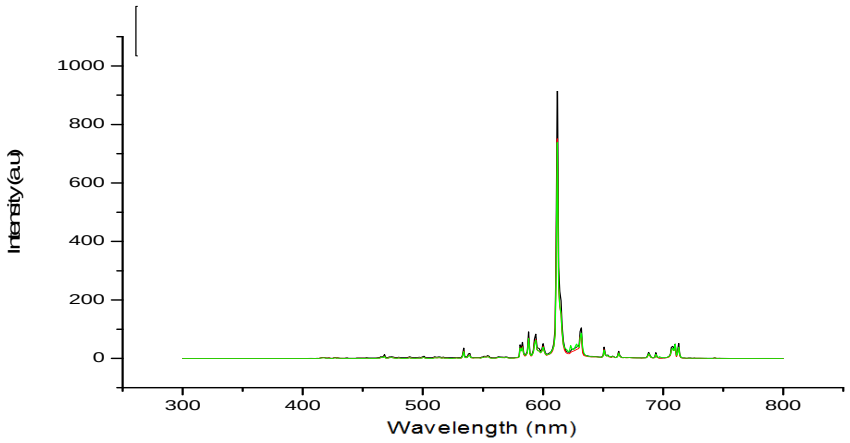

Figure 6.29 Overlay of the CL defocused beam emission spectra presented in Figure 6.28.

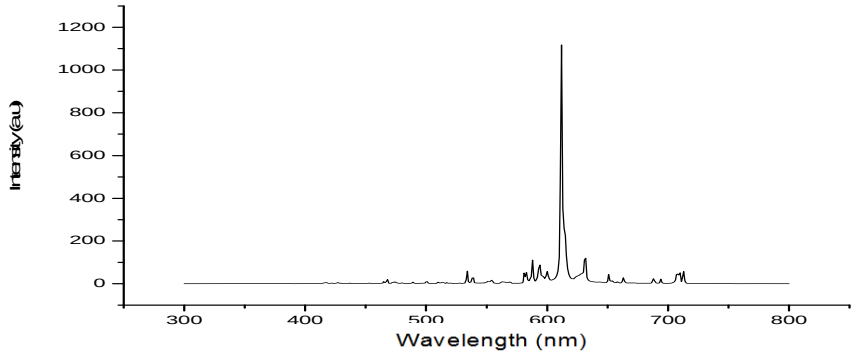

(a)

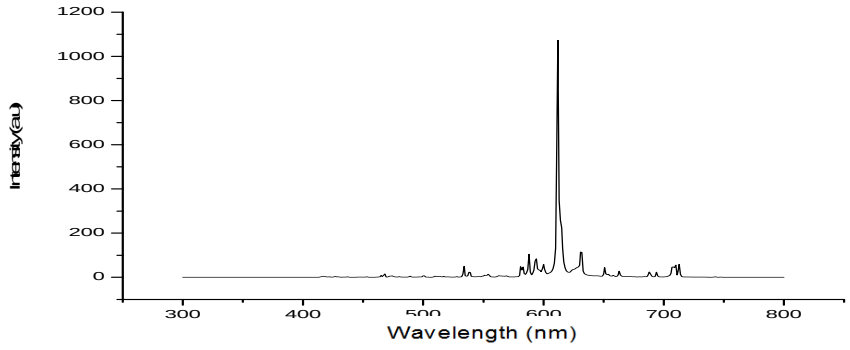

(b)

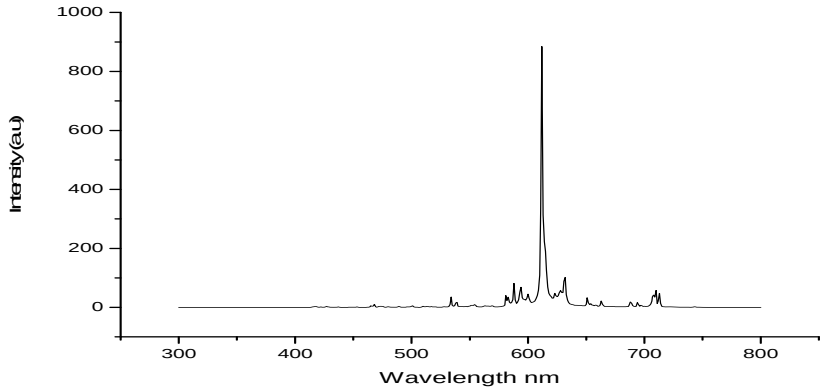

(c)

Figure 6.30 The CL focused beam emission spectra for samples (a) 4-1:1, (b) 5-1:2 and (c) 6-1:3 prepared from methanolic solutions and fired/annealed at 900°C all three samples were excited using 5000V/50uA

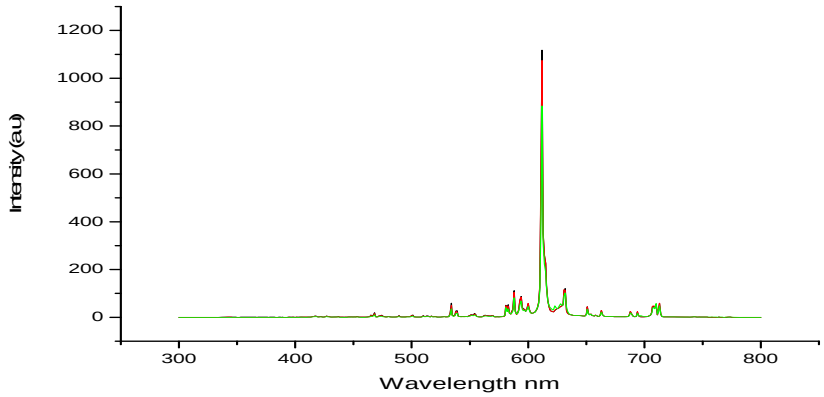

Figure 6.31 Overlay of the CL focused beam emission spectra presented in Figure 30.

The CL (5000V, emission current 9.6μA) defocused and focused spectra of the products prepared from the precursors originating in the ethanolic solutions are shown in Figures 6.32 and 6.33. They are all more simplified than those found for their respective PL emission spectra and those for the 1:2 and 1:3 samples typical of cubic$Y_2O_3:Eu^{3+}$. Even the 1:1 sample showed evidence of a spectrum that though very weak was dominated by the 612nm emission of the cubic$Y_2O_3:Eu^{3+}$. Either the cubic material is more sensitive to Cathodoluminescence and hence this is all that is seen or the energy of the X-rays was enough to allow oxidation of the monoclinic $Y_4O_5Cl_2:Eu^{3+}$ to the cubic $Y_2O_3:Eu^{3+}$ and hence further oxidation took place during the Cathodoluminescence experiments for these materials. The latter explanation is probably less likely to be true.

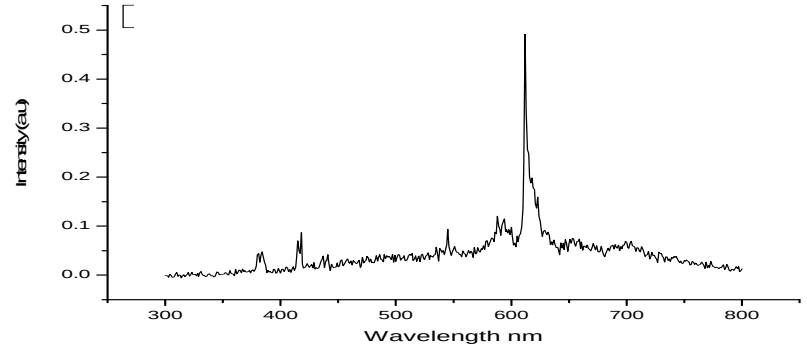

(a)

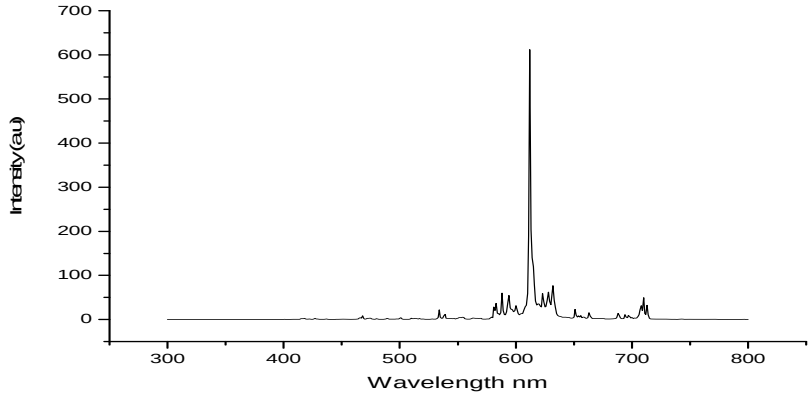

(b)

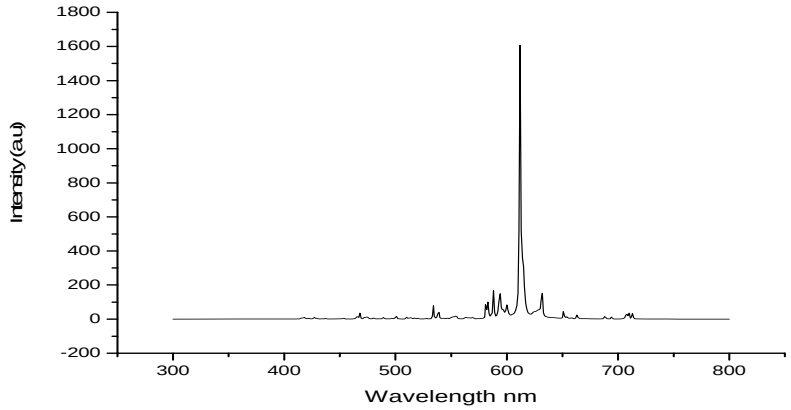

(c)

Figure 6.32 The CL defocused beam emission spectra for samples (a) 10-1:1, (b) 11-1:2 and (c) 12-1:3 prepared from ethanolic solutions and fired/annealed at 900°C all three samples were excited using 5000V/50uA

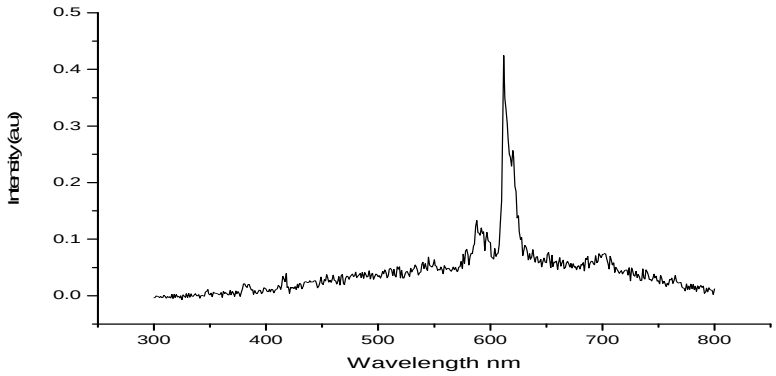

(a)

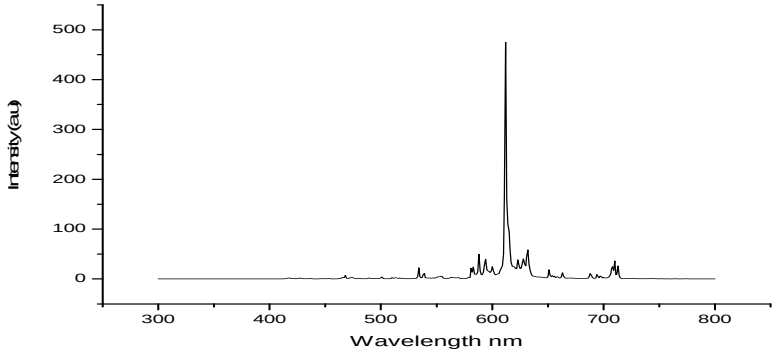

(b)

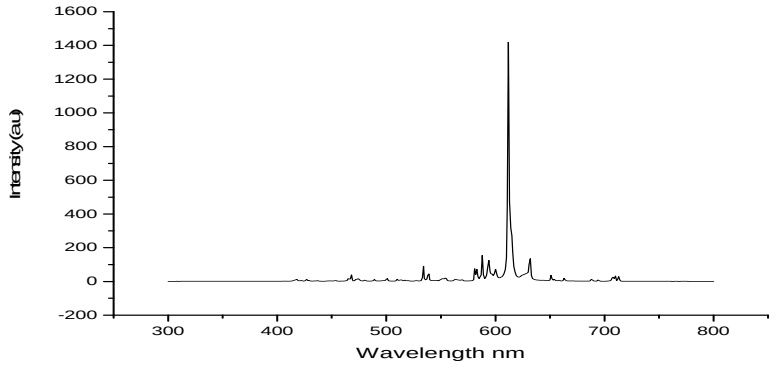

(c)

Figure 6.33 The CL focused beam emission spectra for samples (a) 10-1:1, (b) 11-1:2 and (c) 12-1:3 prepared from ethanolic solutions and fired/annealed at 900°C all three samples were excited using 5000V/50uA

6.4.6. ATR-FTIR Spectra

The ATR- spectra from the samples prepared at 900°C are summarised in Table 6.6 and 6.7. The spectra presented in Figure 6.21 show the presence of bands that can be ascribed to the presence of carbon dioxide and some OH groups in this respect there are some similarities to the 650°C spectra. The O-H deformation mode of H_2O is observed to be present as a weak shoulder at approximately 1636 cm^{-1} to the high frequency side of the strong CO_3^{2-} ν_3 asymmetric stretch doublet at 1523 and1403 cm^{-1}. Although, there is still the wide absorption band between 3600 to 3000 cm^{-1} that appears to be split into two weak peaks. The lower frequency CO_3^{2-} ν_3 asymmetric stretch peak of the doublet at 1400 cm^{-1} has shifted in wavelength compared to the 650°C samples. Also the CO_3^{2-} deformation has resolved as a weak peak at 850 cm^{-1}.
The position of the CO_2 bands in these samples are similar to those found in [(Y,Eu)$OHCO_3.H_2O$]. This finding was explained in chapter 5 in section 5.47 and is summarised below. It is clear from these results that the combustion fuel that was present in the samples in conjunction with the higher annealing temperature (900°C) was sufficient to raise the temperature for nanometer sized crystallites of the cubic $Y_2O_3:Eu^{3+}$ phase to form. The infrared spectra show the presence of bands due to the existence of CO_2 in the lattice. This is we believe due to the reaction of the surface of the nanometer sized particles with the atmosphere. In this work the $Y_2O_3:Eu^{3+}$ was formed from firing a precursor containing the long chained alkylammonium chloride and $YCl_3:Eu^{3+}$. The precursor itself was formed by reducing an alcoholic solution containing both of these components as starting materials. So the metal oxide was prepared by firing the metal chloride. This was to prepare nanometer sized particles of the metal oxide. In the past we have prepared larger nanometer sized particles of the metal oxide that were prepared by the hydrothermal decomposition of urea that facilitated the homogeneous precipitation of spherical submicron europium-doped hydroxycarbonate phosphor precursor particles. It is useful to explain this latter method here to help to understand the infrared data obtained in this work.This method is dependent on the addition of, and hydrothermal decomposition of, urea in acid solution in the presence of metal salts that are soluble at acid pH's. The chemistry involved includes:-
Aqueous decomposition of urea (<85 ºC, ~ pH 3) resulting in the following ions,

6.3. $H_2NCONH_2 \rightarrow NH_4^+ + OCN^-$

The cyanate ion rapidly reacting thus,

6.4. $OCN^- + 2H^+ + 2H_2O \rightarrow H_2CO_3 + NH_4^+$

In the presence of Y^{3+} and Eu^{3+} cations which are added as acid salts the solution pH drops to ~2.5. The urea is added and the resulting hydroxonium ions (H_3O^+) promote

urea decomposition. The subsequent release of carbonate ions causes precipitation of the metal hydroxycarbonate phosphor precursor, once the concentration of reactants reaches supercritical saturation

6.5. $[(Y,Eu)OH(H_2O)_n]^{2+} + H_2CO_3 \rightarrow [(Y,Eu)OHCO_3.H_2O] + (n-1)\ H_2O + 2H^+_{(aq)}$

Careful firing of the precursor particles allows their spherical morphology to be partially maintained in the resulting phosphor particles. This method for the preparation of cubic $Y_2O_3:Eu^{3+}$ has previously been reported for the dopant concentration range from 0.2 mole fraction to $1x10^{-3}$ mole fraction Eu^{3+}. Both by ourselves and others [3-19]. In the current work the presence of the surface of the very small particles of $Y_2O_3:Eu^{3+}$ reacts with the atmosphere adsorbing CO_2 and H_2O to form $[(Y, Eu)OHCO_3.H_2O]$ reversing the above reaction. This shows that cubic $Y_2O_3:Eu^{3+}$ is thermodynamically unstable in the presence of carbon dioxide and water vapour and reverts to the metal hydroxyl-carbonate precursor.

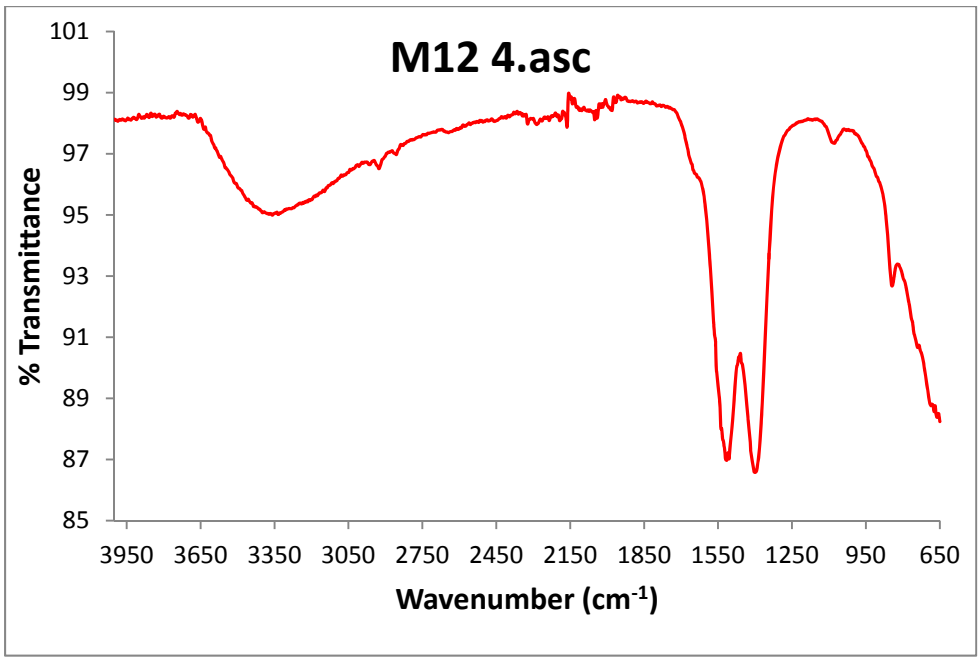

Sample-4, 1 to 1

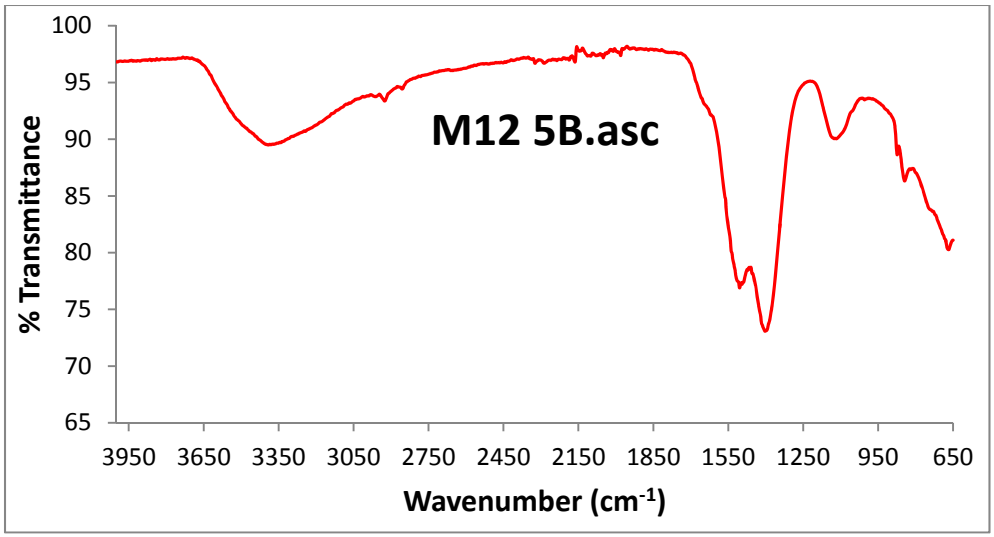

Sample-5, 1 to 2

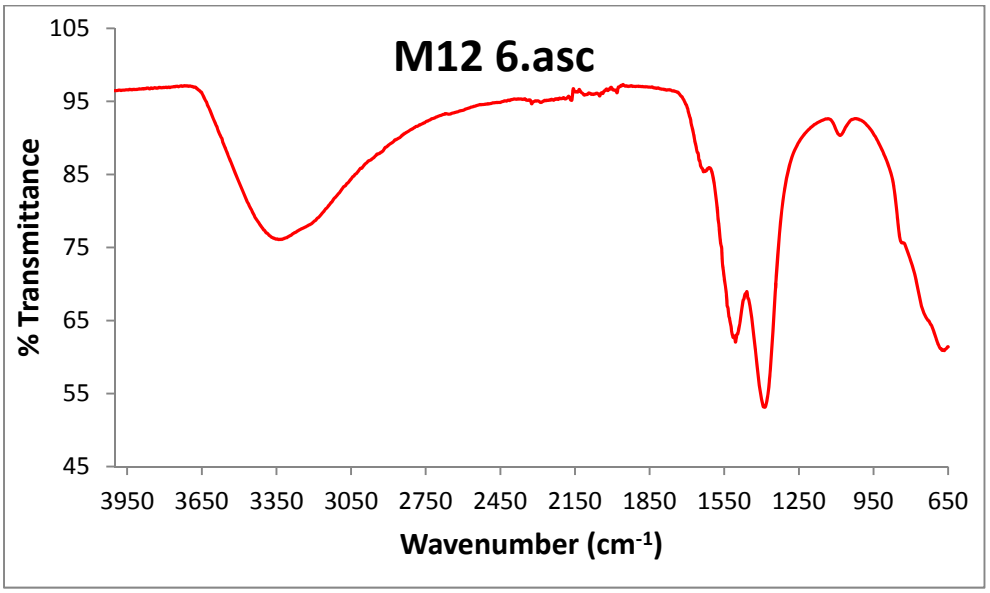

Sample-6, 1 to 3

Figure 6.34 ATR spectra of the 900°C samples 4, 5, 6 prepared from methanolic solution with metal ion to alkylammonium chloride ratios 1:1 (4), 1:2 (5) and 1:3(6).

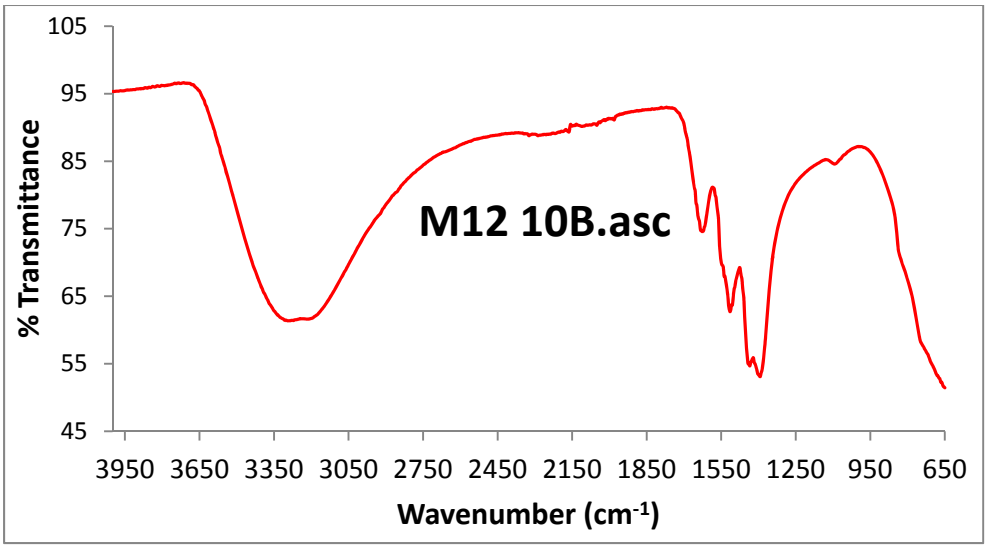

Sample 10, 1 to 1

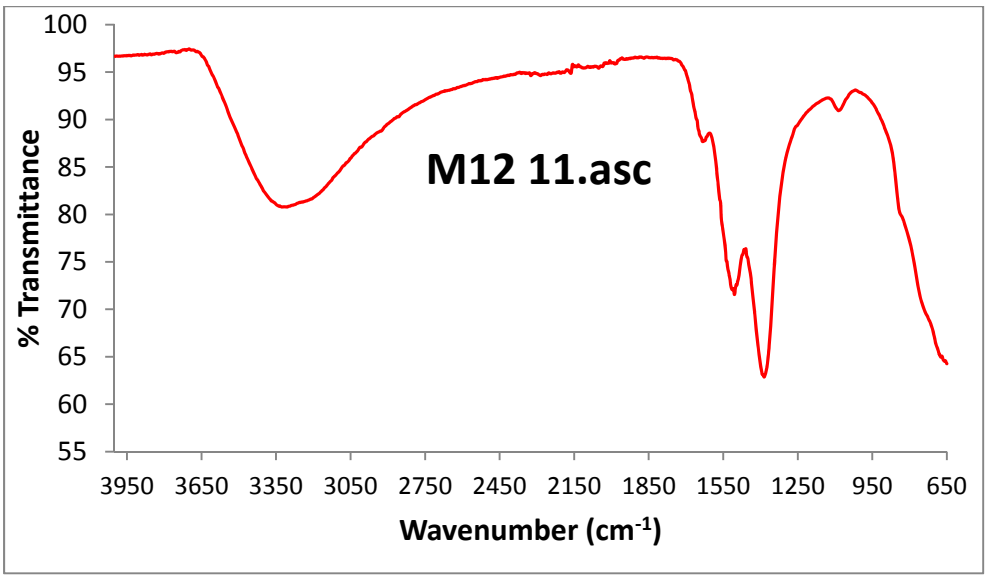

Sample 11, 1 to 2

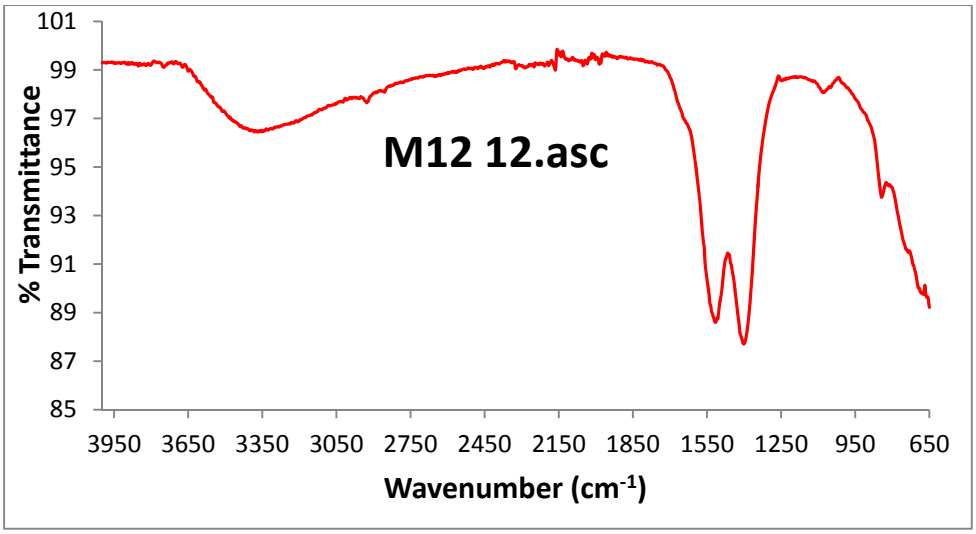

Sample 12, 1 to 3

Figure 6.35 ATR spectra of the 900°C (samples 10, 11, 12), prepared from ethanolic solution with metal ion to alkylammonium chloride ratios 1:1 (10), 1:2 (11) and 1:3 (12) in KBr discs.

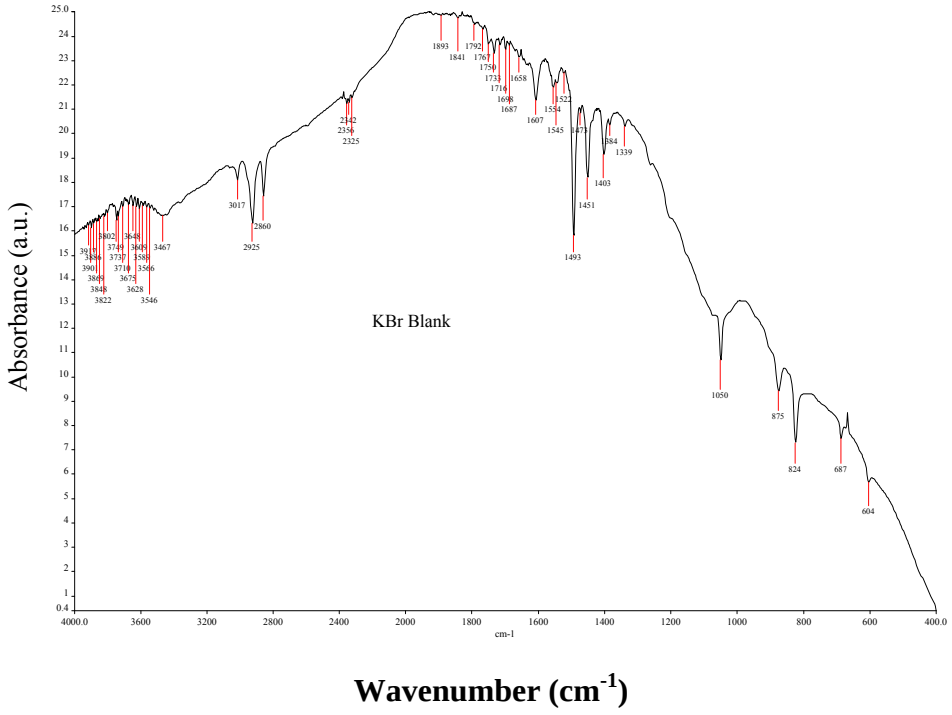

Figure 6.36 FTIR spectrum of KBr pure material-blank.

Table 6.6

Materials prepared from methanolic solution and fired at 900°C

Wavenumber/cm^{-1}

3600-3000	*(m)*	ν_{as} (O-H)
2852	*(m)*	ν_s (O-H)
1636	*(w)*	δ (O-H)
1515	*(m)*	ν_{as} (CO_3^{2-})
1402	*(s)*	ν_{as} (CO_3^{2-})
1082	*(w)*	ν_s (CO_3^{2-})
844	*(w shoulder)*	δ (CO_3^{2-})

Table 6.7

Materials prepared from ethanolic solution and fired at 900°C

Wavenumber/cm^{-1}

3600-3000	*(m)*	ν_{as} (O-H)
2251	*(m)*	ν_s (O-H)
1636	*(shoulder)*	δ (O-H
1523	*(s)*	ν_{as} (CO_3^{2-})
1404	*(s)*	ν_{as} (CO_3^{2-})
1086	*(w)*	δ (O-H)
851	*(w)*	δ (CO_3^{2-})

6.5. Conclusions

It was shown that nanometer sized crystallite particles of cubic $Y_2O_3:Eu^{3+}$ can be prepared from metal chloride precursors formed in micelles encapsulated by alkylammonium chains (the fuel) using a combustion synthetic method at 900°C. This is in keeping with the previous work [1] but in this experiment 900°C was the maximum temperature used and not 1350°C. The method produced a range of morphologies influenced by the alkylammonium chloride concentration, in particular including residual remnant micellar forms as spheres, tubules, and macro- lamellar sheets (of these aforementioned forms).It was clear from this work that the combustion fuel that was present in the samples prepared at 650°C was insufficient to raise the temperature above 900°C for long enough time period (if at all) for the cubic $Y_2O_3:Eu^{3+}$ phase to form. For both the samples prepared from methanol and ethanol the dominated phases found at 650°C were two forms of YOCl. Further we have characterised the nano-particles and demonstrated that they manifest many of the properties (CL and PL spectral properties) of bulk cubic $Y_2O_3:Eu^{3+}$ for the samples fired at 900°C.However we have also detected the presence of CO_2 bands in the infra red spectra of the cubic $Y_2O_3:Eu^{3+}$ crystallites. These bands are similar in position to those found in $[(Y, Eu)OHCO_3.H_2O]$, and are explained as arising from the spontaneous reaction of the surface of the nanometer sized particles of cubic $Y_2O_3:Eu^{3+}$ with atmospheric CO_2 and water vapour. This indicates that nanometer sized particles of cubic $Y_2O_3:Eu^{3+}$ are thermodynamically unstable in the atmosphere and must be protected against such back reactions. This could be achieved with surface coatings. A number of conclusions can be drawn from the work reported in this chapter many in common with the conclusions of chapter 5.

1) We have shown that nanometer sized particles of cubic $Y_2O_3:Eu^{3+}$ can be prepared from metal chloride precursors formed in micelles encapsulated by alkylammonium chains (the fuel) by using a combustion synthetic method at 900°C. This finding is in keeping with the earlier report [1] but the understanding of the reactions and the chemistry is now proving to be much better.
2) The method produces a range of morphologies that are influenced by the initial alkylammonium chloride concentration, in particular remnant micellar forms are present such as spheres, tubules, and macrolamellar sheets of these aforementioned forms.
3) Evidence of morphologies and particle size being controlled by the initial micellar structures was found in the materials fired at both 650°C and 900°C.
4) It is clear from this work that the combustion fuel which was present in the samples prepared at 650°C was insufficient to raise the temperature over 900°C for a long enough time period (if at all) for the cubic $Y_2O_3:Eu^{3+}$ phase to form.

5) Further at 900°C we have characterised the nanometre sized phosphor particles and demonstrated that they manifest the properties (CL and PL spectral properties) of bulk cubic $Y_2O_3:Eu^{3+}$. Through the 1:1 material made from ethanol did not convert.
6) We have also observed $_{bands}$ due to metal hydroxycarbonate in the infrared spectra of the cubic $Y_2O_3:Eu^{3+}$ nanoparticles. These bands are similar in position to those found in bulk [(Y,Eu)$OHCO_3.H_2O$], and are explained as arising from the spontaneous reaction of the surface of the nanometer sized particles of cubic $Y_2O_3:Eu^{3+}$ with atmospheric CO_2 and water vapour. This indicates that nanometre sized particles of cubic $Y_2O_3:Eu^{3+}$ are thermodynamically unstable in the atmosphere and must be protected against such back reactions. This could be achieved with surface coatings.

Finally confirming the finding in chapter 5 from the findings of this chapter it would appear that the use of sacrificial organised organic structures for the incorporation of inorganic precursors offers great potential as a method to control the morphology and size of nanometre sized particles. However during the CL studies we noticed subtle changes in these spectra as a function of applied voltage and beam current, when these changes are understood they will be published elsewhere.

References

[1] T. Ireland and J.Silver."Facile self-assembly of yttrium oxide europium phosphor from Solution using a sacrificial Micellar phase". Journal of the Electrochemical Society. 2, 52-54, 1999.

[2] Y.Nishisu and M.Kobayashi. "Synthetic method for the production range of particle size for Y_2O_3:Eu." U.S. Patent 5,413.736-737, 1995.

[3] Y.D.Jiang, Z.L. Wang, F. Zhang, H.G. Paics and C.J. Summers."Spherical particles for high definition display screens". Journal Material. Res 13, 2950-2955, 1998.

[4] J.A.Cooper, H.G Paris, S.R.Stock, S.Yeng and C.J.Summers." Particle size effect on the crystal structure of Y_2O_3:Eu particles." Journal SID. 6,163-164, 1998.

[5] A.Vecht, C.Gibbons, D.Davies, X.P.Jing, P.Marsh, T.G.Ireland, J.Silver, A. Newport and D. Barber."Engineering phosphors for field emission display." Journal Vac. Sci. Tech. B. 17, 750-751, 1999.

[6] X.P.Jing, T.G.Ireland, C.Gibbons, D.J.Barber, J.Silver, A.Vecht, G.Fern, P.Trogwa and D.C. Morton." Control of Y_2O_3:Eu spherical phosphor size ,assembly and properties." Journal of the Electrochemical Society 146, 4654-4656, 1999.

[7] M.I.Martinez-Rubio, T.G.Ireland, J.Silver, G.Fern, C.Gibbons and A.Vecht. " Effect on EDTA on controlling nucleation and morphology in the synthesis of ultrafine Y_2O_3:Eu phosphors Journal. Solid State Chem. Electrochem and Solid State Lett. 3. 446-448, 2000.

[8] A.Vecht, M.I.Martinez-Rubio, T.G.Ireland, J.Silver, G.Fern and C. Gibbons. "Factors effecting efficiency in submicron size phosphors for high definition display."SID '00 Digest, 31. 15-17, 2000.

[9] M.I.Martinez-Rubio, T.G.Ireland, J.Silver, G.Fern and M.J. Snowden. " Novel Method for the Synthesis of spherical particles of the Y_2O_3: Eu Phosphor Using a Copolymer Microgel of Nipam and Acrylic Acid". Langmuir 17, 7145-7149, 2001.

[10] J.Silver, M.I.Martinez-Rubio, T.G.Ireland, G.R Fern and R.Withnall. "The effect of particle morphology and crystallite size on upconversion

luminescence property of erbium and yttrium co-doped yttrium oxide." Journal. Phys. Chem. 105,948-950, 2001.

[11] J.Silver, R.Withnall, A. Newport, M.I.Martinez-Rubio, T.G.Ireland, P.J. Marsh and A.Vecht. "Yttrium up-converting phosphors Part-2 temperature depend up conversation luminescence" SID '01 Digest .32**,** 756-759, 2001.

[12] J.Silver, M.I.Martinez-Rubio, T.G.Ireland, G.R Fern and R.Withnall. "Yttrium oxide up-converting phosphors Part-3, up conversation luminescence emission from europium doped yttrium". Journal. Phys.Chem, B. 105, 9107- 9110, 2001.

[13] M.I.Martinez-Rubio, T.G.Ireland, G.R.Fern, J.Silver and M.J.Snowden. " A synthetic method for the production of a range of Particle sizes for Y_2O_3 : Eu phosphors using a copolymer microgel of NIPAM." Journal of the Electrochemical Society. 149, 253-255, 2002.

[14] J.Silver, R.I. Galliano, G.R. Fern, T.G. Ireland and R. Withnall. "A novel synthesis of Y_2O_3 : Eu phosphor using carbon dioxide and Ammonia for high definition CRT."SID '02 Digest.33, 12-15, 2002.

[15] J.Silver, N. Wilstead. D.Nicholas and A.Vecht. "Rare earth element anti stock phosphors emission." SID '02 Digest.33, 388-390, 2002.

[16] J.Silver, M.I. Martinez-Rubio, S.Gebretensae, G.R.Fern, M.J.Snowden and R.Withnall. " Yttrium oxide up-conversion phosphors luminescence." SID '02 Digest.33, 393-395, 2002.

[17] J.Silver, M.I.Martinez-Rubio, T.G.Ireland, G.R Fern and R.Withnall. "Yttrium oxide up-conversion phosphors Part-4, up conversation luminescence emission from europium doped yttrium oxide under 632.8nm light excitation." Journal. Phys.Chem. B. 107, 1548-1550, 2003.

[18] J.Silver, T.G. Ireland and R.Withnall." fine control of the doped level in cubic of Y_2O_3 : Eu phosphor."Journal. Electrochem. Soc. 151, 66-89, 2004.

[19] M. Konaissmy, D. Jeyakumar, R. Jagannathan and M. Mohan." Energy transfer and upconversion luminescence property of Y_2O_3 : Eu phosphor." Journal. Material. Res. Bull. 31, 1013-1016, 1996.

[20] D.H.Templetoan and C.H.Dauben. "Crystal Structures of Rare Earth Oxychlorides." Journal American. Chem. Soc, 75, 6069-6070, 1953.

[21] W.H. Zachariasen. "Crystal chemical studies of the 5f-series of elements. XII. New compounds representing known structure types." Journal Acta Crystallographica, 2, 388-391, 1949.

[21a] L.M.Seaverson and J.D.Corbet. "Synthesis and characterization of oxide interstitial derivatives of zirconium monochloride and monobromide." Journal Inorg.Chemistry. 22,3202-3210, 1983.

[22] L.S.DentGlasser." Crystallography and its applications." Van Nostrand Reinhold Wokingham UK. 23-28, 1982.

[23] K.L. Chopra. "Thin Film Phenomena". McGraw-Hill New York. London 45-49, 1969.

[24] D.A Skoog and J. J Leary. "Principle of instrumental analysis". 4th Ed. Saunders College of publishing, London 67-74, 1992

[25] M.Tanaka, Y. Nishisu, M. Kobayashi, A.Kurita, H.Hanzawa and Y.Kanematsu." Optical characterization of spherical fine particles of glassy Eu3+ doped yttrium basic carbonates." Journal. Non-Crystalline Solids .318, 175-185, 2003.

[26] L.Muresan,E.J. Popovici,R. Grecu and L.B.Tudoran." Studies on the synthesis of europium activated yttrium oxide by wet chemical method. 1. Influence of precursor quality on phosphor photoluminescence properties." Journal. Alloys and Compounds. 471, 421-427, 2009.

[27] N.B.Colthup, L.H. Daly and S.E.Wiberley." Introduction to Infrared and Raman Spectroscopy". 3rd edition, Academic Press Ltd. London.1990.

[28] J.Silver and R.Withnall. "Probes of structural and electronic environments of phosphor activators." Journal Chem.104, 2833-2855, 2004.

[29] E.Husson, C. Proust, P. Gillet and J.P.Itié." Phase transition in yttrium oxide at high pressure studied by Raman spectroscopy." Journal Material. Res.34, 2085-2092, 1999.

[30] R.B.Hunt and R.G.Pappalardo.” Fast excited-state relaxation of Eu-Eu pairs in commercial $Y_2O_3:Eu^{3+}$ phosphors.” Journal. Lumin. 34, 133-146, 1985.

[31] G. Schaack and J.A. Köningstein.” Phonon and electronic Raman spectra of cubic Rare earth-oxides and isomorphous yttrium oxide.” Journal. Opt. Soc.American. 60, 1110-1115, 1970.

[32] W.B. White and V.G.Keramidas.” Vibrational spectra of oxides with the C-type rare earth oxide structure.” Journal Spectrochimica Acta part A.28, 501-509,1972.

[33] D. Bloor and J.R.Dean.”Spectroscopy of rare earth oxide systems. I. Far infrared spectra of the rare earth sesquioxides, cerium dioxide And nonstoichiometric praseodymium and terbium oxides.” Journal. Phys. C and Solid State Phys. 5, 1237-1252, 1972.

[34] Y.Repelin, C.Proust, E.Husson and J.M.Beny.” Vibrational spectroscopy Of the C-form of yttrium oxide.” Journal. Solid State Chem. 118, 163-169.1995.

[35] B.Aiken, W.P.Hsu and E.Matijevic.” Preparation and Properties of Monodispersed Colloidal Particles of Lanthanide Compounds: III, Yttrium (III) and Mixed Yttrium (III)/Cerium (III) Systems.” Journal. American. Ceram. Soc. 71, 845-853, 1988.

[36] S.Sohn, Y. Kwon, Y. Kim and D. Kim.” Synthesis and Characterization of near- monodisperse yttria particles by Homogeneous precipitation method Powder Technology.” Journal of Solid State Chem. 142, 136-153, 2004.

Chapter Seven

7.0. $Y_2O_3:Eu^{3+}$ Materials from the [(Y, Eu) Cl_3] - ($C_8H_{17}NH_3Cl$)

7.1 Introduction

In chapter 5, the effect of looking at how [(Y,Eu)Cl_3] - ($C_{16}H_{33}NH_3Cl$) precursor materials led to different fired phosphors depending on firing conditions, atmosphere and whether the precursors were prepared from methanolic or ethanolic solutions was reported. Instead of just cubic $Y_2O_3:Eu^{3+}$ being formed it was found that in the reaction of [(Y, Eu)Cl_3]-($C_8H_{17}NH_3Cl$) two other phases:- $YOCl:Eu^{3+}$ and $Y_4O_5Cl_2$:-Eu^{3+} were also formed in the case of the materials prepared from ethanol. In chapter 6 the preparation of nanoparticles phosphors from [(Y, Eu) Cl_3] - ($C_{12}H_{25}NH_3Cl$) are reported using similar preparative methods. In chapter 6 the main finding was similar to chapter 5 but YOCl: Eu^{2+} was more dominant at 650 °C. In this chapter the preparation of nanoparticles phosphors from [(Y, Eu) Cl_3] - ($C_8H_{17}NH_3Cl$) are reported using similar preparative methods to those in chapters 5 and 6.As stated earlier the aims of this thesis were motivated by widespread interest on the synthesis and properties of phosphors made up of highly crystalline sub micrometer sized particles. The studies presented in this chapter again add/supplement the work of our group and others on methods of preparing the cubic $Y_2O_3:Eu^{3+}$ phosphor [2-19]. In particular we were interested in the influence of the alkylammonium chain length of the precursor on the final products in the combustion synthesis; we extend this interest in this chapter to the study of yet smaller chain lengths. As stated in the introduction in chapter 5 “one of the problems with making such sub micrometer sized particles; is that during annealing of the precursor particles at high temperatures (often necessary for good crystallite quality and hence emission properties) the particles tend to sinter”. In the chapter 5 and 6 we demonstrated that one way to partially alleviate this problem is to synthesise the particles as rapidly as possible at a high temperature. Combustion synthesis has been shown in those chapters to be an ideal method to do this. However we have shown that the use of the method depends on the nature of the fuel and the amount present as well as the amount of oxygen present. The first report [1] of facile self-assembly of the red emitting phosphor yttrium oxide europium ($Y_2O_3:Eu^{3+}$) from solution using a sacrificial micellar phase appeared in 1999. The micellar phase was assembled using the alkylammonium chloride salt ($C_{12}H_{25}NH_3Cl$) in an ethanolic solution. The resulting fine powder had smaller particles, ranging in size from 0.1 to 1.0 μm, than the commercial cubic $Y_2O_3:Eu^{3+}$ phosphor [1]. This chapter reports a study where the chain length is smaller ($C_8H_{17}NH_3Cl$). So in this case there is less combustion fuel. As in Chapters 5 and 6 the results discussed in this chapter were obtained using a more sophisticated way to control the rate of crystallization of the phosphor particles. This was to vary the ratio of phosphor precursor to fuel. In the

previous chapters the presence of more fuel around the phosphor precursors was found to facilitate/influence the combustion process and the products formed. Here the overall amounts of fuel are less so the effect of reduced fuel could be studied. So in this chapter the dodecylalkylammonium hydrochloride chain ($C_8H_{17}NH_3Cl$) was used as fuel and now the affect of varying the ratio of this to the [(Y, Eu)$OHCO_3.H_2O$] precursor on the Cathodoluminescence (Cl) and photoluminescence (PL) properties of the resulting phosphors is discussed. The following systems were studied;-

1. [Y,Eu]Cl_3 - ($C_8H_{17}NH_3Cl$)-6 experiments in the ratio of 1:1, 1:2, 1:3with ethanol (3 fired at 650°C and 3 fired at 900°C).

2. [Y,Eu]Cl_3 - ($C_8H_{17}NH_3Cl$)-2 experiments in the ratio of 1:1, with methanol (1 fired at 650°C and 1 fired at 900°C).

The temperatures 650°C and 900°C were chosen to be above the formation temperature of YOCl.

7.2 Experimental

For the experimental technique refer to chapter 4 paragraph 4.6 experiments 10/10a. Preparations of [(Y, Eu) Cl_3] - ($C_8H_{17}NH_3Cl$) n (for n = 1, 2, 3) were carried out with materials prepared from methanolic and ethanolic solutions. Attenuated total reflectance (ATR)-Fourier transform infrared (FTIR) spectra were obtained using a Perkin Elmer Spectrum One FTIR spectrometer. This technique is used to study vibrational, rotational, and other low-frequency modes in a system [13, 21]. The crystalline phases of the products were determined by X-ray powder diffraction (XRPD) using a Bruker D8 Advance X-ray powder diffractometer. (See for detail to chapter 3 ref 3.2). XRPD studies have been used to identify the phases present in the combusted products synthesized in this work, and their degree of disorder/order and their crystallite sizes [10, 22]. Diffractograms were collected using the fired powders in a conventional holder, or mounted on aluminium pin stub or on an aligned silicon substrate [6, 7, 23, 24].Field emission scanning electron microscopy (FESEM) was used to study the microstructure of the samples using a Zeiss Supra VP 35 instrument. The samples were mounted on carbon tabs attached to aluminium pin stubs and sputter coated with a thin conducting layer of gold. The PL excitation and emission spectra were obtained using a Bentham (Reading, UK) M300 programmable grating monochromator photometer system with computer controlled wavelength scanning and intensity data collection, using in the visible region a 1800 lines/mm grating. The stepping motor and sine drive allows wavelength scanning to be completely controlled from a remote stepping drive unit (SMD3B). Sample excitation and collection was collected inside an in-built sealed chamber connected to the M300 monochromator via

a fibre-optic bundle. The Cl measurement data and spectra were undertaken using a high-vacuum chamber with a Kimball Physics Inc. (Walton, USA), model EGPS-7 electron gun. The Cl luminance measurements were obtained by means of a Jeti spectroradiometer (Specbos 1201, Jeti Technische Instrument GmbH, and Jena, Germany). The phosphor screens were excited with electron beam energies from 1000 to 5000V, and emission currents from 1.1 to 9.8μA/cm^2, with an electron beam spot size of 9 mm for defocused measurements and 1.41 mm for the focussed measurements. For some of the samples, Cl emission and excitation spectra were obtained using the Bentham system previously described except that the fibre optic bundle was disconnected from the in-built sealed chamber and attached to a telescope (TEL 301D).For the Cl luminance measurements and spectra of the prepared samples phosphor screens were prepared in the following manner. After cleaning the aluminium pin stubs in an ultrasonic bath containing ethanol, followed by drying in an oven at a temperature of 100°C they were weighed. A stub was then placed in an electrochemical cell containing an ultrasonically dispersed solution of the phosphor powder (0.5g), in an electrolyte solution of magnesium nitrate (0.075g/L) and isopropanol (50ml). The stub was positioned with its flat surface forming a meniscus with the surface of the phosphor/electrolyte solution and acted as an electrode, the counter electrode being a strip of magnesium ribbon. A field of 300V was applied facilitating the coating of the stub by electrode position. This procedure was repeated till all the stubs were coated with 3mg (±0.1mg) of phosphor. After drying the stubs at 100°C they were introduced into the vacuum chamber for CL measurements.

7.3 Results and Discussion

7.3.1 Products prepared with methanol and ethanol at temperatures of 650°C.

7.3.1.1 Sample appearance: - Products (samples) prepared from precursors methanolic and ethanolic solutions were fired at a temperature of 650°C and observed to be light grey in colour, where as the samples prepared at 900°C were all white powders. Under 254nm excitation the samples prepared at 650°C displayed a weak red luminescence which was in contrast to the strong red luminescence from the samples prepared at 900°C that is characteristic of the $Eu^{3=}$ ion in cubic Y_2O_3. The strongest red luminescence comes from 1:3 material sample ratios and at 900°C. As stated above only four samples were studied at 650°C they are:-

3. [Y,Eu]Cl_3 - ($C_8H_{17}NH_3Cl$) - 1:1, with methanol.

4. [Y,Eu]Cl_3 - ($C_8H_{17}NH_3Cl$) - 1:1, 1:2, 1:3 with ethanol.

7.3.1.2. SEM Studies: - Firstly the samples prepared from methanolic and ethanolic solutions that were fired at a temperature of 650°C. In Figure 7.1 FESEM micrographs

of the sample annealed at 650°C prepared from metal chloride to alkylammonium chloride ratios of 1:1 (a, b, c, d &e), in methanol are presented. It can be seen that a number of morphological forms are present. Large straw-like sheets are shown to be formed from intergrowths of thin needles.

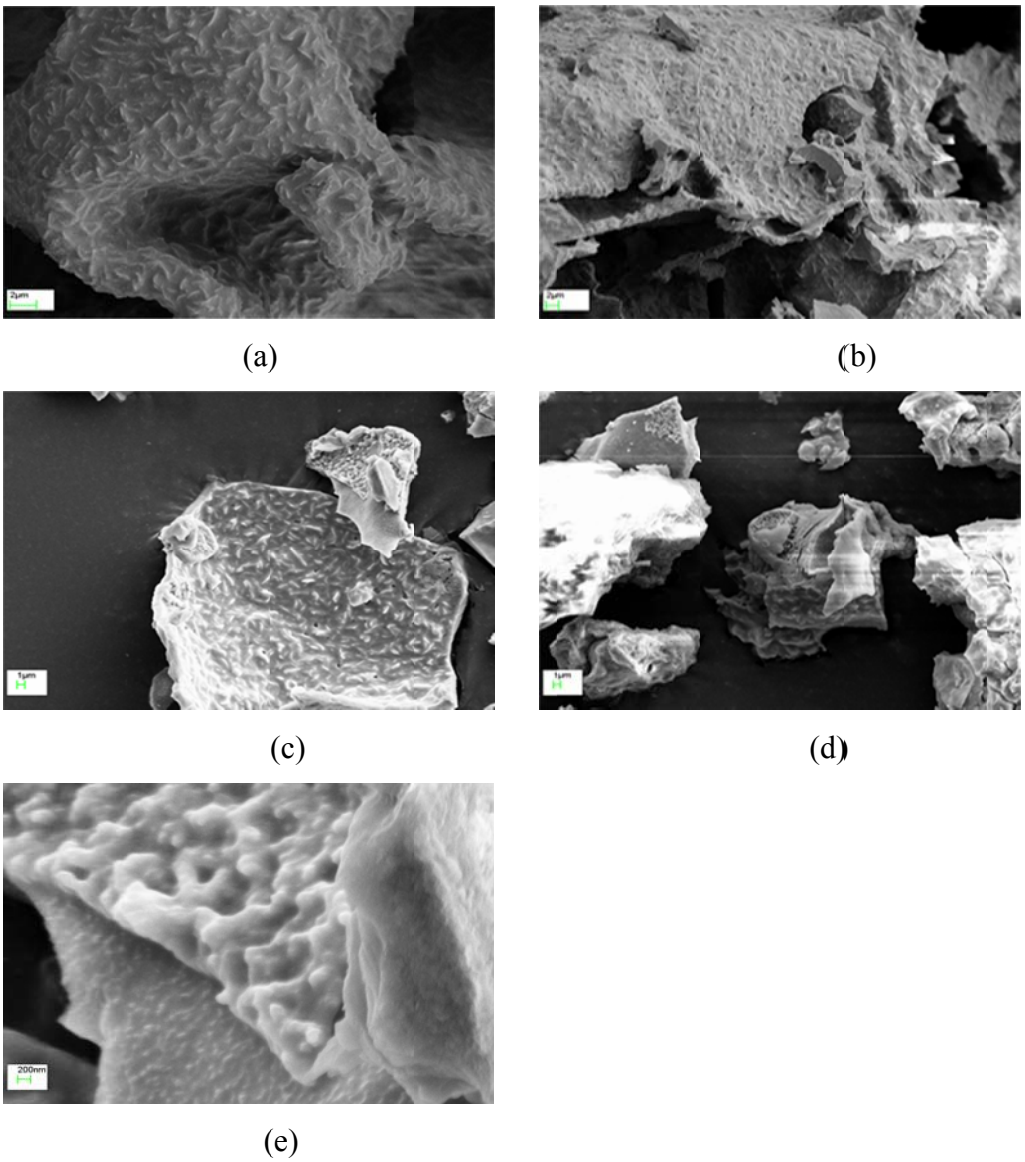

(a) (b)

(c) (d)

(e)

Figure 7.1 FESEM images of phosphor samples fired at 650°C from precursors prepared from methanolic solutions using metal chloride to alkylammonium chloride ratios of (a,b,c,d and e) 1:1, In (e), the bar is 200nm, in (c) and (d) it is 1µm and in (a) and (b) it is 2µm.

These sheets show evidence of melting at the temperature of firing. The spherical, tubular and lamellar structures seen in the earlier chapters are not in evidence in the SEMs of this sample. In Figure 7.2, FESEM micrographs of samples annealed at 650°C prepared from metal chloride to alkylammonium chloride ratios of 1:1 (a,b,c and d), 1:2 (e,f,g,h,j,k and l) and 1:3 (m,n,o and p) in ethanol are presented.

Here there is evidence of much less melting than in Figure 7.1; the structures seen are much more delicate with the presence of thin films of material with spaces between the structures. In agreement to the results of the methanol SEMs (Figure 7.1), it can be seen in Figure 7.2 that for all ratios there is evidence for sheet like structures, but in these cases more porous areas are noticeable between the sheets where the long chain alkylammonium molecules have been consumed in the firing. There is little evidence for the variety or indeed number of morphological forms found in the previous two chapters though in Figure 7.2j their appears to be some evidence for the remains of more complex structural forms. These smaller forms are formed from intergrowths of thin structures that have dimensions up to 200nm in length. In summary the predominant structures are those that have assembled into large lamellar sheets that in these images are often two structural units in thickness similar to those observed in the previous chapters. In many of the SEMs presented in Figures 7.2 it can be seen that there is evidence of structures where the surfaces appear to be smooth suggesting they neared meltdown this is thought to be due to the presence of ethanol rather than methanol (see Figure 7.1) driving the surface temperature higher during the synthesis. It is only a surface effect as the XRPD data (see below) show no evidence for the high temperature cubic $Y_2O_3:Eu^{3+}$ phase.

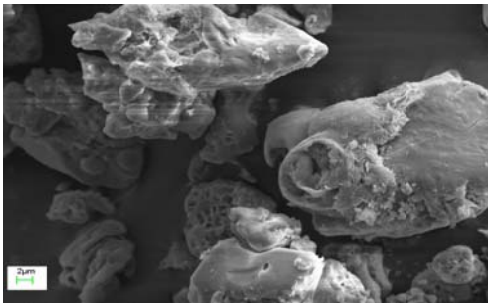

(a)

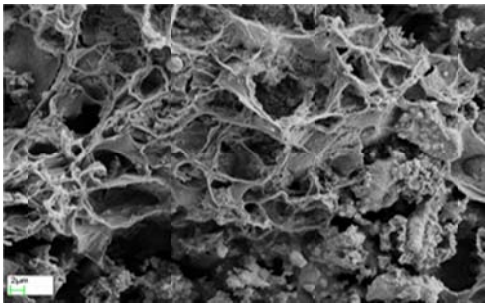

(b)

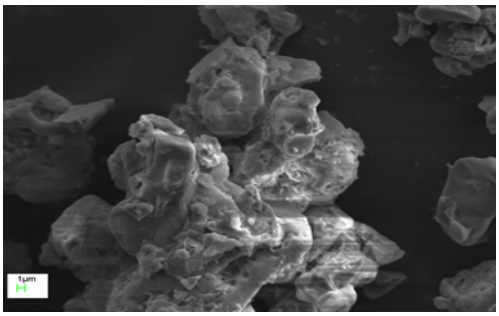

(c)

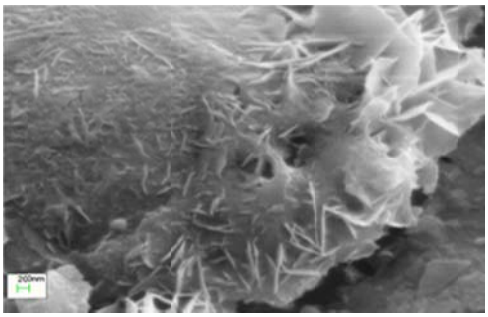

(d)

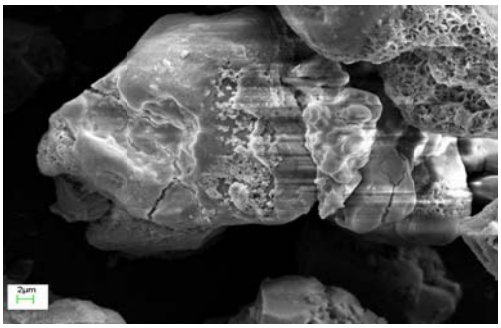

(e)

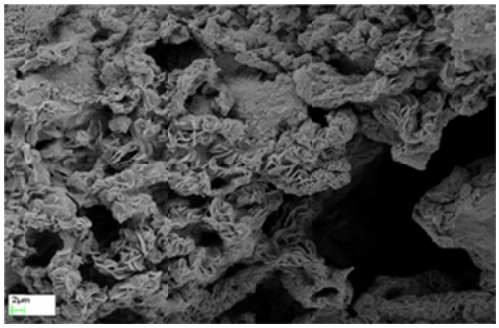

(f)

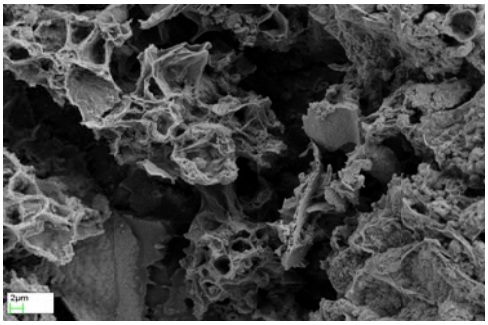

(g)

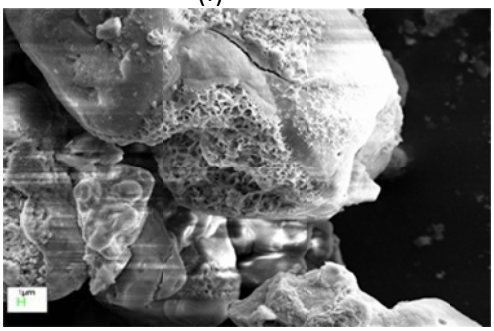

(h)

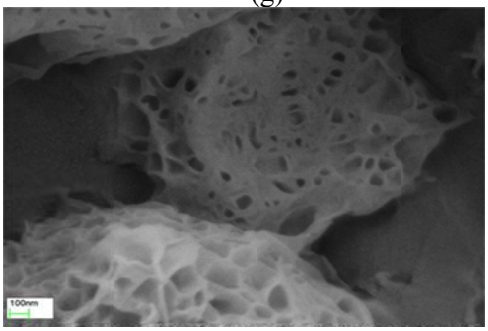

(i)

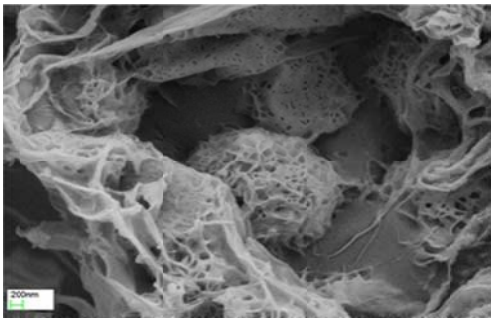

(j)

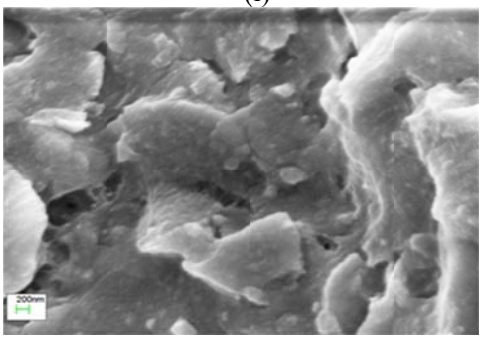

(k)

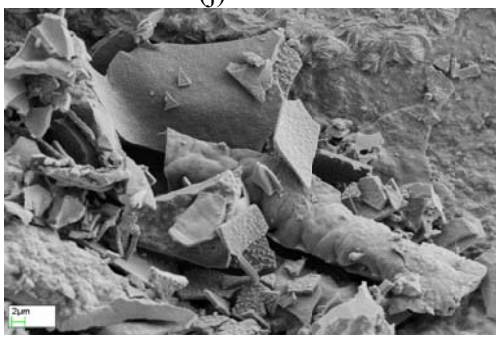

(m)

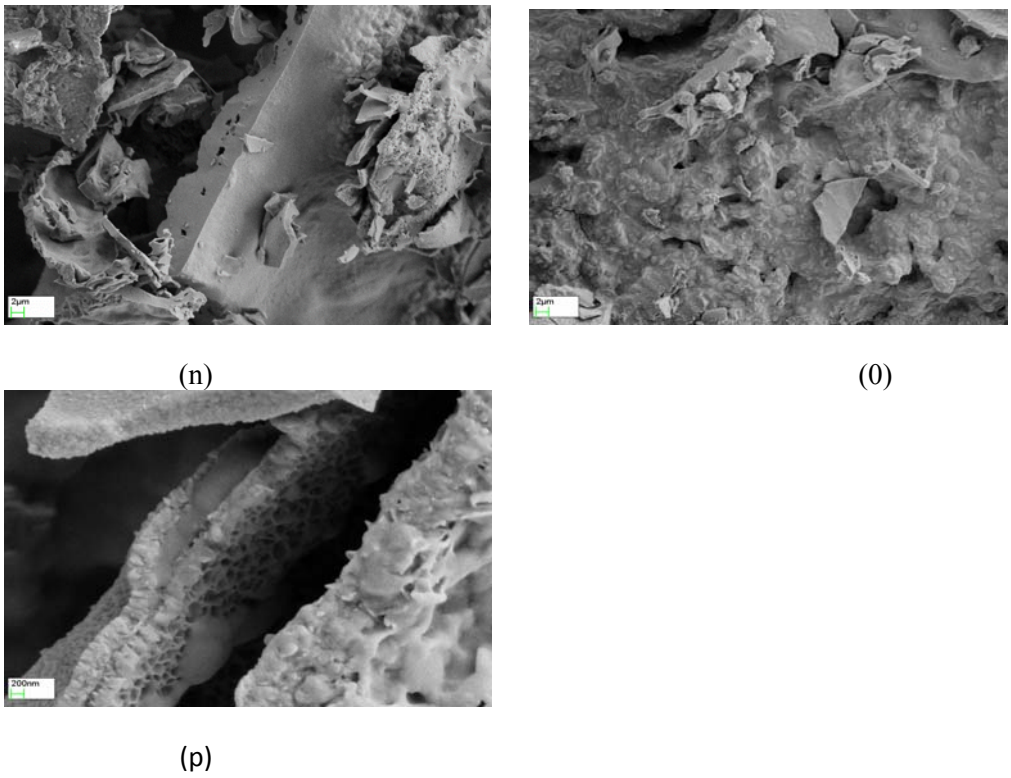

(n) (0)

(p)

Figure 7.2 FESEM images of phosphor samples fired at 650°C from precursors prepared from ethanolic solutions using metal chloride to alkylammonium chloride ratios of 1:1 (a,b,c and d),1:2 (e,f,g,h,i,j and k),1:3 (m,n,o and p). In (c and h), the bar is 1μm. In (a.b,e.f.g, ,m,n and o), the bar is 2μm. In (i) the bar is 100nm. In (d,j.k and p) the bar is 200nm .

7.3.2 Studies on the samples produced at. 650°C

7.3.2.1 Sample structures (from XRPD data)

The XRPD Diffractograms of the 1:1 sample prepared from the methanolic solutions and fired at 650°C showed evidence for a large amount of nanocrystalline material. There was no evidence for cubic $Y_2O_3:Eu^{3+}$ in the XRPD data. The XRPD data of the samples prepared from ethanolic solutions and fired at 650°C are presented in Figure 7.3 for the 1:1 , 1:2 and 1:3 ratios,. There was little evidence of anything different to that prepared from methanol, and again there is evidence of nanocrystalline material in Figure 7.3. Again there was no evidence for cubic $Y_2O_3:Eu^{3+}$ in these XRPD plots. From the fitting to the data presented in Figure 7.3 it was found that the 1:1 and 1:2 ratios continued YOCl in nanocrystalline form (two phases of YOCl were found to be present see Table 7.1) for 1:3 data the material was studies on a Silica stub (see sharp S_1 peaks in figure 7.3(c)). For the 1.3 ratio the XRD data was difficult to fit. The best fitting gave four materials as follows: 1.The main material was around 50% was for TriYttrium Tetra oxide chloride phase. 2. The second material was around 23% with large error with a reacted Yttrium chloride phase. 3. The third material found to be a cubic phase with larger cell size like Y_2O_3 but was identified as a rare earth oxide

phase. 4. The last phase was identified as Yttrium oxide chloride with a different cell to those found in the 1:1 and 1:2 ratios.

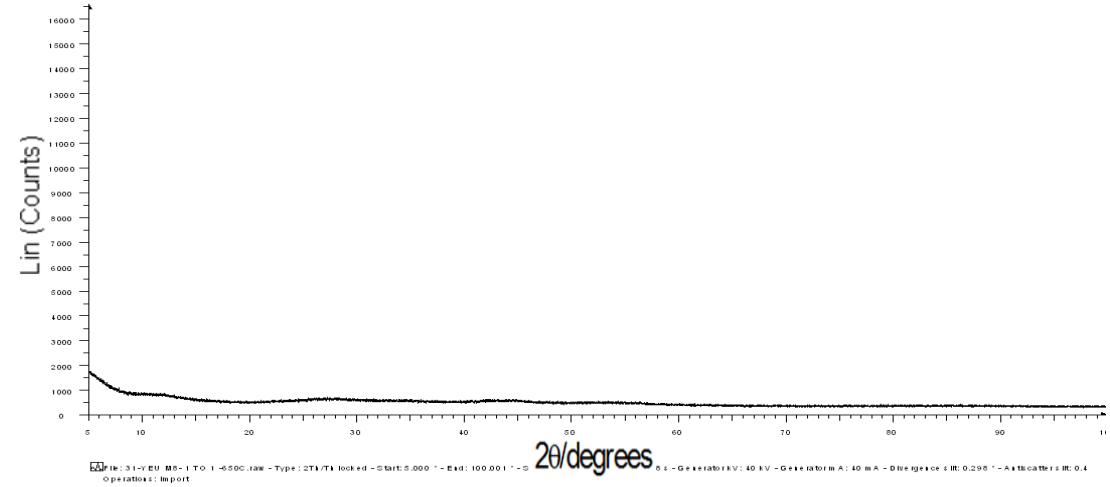

(a)

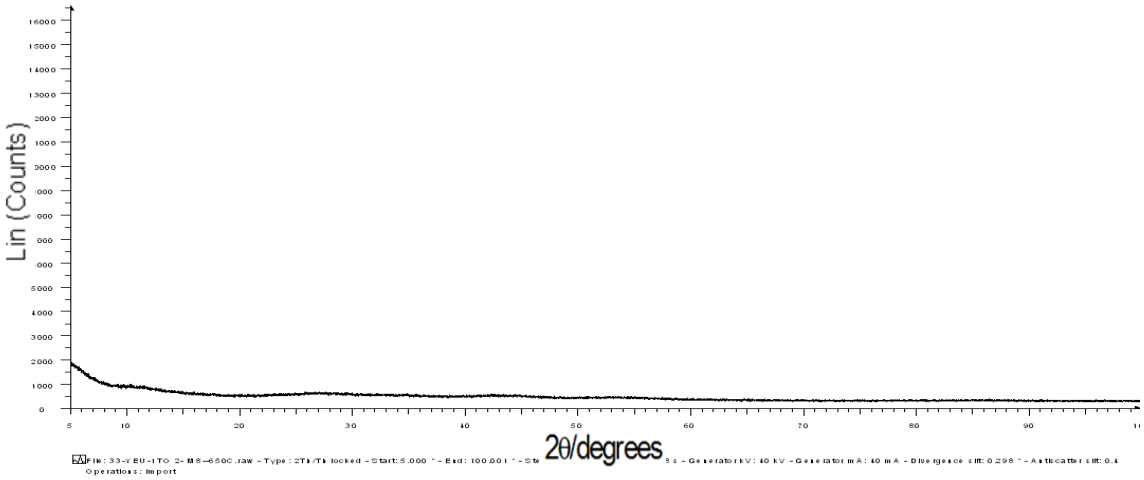

(b)

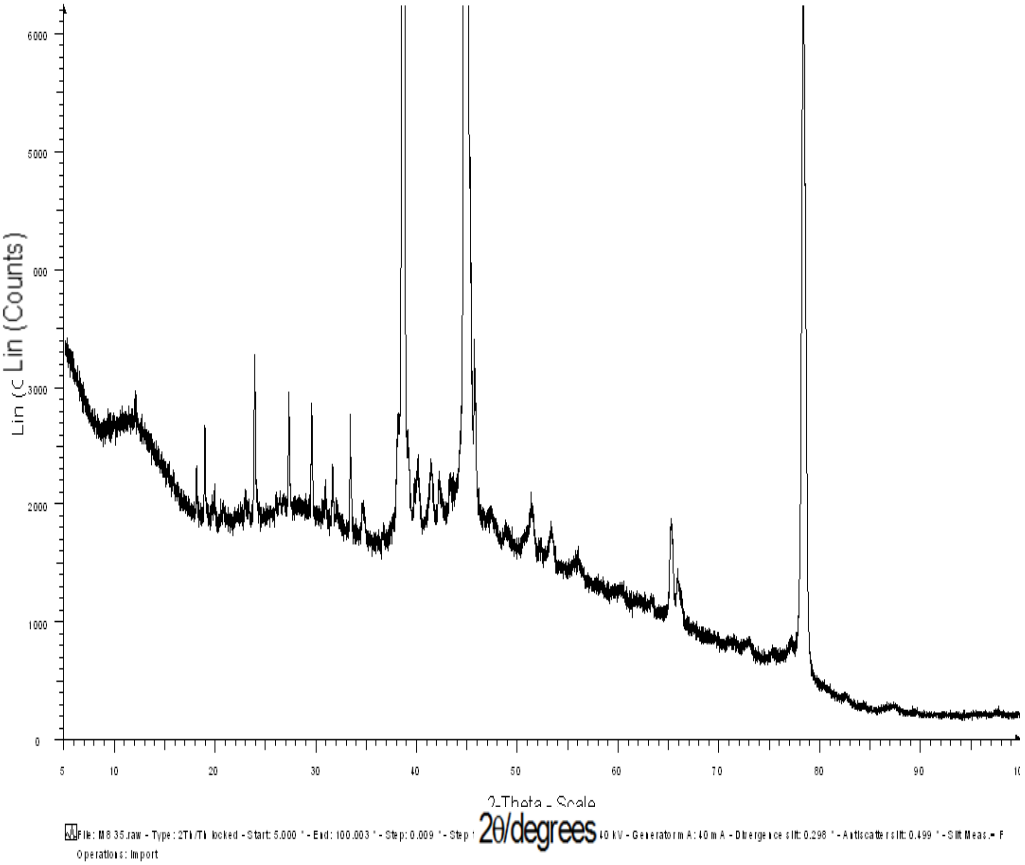

(c)

Figure 7.3 XRPD diffractograms of the samples annealed at 650°C prepared from ethanolic solution, metal ion to alkylammonium chloride ratios; a, b and c.

Table 7.1 Cell parameters for the yttrium oxy chloride phases found in the materials fired at 650°C prepared from ethanol.

	1:1	1:2	1:3
Yttrium oxide chloride YOCl R-3m -1 %	a= 4.999(25)(Å) c= 28.00(23)(Å) 8.93(79)	a=5.000(31)(Å) c=28.00(21)(Å) 13.7(11)	a =5.7806 (24) (Å) c= 26.791(19) (Å) 23(14)
Yttrium oxide chloride YOCl R-3m -2 %	a= 4.178(14) (Å) c=20.463(71)(Å) 91.07(79)	a=4.187(18)(Å) c= 20.371(73)(Å) 86.3(11)	
Yttrium oxide chloride YOCl P4/nmm [20]	a= 3.903 (2) c= 6.597 (4)		a= 3.995 (51) c= 6.758 (12) 12.8 (33) %
Yttrium oxide chloride YOCl P4/nmm [20a]	a= 3.900 (2) c= 6.604 (2)		
Yttrium oxide chloride YOCl R-3m [20b]	a= 3.7895 (5) c= 28.03 (1)		
Tri Yttrium Tetra oxide Chloride %			a=4.0414 (17) (Å) b= 13.6516(89)(Å) c= 11.1531(44)(Å) 51.10 (91)
Yttrium oxide (Cubic Y_2O_3) %			a =11.3274 (44) (Å) c= 13.30(24) (Å) 48.90 (91)

7.3.3 Photoluminescent Spectra: The PL excitation and emission spectra of the samples prepared at 650°C using 1:1, 1:2 and 1:3 ratio precursor products as prepared from ethanolic solutions are displayed in Figure 7.4 and 7.5. Those for the 1:1 and 1:2 support the XRPD data in that they have similar spectral features of varying intensities yet they are different to that of cubic $Y_2O_3:Eu^{3+}$. In addition the excitation spectra of the above products have peaks with weak absorption strength, an increase in the absorption bands intensity is seen for the 1:2 sample that contained higher concentrations of alkylammonium chloride originally. The emission and excitation spectra resemble those found for the ethanolic solutions reported in Chapters 5 and 6. The strong broad band observed at 254nm in cubic $Y_2O_3:Eu^{3+}$ due to the Eu^{3+} - O^{2-}

charge transfer transition is absent, although the usual lower intensity absorption lines due to the electronic transitions within the $4f^6$ configurations are present, some of which show a peak wavelength shift. The emission spectra of these samples are very weak, the strong sharp emission peak found at 611nm in cubic $Y_2O_3:Eu^{3+}$ due to the $^5D_o \rightarrow {}^7F_2$ transition is absent for the higher ratio samples where a broader peak centred at approximately 615nm is seen. Also absent in all three samples are the set of emission peaks with a maximum at 709nm due to the $^5D_o \rightarrow {}^7F_4$ of the Eu^{3+} ion in cubic Y_2O_3. The very weak spectra of the 1:3 samples showed nothing in both the emission and excitation spectra, possibly because so little sample was left, or because the material identified in the XRPD was very different from the 1:1 and 1:2 materials.

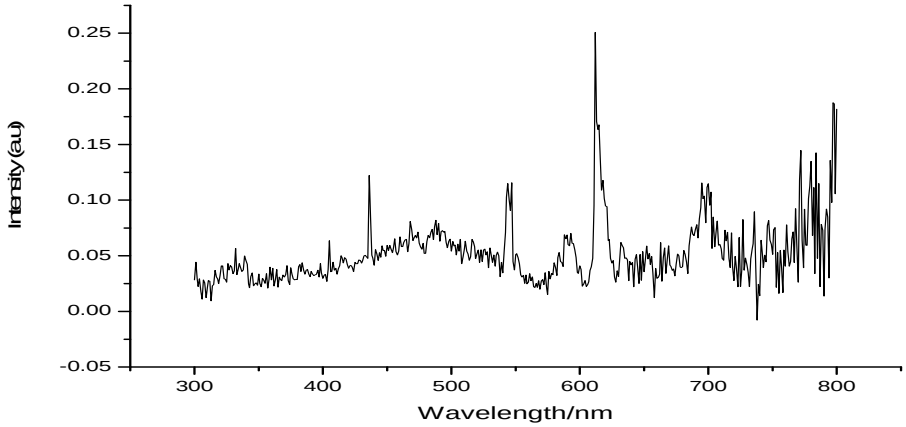

Emission (a)-1to1 ethanol at 650°C

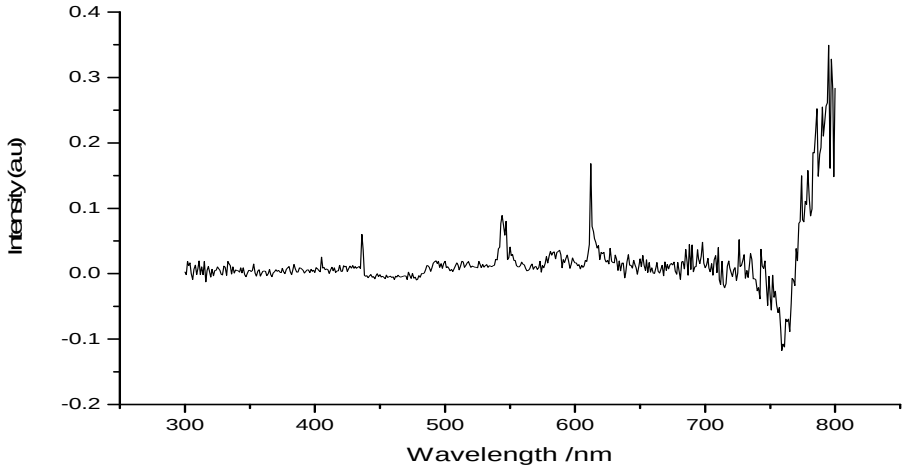

Emission (b)-1to 2 ethanol at 650°C

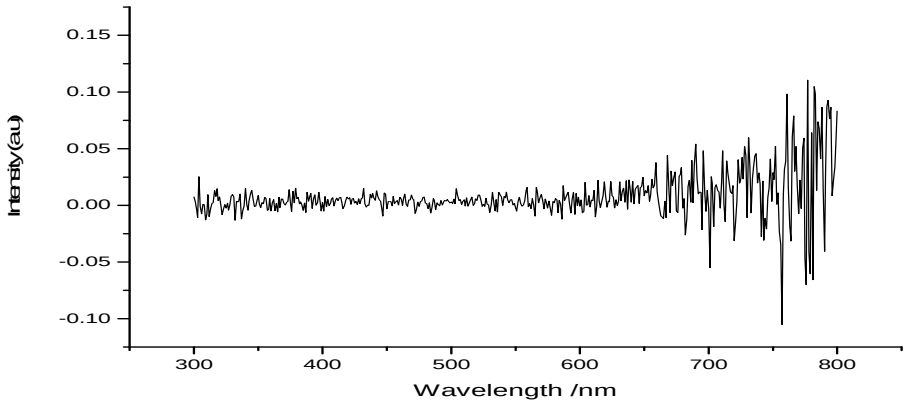

Emission (c)-1to 3 ethanol at 650°C

Figure 7.4 Photoluminescent emission spectra of the samples prepared at 650°C from ethanolic solution a-1:1, b-1:2 and c-1:3 ratio samples (excitation wave length 254nm).

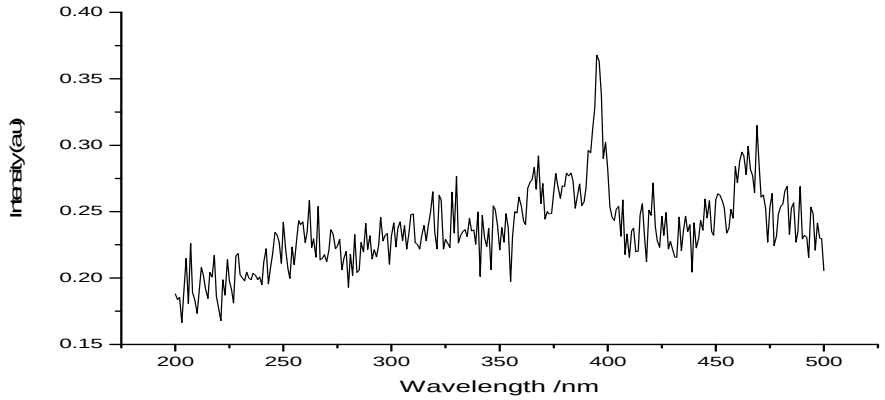

Excitation a-1to1 ethanol at 650°C

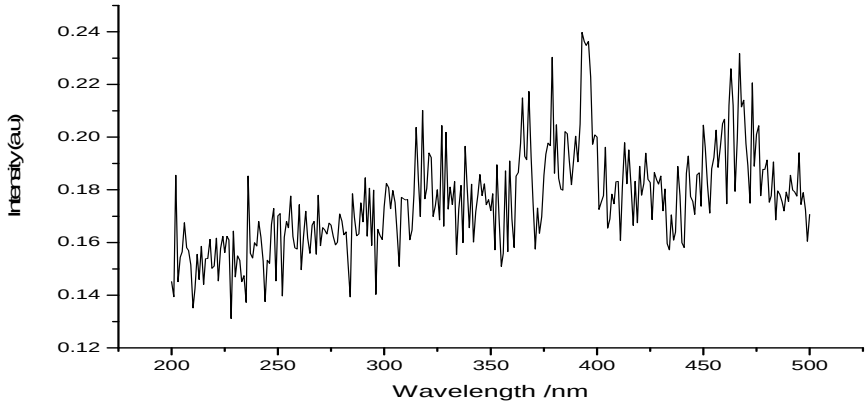

Excitation b-1to 2 ethanol at 650°C

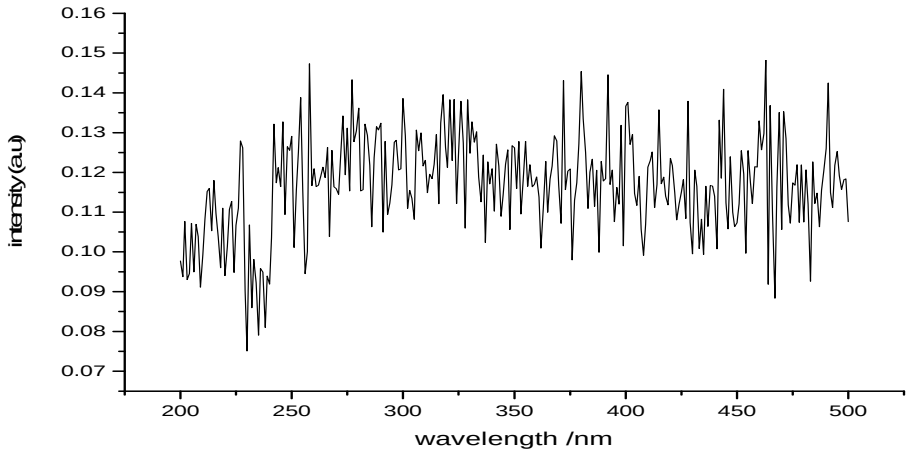

Excitation c-1to 3 ethanol at 650°C

Figure 7.5 Photoluminescent excitation spectra of the samples prepared at 650°C from ethanolic solution: a- 1:1, b- 1:2 and c- 1:3 ratio samples. Excitation monitored at 612 nm.

7.3.4 Cathodoluminescence Spectra

The CL (5000V, emission current 50μA) spectra of the samples prepared from ethanol at 650°C using the products produced from the 1:1, 1:2 ratios are presented in figures 7.6 and 7.7. The spectra obtained using the defocused beam and of the focused beam are all alike though for the 1:1 and 1:2 ratios though that in figure 7.6(a) is very weak and in all cases there is evidence of the cubic phase being formed in the beam. Surprisingly the sample in the focused beam (see figures 7.6 a,b,c,) show less conversion to the cubic phase, although in the defocused beam (figures 7.7 a,b) some cubic was observed. Again this is not because CL is more sensitive to the cubic phase but is in fact due to the conversion of the samples to cubic in the electron beam. Again this is because the samples are made up of very small particles of a precursor phase to that of the cubic $Y_2O_3:Eu^{3+}$ phosphor and the electron beam having sufficient energy to convert these particles into the cubic phase.

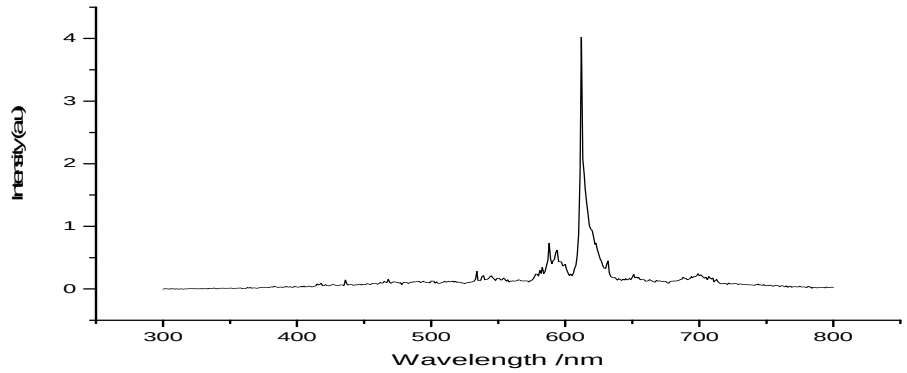

Focused (a)-1to1 at 650°C ethanol 5000V at 50uA

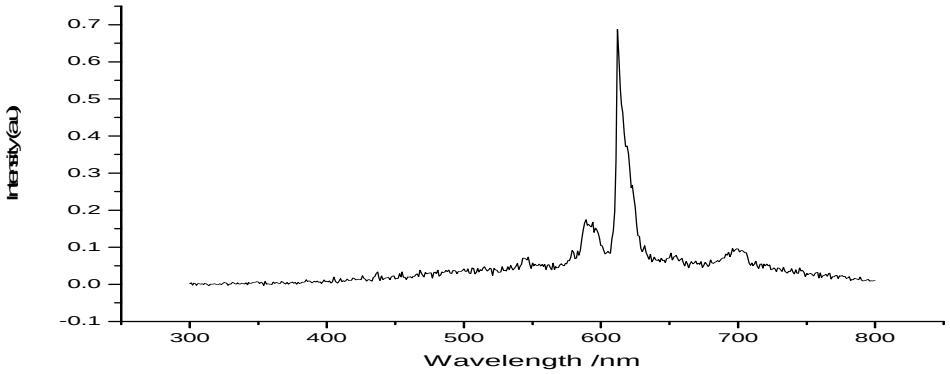

Focused (b)-1to 2 at 650°C ethanol 5000V at 50uA

Figure 7.6 Cathodoluminescent spectra of the 650°C samples prepared from ethanol. Focused beam. (a)-1:1, (b)- 1:2, at 5000V/50uA.

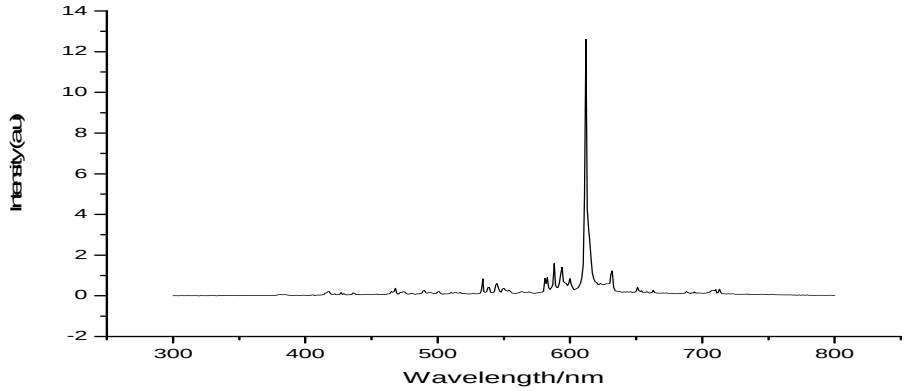

Defocused (a)-1to1 at 650°C ethanol 5000V at 50uA

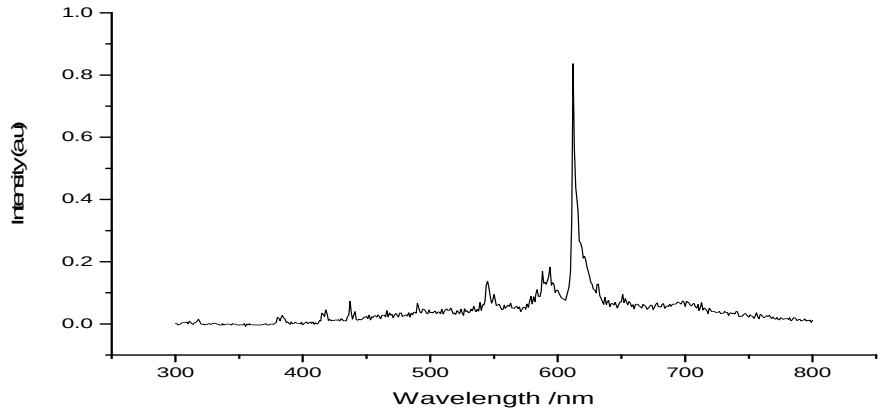

Defocused (b) -1 to 2 at 650°C ethanol 5000V at 50uA

Figure 7.7 Cathodoluminescent spectra of the 650°C samples prepared from ethanol. Defocused beam: (a)-1:1, (b)-1:2, at 5000V/50uA.

7.3.5 FTIR Spectra: - The FTIR spectral assignments of the samples prepared from ethanol at 650°C are summarised in Table 7.2, all show the presence of bands that can only be ascribed to the presence of metal hydroxycarbonate. Firstly for the samples prepared from ethanol at 650°C the FTIR spectra show the presence of bands that are ascribed to a mixture of $Y_{0.98}Eu_{0.02}(OH)CO_3$, $(Y_{0.98}Eu_{0.02})_2O(CO_3)_2$ and $(Y_{0.98}Eu_{0.02})_2O_2CO_3$, although the possibility that some chloride ions are present in some of the species cannot be ruled out. The basic europium doped yttrium carbonate, $Y_{0.98}Eu_{0.02}(OH)CO_3$, could have been formed from the surface reaction of YCl_3 with H_2O and CO_2 produced from the combustion of the alkylammonium cations.

$$2(Y,Eu)Cl_3 + 3H_2O \rightarrow (Y_{0.98}Eu_{0.02})_2O_3 + 6HCl \quad (7.1)$$

$$(Y_{0.98}Eu_{0.02})_2O_3 + 2CO_2 + H_2O \rightarrow 2Y_{0.98}Eu_{0.02}(OH)CO_3 \quad (7.2)$$

As $Y_{0.95}Eu_{0.05}(OH)CO_3$ was reported to lose most of its hydroxide to give $(Y_{0.95}Eu_{0.05})_2O(CO_3)_2$ and $(Y_{0.95}Eu_{0.05})_2O_2CO_3$ when it was calcined at 550°C for 1 h in a muffle furnace [25], it is likely that a similar decomposition occurred, albeit incompletely, under the rapid combustion conditions at a set temperature of 650°C in the present work. Figure 7.8 present FTIR spectra of these samples in the 3600 – 700 cm^{-1} range; the broad band observed in the region of 3600-3000 cm^{-1} is assigned to the O-H stretching vibration of the hydroxycarbonate. The triplet of bands observed at 1626 cm^{-1}, 1553 and 1346 cm^{-1} is attributed to C-O stretching vibrations of CO_3^{2-} anions; the first component having some C=O character and the last two most likely being due to antisymmetric C-O stretching modes of CO_3^{2-} anions [26]. Furthermore, the weak band at 1093 cm^{-1} is assigned to a symmetric C-O stretching vibration of the CO_3^{2-} anions [27]. The inhomogeneous broadening of the various vibrational bands in

the spectra of these samples is due to the disorder within the lattices when the products are formed at 650°C. It is not possible to identify bands due to Y-Cl stretching vibrations in these FTIR spectra as they are expected to appear below the low wavenumber cut-off at *ca.* 749 cm^{-1}.

Table 7.2 Materials prepared from ethanolic solutions and fired at 650°C

Wavenumber/cm^{-1}		
3600-3000	*(m)*	ν (O-H)
	(m)	ν_s (O-H)
1626	*(shoulder)*	δ (O-H)
1553	*(s)*	ν_{as} (CO_3^{2-})
1446	*(s)*	ν_{as} (CO_3^{2-})
1093	*(w)*	δ (O-H)
749	*(w)*	δ (CO_3^{2-})

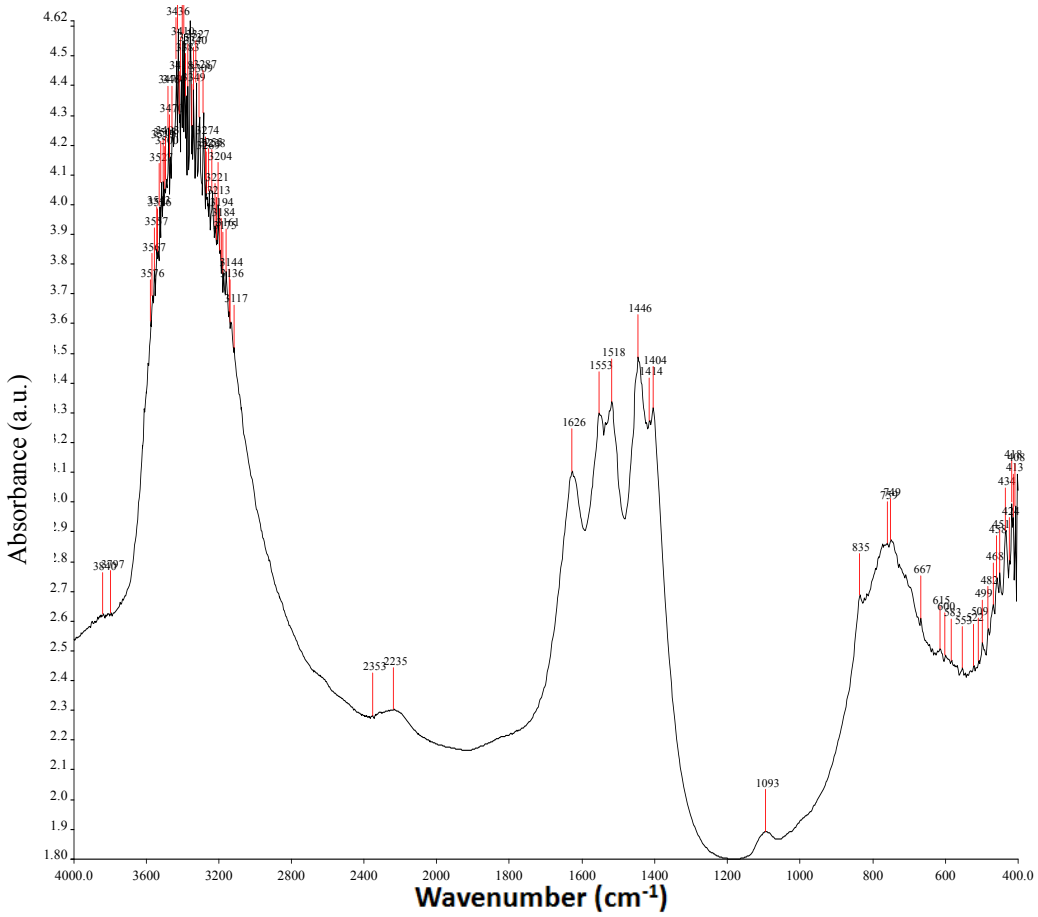

(a)

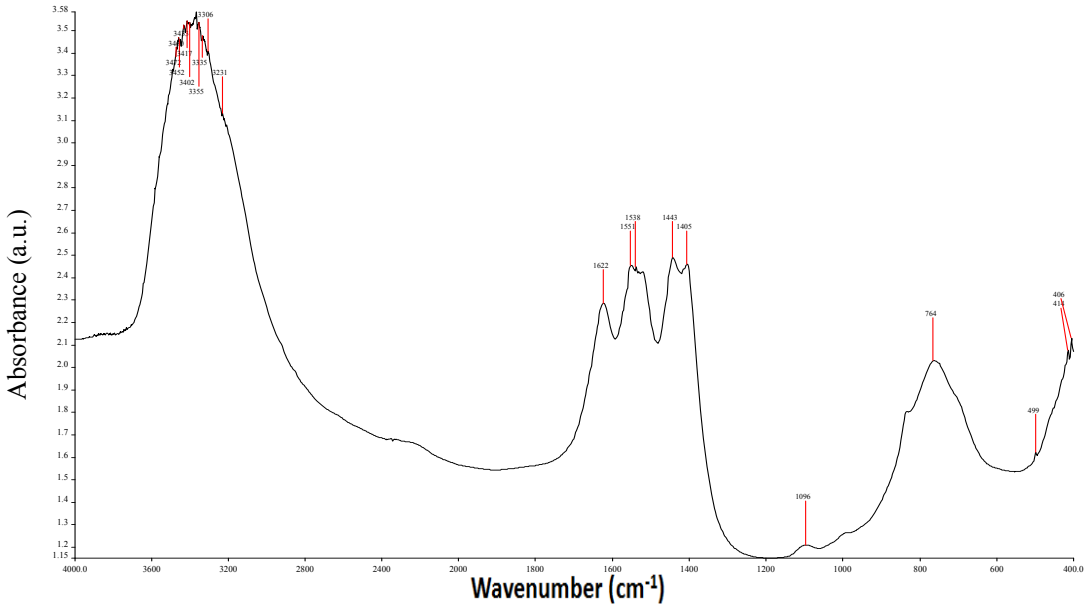

(b)

Figure 7.8 FTIR spectra of the 650°C, samples (a), (b) prepared from ethanolic solution with Metal ion to alkylammonium chloride ratios 1:1 (a), 1:2 (b) in KBr discs.

7.3.6. Conclusions so far

It is clear from these results so far that the presence of the combustion fuel in the samples prepared at 650°C was insufficient to raise the temperature high enough to form the cubic $Y_2O_3:Eu^{3+}$ phase or that the furnace temperature was insufficient. In addition no evidence of the material $Y_4O_5Cl_2$ phase that was found in Chapters 5 and 6 were present in chapter 7 this was showing that the temperature in chapter 7 did not got high enough to form this phase of $Y_4O_5Cl_2$. All the 650°C FTIR spectra are similar, although the emission spectra do indicate that for the higher fuel ratios that a greater degree of order is found. It is interesting that there is no evidence for chloride containing phases for the samples prepared from either ethanol or methanol where the shorter chained alkylammonium salt has been used unlike the findings in chapter 5.

7.4 Studies on the samples produced at 900°C

7.4.1 Products prepared with methanol and ethanol at a temperature of 900°C.

Products (samples) prepared from precursors methanolic and ethanolic solutions were fired at a temperature of 900°C and observed to be all white powders in colour. Under 254nm excitation the samples prepared at 650°C displayed a weak red luminescence which was in contrast to the strong red luminescence from the samples prepared at 900°C that is characteristic of the $Eu^{3=}$ ion in cubic Y_2O_3. The strongest red luminescence comes from 1:3 material sample ratios prepared at 900°C.

7.4.2 SEM Studies

The phosphor samples annealed at 900°C are now discussed. In Figures 7.9, 7.10, 7.11 and 7.12 SEM micrographs of phosphor samples prepared from methanolic and ethanolic solutions respectively. SEM micrographs of the material prepared from methanol (fired at 900°C at metal chloride to alkylammonium chloride ratios of 1:1 (Figure 7.9 a to e), are presented. As in the samples fired at 650°C large straw-like sheets are shown to be formed, though here from intergrowths of small crystals rather thin needles. These sheets show evidence of melting at the temperature of firing. The spherical, tubular and lamellar structures seen in the earlier chapters are not in evidence in the SEMs of this sample.

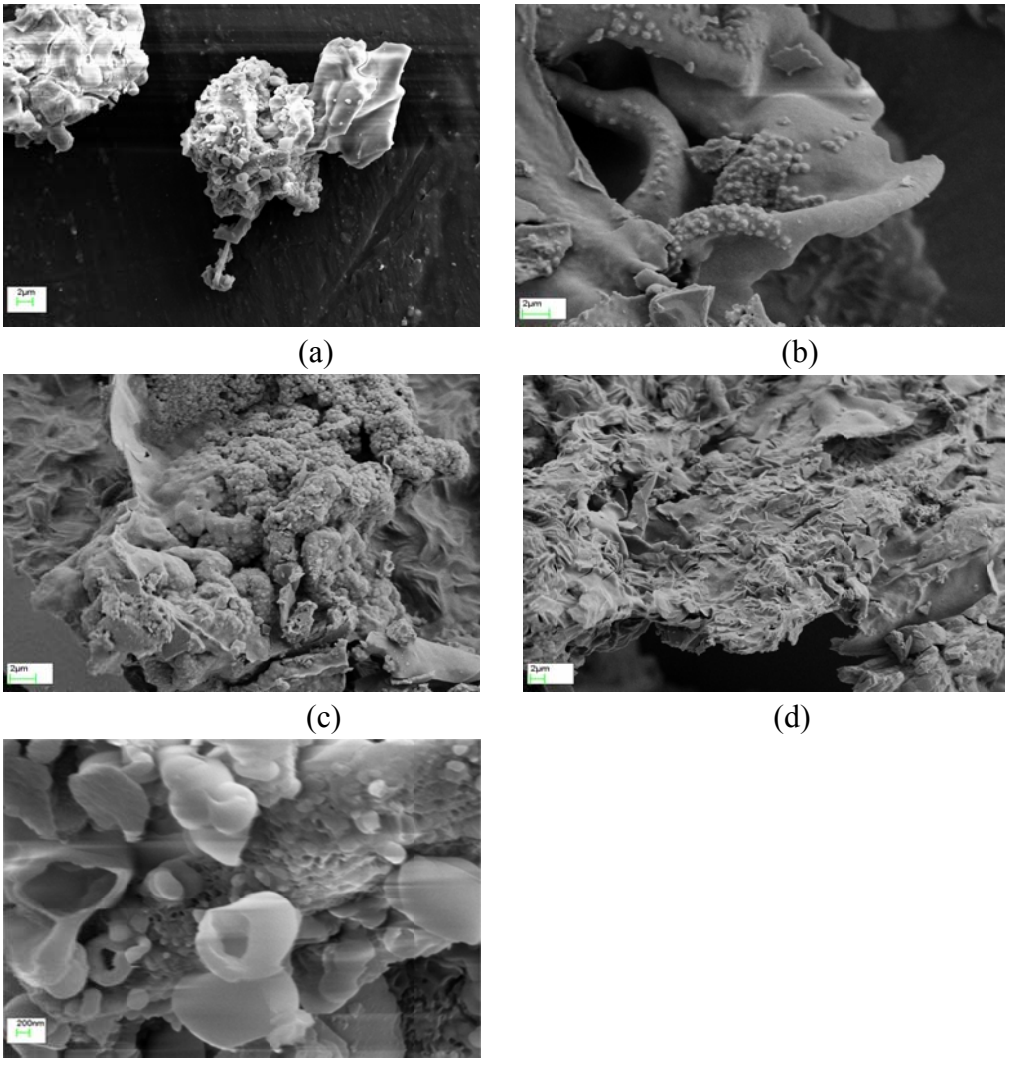

(a) (b) (c) (d) (e)

Figure 7.9 FESEM images of phosphor samples prepared from methanolic solutions then fired at 900°C using a metal chloride to alkylammonium chloride ratios of 1to1(a, b, c, d, and e). In a, b, c and d the bar is 2 μm and in e it is 200nm.

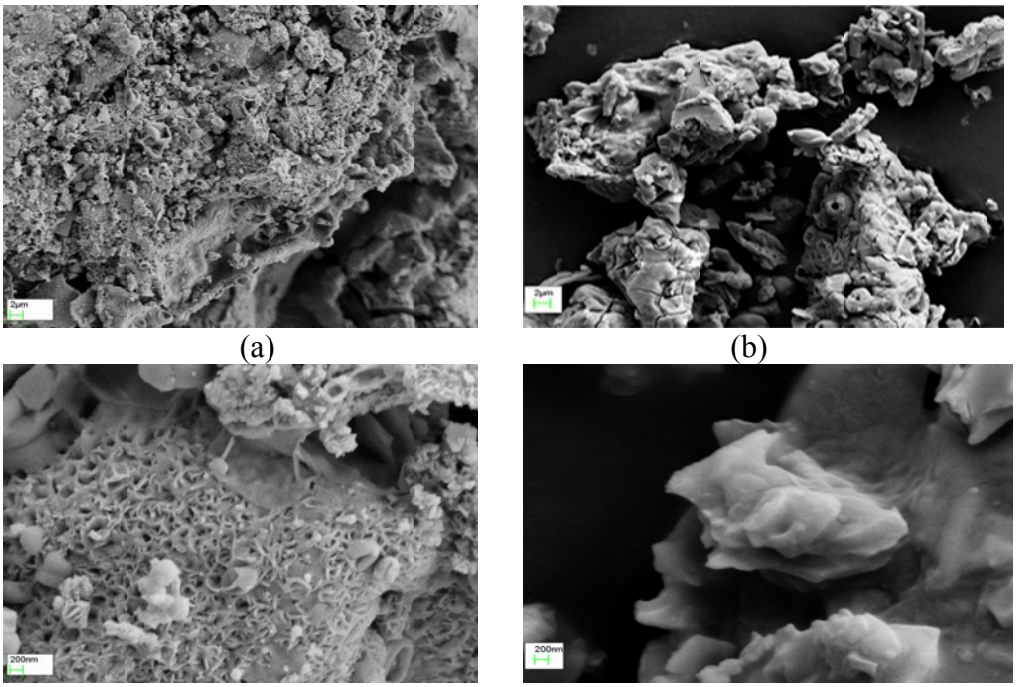

(a) (b)

(c) (d)

Figure 7.10 FESEM images of phosphor samples prepared from ethanolic solutions then fired at 900°C using a metal chloride to alkylammonium chloride ratios of 1to1(a, b, c, and d). In a and b the bar is 2 μm and in c and d it is 200nm.

It is interesting to note that in Figure 7.10 (a-d) here there is evidence of much more melting than in Figure 7.2; the structures seen are much less delicate but there are remnant of the presence of thin films of material with spaces between the structures. In agreement to the results of the methanol SEMs (Figure 7.9), it can be seen in Figure 7.10 that for this ratio there is evidence for sheet like structures, but in this case less porous areas are noticeable between the sheets where the long chain alkylammonium molecules have been consumed in the firing.

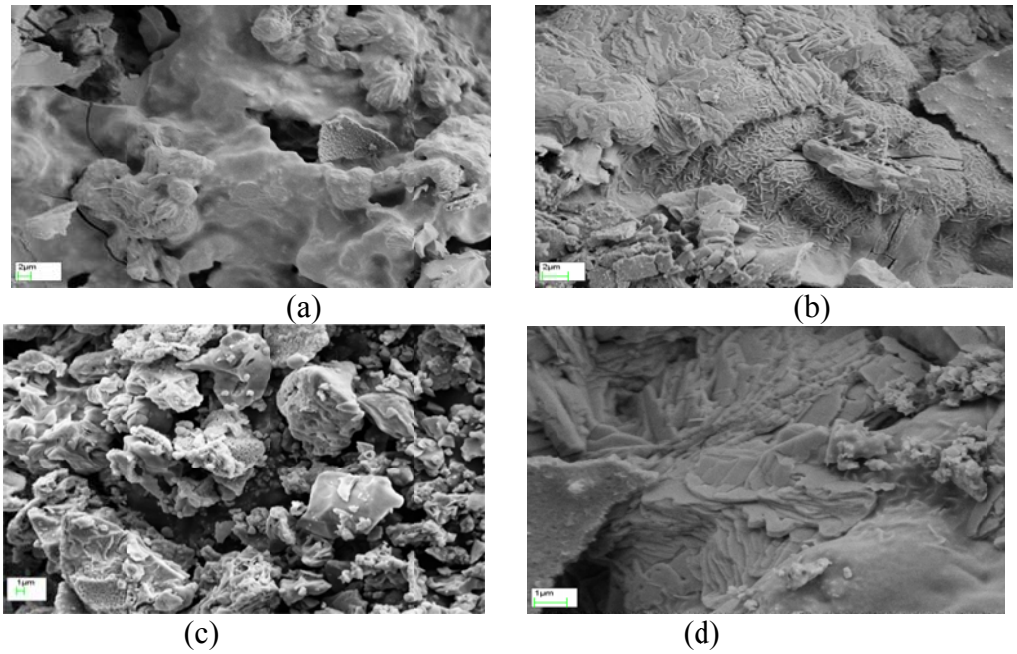

(a) (b)

(c) (d)

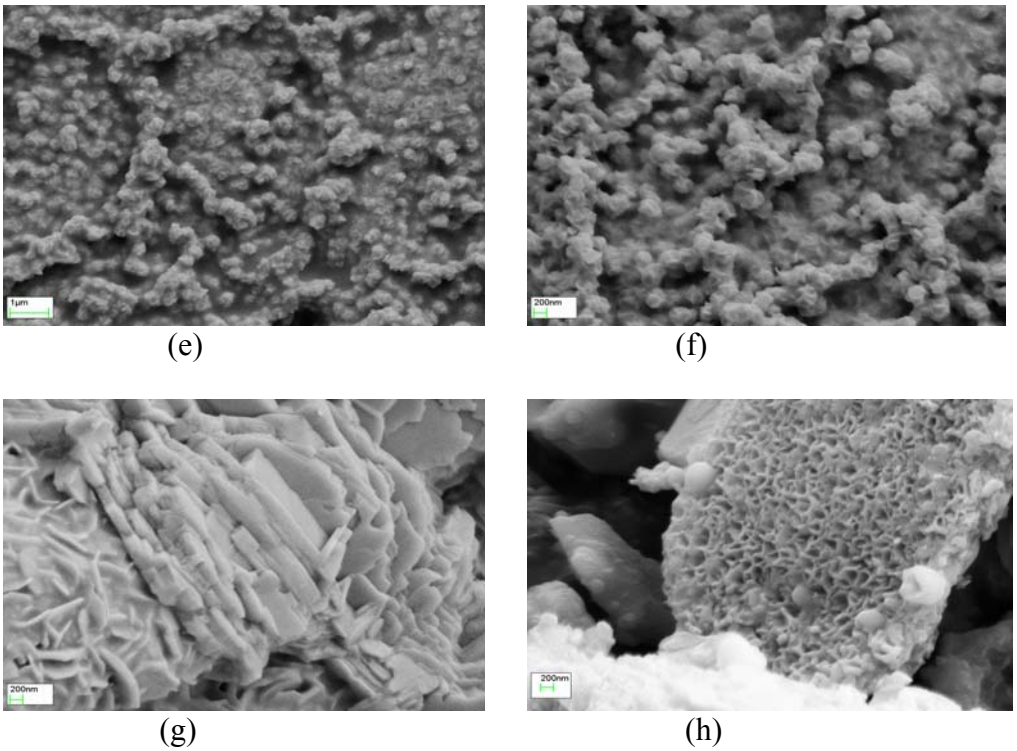

(e) (f)

(g) (h)

Figure 7.11 FESEM images of phosphor samples prepared from ethanolic solutions then fired at 900°C using a metal chloride to alkylammonium chloride ratios of 1to2 (a, b, c, d,e,f,g. and h).In a, and b the bar is 2 µm. c, d, and e the bar is 1 µm and in f, g, h. it is 200nm.

In Figure 7.11 (a-h) for the 1:2 ratio there is also evidence of much more melting than in Figure 7.2; again the structures seen are much less delicate but there are remnant of the presence of thin films of material with spaces between the structures (see figures 7.11(a-d). In figures 7.11(e and f) there is evidence of spherical/oval shaped structures that could be of micellar origin which were not seen in figure 7.10. In figures 7.11(g) there is evidence of crystals melted together, whereas in figure 7.11(h) there are similar structures found for the same material fired at 650°C (see Figure 7.2 (g and h). Again in agreement to the results of the methanol SEMs (figure 7.9), it can be seen in figure 7.11 that for this ratio there is evidence for sheet like structures.

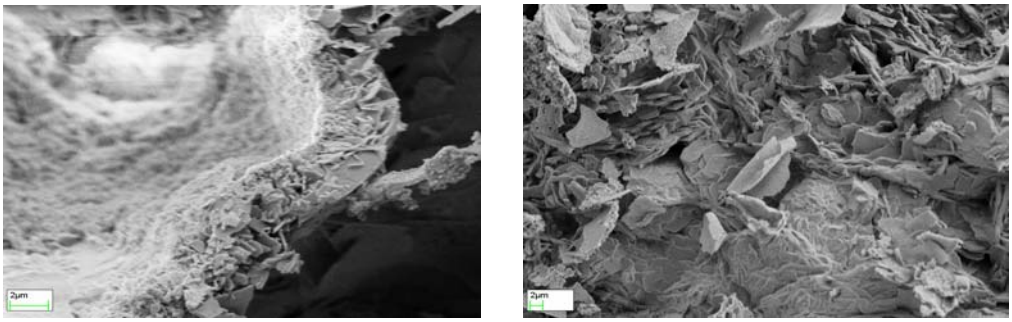

(a) (b)

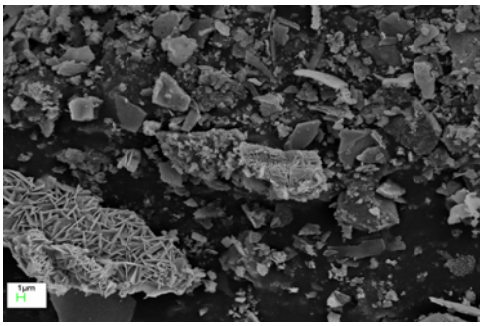

(c)

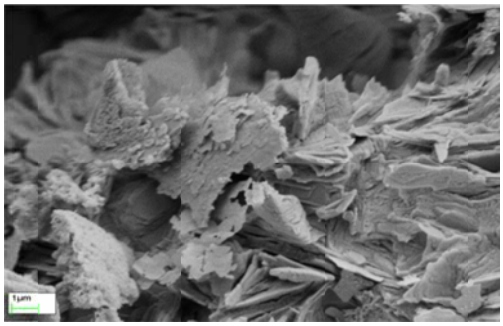

(d)

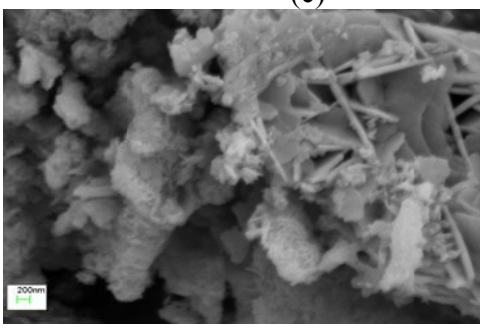

(e)

Figure 7.12 FESEM images of phosphor samples prepared from ethanolic solutions then fired at 900°C using a metal chloride to alkylammonium chloride ratios of 1to3(a, b, c, d, and e).In a, and b the bar is 2 µm. c, and d the bar is 1 µm and in e it is 200nm.

In Figure 7.12 (a-e) (the 1:3 ratio material) there evidence of many sheet like structures that are very micellular like in appearance, with crystals between the sheets. Again more melting than in Figure 7.2 is apparent. In Figure 7.12 (c) there are many small spherical structures as well as sheet structures. These are less aggregated than those in Figures 7.11(e and f). Again in agreement to the results of the methanol samples images (Figure 7.9), it can be seen in figure 7.12 that for this ratio there is much evidence for sheet like structures. In Figures 7.10, 7.11 and 7.12 there is little evidence for the variety or indeed number of morphological forms found in the previous two chapters, though in Figure 7.12 their appears to be some evidence for the remains of more complex structural forms. In agreement with the previous chapters the thin structures that have dimensions up to 200nm in length. In summary the predominant structures are those that have assembled into large lamellar sheets that in these images are often two structural units in thickness similar to those observed in the previous chapters. In many of the SEMs presented in figures 7.9 to 7.12 it can be seen that there is evidence of structures where the surfaces appear to be smooth suggesting they neared meltdown this is thought to be due to the presence of ethanol rather than methanol.

7.4.3. Sample structures (from XRPD data):- All the samples that were produced under the 900°C conditions from methanolic and ethanolic solutions showed the presence of crystalline material and all showed some traces of a similar XRPD (see Figure 7.13&7.14) pattern identified as cubic $Y_2O_3:Eu^{3+}$ on top of a much broader

pattern similar to those reported in the last two chapters 5 and 6. The 1:1 sample prepared from the methanolic solution had XRPD data that showed the presence of both cubic $Y_2O_3:Eu^{3+}$ (16.1%) and mono clinic $Y_2O_3:Eu^{3+}$ (83.89 % this is the first time evidence for monoclinic $Y_2O_3:Eu^{3+}$ was found in this experimental work. Powdered methanol sample 38 was used for the XRD experiment.

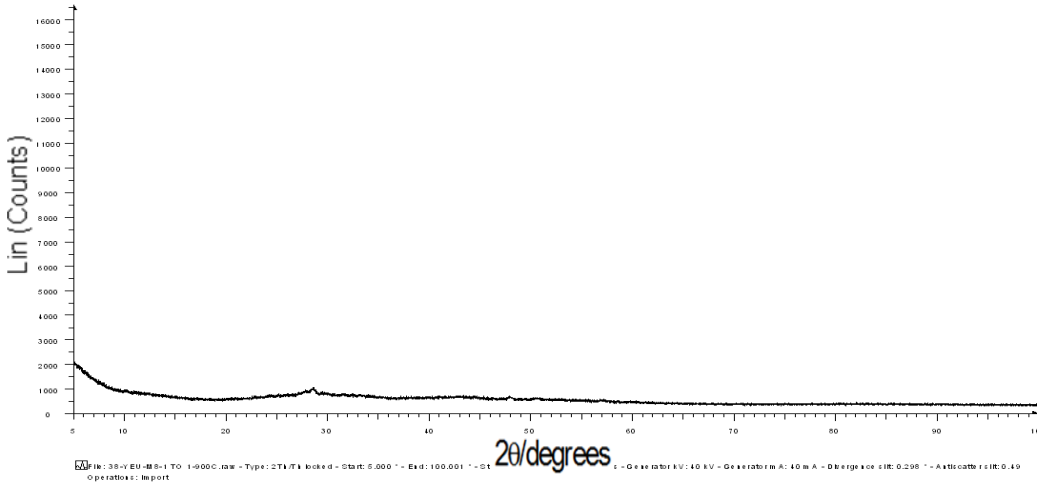

38 1to 1

Figure 7.13 XRPD diffractograms of the sample prepared from methanolic solution then fired/annealed at 900°C, metal ion to alkylammonium chloride ratios.1:1(38) from the powder.

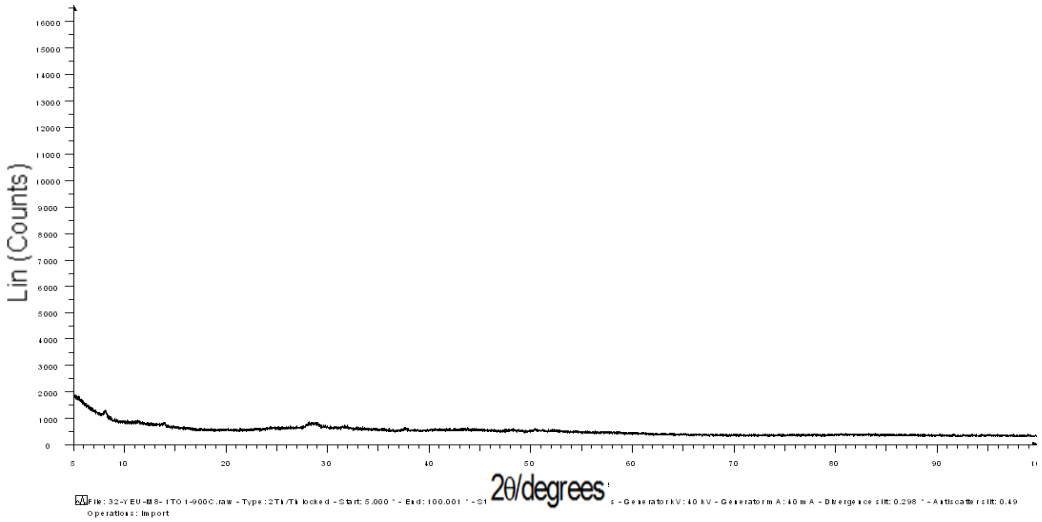

32- 1 to 1 ethanol from the powder

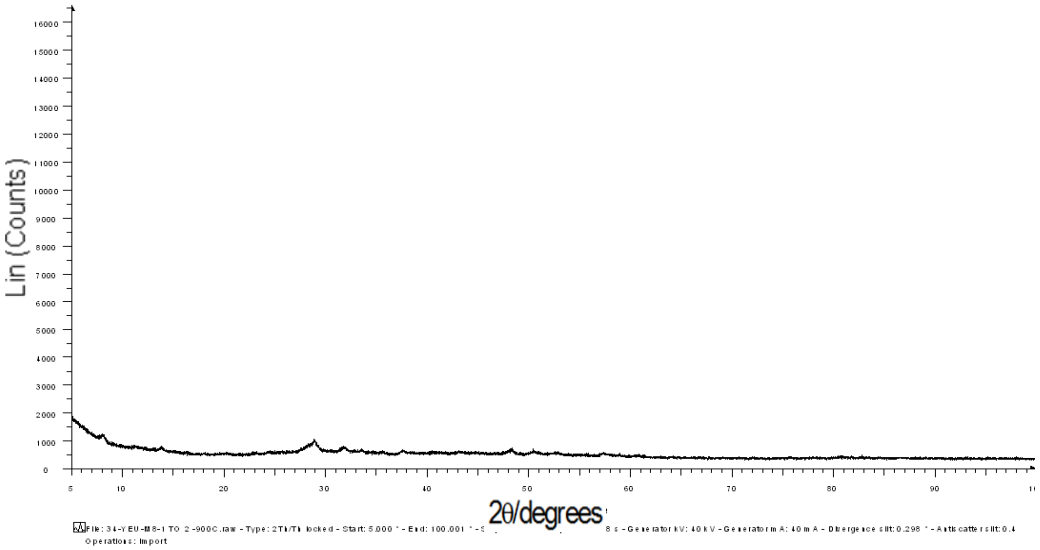

34- 1 to 2 ethanol from the powder

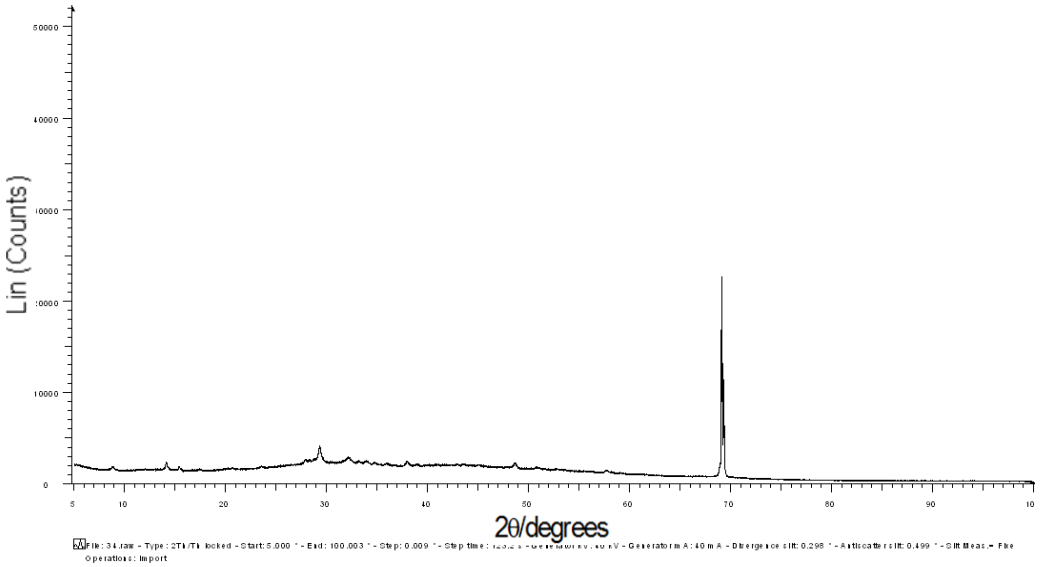

34-1 to 2 ethanol on Silicon

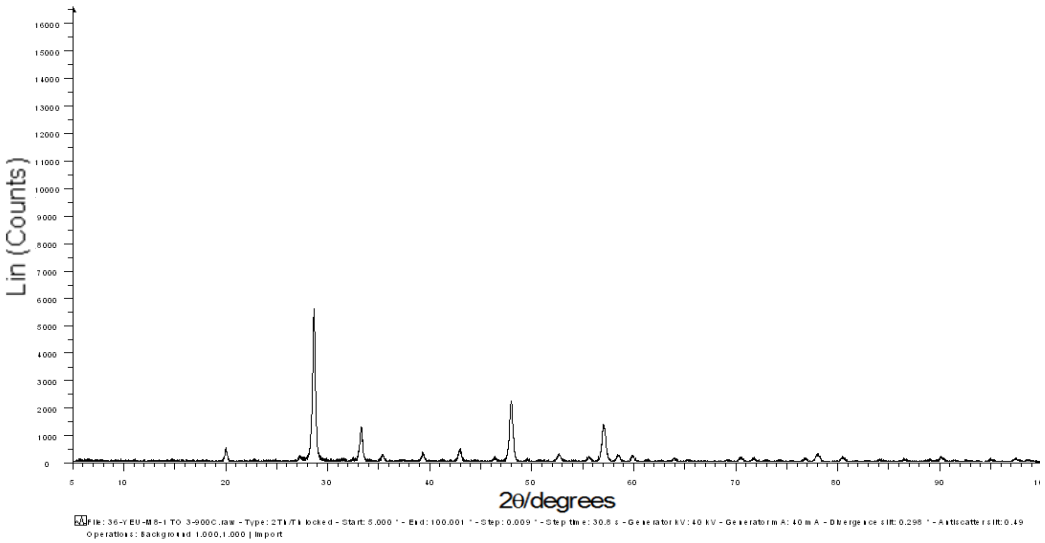

36 -1 to 3 ethanol from the powder

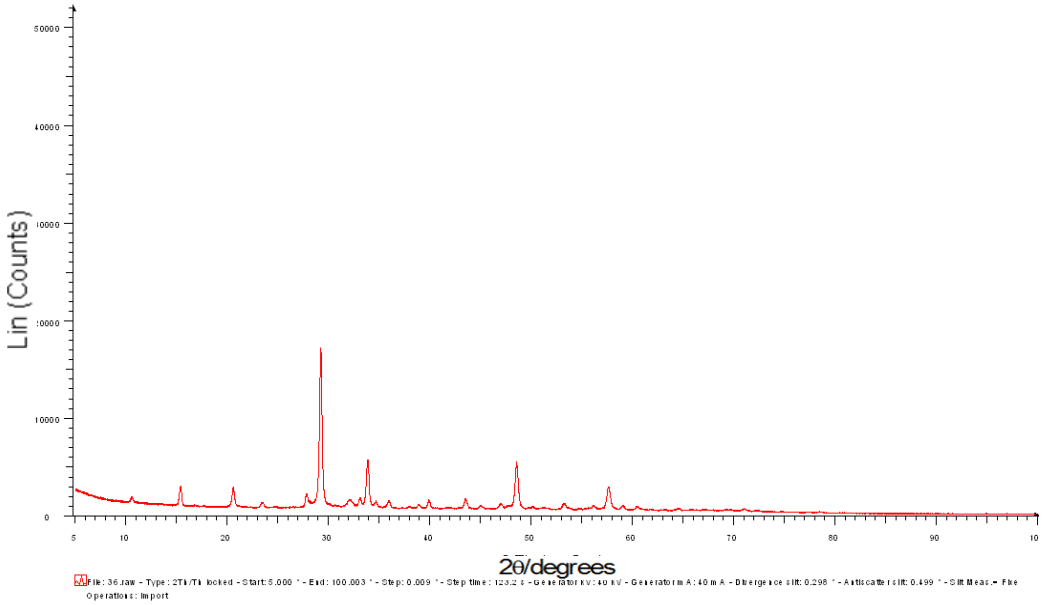

36-1 to 3 ethanol on silicon

Figure 7.14 XRPD diffractograms of the samples prepared from ethanolic solution then fired/annealed at 900°C, metal ion to alkylammonium chloride ratios.1:1(32), 1:2 (34),1:3 (36).

The samples that were produced under the 900°C conditions from ethanolic solution showed differing behaviour. The 1:1 sample had an XRPD pattern (see figure 7.14 (32)) that is typical of the presence of two forms of $YOCl:Eu^{3+}$ and both cubic and monoclinic $Y_2O_3:Eu^{3+}$. The 1:2 sample showed very similar results but the results of

each is different. The 1:3 sample had XRPD data that only showed the presence of cubic and monoclinic $Y_2O_3:Eu^{3+}$ forms.

Table 7.3
Cell parameters for the yttrium oxychloride phase $Y_2O_3:Eu^{3+}$ found in the materials fired at 900°C prepared from methanol and ethanol.

Methanol	a (Å)	b (Å)	c (Å)	Beta	Phase %
38 1:1					
Cubic $Y_2O_3:Eu^{3+}$	10.6216*				16.101*
Monoclinic $Y_2O_3:Eu^{3+}$	14.9998*	3.5737*	8.9863*	99*	83.899*
Ethanol					
32 1;1					
YOCl:Eu^{3+} R-3m-1	4.804(13)		28.14(18)		5.101(48)
YOCl:Eu^{3+} R-3m-2	4.115(140		20.751(94)		88.12(83)
Cubic $Y_2O_3:Eu^{3+}$	10.581(64)				2.23(13)
Monoclinic $Y_2O_3:Eu^{3+}$	13.970 (12)	3.4989 (26)	8.7002(70)	99.909(52)	4.55(89)
34 1:2					
YOCl:Eu^{3+} R-3m-1	4.74(11)		28.0(12)		6.592(54)
YOCl:Eu^{3+} R-3m-2	4.132(40)		20.08 (23)		86.50(71)
Cubic $Y_2O_3:Eu^{3+}$	10.6230(15)				2.908(89)
Monoclinic $Y_2O_3:Eu^{3+}$	13.9681(99)	3.5389(16)	8.3870(71)	98.288(12)	4.00(78)
36 1:3					
Cubic $Y_2O_3:Eu^{3+}$	10.62102 (26)				49.4(47)
Monoclinic $Y_2O_3:Eu^{3+}$	13.885(43)	3.6119(78)	8.038(23)	98.66(23)	50.6(47)

*The fit is not good enough for errors to be meaningful.

The fact that all four samples contained monoclinic $Y_2O_3:Eu^{3+}$ forms was not expected as this is a high temperature phase and was not found in the methods studied in Chapters 5 and 6 .her the alkylammonium chain length was smaller so it might have expected that the materials would not reach such a high temperature with a shorter chain, clearly this was clearly this was wrong assumption and this will be discussed later in this chapter.

7.4.4. Photoluminescent Spectra: - The PL excitation spectrum1:1 of the sample made from methanolic solution was not typical of cubic $Y_2O_3:Eu^{3+}$, as were the emission spectrum butt the spectrum had excitation bands. The excitation and emission spectra are presented in Figure 7.15 for the 1:1, 900°C sample. A comparison of Figure 7.15 with Figure 6.21 shows accurately small band between 250 and 300nm and between 420 and 450nm. In the Figure 6.5 Photoluminescent Excitation spectra of the YOCl material are shown these are very weak. The stronger spectra in Figure 7.15 is dominated by the presence of cubic emission spectrum this is amassing that as only 2.3% of the cubic material was present. The emission spectrum in Figure 7.16 is much stronger than those of the YOCl shown in Figure 6.7and is dominated by the wave length bands due to cubic and monoclinic material $Y_2O_3:Eu^{3+}$. Hence the photoluminescent spectra also confirmed the presence of cubic and monoclinic material $Y_2O_3:Eu^{3+}$.

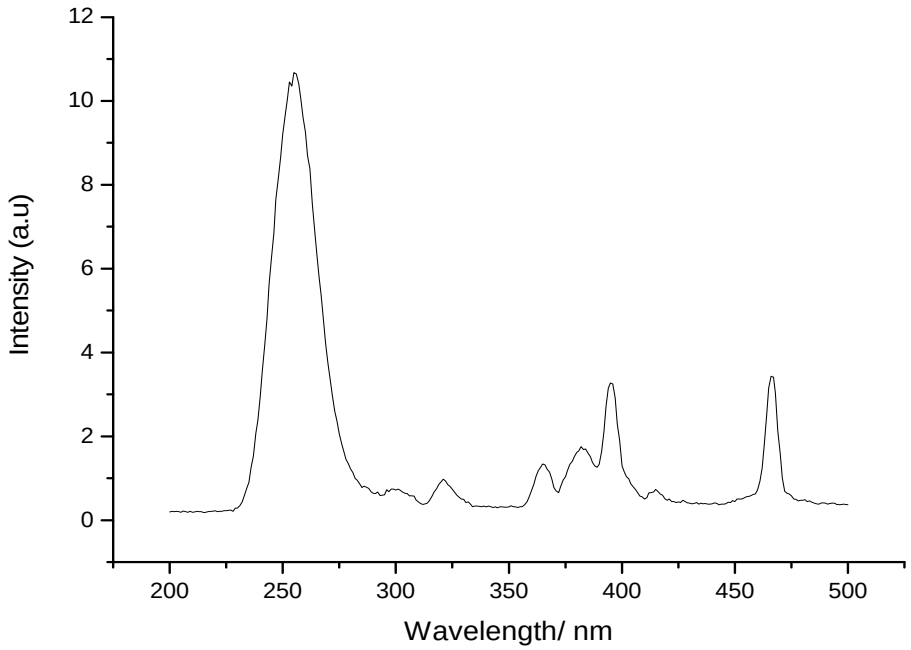

Excitation spectra-38-1 to 1 methanol

Figure 7.15 Photoluminescent excitation spectra of the 900°C sample prepared from methanolic solution. Excitation spectra 1:1-38. Excitation monitored at 612 nm.

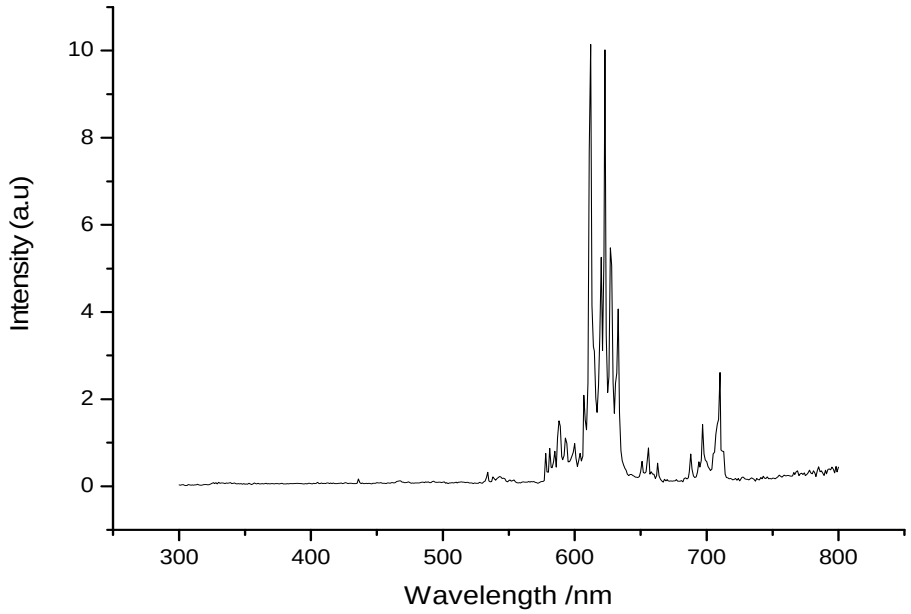

Emission spectra, 38-1 to 1 methanol

Figure 7.16 Photoluminescent emission spectra of the 900°C sample prepared from methanolic solution. Emission spectra 1:1-38. Excitation wavelength 254nm.

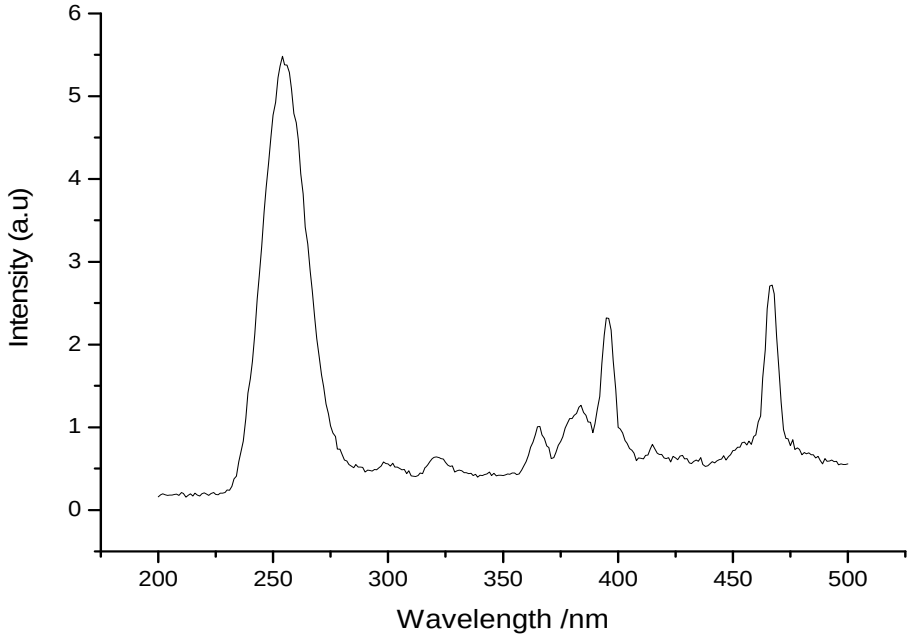
Intensity (a.u)
Wavelength /nm
0
1
2
3
4
5
6
200
250
300
350
400
450
500

(a)

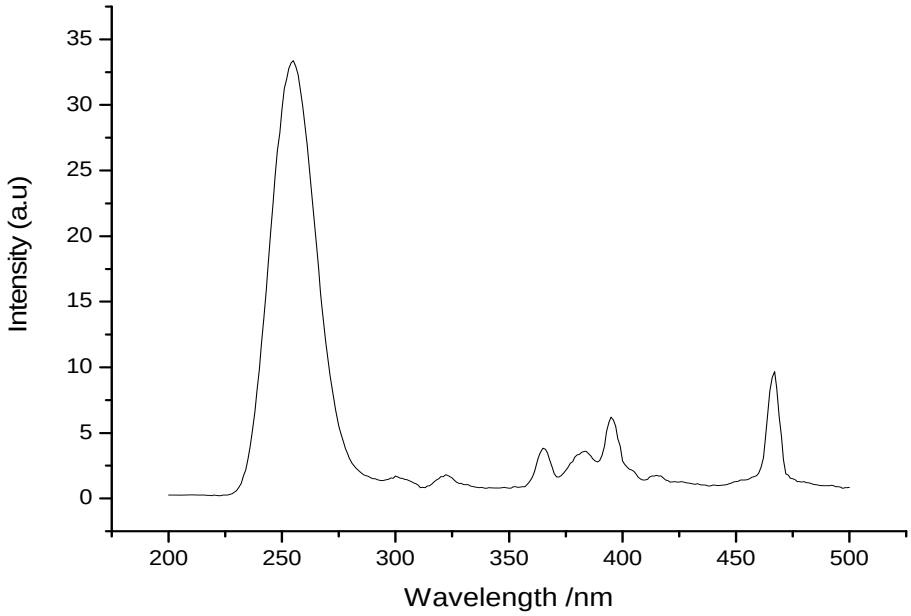
Intensity (a.u)
Wavelength /nm
0
5
10
15
20
25
30
35
200
250
300
350
400
450
500

(b)

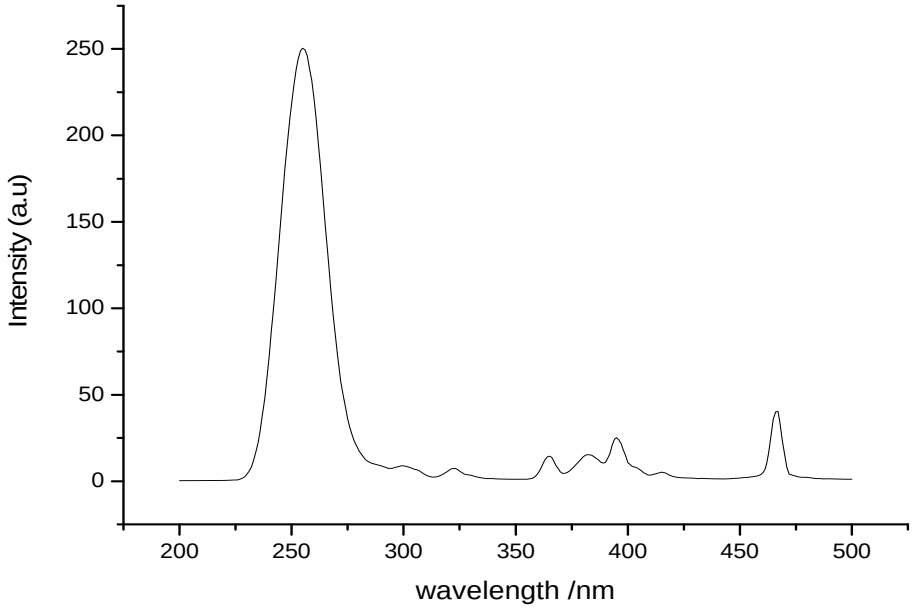

(c)

Figure 7.17 Photoluminescent excitation spectra of the 900°C samples prepared from ethanolic solution for (a) 1:1-32, (b) 1:2-34, (c) 1:3-36. Excitation monitored at 612 nm.

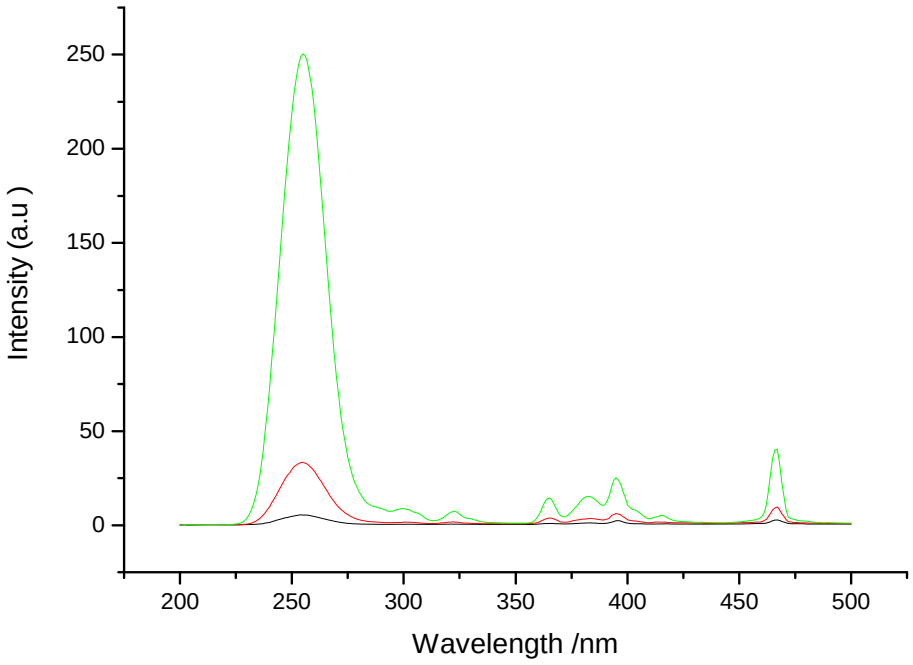

Figure 7.18 Photoluminescent excitation spectra of the 900°C samples prepared from ethanolic solution. Overlay excitation graphs 1:1-32-black-bottom, 1:2-34,red (mid), 1:3-36,green,top. Excitation monitored at 612 nm.

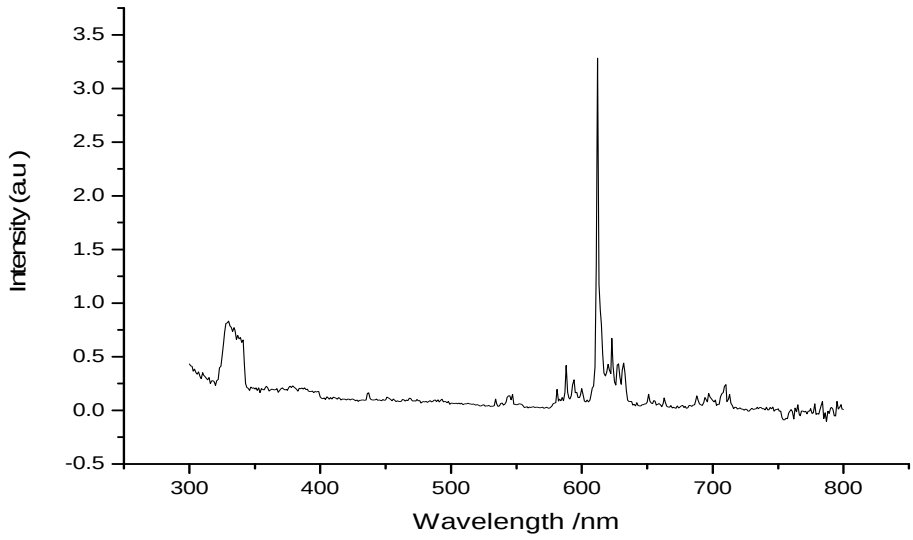

(a)

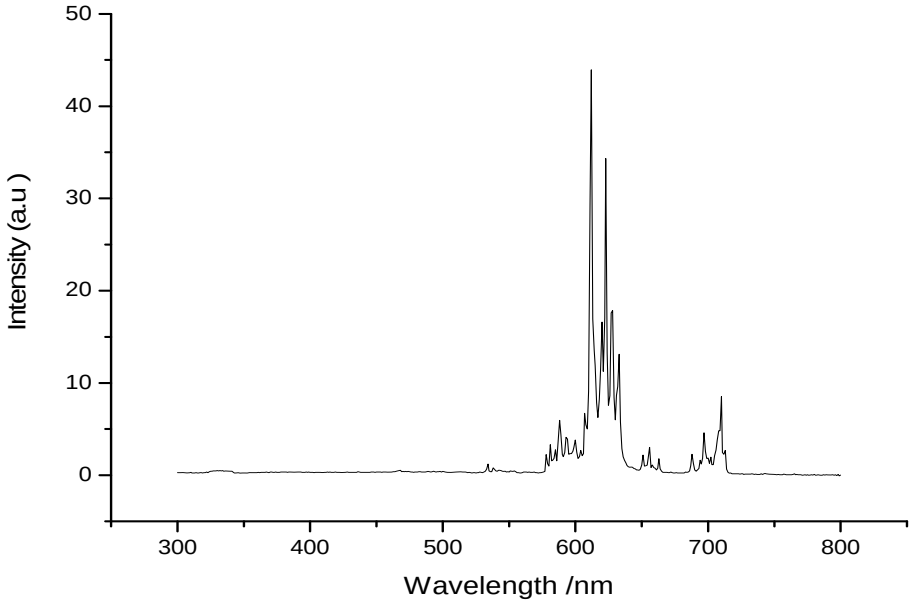

(b)

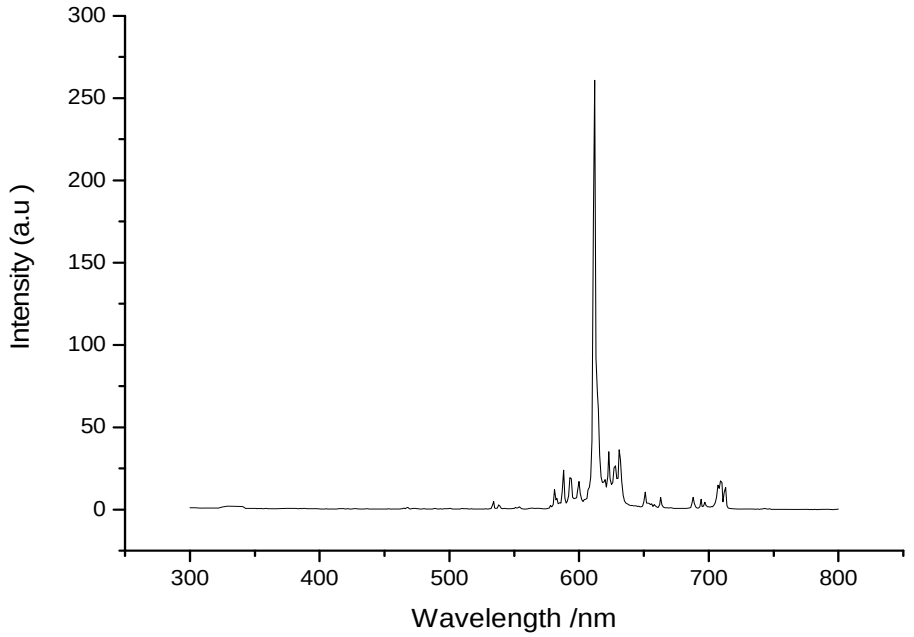

(c)

Figure 7.19 Photoluminescent emission spectra of the 900°C samples prepared from ethanolic solution. Emission spectra (a)1:1-32,(b) 1:2-34,(c) 1:3-36 .
Excitation wavelength 254nm.

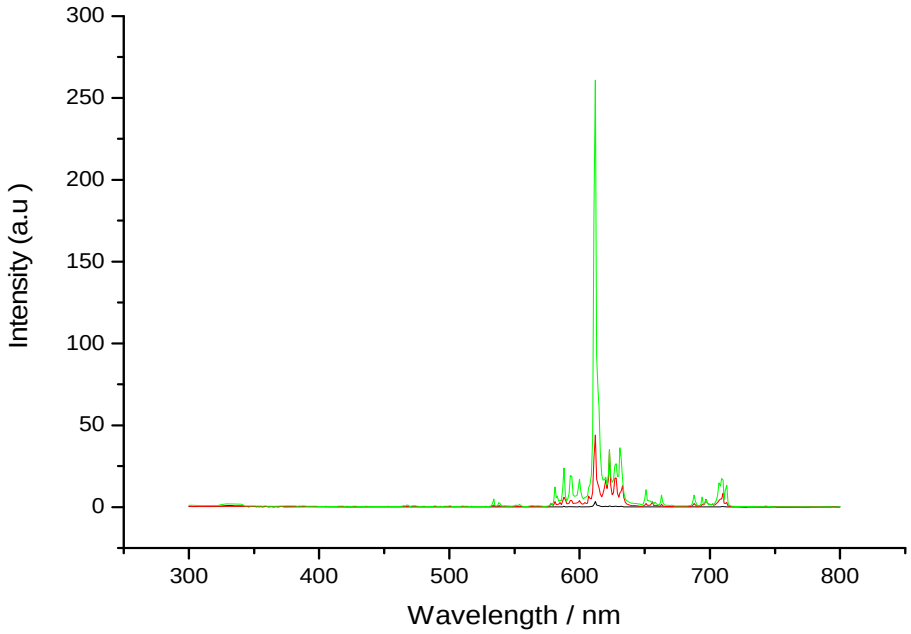

Figure 7.20 Photoluminescent emission spectra of the 900°C samples prepared from ethanolic solution. Overlay of the emission graphs 1:1-32 black, 1:2-34 red, 1:3-36 green. Excitation wavelength 254nm.

The Photoluminescent spectra of the samples made Ethanolic solution are presented in Figure 7.17 and 7.18. The excitation spectra are similar to that in Figure 7.15 and can be explained in the same way as that of the sample prepared from methanolic solution. The spectrum of the 1.3 sample Figure 7.17(c) it is much more in a sense and it is clearer in the light of the above discussion, 1s due to the presence of only and monoclinic material $Y_2O_3:Eu^{3+}$. The samples 1:1 and 1:2 are much weaker but still only show evidence for the latter two compounds. The Photoluminescent Emission spectra of these three materials are presented in Figure 7.18.The strongest spectrum is in Figure 7.18(c) for the 1:3 compound and is typical of the cubic $Y_2O_3:Eu^{3+}$.Figures 7.18(a) and 7.18(b) both show evidence of cubic $Y_2O_3:Eu^{3+}$. But in addition we can observe in Figure 7.18(b) also shows the presence of some monoclinic material $Y_2O_3:Eu^{3+}$.

7.4.5 Cathodoluminescence Spectra:- The CL (5000V, emission current 9.6μA) defocused and focused spectra of the products prepared from the precursors originating in the methanolic solutions are shown in Figures 7.21, and 7.22; they are all similar and typical of cubic$Y_2O_3:Eu^{3+}$. So here again the cubic material dominates the Cl emission.

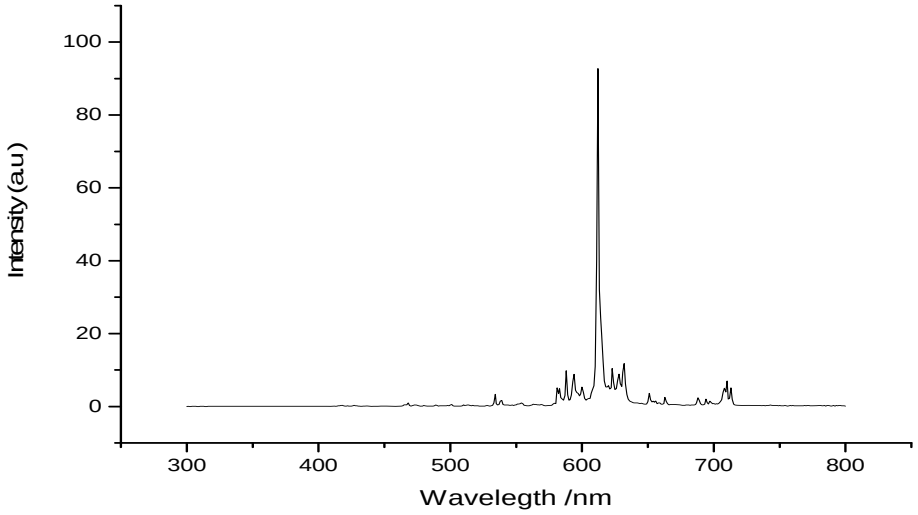

Figure 7.21 The Cl defocused beam emission spectra for samples 38-1:1 prepared from methanolic solutions and fired/annealed at 900°C the samples was excited using 5000V/50uA.

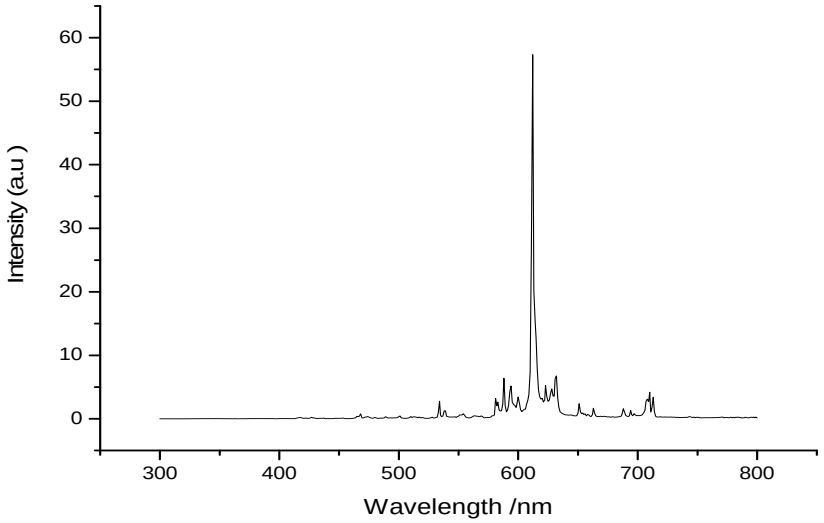

Figure 7.22 The Cl focused beam emission spectra for samples 38-1:1 prepared from methanolic solutions and fired/annealed at 900°C. The sample was excited using 5000V/50uA.

The CL (5000V, emission current 9.6μA) defocused and focused spectra of the products prepared from the precursors originating in the ethanolic solutions are shown in Figures 7.23 and 7.24. They are all more simplified than those found for their respective PL emission spectra and those for the 1:2 and 1:3 samples typical of cubic$Y_2O_3:Eu^{3+}$. Even the 1:1 sample showed evidence of a spectrum that though very weak was dominated by the 612nm emission of the cubic$Y_2O_3:Eu^{3+}$.

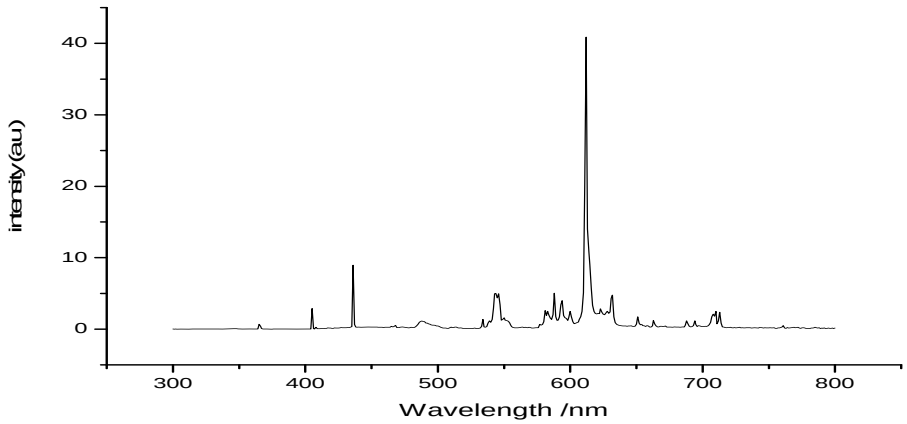

(a)

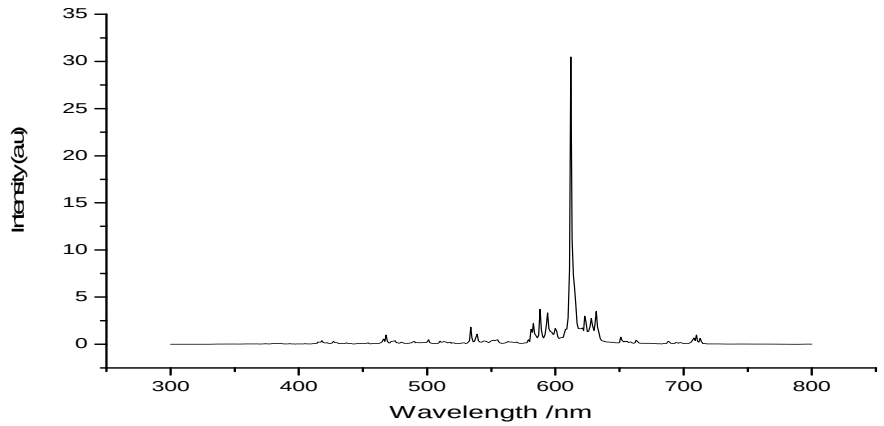

(b)

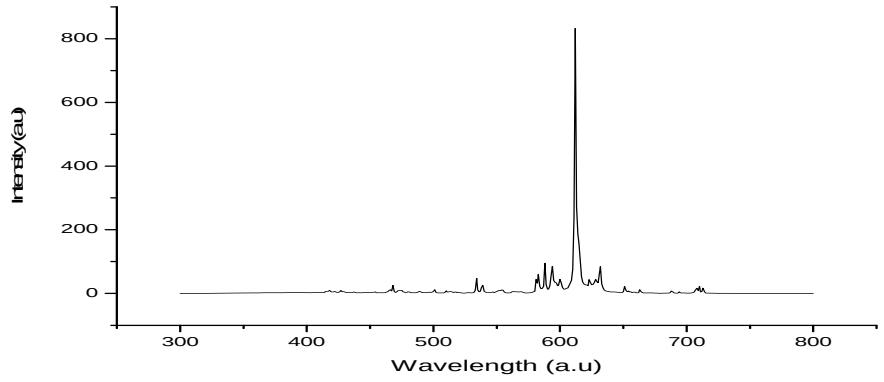

(c)

Figure 7.23 The Cl defocused beam emission spectra for samples (a) -1:1, (b) -1:2 and (c) -1:3 prepared from ethanolic solutions and fired/annealed at 900°C. All three samples were excited using 5000V/50uA.

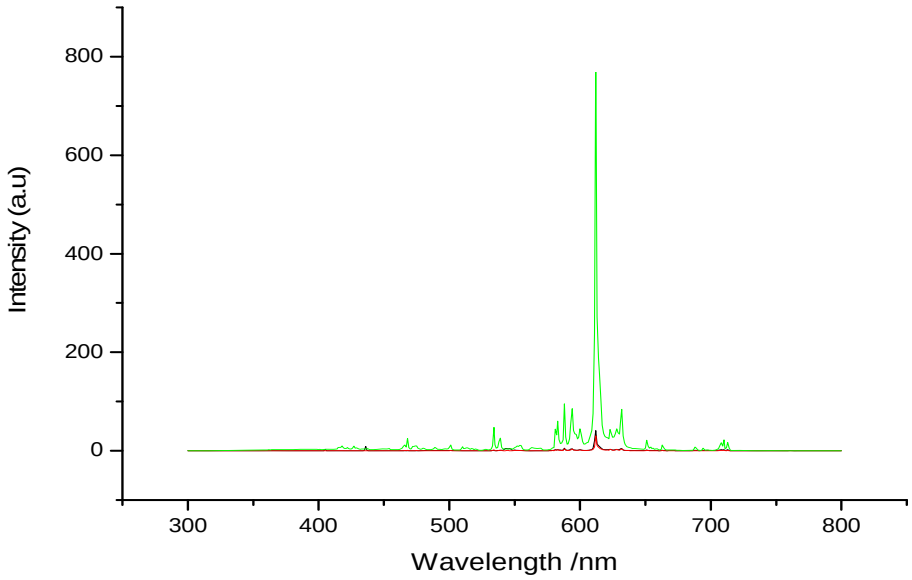

Figure 7.24 The Cl defocused beam emission spectra overlay for samples (a) -1:1black, (b) -1:2 red and (c) -1:3 green prepared from ethanolic solutions and fired/annealed at 900°C all three samples were excited using 5000V/50uA.

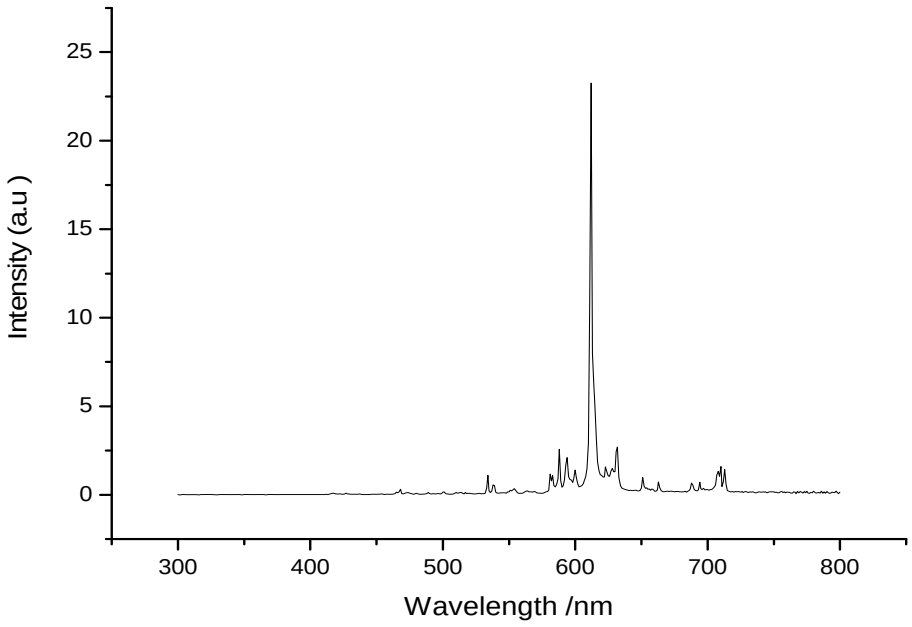

(a)

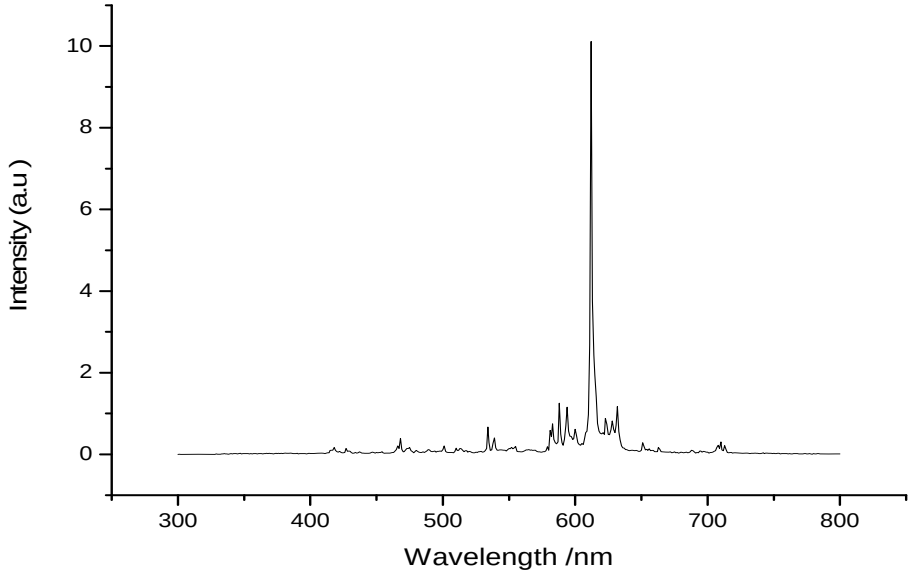

(b)

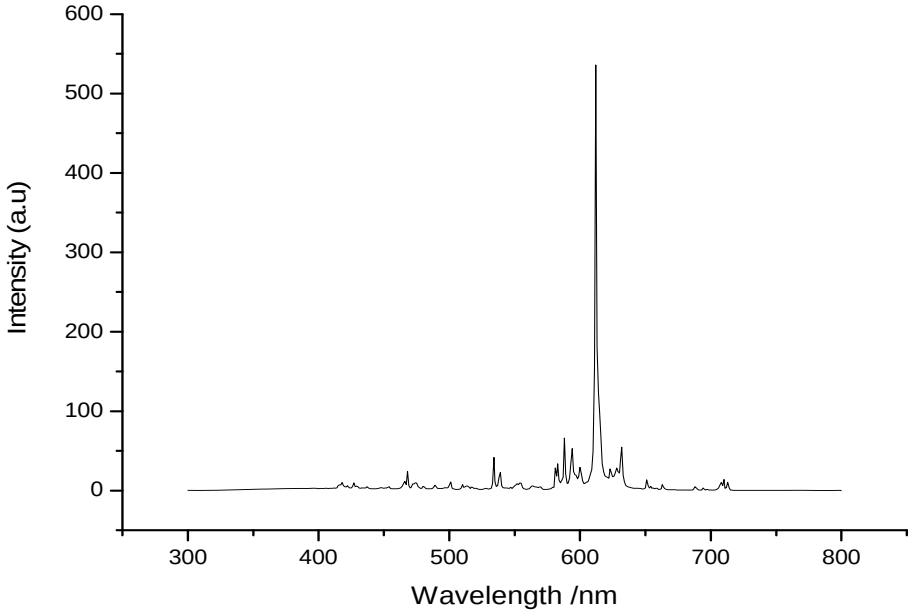

(c)

Figure 7.25 The Cl focused beam emission spectra for samples (a) -1:1, (b) -1:2 and (c) -1:3 prepared from ethanolic solutions and fired/annealed at 900°C all three samples were excited using 5000V/50uA.

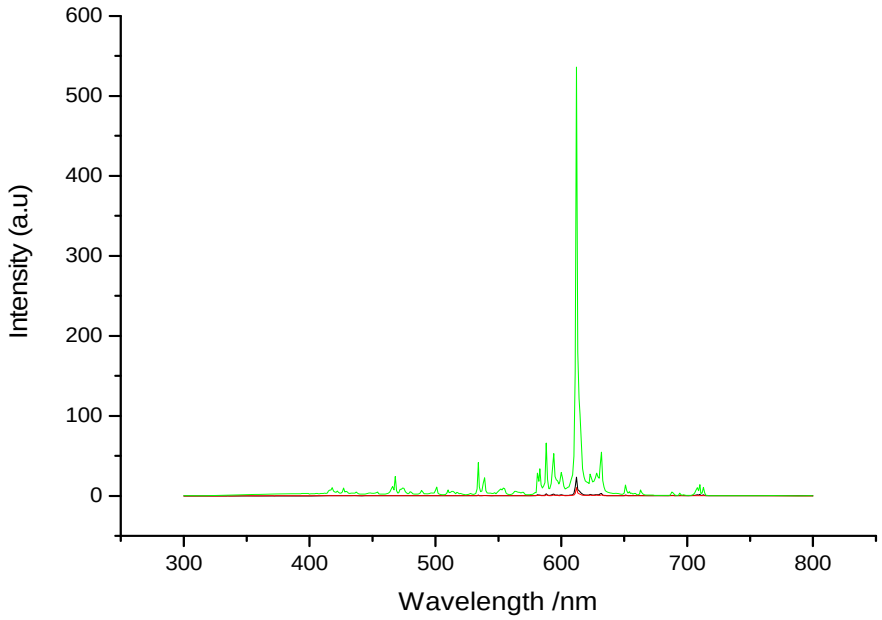

Figure 7.26 The Cl focused beam emission spectra overlay for samples (a) -1:1black, (b) -1:2 red and (c) -1:3 green prepared from ethanolic solutions and fired/annealed at 900°C all three samples were excited using 5000V/50uA.

7.4.6 FTIR Spectra

The data found for the 1:1material from methanol and the 1:1, 1:2 and 1:3materilas from ethanol, all the four materials gave similar Infra Red Data to those found for the 900°C materials in Chapters 5 and 6. The explanation of the Infra Red spectrum reported in paragraph 7.4.7 is the same. This is because we are looking at surface of the material sample with this special technique. The FTIR spectra from the samples prepared at 900°C are summarised in Table 7.4 the spectra presented in Figure 7.27, 7.28, show the presence of bands that can be ascribed to the presence of carbon dioxide and some OH groups in this respect there are some similarities to the 650°C spectra. The O-H deformation mode of H_2O is observed to be present as a weak shoulder at approximately 1626 cm^{-1} to the high frequency side of the strong CO_3^{2-} ν_3 asymmetric stretch doublet at 1553and 1446 cm^{-1}. Although, there is still the wide absorption band between 3600 to 3000 cm^{-1} that appears to be split into two weak peaks. The lower frequency CO_3^{2-} ν_3 asymmetric stretch peak of the doublet at 1446 cm^{-1} has shifted in wavelength compared to the 650°C samples. Also the CO_3^{2-} deformation has resolved

as a weak peak at 749 cm^{-1}.The positions of the CO_2 bands in these samples are similar to those found in
[(Y, Eu)$OHCO_3.H_2O$]. This finding will be explained below. It is clear from these results that the combustion fuel that was present in the samples in conjunction with the higher annealing temperature (900°C) was sufficient to raise the temperature for nanometer sized crystallites of the cubic $Y_2O_3:Eu^{3+}$ phase to form. The infrared spectra show the presence of bands due to the existence of CO_2 in the lattice. This is we believe due to the reaction of the surface of the nanometer sized particles with the atmosphere. In this work the $Y_2O_3:Eu^{3+}$ was formed from firing a precursor containing the long chained alkylammonium chloride and $YCl_3:Eu^{3+}$. The precursor itself was formed by reducing an alcoholic solution containing both of these components as starting materials. So the metal oxide was prepared by firing the metal chloride. This was to prepare nanometer sized particles of the metal oxide. In the past we have prepared larger nanometer sized particles of the metal oxide that were prepared by the hydrothermal decomposition of urea that facilitated the homogeneous precipitation of spherical submicron europium-doped hydroxycarbonate phosphor precursor particles. It is useful to explain this latter method here to help to understand the infrared data obtained in this work. This method is dependent on the addition of, and hydrothermal decomposition of, urea in acid solution in the presence of metal salts that are soluble at acid pH's. The chemistry involved includes:-
aqueous decomposition of urea (<85 ºC, ~ pH 3) resulting in the following ions,

$$H_2NCONH_2 \rightarrow NH_4^+ + OCN^- \qquad (7.3$$

the cyanate ion rapidly reacting

$$OCN^- + 2H^+ + 2H_2O \rightarrow H_2CO_3 + NH_4^+ \qquad (7.4$$

In the presence of Y^{3+} and Eu^{3+} cations which are added as acid salts the solution pH drops to ~2.5. The urea is added and the resulting hydroxonium ions (H_3O^+) promote urea decomposition. The subsequent release of carbonate ions causes precipitation of the metal hydroxycarbonate phosphor precursor, once the concentration of reactants reaches supercritical saturation.

$$[(Y, Eu)OH(H_2O)_n]^{2+} + H_2CO_3 \rightarrow [(Y,Eu)OHCO_3.H_2O] + (n-1)\ H_2O + 2H^+_{(aq)} \qquad (7.5$$

Careful firing of the precursor particles allows their spherical morphology to be partially maintained in the resulting phosphor particles. This method for the preparation of cubic $Y_2O_3:Eu^{3+}$ has previously been reported for the dopant concentration range from 0.2 mole fraction to 1mmole fraction Eu^{3+}. Both by ourselves and others [3-19].In the current work the presence of the surface of the very small particles of $Y_2O_3:Eu^{3+}$ reacts with the atmosphere adsorbing CO_2 and H_2O to form [(Y, Eu)$OHCO_3.H_2O$] reversing the above reaction. This shows that cubic $Y_2O_3:Eu^{3+}$ is

thermodynamically unstable in the presence of carbon dioxide and water vapour and reverts to the metal hydroxyl-carbonate precursor.

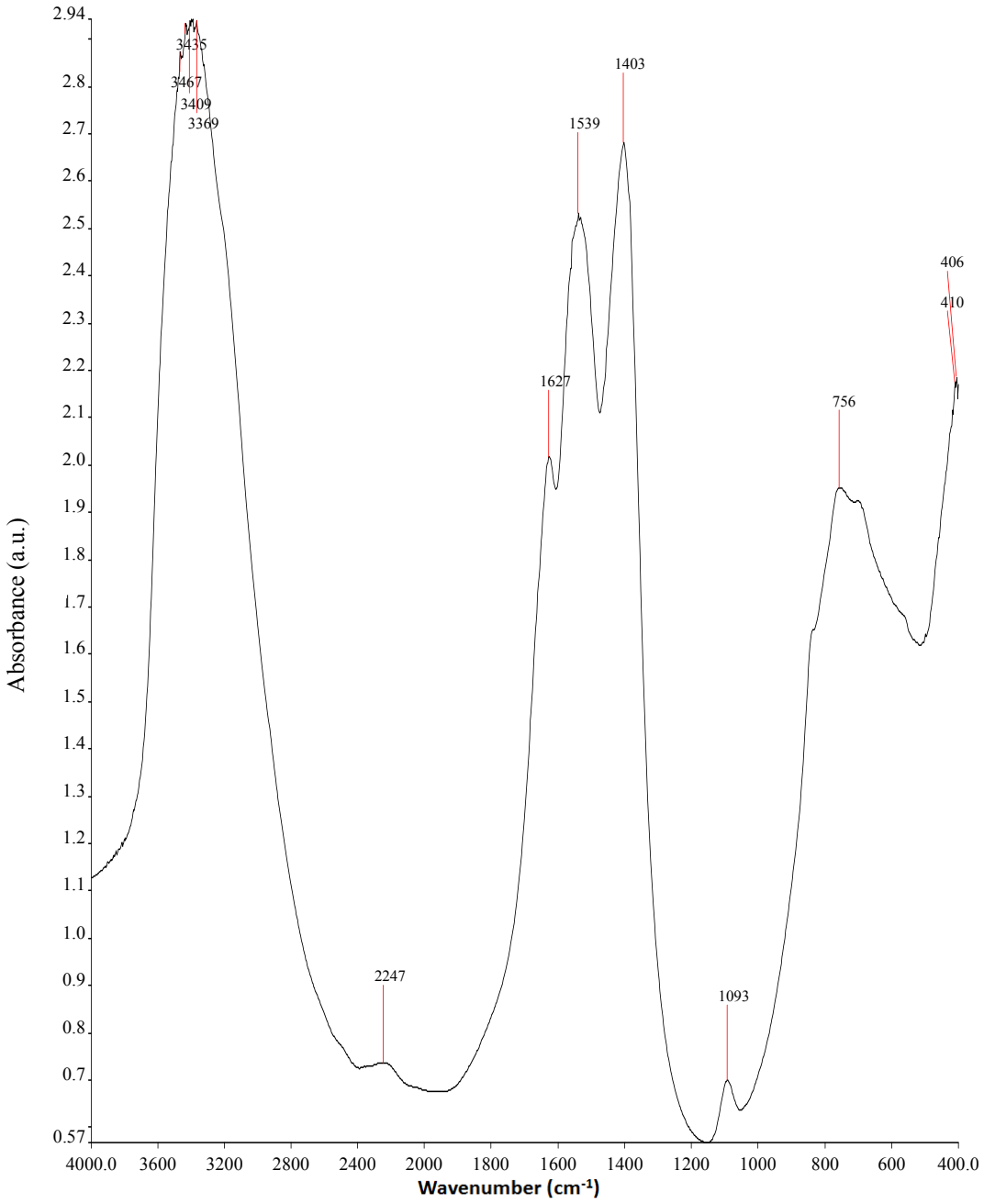

Figure 7.27 FTIR spectra of the 900°C, sample 38 prepared from methanolic solution with metal ion to alkylammonium chloride ratios 1:1 (in KBr discs).

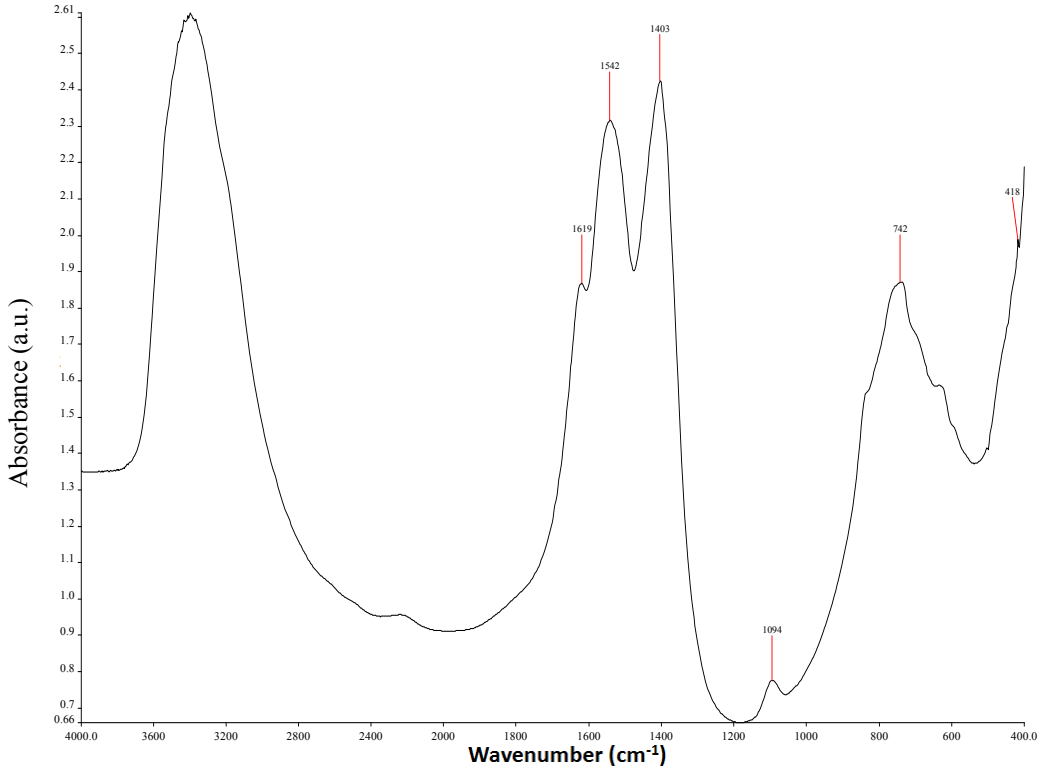

Sample 32, 1 to 1

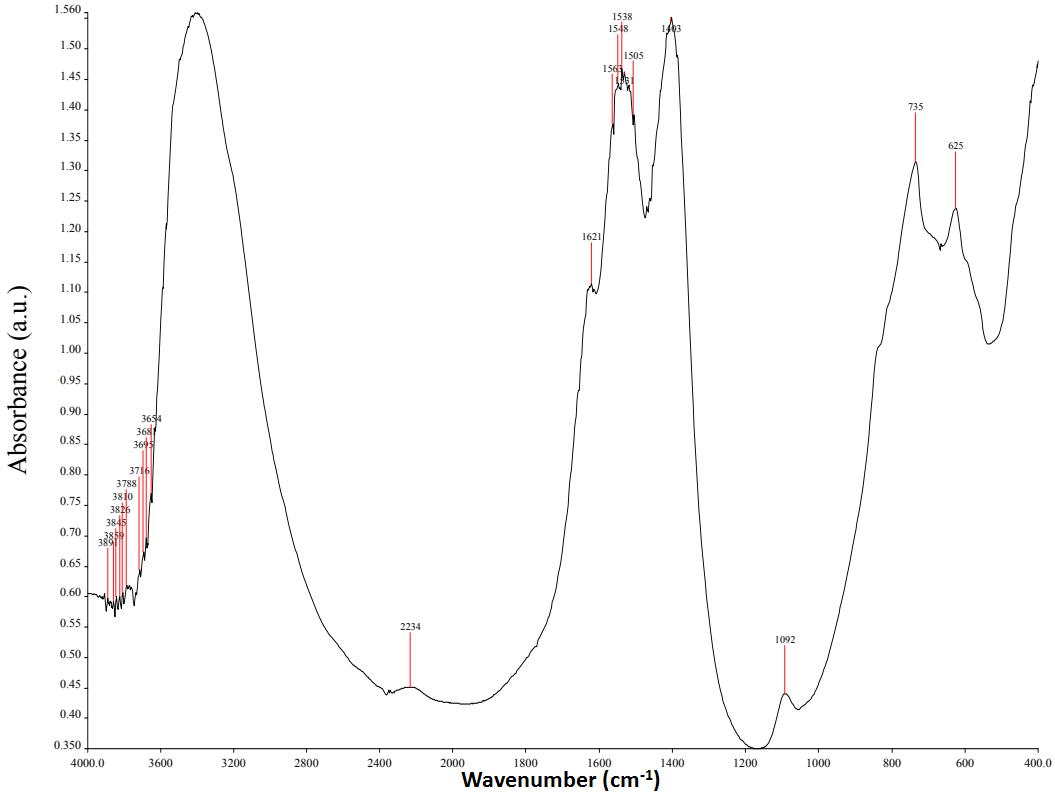

Sample 34, 1 to 2

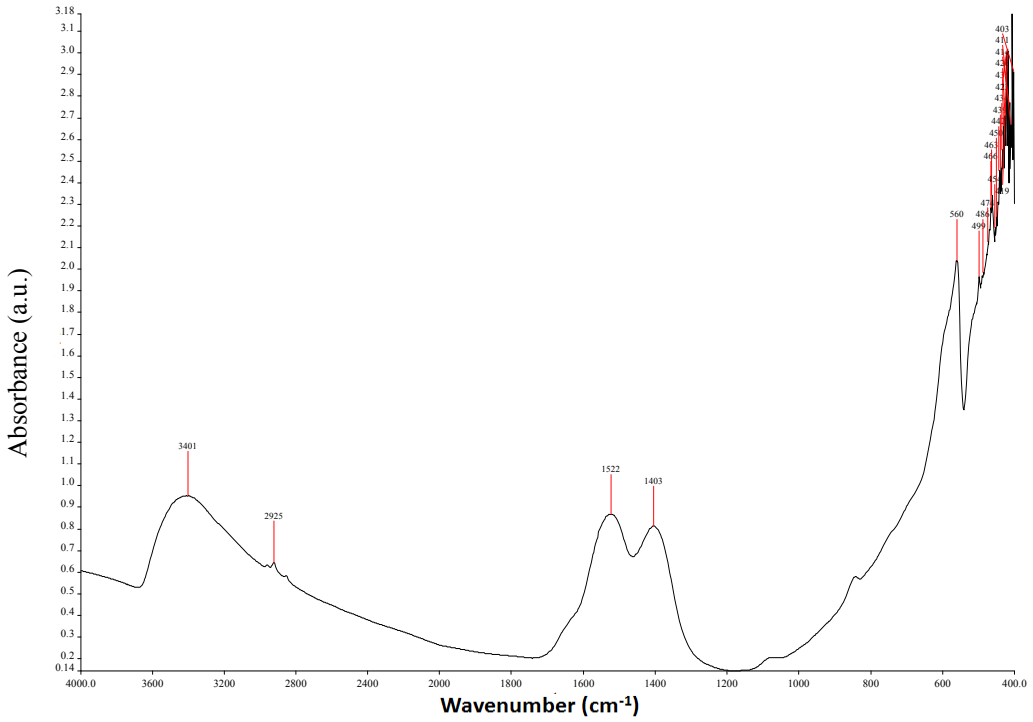

Sample 36, 1 to 3

Figure 7.28 FTIR spectra of the 900°C (samples 32, 34, 36), prepared from ethanolic solution with metal ion to alkylammonium chloride ratios 1:1 (32), 1:2 (34) and 1:3 (36) (in KBr discs)

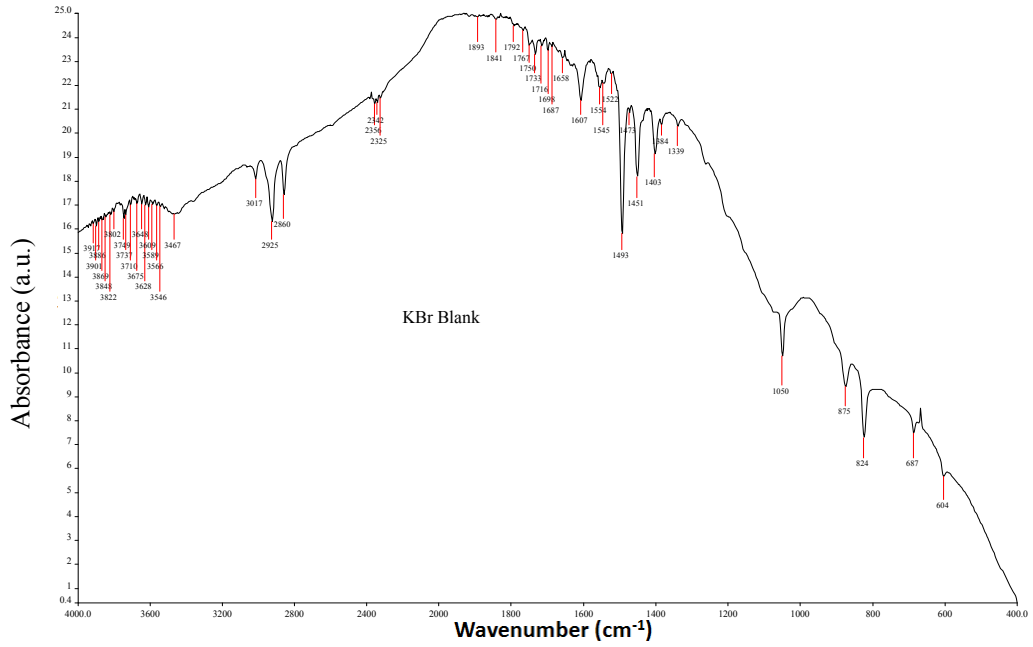

Figure 7.29 FTIR spectrum of KBr pure material-blank.

Table 7.4 Materials prepared from methanolic solutions and fired at 900°C

Wavenumber/cm^{-1}		
3600-3000	*(m)*	ν (O-H)
1627	*(w)*	δ (O-H)
1539	*(m)*	ν_{as} (CO_3^{2-})
1403	*(s)*	ν_{as} (CO_3^{2-})
1093	*(w)*	δ (O-H)
~756	*(w shoulder on cut-off)*	δ (CO_3^{2-})

Table 7.5 Materials prepared from ethanolic solutions and fired at 900°C

Wavenumber/cm^{-1}		
3600-3000	*(m)*	ν (O-H)
	(m)	ν_s (O-H)
1619	*(shoulder)*	δ (O-H)
1542	*(s)*	ν_{as} (CO_3^{2-})
1403	*(s)*	ν_{as} (CO_3^{2-})
1094	*(w)*	δ (O-H)
742	*(w)*	δ (CO_3^{2-})

7.5. Conclusions

A number of conclusions can be drawn from the work reported in this chapter that differ from those reported in chapters 5 and 6:-

1) Some nanometre sized particles of cubic $Y_2O_3:Eu^{3+}$ were prepared in all four materials reported in this chapter, but the only material where a significant quantity was found was in the 1:3 sample prepared from ethanolic solution and fired at 900°C. the other three samples were found to contain much less of the cubic material though they were all prepared from metal chloride precursors formed in micelles encapsulated by alkylammonium chains (the fuel) by using a combustion synthetic method at 900°C. This finding indicates that the shorter alkylammonium chain used in this chapter provided insufficient fuel to convert the majority of each sample to the cubic phase except for when it was present in a larger ratio than 1:2.
2) The surprising finding was that unlike the findings in chapters 5 when the shorter alkylammonium chain was used evidence for the presence of the high temperature monoclinic $Y_2O_3:Eu^{3+}$ phase was found. This surprising finding is not fully understood as this phase usually forms at temperatures well above 1000°C. The most likely explanation is that the structure of the very small

nanoparticles was dominated by the surface and surface energy allowed the phase to form at lower temperature, as the shorter alkylammonium chains burnt faster and exposed the small inorganic particles to oxygen.

3) In keeping with the results of chapters 5 and 6 the method still produces a range of morphologies that are influenced by the initial alkylammonium chloride concentration, in particular remnant micellar forms are present such as spheres, tubules, and macrolamellar sheets of these aforementioned forms.
4) Evidence of morphologies and particle size being controlled by the initial micellar structures was found in the materials fired at both 650°C and 900°C in keeping with the work in the earlier chapters.
5) It is clear from this work that the combustion fuel which was present in the samples prepared at 650°C was insufficient to raise the temperature over 900°C for a long enough time period (if at all) for the cubic $Y_2O_3:Eu^{3+}$ phase to form.
6) In fact at 650°C only evidence for YOCl and a Y_3O_4Cl present.
7) Further we have characterised the nanometre sized phosphor particles fired at both 650°C and demonstrated that they only manifest some CL spectral properties of bulk cubic $Y_2O_3:Eu^{3+}$, and these are not related to structural evidence.
8) In keeping with the findings in chapters 5 and 6 infra-red bands due to metal hydroxycarbonate in the infrared spectra of the cubic $Y_2O_3:Eu^{3+}$ nanoparticles were observed. These bands are similar in position to those found in bulk [(Y,Eu)$OHCO_3.H_2O$], and are explained as arising from the spontaneous reaction of the surface of the nanometre sized particles of cubic $Y_2O_3:Eu^{3+}$ with atmospheric CO_2 and water vapour. This indicates that nanometre sized particles of cubic $Y_2O_3:Eu^{3+}$ are thermodynamically unstable in the atmosphere and must be protected against such back reactions. This could be achieved with surface coatings.
9) In fact all the samples fired at both 650°C and 900°C irrespective of formula or phase showed the presence of infra-red bands due to metal hydroxycarbonate and these are explained as in 8 above.

Finally from the findings of the work reported in this chapter it would appear that though the use of sacrificial organised organic structures for the incorporation of inorganic precursors offers great potential as a method to control the morphology and size of nanometre sized particles the exact size and amount of the structures has a profound effect on the chemistry of the resulting particles.

References

[1] T. Ireland and J.Silver."Facile self-assembly of yttrium oxide europium phosphor from Solution using a sacrificial Micellar phase". Journal of the Electrochemical Society. 2, 1.52-54, 1999.

[2] Y.Nishisu and M.Kobayashi. "Synthetic method for the production range of particle size for Y_2O_3:Eu." U.S. Patent 5,413.736-737, 1995.

[3] Y.D.Jiang, Z.L. Wang, F. Zhang, H.G. Paics and C.J. Summers."Spherical particles for high definition display screens". Journal Material. Res 13, 2950-2955, 1998.

[4] J.A.Cooper, H.G Paris, S.R.Stock, S.Yeng and C.J.Summers." Particle size effect on the crystal structure of Y_2O_3:Eu particles." Journal SID, 6. 163-164, 1998.

[5] A.Vecht, C.Gibbons, D.Davies, X.P.Jing, P.Marsh, T.G.Ireland, J.Silver, A. Newport and D. Barber."Engineering phosphors for field emission display." Journal Vac. Sci. Tech. B. 17, 750-751, 1999.

[6] X.P.Jing, T.G.Ireland, C.Gibbons, D.J.Barber, J.Silver, A.Vecht, G.Fern, P.Trogwa and D.C. Morton." Control of Y_2O_3:Eu spherical phosphor size, assembly and properties." Journal of the Electrochemical Society 146, 4654-4656, 1999.

[7] M.I.Martinez-Rubio, T.G.Ireland, J.Silver, G.Fern, C.Gibbons and A.Vecht. " Effect on EDTA on controlling nucleation and morphology in the synthesis of ultrafine Y_2O_3:Eu phosphors." Journal. Solid State Chem. Electrochem and Solid State Lett. 3. 446-448, 2000.

[8] A.Vecht, M.I.Martinez-Rubio, T.G.Ireland, J.Silver, G.Fern and C. Gibbons. "Factors effecting efficiency in submicron size phosphors for high definition display." SID '00 Digest 31, 15-17, 2000.

[9] M.I.Martinez-Rubio, T.G.Ireland, J.Silver, G.Fern and M.J. Snowden. " Novel Method for the Synthesis of spherical particles of the Y_2O_3: Eu Phosphor Using a Copolymer Microgel of Nipam and Acrylic Acid". Langmuir 17, 7145-7149, 2001.

[10] J.Silver, M.I.Martinez-Rubio, T.G.Ireland, G.R Fern and R.Withnall. "The effect of particle morphology and crystallite size on upconversion luminescence property of erbium and yttrium co-doped yttrium oxide." Journal. Phys. Chem. 105,948-950, 2001.

[11] J.Silver, R.Withnall, A. Newport, M.I.Martinez-Rubio, T.G.Ireland, P.J. Marsh and A.Vecht. "Yttrium up-converting phosphors Part-2 temperature depend up conversation luminescence SID '01 Digest .32, 756-759, 2001.

[12] J.Silver, M.I.Martinez-Rubio, T.G.Ireland, G.R Fern and R.Withnall. "Yttrium oxide up-converting phosphors Part-3, up conversation luminescence emission from europium doped yttrium." Journal. Phys.Chem, B. 105, 9107- 9110, 2001.

[13] M.I.Martinez-Rubio, T.G.Ireland, G.R.Fern, J.Silver and M.J.Snowden. " A synthetic method for the production of a range of Particle sizes for Y_2O_3 : Eu phosphors using a copolymer microgel of NIPAM." Journal of the Electrochemical Society. 149, 253-255, 2002.

[14] J.Silver, R.I. Galliano, G.R. Fern, T.G. Ireland and R. Withnall. "A novel synthesis of Y_2O_3 : Eu phosphor using carbon dioxide and Ammonia for high definition CRT."SID '02 Digest.33, 12-15, 2002.

[15] J.Silver, N. Wilstead. D.Nicholas and A.Vecht. "Rare earth element anti stock phosphors emission." SID '02 Digest.33, 388-390, 2002.

[16] J.Silver, M.I. Martinez-Rubio, S.Gebretensae, G.R.Fern, M.J.Snowden and R.Withnall. " Yttrium oxide up-conversion phosphors luminescence." SID '02 Digest.33, 393-395, 2002.

[17] J.Silver, M.I.Martinez-Rubio, T.G.Ireland, G.R Fern and R.Withnall. "Yttrium oxide up-conversion phosphors Part-4, up conversation luminescence emission from europium doped yttrium oxide under 632.8nm light excitation." Journal. Phys.Chem. B. 107, 1548-1550, 2003.

[18] J.Silver, T.G. Ireland and R.Withnall." fine control of the doped level in cubic of Y_2O_3 : Eu phosphor."Journal. Electrochem. Soc. 151, 66-89, 2004.

[19] M. Konaissmy, D. Jeyakumar, R. Jagannathan and M. Mohan." Energy transfer and upconversion luminescence property of Y_2O_3 : Eu phosphor." Journal. Material. Res. Bull. 31. 1013-1016, 1996.

[20] D.H.Templetoan and C.H.Dauben. "Crystal Structures of Rare Earth Oxychlorides." Journal American. Chem. Soc, 75, 6069-6070, 1953.

[20a] W.H. Zachariasen. "Crystal chemical studies of the 5f-series of elements. XII. New compounds representing known structure types." Journal Acta Crystallographica, 2. 388-391, 1949.

[20b] L.M.Seaverson and J.D.Corbet. "Synthesis and characterization of oxide interstitial derivatives of zirconium monochloride and monobromide." Journal Inorg.Chemistry, 22.3202-3210, 1983.

[21] D.J.Gardiner, and P.R.Graves."Practical Raman spectroscopy." Springer-Verlag. 30-40, 1989.

[22] L.S.DentGlasser." Crystallography and its applications." Van Nostrand Reinhold Wokingham UK. 23-28, 1982.

[23] K.L. Chopra. "Thin Film Phenomena". McGraw-Hill New York. London 45-49, 1969.

[24] D.A Skoog and J. J Leary. "Principle of instrumental analysis". 4th Ed. Saunders College of publishing. London. 67-74, 1992

[25] M.Tanaka, Y. Nishisu, M. Kobayashi, A.Kurita, H.Hanzawa and Y.Kanematsu." Optical characterization of spherical fine particles of glassy Eu3+ doped yttrium basic carbonates." Journal. Non-Crystalline Solids .318, 175-185, 2003.

[26] L.Muresan,E.J. Popovici,R. Grecu and L.B.Tudoran." Studies on the synthesis of europium activated yttrium oxide by wet chemical method. 1. Influence of precursor quality on phosphor photoluminescence properties." Journal. Alloys and Compounds. 471, 421-427, 2009.

[27] N.B.Colthup, L.H. Daly and S.E.Wiberley. Introduction to Infrared and Raman Spectroscopy," 3rd edition, Academic Press Ltd. London 1990.

[28] J.Silver and R.Withnall. "Probes of structural and electronic environments of phosphor activators." Journal Chem.104, 2833-2855, 2004.

[29] E.Husson, C. Proust, P. Gillet and J.P.Itié." Phase transition in yttrium oxide at high pressure studied by Raman spectroscopy." Journal Material. Res.34, 2085-2092, 1999.

[30] R.B.Hunt and R.G.Pappalardo." Fast excited-state relaxation of Eu-Eu pairs in commercial $Y_2O_3:Eu^{3+}$ phosphors." Journal. Lumin. 34, 133-146, 1985.

[31] G. Schaack and J.A. Köningstein." Phonon and electronic Raman spectra of cubic Rare earth-oxides and isomorphous yttrium oxide." Journal. Opt. Soc.American. 60, 1110-1115, 1970.

[32] W.B. White and V.G.Keramidas." Vibrational spectra of oxides with the C-type rare earth oxide structure." Journal Spectrochimica Acta part A.28, 501-509,1972.

[33] D. Bloor and J.R.Dean."Spectroscopy of rare earth oxide systems. I. Far infrared spectra of the rare earth sesquioxides, cerium dioxide And nonstoichiometric praseodymium and terbium oxides." Journal. Phys. C and Solid State Phys. 5, 1237-1252, 1972.

[34] Y.Repelin, C.Proust, E.Husson and J.M.Beny." Vibrational spectroscopy Of the C-form of yttrium oxide." Journal. Solid State Chem. 118, 163-169.1995.

[35] B.Aiken, W.P.Hsu and E.Matijevic." Preparation and Properties of Monodispersed Colloidal Particles of Lanthanide Compounds: III, Yttrium (III) and Mixed Yttrium (III)/Cerium (III) Systems." Journal. American. Ceram. Soc. 71, 845-853, 1988.

[36] S.Sohn, Y. Kwon, Y. Kim and D. Kim." Synthesis and Characterization of near- monodisperse yttria particles by Homogeneous precipitation method Powder Technology." Journal of Solid State Chem. 142, 136-153, 2004.

Chapter Eight

Conclusions

The work presented in chapters 5, 6, 7 describes the methods by which the materials studied were synthesized. The synthetic methods used was based on (but modified from) one that was previously published by our group [1].The preparations all made use of amine hydrochlorides $(C_nH_{2n+1})NH_3Cl$ (n = 8, 12, 16) to form micellar phases (see chapter 2 section,2.6) in methanol or in ethanol and these were used to self assemble yttrium and europium cations from $YCl_3:Eu^{+3}$ (Eu 2.0 Mol%). In this work studies on the synthesis of cubic $Y_2O_3:Eu^{3+}$ from $[(Y, Eu)Cl_3]$ - $(C_{16}H_{33}NH_3Cl)n$ (for n = 1, 2, 3) materials, gave evidence for a number of different intermediate compounds reported in chapters 5, 6, 7 . The resulting fine powders all had smaller particles sizes, (ranging in size from 0.1 to 1.0 μm), than the commercial cubic $Y_2O_3:Eu^{3+}$ phosphor evidence for:-

1. YOCl
2. $Y_4O_5Cl_2$
3. Y_3O_4Cl

Was found. In fact, the "YOCl" species has been reported as a compound crystallising in both PbFCl and YOF-type structures [2, 3]. Furthermore, both $Y_4O_5Cl_2$ (≡ "$2YOCl.Y_2O_3$") [4] and Y_3O_4Cl (≡"$YOCl.Y_2O_3$") [5, 6] have also been reported. A number of conclusions can be drawn from the work reported herein for the materials prepared from the ethanolic solutions:-The materials prepared from ethanol at 650°C were shown to be the two forms of YOCl, and monoclinic $Y_4O_5Cl_2:Eu^{3+}$ this was converted to a more pure form of monoclinic $Y_4O_5Cl_2:Eu^{3+}$ at the higher temperature (over 900°C). It should be remembered that the presence of the yttrium hydroyoxycarbonate type layer protected the monoclinic $Y_4O_5Cl_2:Eu^{3+}$ in the materials prepared at 900°C from further reaction with the atmosphere. Finally from the findings of this work it would appear that the use of sacrificial organized organic structures for the incorporation of inorganic precursors offers great potential as a method to control the morphology and size of nanometre sized particles. Future work that is needed to follow that reported in this thesis would include a systematic investigation of what other yttrium oxide based phosphors could be prepared by composition of micellar precursors. Obvious candidates include Y_2O_3 precursors doped with Tb^{3+} and Gd_2O_3 doped with Tb^{3+} to produce green phosphors. The work could also extended by used such micellar based precursors in conjunction with sulfur to form Y_2O_2S lattices doped with Eu^{3+} or Tb^{3+} . Up- converting phosphors based on Y_2O_3 precursors doped with Er^{3+} Er^{3+} and Yb^{3+}, Th^{3+} and Er^{3+} could also be made based on the methods described. Many of these suggested phosphors are used commercially at the present time, but no one has exploited nano particles of these materials for industrial applications yet.

Chapter 8 Conclusions

It should be remembered that cubic $Y_2O_3:Eu^{3+}$ is still used in fluorescent lighting as the red phosphor, and hence nano-particles of this phosphor could have applications in lighting as less phosphor would be used to form layers two or three particles thick compared with μm sized particles. In this regard it would also be worth studying the stability of the Photoluminescent properties of the nanoparticles over time. In the conditions found in fluorescent tubes.

References

[1] T. Ireland and J.Silver."Facile self-assembly of yttrium oxide europium phosphor from Solution using a sacrificial Micellar phase". Journal of the Electrochemical Society. 2, 1.52-54, 1999.

[2] E. Garcia, J.D. Corbett, J.E. Ford and W.J. Vary." Stability of Rare-Earth Oxychloride Phases: Bond Valence Study." Journal Inorg. Chem. 24, 494- 496.1985.

[3] H.G. Brittain and G.Meyer." Luminescence and energy migration in Eu^{3+}-containing scheelites with different anions." Journal. Less Common Metals.126, 170-175,1986.

[4] L. Markovskii, E.Pesina, A.Omel'chenko and D. Kondrashev." The formation of $Y_2O_3Cl_2$."Russ, Journal Inorg Chem.14.10-11, 1969.

[5] S. Natansohn. "The synthesis and structure of rare-earth and indium tellurates, R2TeO6." Journal of Inorganic and Nuclear Chemistry. 30,3123-3125,1968.

[6] H.P. Beck, B. Naturforsch and B. Anorg." Low-temperature routes to new structures for yttrium, holmium, erbium, and thulium oxychlorides." Journal Chem Org. 32B,1015-1017,1977.

.

Appendices

Appendices

A number of papers have already been published on this work and of course more will be forthcoming. These include:-

Conference Papers

"**A Study of Small Particle Yttrium Oxide Type Phosphors prepared from Solution using a Sacrificial Micellar Phase as a Combustion Fuel**"
K. Saltoun, T. G. Ireland, G. R. Fern, R.Withnall and J. Silver.
22nd International Conference on Raman Spectroscopy, Date: AUG 08-13, 2010 Boston MA (paper)

"**Surface Studies of Y_2O_3:Eu, YAG:Ce, Y_2O_2S:Pr and Gd_2O_2S:M (M = Pr or Tb) Phosphors**"
Jack Silver, Robert Withnall, Terry G. Ireland Xiao Yan, Kelly Saltoun and Jesus J. on 18th International Display Workshop, Nagoya, Japan, 8th December, 2011 (paper).

Publications (listed below and included in the next pages).

Surface Studies of Y2O3:Eu, YAG:Ce, Y2O2S:Pr and Gd2O2S:M (M = Pr or Tb) Phosphors,
Jack Silver, Robert Withnall, Terry G. Ireland, Xiao Yan, Kelly Saltoun and Jesus J. Ojeda, Proc. IDW, 731-734 (2011).

A Study of Small Particle Yttrium Oxide Type Phosphors prepared from Solution using a Sacrificial Micellar Phase as a Combustion Fuel
K. Saltoun, TG. Ireland, TG; Fern, R.Withnall and J. Silver.
22nd International Conference on Raman Spectroscopy, Date: AUG 08-13, 2010 Boston MA *XXII INTERNATIONAL CONFERENCE ON RAMAN SPECTROSCOPY* Volume: 1267 Pages: 609-610, (2010).

Paper almost ready to be submitted

Templated Combustion Synthesis of Europium Doped Yttrium Oxychloride and Yttrium Oxide Nanoparticle Phosphors

Kelly Saltoun,[a] Terry G. Ireland,[a] George R. Fern,[a] Robert Withnall[a](the late) and Jack Silver.

Raman spectra of nanocrystalline yttrium oxychlorides prepared by a novel templating method

R. Withnall*, J. Silver, T.G. Ireland, K. Saltoun and G.R. Fern